

# **TIME VARYING PROBABILITY OF FAILURE OF STEEL FLOOR BEAMS SUBJECTED TO REAL FIRE**

by

**J.R.LAW, HNC(Mining), BSc, BE(Civil)**



Supervised by  
P. Clancy

A thesis submitted in fulfillment of the requirements for the degree of  
Master of Engineering at the Victoria University of Technology.

School of the Built Environment  
(Thesis undertaken in the former Department of Civil and Building Engineering)  
Victoria University of Technology  
Victoria  
Australia

December 1997

FTS THESIS  
628.9222011 LAW  
30001005971983

Law, J. R  
Time varying probability of  
failure of steel floor beams  
subjected to real fire

## TABLE OF CONTENTS

### CHAPTER 1: INTRODUCTION

1.0 Introduction	2
1.1 Aim	3
1.1.1 General	3
1.1.2 Specific	4

### CHAPTER 2: FIRE SEVERITY SUBMODEL

2.0 Introduction	7
2.1 Standard Fire	7
2.2 Real Fire	9
2.3 Heat Sources and Loses in Post-Flashover Fires.	11
2.3.1 Rate of Heat Release	12
2.3.2 Heat Loss by Convection through Openings	14
2.3.3 Heat Loss to the Walls	15
2.3.4 Heat Loss Through Openings	17
2.4 The Effect of Ventilation and Fire Load Density on Post-flashover Fires	18
2.4.1 Transition Criteria between Ventilation and Fuel Control	20
2.4.2 Opening factor	22
2.5 Fire load density	23
2.5.1 Fire load statistics	24
2.5.2 Fuel type	27
2.6 Mathematical models for compartment fire temperatures	29
2.6.1 Kawagoe and Sekine, 1963	29
2.6.2 Magnusson and Therlandersson, 1970	31

2.6.3	Babrauskas and Williams, 1978	32
2.6.4	Law, 1983	33
2.6.5	Lie, 1976	34
2.6.6	Harmathy, 1983	36
2.7	Summary of compartment fire models	38
2.8	Selection of Fire Severity Sub-Model	38
2.9	Comparison of Predictions of Selected Fire Severity Submodel with Test Results and Predictions of Other Models.	40
2.9.1	Comparison with Kawagoe's results	43
2.9.2	Comparison between alternative models.	45
2.9.3	Comparison between Lie model and experimental results (Butcher)	46
2.9.4	Comparison between Lie model and experimental results (Lathem)	49
2.10	Summary	51
2.10	Conclusion	52

## CHAPTER 3: HEAT TRANSFER SUBMODEL

3.0	Introduction	55
3.1	Heat Transfer	56
3.1.1	Convection	56
3.1.2	Radiation	58
3.1.3	Conduction	60
3.2	Prediction of Temperature of Fire Exposed Members	62
3.2.1	Numerical Methods	63
3.2.2	Comparison with Test Results	65
3.2.3	Commentary	65
3.3	Current Recommendations for the Calculation of the Temperature of Steel Members	66
3.3.1	Simplified Heat Transfer Analysis	66

3.3.1.1	Simplified Heat Transfer Analysis of Unprotected Steel Members	66
3.3.1.2	Simplified Heat Transfer Analysis of Insulated Steel Members	71
3.3.1.3	Considerations for Three Sided Exposure	76
3.3.1.4	Density of steel	79
3.3.1.5	Thermal Conductivity of Steel	79
3.3.1.6	Thermal Conductivity of Insulation	80
3.3.1.7	Influence of Moisture	83
3.3.2	Regression Method	86
3.4	Selection of Thermal Submodel	87
3.4.1	Calculation of Unprotected Steel Temperature	89
3.4.1.1	Heat Transfer Coefficient and Emissivity	89
3.4.1.2	Specific Heat of Steel	90
3.4.1.3	Time Step	91
3.4.1.4	Comparison between Calculated Steel Temperature Versus Time Curve and Experimental Test Data - Uninsulated steel	92
3.4.2	Calculation of Insulated Steel Temperature	96
3.4.2.1	Arrangement of Insulation	97
3.4.2.2	Thermal Conductivity	97
3.4.2.3	Thermal Conductivity - Derived from Test Data	100
3.4.2.4	Comparison between Calculated Steel Temperature-Time Curve and Experimental Test Data - Insulated Steel	106
3.5	Conclusion	108

## CHAPTER 4: MECHANICAL PROPERTIES SUBMODEL

4.0	Introduction	111
4.1	Mechanical Properties of Steel	112

4.1.1	Stress -Strain at Room Temperature	112
4.1.2	Stress - Strain at Elevated Temperature	113
4.2	Measurement of Stress-Strain Relationships	113
4.2.1	Steady State Tests	114
4.2.2	Transient Heating Tests	115
4.3	Models of Stress-Strain Relationships	116
4.4	Models of Variation of Steel Strength with Temperature	119
4.4.1	Influence of Creep and Heating Rate on Time and Temperature of Collapse	121
4.4.2	Effective Yield Stress of Steel at Elevated Temperature	124
4.5	Strength Reduction Model for Australian Steel	130
4.5.1	Current Model	132
4.5.2	Alternative Strength Reduction Model	136
4.5.3	Alternative Strength Reduction Model -Three Sided Exposure	136
4.6	Comparison between Strength Reduction Model and Test Results	138
4.7	Conclusion	143

## CHAPTER5: STRUCTURAL SUBMODEL

5.0	Introduction	145
5.1	Statically Determinate Beams	146
5.2	Plastic Analysis	147
5.2.1	Ambient Temperature	147
5.2.2	Elevated Temperature - Four sided Exposure	149
5.2.3	Elevated Temperature - Three Sided Exposure	150
5.3	Flexural Capacity	153
5.3.1	Comparison between Measured and Calculated Moment Capacity for Four Sided Exposure	154
5.4	Conclusion	156

## CHAPTER 6: LOAD SUBMODEL

6.1	Load Model - Code Requirement	159
6.2	Load Model - Probabilistic	160
6.2.1	Dead Load	160
6.2.2	Live Load	161

## CHAPTER 7: RELIABILITY MODEL

7.0	Introduction	164
7.1	Reliability Theory	164
7.1.1	Calculation of Probability of Failure	164
7.1.2	Second Moment Methods	167
7.1.3	Advanced Second Moment Method	170
7.1.4	Simulation Method	171
7.2	Commentary	173
7.3	Reliability Sub-Model	176

## CHAPTER 8: MODEL FOR PREDICTING THE PROBABILITY OF FAILURE OF STEEL FLOOR BEAMS IN REAL FIRE

8.0	Introduction	179
8.1	Description of Reliability Model	179
8.1.1	Fire Severity Submodel	180
8.1.2	Heat Transfer Submodel	180
8.1.3	Mechanical Properties Submodel	181
8.1.4	Structural Response Submodel.	184
8.1.5	Load Submodel	182
8.1.6	Reliability Submodel	183
8.2	Program Operation	184
8.2.1	Variance Reduction	186
8.3	Validation of model	189

8.3.1 General Comparison - Ambient Temperature	190
--	-----

## CHAPTER 9: SENSITIVITY ANALYSIS

9.0 Sensitivity Analysis	193
9.1 Fire load density	194
9.1.2 Probability of Failure - Time Independent	195
9.1.2.1 Mean value of fire load density	195
9.1.2.2 Coefficient of variation of fire load density	197
9.1.2.3 Probability density function	201
9.1.3 Probability of Failure - Time Varying	203
9.1.3.1 Mean value of fire load density	204
9.1.3.2 Coefficient of variation of fire load density	207
9.1.4 Conclusion	209
9.2 Probability of Failure as a function of Ventilation	210
9.2.1 Opening Factor	210
9.2.2 Probability of Failure - Time Independent	211
9.2.2.1 Variation in mean value of opening factor	211
9.2.2.2 Variation in coefficient of variation of opening factor	212
9.2.3 Probability of failure - Time varying	213
9.2.3.1 Variation in mean value of opening factor	213
9.2.3.2 Variation in the coefficient of variation of opening factor	215
9.2.4 Discussion	216
9.2.5 Conclusion	219
9.3 Insulation thickness	220
9.3.1 Probability of failure - Time independent	221
9.3.2 Probability of failure - Time dependent	222
9.4 Load ratio and load type	224
9.4.1 Probability of Failure - Time independent	226
9.4.1.1 Variation in load type ratio	226

9.4.1.2	Variation in load ratio	227
9.4.2	Probability of Failure - Time varying	228
9.4.2.1	Variation in load type ratio	228
9.4.2.2	Variation in load ratio	230
9.4.3	Conclusion	232
9.5	Exposure condition	233
9.5.1	Probability of Failure - Time dependent	233
9.5.1	Probability of Failure - Time dependent	234
9.6	Strength reduction model	235
9.6.1	Probability of failure	236
9.6.2	Conclusion	237
9.7	Conclusion	238

## List of Figures and Tables used in Chapter 2:

- Figure 2.1 Standard temperature-time curve specified for the fire resistance test AS 1530 Part 4.
- Figure 2.2 Real fire development in an enclosure.
- Figure 2.3 The effect of ventilation opening on the potential enthalpy release rate in a compartment fire (after Babrauskas).
- Figure 2.4 Frequency distribution of room fire load data for private office building (after Culver) and fitted theoretical distribution.
- Figure 2.5 Cumulative frequency distribution of fire load data for office buildings (after Pettersson) and fitted theoretical distributions.
- Figure 2.6 Average combustion gas temperature ( $^{\circ}\text{C}$ ) for different fuels and types of ignition. Fire load density =  $15 \text{ kg/m}^2$ ; opening parameter =  $0.06 \text{ m}^{1/2}$  after [Lathem, 1987].
- Figure 2.7 Temperature time curve for a range of opening factors 1) =  $0.03 \text{ m}^{1/2}$ ; 2) =  $0.06 \text{ m}^{1/2}$ ; 3) =  $0.12 \text{ m}^{1/2}$ ; (Fire load density =  $40 \text{ kg/m}^2$ ).
- Figure 2.8 Temperature time curve for a range of fire loads. (1 =  $20 \text{ kg/m}^2$ ; (2 =  $40 \text{ kg/m}^2$ ; (3 =  $60 \text{ kg/m}^2$  (Fire load referenced to floor area); Opening parameter,  $F = 0.08 \text{ m}^{1/2}$ .
- Figure 2.9 Comparison between temperature-time curves obtained by solving a heat balance and those described by expression (2.17) for ventilation controlled fires in compartments bounded by predominantly heavy materials ( $\rho \geq 1600 \text{ kg/m}^3$ ) [after Lie, 1992].
- Figure 2.10 Comparison between temperature-time curves obtained by solving a heat balance and those described by expression (2.17) for ventilation controlled fires in compartments bounded by predominantly light materials ( $\rho < 1600 \text{ kg/m}^3$ ) [after Lie, 1992].
- Figure 2.11 Comparison between gas temperature curves calculated using the Lie model and that adopted for use in the Swedish Building Regulations.
- Figure 2.12 Comparison between theoretical and experimental temperature-time curves. Fire load density =  $60 \text{ kg/m}^2$ .
- Figure 2.13 Comparison between theoretical and experimental temperature-time curves. Fire load density =  $30 \text{ kg/m}^2$ .

- Figure 2.14 Comparison between theoretical and experimental temperature-time curves. Fire load density = 15 kg/m<sup>2</sup>.
- Figure 2.15 Comparison between theoretical and experimental temperature-time curves. Opening factor = 0.06 m<sup>-1/2</sup>. Fire load density = 10, 15 and 20 kg/m<sup>2</sup> - Author.
- Figure 2.16 Comparison between theoretical and experimental temperature-time curves. Fire load density = 15 kg/m<sup>2</sup>. Opening factor = 0.03, 0.06 and 0.12 m<sup>-1/2</sup> - Author.
- Table 2.1 Top line - Required dimensions of windows for a range of compartments fitted with a standard door (2.0\*0.9 m), to achieve near stoichiometric burning. Bottom line - Minimum fuel load expressed in kg/m<sup>2</sup> of floor area (cribs/furniture) at which fuel control burning occurs. Opening factor = 0.08 m<sup>-1/2</sup>.
- Table 2.2 Variable fire load densities in offices,  $q_f$ , per unit floor area (MJ/m<sup>2</sup>).

#### List of Figures and Tables used in Chapter 3:

- Figure 3.1 Influence of variation in emissivity on average temperature of insulated and uninsulated steel members.
- Figure 3.2 Temperature time curve of a lightly insulated steel beam calculated using a temperature dependent specific heat of steel and a constant value specific heat.
- Figure 3.3 Influence of heat transfer coefficient on calculated steel temperature.
- Figure 3.4 Relationship between the 1983 and 1990 recommendations for the calculation of the temperature of heavily insulated steel members.
- Figure 3.5 Heating rate of insulated steel sections as a function of exposed surface area to mass ratio (ESM).
- Figure 3.6 Temperature time curve of a lightly insulated steel beam calculated using a temperature dependent thermal conductivity ( $\lambda$ ) of insulation and a constant value of thermal conductivity based on expected maximum steel temperature.
- Figure 3.7 Temperature rise of 250 UB steel beams exposed to the standard fire and protected by a range of insulation thicknesses.

- Figure 3.8 Relative change in the calculated average maximum steel temperature as a function of time increment.
- Figure 3.9 Comparison of experimental and calculated steel temperature using Equation (3.14).
- Figure 3.10 Comparison between measured steel temperatures, obtained from simulated office fire, and calculated steel temperature using one-dimensional heat transfer.
- Figure 3.11 Comparison between calculated and test data of free standing column exposed to natural fire.
- Figure 3.12 Comparison between calculated and test data of free standing column exposed to natural fire.
- Figure 3.13 Arrangement of insulation.
- Figure 3.14 Comparison between experimental and calculated temperature-time curves in which Equation (3.24) was used to represent the thermal conductivity of the insulation - 3 - sided exposure.
- Figure 3.15 Comparison between experimental and calculated temperature-time curves in which Equation (3.24) was used to represent the thermal conductivity of the insulation - 4 - sided exposure.
- Figure 3.16 Method of calculating slope of temperature-time response curve.
- Figure 3.17 Variation in calculated thermal conductivity as a function of moisture content.
- Figure 3.18 Values of thermal conductivity derived using experimental data in Equation (3.21) for temperatures up to 100 °C.
- Figure 3.19 Values of thermal conductivity derived using experimental data in Equation (3.14) for temperatures over 100 °C.
- Figures 3.20 - 3.24 Comparison of modelled and measured temperatures of insulated steel beams exposed to fire on three and four sides for a range of insulation thicknesses (INS) and mass to surface area ratios (ESM).

Table 3.1	Emissivities of surfaces in fire compartment Drysdale (1985).
Table 3.2	Ratio of temperature of top flange to bottom flange for box protected steel beams.
Table 3.3	Thermal conductivity, $\lambda$ , (W/m°C) of some insulation materials as a function of insulation temperature.
Table 3.4	Calculation of delay time due to moisture.

#### List of figures and Tables used in Chapter 4.

Figure 4.1	Variation with temperature of the stress - strain curve of Australian Grade 250 steel.
Figure 4.2	Various proposed yield stress reduction models.
Figure 4.3	Stress-strain curves at elevated temperature for Fe 360 steel.
Figure 4.4	Reduction in effective yield stress, expressed as a ratio of yield stress at ambient conditions, for a range of strains at first yield from ECCS and EC3.
Figure 4.5	Reduction in effective yield stress, expressed as a ratio of yield stress at ambient conditions, for a range of total strains from British Standards BS 4760 and BS 5059, (combined Grades 43 and 50 steel sections).
Figure 4.6	Tensile curves for a Grade 43A steel derived from transient tests.
Figure 4.7	Comparison between strength reduction models based on Equations (4.2) and (4.3) and that given in BS 5950: Part 8.
Figure 4.8	Strength reduction models. Curve AA - AS 4100. BB - derived

polynomial based on test data of Grade 250 and 350 steel.

- Figure 4.9 Influence of linear temperature gradient on moment capacity. Numbers in legend indicate ratio of the temperature of the compression flange/temperature of the tensile flange i.e.  $T_{top}/T_{bottom} = 0.6$ .
- Figure 4.10 Moment capacity ratio as a function of bottom flange temperature ( $T_{btm.}$ ) and linear temperature gradient  $1 - T_{top}/T_{bottom}$  for Australian sections - Author.
- Figure 4.11 Comparison between strength reduction models and test data (four sided exposure).
- Figure 4.12 Comparison between calculated and experimental time to failure.
- Table 4.1 Variation in steel temperature at 1% strain for a range of heating rates and two levels of stress, ( AS 1205 Grade 250 steel).
- Table 4.3 Comparison between measured and calculated time to failure using AISC/AS4100 and proposed strength reduction model, Equation 4.4 and 4.5. [Test Data - BHP Melbourne Research Laboratories (MRL), 1983].
- Table 4.5 Comparison between measured and calculated time to failure using proposed strength reduction model, Equation 4.4 and 4.5 and proposed heat transfer models. [Test Data - BHP Melbourne Research Laboratories (MRL), 1983].

#### List of Figures and Tables used in Chapter 5.

- Figure 5.1 Loading arrangement - point load.
- Figure 5.2 Loading arrangement - uniformly distributed load.

- Figure 5.3 Stress-strain distribution for plastic analysis.
- Figure 5.4 (a) - ideal elastic-plastic moment curvature relationship.  
(b) - actual moment curvature relationship for different section shapes.
- Figure 5.5 Stress distribution four sided exposure.
- Figure 5.7 Moment capacity ratio as a function of bottom flange temperature ( $T_{btm.}$ ) and linear temperature gradient  $1 - T_{top}/T_{bottom}$  for Australian sections - Author .
- Table 5.1 Comparison between calculated moment capacity using AS 4100 model and measured capacity at collapse. Test data derived from BHP MRL Reports (1983).
- Table 5.2 Comparison between calculated moment capacity using Equation (4.4) model and measured capacity at collapse. Test data derived from BHP MRL Reports (1983).

#### List of Figures and Tables used in Chapter 6.

- Figure 6.1 Statistical distribution of live load (figure based on 50 m<sup>2</sup>).
- Table 6.1 Statistical properties of office floor live loads ( $A_{Trib.}$  = tributary area).

#### List of Figures and Tables used in Chapter 7.

- Figure 7.1 Inconsistency in safety index due to variation in volume of failure region.

- Figure 7.2 Simulated load distribution and variation in mean value and shape of distribution of resisting moment of steel beam exposed to fire for 0 - 150 minutes.
- Figure 7.3 Comparison between the shape of the resisting moment distribution obtained by simulation and that obtained using second moment methods in which the resisting moment is assumed to be lognormally distributed - Author.

#### List of Figures and Tables used in Chapter 8.

- Figures 8.1 A-Top), B-Mid) and C-Btm.) - Frequency distribution of fire load density ( main chart) and fire load at failure (insert) [ fire load: A) = 18 kg/m<sup>2</sup> floor area; B) = 12 kg/m<sup>2</sup>; C) = 6 kg/m<sup>2</sup>; opening factor = 0.08 m<sup>1/2</sup>; Ins = 20 mm]- Author.
- Figure8.2 Distribution of fire load at failure as a function of insulation thickness [Fire load = 40 kg/m<sup>2</sup>; Ventilation parameter = 0.04 m<sup>1/2</sup>] - Author.
- Table 8.1 Statistical properties used in heat transfer submodel.
- Table 8.2 Table of minimum fire load to be used in simulation for given design fire load , Author.
- Table 8.3 Comparison between code and simulated safety index for a range of load ratios -Author.
- Table 8.4 Statistical models for load and resistance effect used in the code development

## List of Figures and Tables used in Chapter 9

- Figure 9.1 Time independent probability of failure as a function of fire load density (FL)  $\text{kg/m}^2$  floor area (opening factor (OF) =  $0.08 \text{ m}^{1/2}$ , COV = 0.35), [Insert shows relationship between -Log Probability of failure and probability of failure] - Author.
- Figure 9.2 Time independent probability of failure as a function of fire load density FL ( $\text{kg/m}^2$ ) and thickness of insulation (mm) - Author..
- Figure 9.3 Probability of failure as a function of fire load density and coefficient of variation of fire load density (OF =  $0.08 \text{ m}^{1/2}$ ) - Author.
- Figure 9.4 Time independent probability of failure as a function of coefficient of variation of fire load density and insulation thickness (based on fire load density of 40 -  $\square$  and 60 -  $\times$   $\text{kg/m}^2$ ; OF =  $0.08 \text{ m}^{1/2}$ ) - Author.
- Figure 9.5 Frequency distribution of fire load for a range of values of coefficients of variation - Author.
- Figure 9.6 Theoretical distributions of fire load density (based on mean fire load density =  $40 \text{ kg/m}^2$  and COV = 0.35).
- Figure 9.7 Time varying probability of failure as a function of fire load density (OF =  $0.08 \text{ m}^{1/2}$  A = 20, = 30, C = 40, D = 60, E =  $80 \text{ kg/m}^2$ ) - Author.
- Figure 9.8 Idealised probability of failure curve.
- Figure 9.9 Time varying probability of failure as a function of COV of fire load density for two mean values fire load density (refer Table 9.2 for details) - Author.

- Figure 9.10 Time independent probability of failure as a function of opening factor ( $m^{1/2}$ ) and insulation thickness (mm). COV of opening factor = 0.1 factor ( $m^{1/2}$ ), FL = 40 kg/m<sup>2</sup> -Author.
- Figure 9.11 Time independent probability of failure as a function of coefficient of variation (COV) of opening factor and insulation parameter ( OF = 0.08 m<sup>1/2</sup> and FL = 40 kg/m<sup>2</sup>) - Author.
- Figure: 9.12 & Table 9.5 Probability of failure as a function opening factor and two values of mean fire load density - Author.
- Figure 9.13 Time varying probability of failure as a function of coefficient of variation of opening factor (refer Table 9.5 for details) - Author.
- Figure 9.14 Time independent probability of failure as a function of thickness of insulation (OF = 0.08 m<sup>1/2</sup>, COV Insulation = 0.1) - Author.
- Figure 9.15 & Table 9.6 Probability of Failure as a function of Insulation Thickness (Fire Load = 18 kg/m; ventilation parameter = 0.08). Insulating material Harditherm 700 -Author.
- Figure 9.16 Probability density of load moment generated by RSB for different ratios of dead load to live load (simply supported beam, point load mid-span) - Author.
- Figure 9.17 Time varying probability of failure as a function of load type ratio of arbitrary point in time live load and dead load (FL =80 kg/m<sup>2</sup>; OF = 0.08 m<sup>1/2</sup>) -Author.
- Figure 9.18 Time varying probability of failure as a function of load type ratio of

arbitrary point in time live load and dead load (FL =40 kg/m<sup>2</sup>; OF = 0.08 m<sup>1/2</sup>) - Author.

- Figure 9.19 Time varying probability of failure as a function of variation in load ratio (FL = 40 kg/m<sup>2</sup>; OF = 0.08 m<sup>1/2</sup>) -Author.
- Figure 9.20 Time varying probability of failure as a function of variation in load ratio (FL = 80 kg/m<sup>2</sup>; OF = 0.08 m<sup>1/2</sup>) - Author.
- Figure 9.21 Time independent probability of failure as a function of exposure condition for medium-high and very-high fire load density ( OF = 0.08 m<sup>1/2</sup>) - Author.
- Figure 9.22 Time varying probability of failure as a function of exposure condition for medium-low and high fire load density (OF = 0.8 m<sup>1/2</sup>) - Author.
- Figure 9.23 Strength reduction model for British steel based on 0.2 and 1.0% proof strain.
- Figure 9.24 Time varying probability of failure for alternative strength reduction models ( FL = 60 kg/m<sup>2</sup>; OF = 0.08 m<sup>1/2</sup>; INS = 30 mm; 4-sided exposure) - Author.
- Table 9.1 Time independent probability of failure as a function of fire load density (FL) kg/m<sup>2</sup> floor area (opening factor ( OF) = 0.08 m<sup>1/2</sup>, COV = 0.35).
- Table 9.2 Probability of failure as a function of fire load density and coefficient of variation of fire load density (OF = 0.08 m<sup>1/2</sup>).
- Table 9.3 Area under tail of distribution with increase in COV (based on Lognormal distribution).

- Table 9.4 Time independent probability of failure as a function of probability density function ( $\overline{FL}$  @ FAIL denotes average fire load density at failure) - Author.
- Table 9.7 Mean and standard deviation of load moment derived from load models and load ratio expressed as a percentage of design capacity.
- Table 9.8 Time independent probability of failure as a function of load ratio.
- Table 9.9 Time independent probability of failure as a function of a reduced maximum nominal design load ratio (FL = fire load density).
- Table 9.10 Period of fire resistance at probability of failure of 0.00022.

## **ACKNOWLEDGEMENTS**

The author would like to thank both James Hardie & Co. Pty. Ltd. NSW and BHP Melbourne Research Laboratories, for making available test data used in this project. I would also like to thank my supervisor, Mr Paul Clancy for his help, guidance and perseverance throughout this project. Lastly, I would like to thank Mr Ian Campbell for pushing me over the line.

## ABSTRACT

A model for estimating the time-dependent reliability of steel beams under real fire conditions has been developed. It gives a more rational basis than time of failure modelling does for design. From risk modelling, some small resistance time from the probabilistic distribution times of failure can be deduced, which gives an acceptably small risk of failure. Time of failure modelling by itself can only give the mean time of failure which could lead to excessive risk if the variability of time of failure is large. The model comprises submodels for fire severity, heat transfer, mechanical properties, loads, structural analysis and reliability. Simple submodels have been adopted commensurate with the level of accuracy of other models in fire safety engineering. The submodel for real fire severity is Lie's. Heat transfer submodels have been adopted for three and four sided exposure and have been taken from work by the European Regional Organisation for Steel Construction and the French Technical Centre for Steel Construction. Three sided arises when the beam supports a concrete slab. The mechanical properties submodel was derived from an empirical fit to available test data. It gave better results than the current model in AS4100. It is appropriate for the model but is too complex for replacing the model in AS4100. The structural model four sided exposure was developed from simple plastic theory. For three sided exposure, discrete element analysis was adopted. The load submodels were lognormal for dead load and Weibull arbitrary point in time values for live load. The Monte Carlo method was adopted for the reliability submodel. The overall model was used to obtain the following sensitivities. An increase of  $10\text{kg.m}^{-2}$  in fire load density can increase the risk of failure by 40%. In relation to the sensitivity of risk to ventilation, a reduction of the opening factor from

0.12 to 0.04 m<sup>0.5</sup> increases the risk of failure approximately 200 times. Doubling the insulation thickness reduces the risk of failure by a factor ten. Increasing the live load has less effect on the risk of failure than increasing the dead load. If the load present is predominantly live load, there is much less risk of failure than if the load is predominantly live load. Four sided exposure has ten times the risk of failure compared with three sided exposure. Accepting larger proof strains reduces the risk of failure; for example, increasing proof strain from 0.2% to 1% reduces the risk of failure by 50%.

## **CHAPTER ONE**

### **INTRODUCTION**

## 1.0 Introduction

Approximately seventy percent of the Building Code of Australia (BCA) is concerned with provisions for the prevention, containment and control of fire. The BCA has evolved over many decades and reflects the traditional approach to fire safety. Many of the regulations pertaining to fire are experience-based and prescriptive in nature. Prescriptive regulations implies procedures and the use of materials with little scope for rational engineering design. Regulations have been added leading to an excess of fire safety requirements with little regard for building function. It has been estimated in a recent review conducted by the Building Regulations Review Task Force, [Grubitts,. 1992], that the additional impost due to unnecessary and inappropriate regulation relating to fire in the building industry amounts to \$250 Million annually. There is a recognised need for cost-effective fire regulations based on a rational engineering design philosophy which maintain Australia's good fire safety record.

A Draft National Building Fire Safety Systems Code [1992] has been developed that adopts a systems approach to building fire safety and protection design, based on risk assessment models (RAM) and fire engineering design techniques. Fire safety systems and subsystems are those assemblages of hardware and equipment such as fire extinguishment, alarms, smoke management, people management and structures and aspects of physical construction that contribute to or influence the level of fire safety of occupants or firefighters. Systems may be active such as sprinklers or passive such as compartment barriers. This systems view of fire safety and protection is a significant departure from the traditional approach to fire engineering. A RAM identifies those combinations of

building subsystems that provide the required level of safety in a cost-effective manner.

The efficacy of such an approach depends on the accurate modelling of the identified subsystems.

A passive system provides fire safety without actively responding to the fire. This includes horizontal and vertical structural separating elements (floors and walls) which act as a barrier to the spread of smoke and flame. Because of the time required to evacuate a building the time based performance of such elements when subjected to fire is an important consideration in the risk assessment of fire safety in buildings.

It is also necessary to consider realistic fires. Currently there are fire models which will predict the critical temperature of steel members, refer subsection (3.2), and hence time to failure of particular elements of construction subject to standard-fire testing. The author is not aware of any work done to model the time dependent reliability of passive subsystems subjected to real fire conditions.

## **1.1 Aim**

### **1.1.1 General**

The aim of the research is to develop a barrier model to estimate the time-dependent reliability of steel floor beams under real fire conditions. The model will make a significant contribution to the development of Risk Assessment Modeling.

### 1.1.2 Specific

It is proposed to obtain time dependent reliability of steel floor beams by developing the following submodels

- a) Fire severity submodel.
- b) Heat transfer submodel.
- c) Mechanical properties submodel.
- d) Loads submodel
- e) Structural analysis submodel.
- f) Reliability submodel.

The aim of each submodel is to model dominant phenomena as simply as possible with an accuracy commensurate with that of current risk assessment models.

An attempt has been made at estimating the reliability of steel beams [Thor, 1976; Beck, 1986], at any time during a fire, that is time independent reliability. A measure of reliability, on its own, is useful only in a comparative sense. An insulated steel beam tested in the standard fire has a probability of failure of one. Such knowledge in itself is not immediately useful. It is not sufficient to know that an event has a certain likelihood of occurring but rather what is the probability of occurrence at a particular time so that one can assess whether occupants will evacuate before structural failure. With this information a more accurate assessment can be made of the risk to life and fire safety systems in buildings.

## **CHAPTER TWO**

### **FIRE SEVERITY SUBMODEL**

## 2.0 Introduction

This chapter aims to describe in published literature important concepts in fire severity. Some existing fire severity models are investigated from which a compartment fire severity submodel is chosen for use in the model. Comparisons of submodel predictions are made with published test results.

All fires referred to in this research are compartment fires. Other fires such as bush fires and oil platform fires are outside the scope of this research.

## 2.1 Standard Fire

Because of the complexity of real fire the response and fire resistance of elements of building construction to exposure to elevated temperature has been determined on the basis of standard fire tests, conducted in accordance with procedures set down in standards and codes. A standard temperature-time curve is used in most countries to for testing full-scale samples of building elements in large furnaces. There is little difference between the curves from the various countries. The Australian standard fire exposure specified in AS 1530 Part 4 is defined by the following:

$$T_f = T_o + (345 * \text{Log}_{10}(8 * t + 1)) \quad (\text{°C}) \quad (2.1)$$

where  $T_o$  = the initial temperature

$T_f$  = the furnace temperature at time  $t$   
(minutes)

The furnace is controlled so that the temperature of thermocouples adjacent to the exposed surface of the element of construction undergoing a fire resistance test follows the standard curve shown in Figure 2.1.

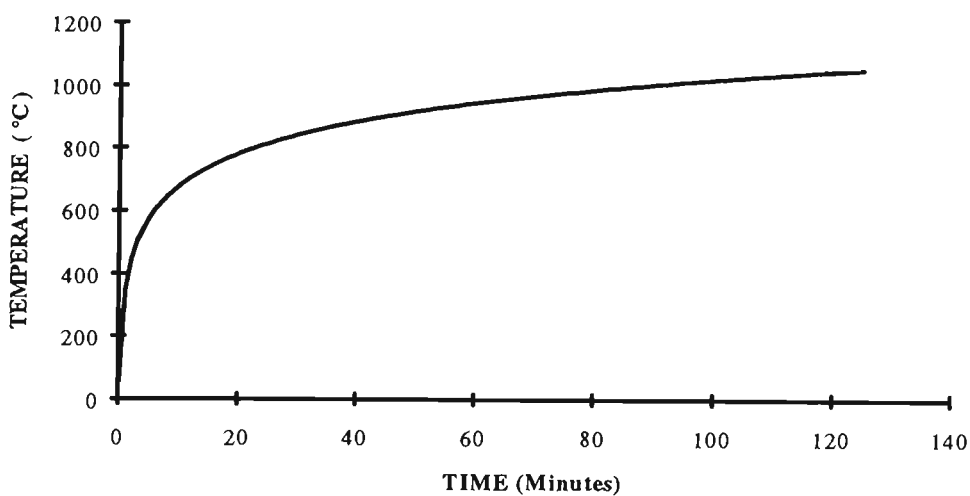


Figure 2.1: Standard temperature-time curve specified for the fire resistance test AS 1530 Part 4.

The heat transferred to the element can vary depending on the fuel used and the furnace design. The reproducibility of fire tests as measured by the coefficient of variation of fire resistance times can be as high as 0.15 [ASTM, 1983].

The standard fire is not a realistic representation of a compartment fire model. It makes no attempt to simulate real compartment fires rather the standard fire has evolved as representing a fire severity that would not be expected to be exceeded in a building fire [Lie, 1992]. It is well recognised Purkis [1988],

that the standard fire test, expressed in terms of maximum temperature and duration of exposure, is more severe than exposure to real fire. The differences between standard fires and real fires are detailed below in the next subsection.

## 2.2 Real Fire

"Real" fire is a complex phenomenon, the nature of which is dependent upon a large number of variables.

A compartment fire is a real fire confined within some enclosure within a building. The rate of increase of temperature, the maximum temperature reached and the duration of the fire can vary over a wide range. The development of fire in a compartment may be divided into three phases [Drysdale, 1987], refer Figure 2.2:

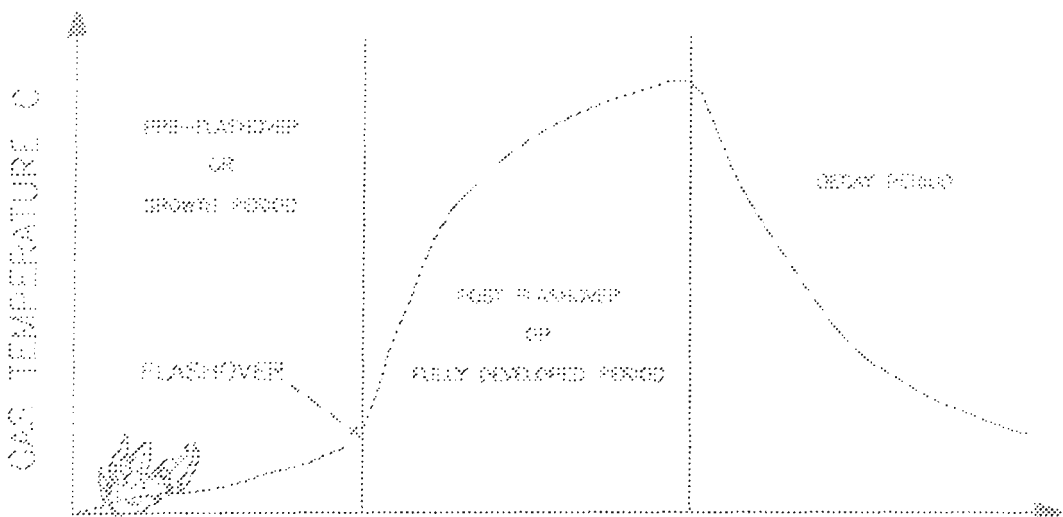


Figure 2.2 - Real fire development in an enclosure.

- a) the growth phase
- b) the fully developed phase
- c) the decay phase

The growth phase is characterised by a localised zone of burning, above which, hot gas is transported in a narrow plume to the ceiling. Provided window openings are small enough sufficient net accumulation of heat will occur in a short period of time, as short as five minutes. The layer of hot gas at the ceiling reaches a temperature whereby enough radiation is produced to simultaneously ignite all combustible surfaces in the enclosure. This sudden involvement of all of the materials and gases in all parts of the room is known as flashover. The foregoing scenario is termed ventilation control. If heat losses are large the fire is fuel controlled. A number of criteria have been used to define flashover [Thomas, 1983]. After flashover the temperature in the compartment rises quickly. The fire will continue to burn - the fully developed phase - until the fuel sources are exhausted, thereafter the compartment temperature will fall - the decay phase.

The amount of combustibles in the enclosure which is referred to as the fire load density effects ventilation and fuel controlled fires. Fire load density increases the duration of ventilation controlled fires and the maximum temperature of fuel controlled fires.

In terms of the fire resistance of structural members the low temperatures in the compartment during the growth phase are not considered significant.

Actual risk of failure of structural members in fire will only occur during the postflashover or fully developed phase of the fire. For this reason, only postflashover compartment fire models will be reviewed here.

Flashover is essentially a phenomenon associated with smaller compartment volumes typical of office or residential buildings. In the case of larger building spaces such as atria, auditoriums and industrial buildings a fully developed fire may occur without flashover of the entire volume. The foregoing is an important distinction in that a fire which could locally cause failure can develop in a building space but are technically not postflashover fires - the object of this study. Such fires require a different modelling approach to that for smaller compartment fires. Much of the research conducted into fire modelling assumes flashover or total involvement of the compartment volume. The plan area of the compartments used in the majority of experiments and from which much of the data used to develop fire models has been obtained, would rarely exceed 50 m<sup>2</sup>.

The following subsection describes the variables affecting post-flashover fires for small to medium compartments.

### **2.3 Heat Sources and Loses in Post-Flashover Fires**

The basis for predicting time of flashover and temperature versus time of post-flashover fires is the first law of thermodynamics. It can be applied in the form of equation 2.2.

$$q_F = q_G + q_W + q_R \quad (2.2)$$

where

- $q_F$  = rate of heat release by combustion inside the compartment
- $q_G$  = rate of heat loss by convection in the openings
- $q_W$  = rate of heat loss through bounding walls, floors and ceilings
- $q_R$  = rate of heat loss by radiation through the openings

### 2.3.1 Rate of Heat Release

The quantity of heat released in the compartment per unit of time by combustion,  $Q_F$ , is given by:

$$Rqm \quad (2.3)$$

- where
- $R$  = mass burning rate of wood cribs
- $q$  = the calorific value of wood
- $m$  = ratio of complete combustion

Kawaoge [1958] using full scale and reduced scale fire tests, demonstrated that the mass burning rate of wood cribs in enclosures (the rate of heat release) can be related to the size and shape of the compartments ventilation opening (air flow factor). The semi-empirical relationship is given by

$$R = 5.5A_w\sqrt{H} \quad (\text{kg/s}) \quad (2.4)$$

where  $A_w$  and  $H$  are the area ( $\text{m}^2$ ) and height (m) of the ventilation opening respectively. Similar expressions to (2.4) were proposed [Thomas et al., 1967; Rockett, 1976] in which the constant was attributed values of 0.5 and 0.4 to 0.61 respectively depending on the discharge coefficient. An alternative relationship is given by Saito [1979] in which the size of the compartment is taken into account and by Law [1983] in which the depth to width ratio of the fire compartment is accounted for. Thomas [1972] demonstrated that the mass burning rate of the fuel as given by equation (2.4) is only appropriate for a limited range of  $A_w\sqrt{H}$ . It was apparent from experimental results that when the ventilation opening was small the flow rate of air into the compartment controlled the combustion process (ventilation control - refer subsection 2.4 and 2.4.1). If the ventilation opening is progressively enlarged a condition is reached such that the rate of burning becomes independent of the size of the opening. In such cases the rate of burning is controlled by a number of parameters (fuel control - refer subsection 2.4 and 2.4.1). The most significant of these parameters is the exposed surface area of the fuel, however specific fuel bed properties such as average thickness

of the fuel, spatial orientation and porosity are also important, [Butcher et al., 1968]: [Bullen, 1977].

A theoretical derivation of equation (2.4) in which stoichiometric burning occurs indicate that radiative feedback from the surrounds has negligible effect. This apparently anomalous result supports the observations of Thomas and is explained Harmathy [1978], by either protection afforded the burning surface by the formation of char or by shielding due to the arrangement of the wood cribs typically used in fire tests. Although some form of equation (2.4) is used to calculate the amount of heat released by the fuel in a number of fire models, it is apparent that its use should be limited to fires in which the fuel source is cellulose.

### **2.3.2 Heat Loss by Convection through Openings**

The dominant heat loss from the compartment is due to the removal of hot gases from the compartment. [Drysdale, 1987]. The exchange of combustion gases is driven by buoyant flow due to the reduced density of the hot gas. The theoretical treatment is based on the fundamental assumption that there is a linear pressure distribution in the vertical direction over the ventilation opening. By means of Bernoulli's equation the gas exchange  $\dot{V}$  is calculated from the following:

$$Q_{G(out)} = \frac{2}{3} C_d B_v (h_f)^{2/3} \rho_f \sqrt{2g \left( \frac{\rho_o}{\rho_f} - 1 \right)} \quad (2.5)$$

$$Q_{G(in)} = \frac{2}{3} C_d B_v (h_o)^{3/2} \rho_o \sqrt{2g \left( 1 - \frac{\rho_f}{\rho_o} \right)} \quad (2.6)$$

where

- $C_d$  = flow coefficient
- $B_v$  = width of opening (m)
- $h_f$  = distance from neutral layer to top of opening  
(m)
- $h_o$  = distance from neutral layer to bottom of opening  
(m)
- $\rho_f$  = density of combustion gases (kg/m<sup>3</sup>)
- $\rho_o$  = density of air (kg/m<sup>3</sup>)
- $g$  = acceleration due to gravity (m/s<sup>2</sup>)

A more realistic treatment must consider rate of burning and ventilation separately in order to accommodate the movement of unburnt volatiles from the compartment.

### 2.3.3 Heat Loss to the Walls

Heat transfer from the hot gas to the walls occurs by two mechanisms: radiation and convection. Both mechanisms are very complex [Siegal and Howell, 1972]. An acceptable modelling approach in which the wall losses are modelled using small number of variables is to consider the walls (including the

ceiling) to be part of an infinite slab. The heat transferred to the walls,  $Q_w$ , is given by the general expression:

$$Q_w = A_w \left[ \sigma \left( \frac{1}{\frac{1}{\varepsilon_f} + \frac{1}{\varepsilon_w}} \right) (T_f^4 - T_w^4) + \alpha (T_f - T_w) \right] \quad (2.7)$$

where

- $A_w$  = total internal surface area of fire compartment (m<sup>2</sup>)
- $\varepsilon_{f \& w}$  = emissivity of the flame and walls
- $T_{f \& w}$  = temperature of flame and walls
- $\alpha$  = convective coefficient of heat transfer

Large-scale turbulence due to the interaction of boundaries, plumes, ceiling jets and openings precludes a specific expression for the convective coefficient of heat transfer  $\alpha$ . Given the assumption of a well stirred reactor and that radiation is dominant at temperatures which occur during fire, either a mean value for the convective coefficient of heat transfer is adopted or a simplified expression, in which the coefficient is temperature dependent, is used [McAdams, 1954].

Heat transfer to the walls must be balanced by the heat transmitted through the walls, stored in the walls and that portion of the energy radiated back into the compartment. Solution of heat loss involves the evaluation of non-linear radiation terms and the inclusion of temperature dependent thermophysical

parameters such as thermal conductivity and specific heat. Additional complexity derives from the influence of different groups of thermophysical parameters have on gas temperature at different stages of a compartment fire [Babrauskas and Williams, 1979].

#### 2.3.4 Heat Loss Through Openings

The quantity of heat dissipated by radiation through openings in the compartment,  $Q_R$ , can be calculated using the Stefan-Boltzman law:

$$Q_R = A_V \sigma (T_f^4 - T_o^4) \quad (2.8)$$

where

$A_V$	=	Area of ventilation openings
$\sigma$	=	Stefan-Boltzmann Constant
$T_{f\&o}$	=	Temperature of flame and outside of compartment.

The emissivity outside the window is generally taken to be that of a black body.

Models developed to predict postflashover temperatures assume that the gas within the compartment is at or near a uniform temperature throughout the compartment volume, except near the floor (the well mixed reactor model) because of small compartment volume, turbulence and radiation [Croce, 1978].

Depending on whether the fire is controlled by the available oxygen or the amount of fuel the heat loss characteristics vary. In the former case the ratio of the total heat loss by each of the three mechanisms  $q_G : q_W : q_R$  is 0.55 : 0.34 : 0.11 whereas in the later case the ratio is 0.81 : 0.14 : 0.05 [Magnusson and Therlandersson, 1974]. In both cases the radiant heat loss through the windows is relatively small the dominant heat loss mechanism being convective gas flow through the openings.

## 2.4 The Effect of Ventilation and Fire Load Density on Postflashover Fires

There are two distinct regimes of burning for postflashover fires, namely, ventilation and fuel controlled fires. The rate of pyrolysis of the fuel is a function of temperature, fuel type and geometry of the fuel. The potential enthalpy of the pyrolysed fuel,  $h_p$ , may not be realised if there is insufficient oxygen in the compartment since the maximum rate of burning is stoichiometric combustion, reduced by some factor due to incomplete mixing [Babrauskas and Williamson, 1978]. The rate of heat release for stoichiometric combustion,  $h_s$ , is related to the mass inflow of air,  $m_{air}$ , expressed in terms of the opening parameter,  $A_w \sqrt{h}$ , refer subsection 2.4.1 for definition, and the gas temperature. Figure 2.3 shows that the actual enthalpy release rate in the compartment,  $h_c$ , will be the lesser of  $h_p$  and  $h_s$  reduced by some factor due to incomplete mixing.

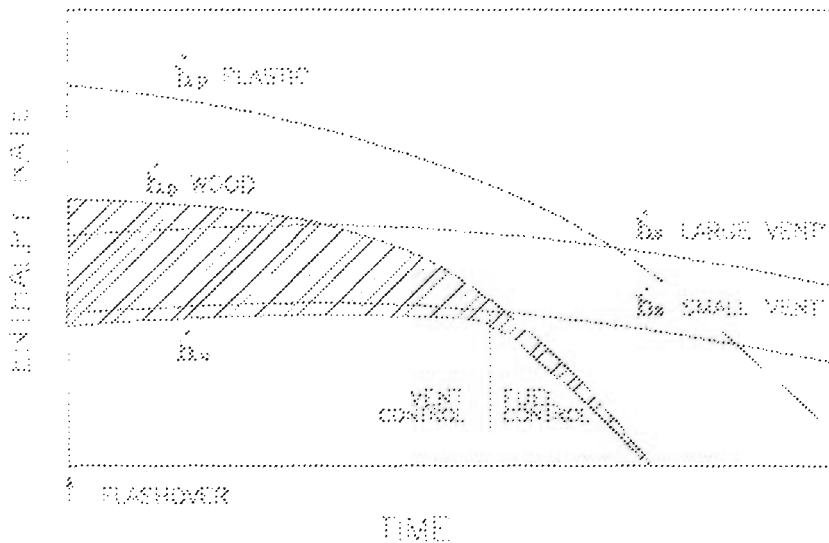


Figure 2.3: The effect of ventilation opening on the potential enthalpy release rate in a compartment fire (after Babrauskas).

When  $h_p > h_s$ , there is more pyrolysed fuel in the compartment than can be burnt inside it - ventilation control. This unburnt fraction of the fuel (the cross-hatched region when the ventilation opening is small) may cause significant flaming and be a potential hazard where it discharges from the compartment. When  $h_p < h_s$ , the enthalpy rate is controlled by the available fuel. The convective flow of excess air into the compartment under fuel control can be large causing a significant dilution of the pyrolysed fuel. Under these conditions the temperature of the compartment is lower. On the other hand the loss of enthalpy due to heating of the unburnt products of pyrolysis in the case of ventilation control, is relatively small in comparison. The compartment temperature will therefore approach a maximum at the point of switchover between ventilation controlled and fuel controlled regimes.

Most compartment fire models assume ventilation control because it is considered the most severe [Pettersson, 1976]. It is evident from Figure 2.3

that the assumption of ventilation control could significantly overestimate the enthalpy rates in a compartment fire. Magnusson and Therlanderrson, [1974], demonstrated that the average gas temperatures of fuel controlled fires are significantly lower and of longer duration than that of ventilation controlled fires. There is little difference in the maximum temperature of insulated steel exposed to either curve while in the case of lightly insulated and uninsulated steel exposed to ventilation controlled fires the steel temperatures are higher.

#### 2.4.1 Transition Criteria between Ventilation and Fuel Control

Transition from a fuel controlled fire to a ventilation controlled fire occurs when enclosure openings are not large to enough to let sufficient oxygen to enter the enclosure to satisfy the oxygen demand of the fire. This occurs when the ratio of fire load,  $Q$ , to window area,  $A_w$ , exceeds approximately 150 kg/m<sup>2</sup> [Thomas et al., 1967]. Alternatively values of the factor,  $A_w \sqrt{h} / A_T$ , greater than 0.1- 0.125  $m^{-1/2}$  correspond to fuel control fires [Thomas & Heselden, 1972]. Here  $A_T$  is the area of the walls and ceiling of the compartment, excluding the ventilation area  $A_w$  ( $A_T$  normally defines the total internal surface area) and  $h$  represents the weighted mean of the height of the ventilation openings in the enclosure. The average value of opening factor for offices obtained from survey data, given as 0.08  $m^{-1/2}$  [Ellingwood and Shaver, 1980] (calculated using the total surface area), lies within this range. Table 2.1 shows the area of window at which the transition between fire regimes would

occur for a range of compartment sizes. Fires in compartments with window areas less than that in Table 2.1 will be controlled by the available oxygen and are likely to produce flaming over the building facade. Compartments in which the window area equals that given in Table 2.1 will burn at maximum temperature while those compartments with larger areas will be fuel controlled. In this case the fire temperatures will be lower and of longer duration.

	COMPARTMENT WIDTH (m)				
DEPTH (m)	3.0	4.0	5.0	6.0	7.0
3.0	1.5 * 0.95 28.0/44.5				
4.0	1.5 * 1.5 24.0/38.4	1.5 * 2.1 23.5/37.6			
5.0	1.5 * 2.0 23.8/38.1	1.5 * 2.7 22.5/36.0	1.5 * 3.3 20.5/32.8		
6.0	1.5 * 2.5 23.5/37.6	1.5 * 3.2 21.0/33.6	1.5 * 4.0 19.7/31.5	1.5 * 4.7 18.7/29.9	
7.0	1.5 * 3.0 23.0/36.8	1.5 * 3.8 20.3/32.5	1.5 * 4.7 19.2/30.7	1.5 * 5.6 18.1/28.9	1.5 * 6.4 17.6/28.1

Table 2.1: Top line - Required dimensions of windows for a range of compartments fitted with a standard door (2.0\*0.9 m), to achieve near stoichiometric burning.

Bottom line - Minimum fuel load expressed in kg/m<sup>2</sup> of floor area (cribs/furniture) at which fuel control burning occurs. Opening factor =  $0.08 m^{-1/2}$ .

A criterion to distinguish between ventilation and fuel controlled fires involving cellulosic fuels [Harmathy, 1986], is given by the following:

$$\text{Ventilation control} \quad \frac{\rho A_w \sqrt{h g}}{A_f} < 0.235 \quad (2.9)$$

$$\text{Fuel control} \quad \frac{\rho A_w \sqrt{h g}}{A_f} > 0.290 \quad (2.10)$$

where  $A_f$ , is the fuel surface area. Based on expression (2.10) the fuel load ( $\text{kg}/\text{m}^2$ ) which would result in fuel control burning is given in Table 2.1. The first value assumes a typical specific surface of the fuel for cribs; the second value uses a value typical of a furnished room. It is apparent from Table 2.1 that for wood based fuels a much larger fuel load (60%) is required in small compartments to achieve fuel control.

For fuels other than cellulose the change in burning regime does not occur, refer Sub-section 2.4.2.

## 2.4.2 Opening Factor

The burning rate of the fuel is linked to the mass flow of air into the compartment through vertical openings in the compartment. The combined influence of the compartment size and the amount and shape of the openings is expressed by the opening factor:

$$\frac{A_w \sqrt{h}}{A_T} \quad (2.11)$$

The terms have been defined in Subsection 2.4.1. Calculation of the opening factor for compartments with a number of openings of different size and shape is given in [Pettersson, 1976]. It is assumed that ordinary glass is immediately destroyed when flashover occurs and that doors are closed. Neither of these

situations may necessarily occur and as a consequence the value of the opening factor may either be smaller than the calculated value or vary from a very small value to a maximum. The foregoing can have a significant effect on temperature development in the fire compartment. In general it is assumed that a ventilation controlled fire with a large opening factor will produce a higher temperature and as a consequence will be more severe. Therefore the assumption made above is a conservative one. It should be noted however fires in which the opening factor is large and the fire load is small is firstly, fuel controlled, and secondly, will burn out very quickly and have little influence on exposed structural steel. Care must be taken in determining the worse case scenario in terms of the effect of fire on the compartments structure. It is not appropriate to consider the amount of ventilation as a sole indicator of potential fire severity but rather the ratio of fire load to window area as noted in subsection 2.4.1.

### **2.5.0 Fire Load Density**

Fire load has been identified as one of the principal variables influencing fire severity [International Iron and Steel Institute, 1993]. All things being equal, the larger the fire load the higher the maximum temperature in the fire compartment and the longer the duration of the fire.

Fire load as it relates to a fire compartment is defined as the quantity of heat,  $Q$ , released during the complete combustion of all combustible material

contained inside the compartment. The total heat,  $Q$ , divided by a reference area, which may be either the total internal surface area,  $A_t$ , or the floor area,  $A_f$ , gives the fire load density,  $q$ . The fire load density are given by the following:

$$q_f = \frac{1}{A_f} \sum m_v H_v \quad (\text{MJ/m}^2) \quad (2.12)$$

$$q_t = \frac{1}{A_t} \sum m_v H_v \quad (\text{MJ/m}^2) \quad (2.13)$$

where  $m_v$  = total mass of combustible material (kg) and  $H_v$  = calorific value of combustible material (MJ/kg). Fire load comprises two components, permanent fire load and variable fire load. The former includes surface materials and all linings and coverings on the walls, roof and floor as well as the load-bearing and non load-bearing-bearing structure or structural members and permanently installed devices, the latter comprises furnishings and contents. Fire loads may be adjusted by a derating factor which accounts for incomplete combustion of the fire load. Some difficulty exists in determining and applying these factors. As a consequence a conservative approach can be adopted where-by such factors are ignored.

### 2.5.1 Fire Load Statistics.

Accurate prediction of temperature versus time in a compartment fire relies on knowledge of the expected fire load density. Fire load statistics for offices

have been determined from a number of surveys. Table 2.2 presents some results from a number of surveys. It can be seen that there is considerable variation between the average values of the variable fire load both between surveys and between different categories of room within each survey. As expected the largest coefficient of variation (COV) in each survey is for 'all rooms' combined. The more general the classification the greater the variation in the fire load. The COV for the classification 'all offices' varies from 0.34 to 1.12. The variation in the results may be due to a combination of national differences and different sampling and evaluation techniques.

Type of fire compartment.	Average (MJ/m <sup>2</sup> )	Standard Deviation MJ/m <sup>2</sup>	Coefficien of Variation	Source
Technical offices	552	138	0.25	Pettersson 1976
Admin' offices	462	143	0.31	
All rooms	526	179	0.34	
Technical offices	280	108	0.39	CIB W14 1983
Admin' offices	420	210	0.5	
All rooms	410	310	0.8	
Admin' offices	380	180	0.47	Bonetti, 1975
All rooms	330	400	1.21	
General office	555	285	0.51	Culver, 1976
Clerical office	415	425	1.02	(Government
All rooms	555	625	1.12	Bld)
General office	525	355	0.67	Culver, 1976
Clerical office	465	315	0.67	(Private Bld)
All rooms	580	535	0.92	

Table 2.2 — Variable fire load densities in offices,  $q_f$ , per unit floor area (MJ/m<sup>2</sup>).

Fire load is a random variable which can be fully described by its first three moments - mean, standard deviation and skewness, or alternatively, by its first two moments and a plot of the frequency distribution of the data.

In order to utilise the available statistics on fire load in a reliability analysis the data must be fitted to a theoretical distribution.

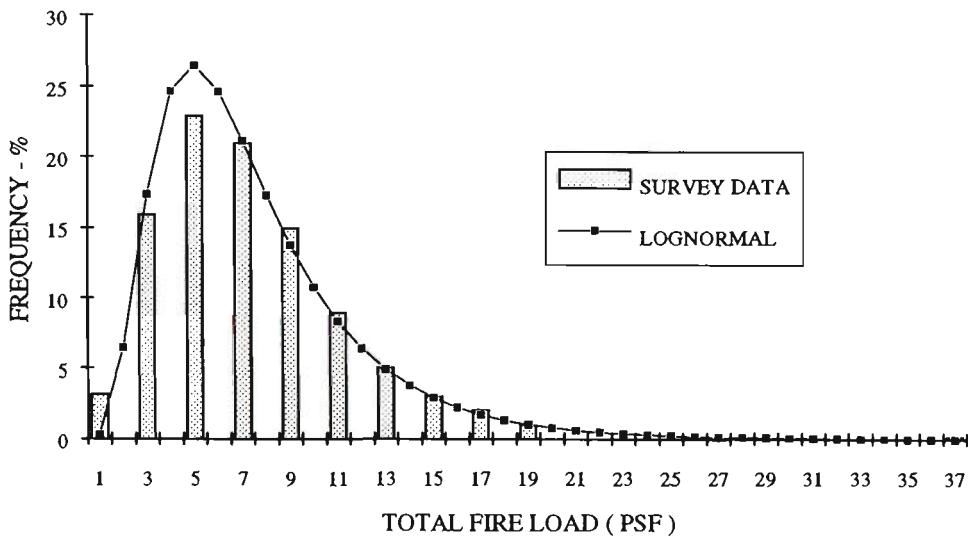


Figure 2.4: Frequency distribution of room fire load data for private office building (after Culver) and fitted theoretical distribution.

Figure 2.4 and 2.5 show a plot of the frequency distribution and cumulative frequency distribution of fire load data obtained from the surveys conducted by Culver [1976] and Pettersson [1976] respectively. Attempts to fit several theoretical distributions to the data show that the data is well represented by a lognormal distribution. Assuming fire load is lognormally distributed is intuitively appealing in that in that the problem of negative results is avoided.

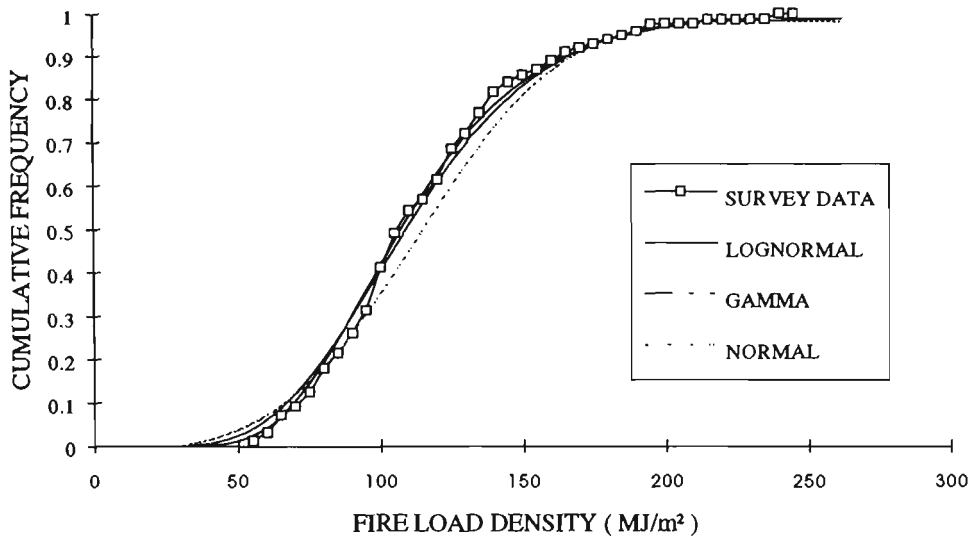


Figure 2.5: Cumulative frequency distribution of fire load data for office buildings (after Pettersson) and fitted theoretical distributions.

### 2.5.2 Fuel Type

The shape of the temperature versus time curve of a postflashover compartment fire can vary significantly depending on the type of fuel. The majority of the fire load in a modern office is cellulose based, however, between 10 and 25 % of the fire load is made up of plastic fuels, [Lathem, 1987]. The combustion enthalpy and rate of heat release for plastics are significantly higher than that for wood. Typically the calorific value of plastics can be up to two and a half times that of wood. The rate of pyrolysis of plastics, under the influence of purely convective heating, is 2 to 3 times greater compared to wood and, under the purely radiative heating, up to 20 times as great [Babrauskas, 1988]. Given the stoichiometric requirement of different fuels the combustion enthalpy per unit mass of air is nearly independent of the type of fuel and is approximately 3000 KJ/kg. As long as a

fire is ventilation control the combustion enthalpy will be much the same despite the type of fuel. Fuel control is essentially a phenomena associated with cellulose based fuels and relates to the rate at which timber is pyrolysed and the formation of char. Plastics however do not exhibit this behaviour, their rapid rate of pyrolysis and different mechanism of decomposition, will, given sufficient oxygen result in much higher temperatures than can be achieved in wood fuel fires.

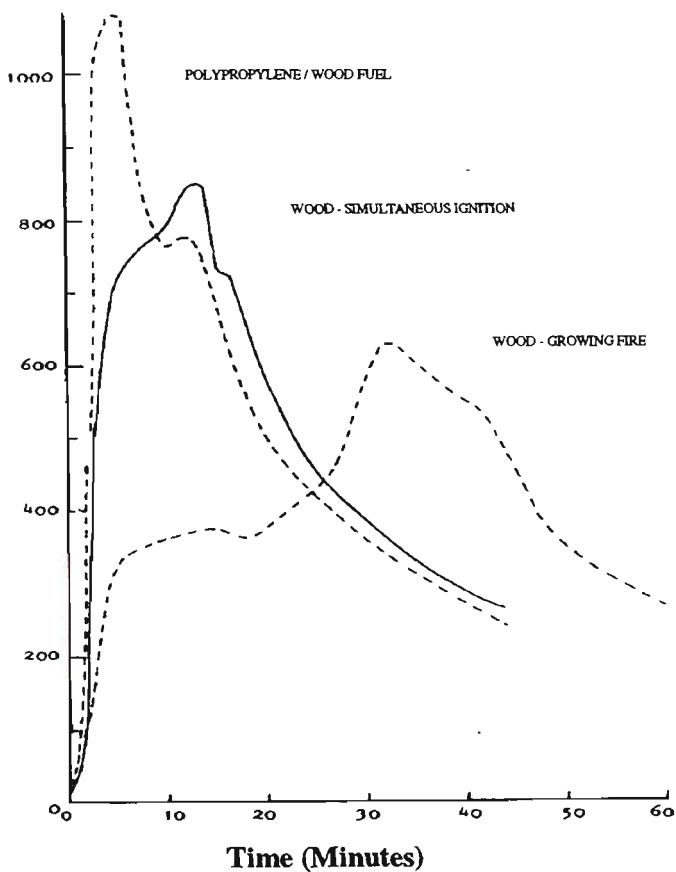


Figure 2.6: Average combustion gas temperature (°C) for different fuels and types of ignition. Fire load density = 15 kg/m<sup>2</sup>; opening parameter = 0.06 m<sup>-1/2</sup> after [Lathem, 1987].

Figure 2.6 shows the influence of mixed-fuel fires in which 25% of the wood fuel was replaced with polypropylene. Mixed-fuel fires are characterised by higher maximum average temperatures of 200 to 300 °C, attained in less than half the time taken for wood fuel fires, followed by a rapid loss in temperature.

The figure also shows the significant reduction in the maximum average temperature and the increase in the time to attain maximum temperature when a fire is allowed to grow naturally, compared with simultaneous ignition of the fuel. As a consequence of the foregoing, noticeable differences can occur between temperature versus time curves obtained from room burn experiments in which realistic fuels and fire initiation are used and those obtained from traditional wood-crib fires.

## **2.6.0 Mathematical Models for Compartment Fire Temperatures**

Several models are reviewed which predict the likely temperature-time history of a potential compartment fire. The objective of such models is to specify for design purposes the thermal stresses to which structural members are exposed during fire. It is necessary that such models are not merely empirical correlations but that they are of sufficient detail to reflect the influence of the more important parameters involved in the fire process.

### **2.6.1 Kawagoe and Sekine, 1963**

Kawagoe (1963) and his coworkers were the first group to attempt to model a compartment fire. The compartment comprised a concrete enclosure with one or more vertical wall openings. Heat loss to the walls was calculated using Schmidts method in which the walls are assumed to be semi-infinite slabs. The emissivity and the surface temperature inside the compartment was assumed to

be uniform. The emissivity of the flame was taken to be 1 and the emissivity of the space outside the window that of a black body. Using the foregoing assumptions an equation of heat balance was set-up and solved iteratively.

Equation (2.4) is used to calculate the rate of burning. The density of the gas within the compartment was calculated assuming a gas temperature of  $\sim 900$  °C. The expression was verified experimentally in a series of full scale and reduced scale tests. The heat of combustion of the fuel source (wood) was modified assuming a ratio of complete combustion of 0.6 (based on experiment). This served to correct for the volatiles lost to the atmosphere during ventilation control and to account for the inflow of excess cold air in the event of fuel control.

The duration of the fire or the time taken to reach the maximum temperature ie. the time taken for all the combustibles to be consumed, is obtained by dividing the total fire load by the rate of burning. The rate of decrease of temperature was obtained by observation of test fires. The predicted compartment temperatures were compared with a series of full scale fire tests in which the ventilation opening and thermal properties of the bounding surfaces were varied.

As a consequence of the foregoing assumptions the model will predict a more rapid increase in the compartment temperature since the rate of inflow of air is overestimated initially and a higher maximum temperature since the decay period of the fire is effectively ignored.

## 2.6.2 Magnusson and Therlandersson, 1970

Magnusson and Therlandersson developed a model to predict the temperature-time curve for the complete process of fire development for wood fuel fires. The model was subsequently used in the "Swedish Fire Engineering Design of Steel Structures" [Pettersson and Magnusson, 1976], to calculate representative gas temperature versus time curves for different fire loads and ventilation conditions represented by the opening factor (2.11).

This model is very similar in structure to that of Kawagoe but differs in some aspects. Firstly the wall thickness is taken to be finite and an explicit finite difference method is used to calculate the heat loss due to conduction. A second and more important difference is that the Swedish researchers attempted to model both the postflashover phase of the fire and the decay period. Although the relationship between the rate of burning and the ventilation opening is accepted in principal (and therefore both models presuppose ventilation control) the Swedish model calculates the variation with time of the rate of heat release in the compartment. This was achieved by varying the rate of heat release-time curve until full agreement was obtained between theoretical and experimental temperature-time curves while satisfying the requirement that the area under the rate of heat release-time curve matched the total heat released in the fire [Magnusson and Therlandersson, 1974]. The foregoing implies that the mass loss of the fuel must not be greater than stoichiometric, that is no excess fuel burning outside the compartment can be accounted for. Essentially the model is correlated to test results by means of

the rate of heat release-time curve. The model assumes a "standard fire compartment" the thermal properties of which are representative of concrete and brick. For compartments constructed of materials with significantly different thermal properties the temperature-time curves for the standard compartment may be converted by means of equivalent fire loads and opening factors.

The procedure involved in calculating the gas temperature-time curve is both lengthy and complicated. It is necessary to use numerical integration techniques (Runga-Kuttas) in which five iterations are performed for each time step; the time step used is one minute. The results of the model are generally presented in graphical form.

### **2.6.3 Babrauskas and Williams, 1978**

This model, as does the previous two models, uses the principal of heat balance to calculate the compartment gas temperature. It involves a more rigorous analysis than the previous two models but does not, however require input data that would not generally be available. The model solves the gas phase heat balance and the heat conduction through the walls simultaneously. The model accommodates change in the burning regime as the fire develops. As a consequence the model does not assume burning near or at stoichiometry nor that rate of burning is directly related to rate of inflow of air as above. The heat conduction equation contains non-linear radiation terms which can

incorporate temperature dependent thermophysical wall properties. The desired calculations are achieved using either explicit, implicit or the Crank-Nicolson finite difference techniques. This model is the basis of the computer program COMPF2 in reference [Babrauskas, 1979].

#### 2.6.4 Law, 1983

Based on the results of a large number of experimental fires [Thomas and Heselden, 1972], Law developed an expression to calculate the maximum gas temperature,  $T_g$ , as a function of the compartment size (internal surface area  $A_i$ ) and area of ventilation opening ( $A$ ) and height ( $H$ ) of ventilation opening:

$$\max T_g = 6000 \frac{(1 - e^{-0.1\eta})}{\sqrt{\eta}} \quad (^\circ\text{C}) \quad (2.14)$$

where

$$\eta = \frac{(A_i - A)}{A\sqrt{H}} \quad (2.14A)$$

The expression ignores the contribution of fire load and presupposes ventilation control. The temperature in the compartment due to the combustion of a given fire load, ( $L$ ), at a given time, ( $\tau$ ), can be calculated using the following:

$$T_g = T_{g(\max)} (1 - e^{-0.5\psi}) \quad (^\circ\text{C}) \quad (2.15)$$

where 
$$\psi = \frac{L}{\sqrt{A(A_i - A)}} \text{ (kg / m}^2\text{)} \quad (2.16)$$

The mass burning rate of the fuel is based on correlation with experimental results:

The above equations are based on average temperatures measured during the fully developed period of wood fuelled fires. The model does not consider the decay period of the fire, nor is any indication given as to the thermal properties of the bounding surfaces on which the equations are based. The model does however show that the shape of the compartment is important in determining the burning rate.

### 2.6.5 Lie, 1976

Lie formulated an algorithm to facilitate studies of fire resistance of buildings components exposed to fires of different severity. The algorithm (2.17) models the temperature versus time curves for ventilation controlled fires, proposed by Kawaoge and Sekine, calculated using heat balance - refer Subsection 2.6.1. The algorithm (2.17) calculates the compartment gas temperature,  $T_g$ , at time  $t$  after flashover, using readily available data in the form of fire load density,  $Q$ , and ventilation parameter,  $F$ :

$$T_g = 250(10F)^{0.1/F^{0.3}} e^{-tF^2} [3(1 - e^{-0.6t}) - (1 - e^{-3t}) + 4(1 - e^{-12t})] + C \left( \frac{600}{F} \right)^{0.5} \text{ (}^\circ\text{C)} \quad (2.17)$$

where  $C$  is a constant to take into account the influence of the properties of the boundary materials on the temperature. The time taken to achieve the maximum temperature (duration of the fully developed phase of the fire)  $\tau$ , is determined by:

$$\tau = \frac{Q}{330 F} \quad (\text{hr}) \quad (2.18)$$

The temperature during the decay period is assumed to decrease linearly at a rate of 10 °C/min or 7 °C/min depending on whether the duration of the fire is less than or greater than one hour. This corresponds with a value of 10 °C/min used in the Swedish building code and values of 15 - 20 °C/min observed in a series of short test fires [Butcher, 1966 & 68]. The temperature course of the fire in the decay period is given by:

$$T_g = -600 \left( \frac{t}{\tau} \right) + T_\tau \quad (\text{}^\circ\text{C)} \quad (2.19)$$

Two materials were chosen as representative bounding materials: one with thermal properties resembling those of a heavy material (high heat capacity and conductivity) and one representing those of a light material (low heat capacity and conductivity). In practice normal weight concretes and bricks are

considered as belonging to the group of heavy materials and lightweight and cellular concretes and plasterboards are considered light materials.

Although formulated in 1974, the Lie algorithm is still well regarded. It is represented in the current edition (Ed. 14 ) of the NFPA Handbook and is the only model presented in the ASCE manual on Structural Fire Protection, [ASCE, 1992]. The model compares well with the only other model currently used in the rational design of structures exposed to real fire [Magnusson and Therlandersson, 1974], - refer Sub-section 2.6.2.

### 2.6.5 Harmathy, 1983

Harmathy has developed the concept of the normalised heat load (NHL) which can be used to correlate "real-world" compartment fires with standard test fires. The method models compartment fires by calculating the NHL, the total heat absorbed by a unit area of the boundaries of a compartment during any fire, divided by the thermal inertia of the boundaries, rather than the gas temperature. The normalised heat load  $H$ , is given by the following equation:

$$H = \frac{1}{\sqrt{k\rho c}} \int_0^{\tau} q dt \quad (2.20)$$

where  $\sqrt{k\rho c}$  = thermal inertia ( $k$ : thermal conductivity,  
 $\rho$ : density,  $c$ : specific heat).

For "real-world" compartment fires,  $H'$ , can be approximated by the following semi-empirical equation:

$$H' = 10^6 \frac{11.0\delta + 1.6}{A_t \sqrt{k\rho c} + 935\sqrt{\Phi A_F L}} (A_F L) \quad (2.21)$$

in which the heat flux to the compartment boundaries is expressed in terms of the main parameters used in the heat balance approach viz., fire load, ( $L$ ), ventilation factor, ( $\Phi$ ), area of the floor, ( $A_F$ ), total area ( $A_t$ ), and thermal inertia. The NHL in standard fire tests,  $H''$ , is a function only of the duration of the test,  $\tau$ , and is described by the following equation:

$$\tau = 0.11 + 0.16E^{-4}H'' + 0.13E^{-9}(H'')^2 \quad (2.22)$$

Harmathy asserts that the destructive potential of "all" fires can be quantified by this single parameter  $H$ . Further, his theory of uniformity of normalised heat load states that  $H$  is approximately the same for the fire enclosure as a whole as for the individual boundary elements. Following from this, the fire resistance period of a compartment can be obtained by calculating  $H'$ , equating  $H'$  with  $H''$  and solving for  $\tau$ .

This is not a compartment fire model as such but rather a correlation of fire test results expressed in terms of the parameters known to influence the

development of fire. The model is not applicable to boundary elements made from or supported by material of high thermal inertia ie., unprotected steel.

## **2.7 Summary of Compartment Fire Models**

The models described in subsections 2.6.1 to 2.6.5 have been developed to predict the temperature-time history of compartment fires. The model by Kawaoge does not model the decay period of the fire and accounts for the thermal properties of the bounding surfaces in an approximate way. Both the model developed by Therlandersson and the model developed by Babrauskis are more rigorous in their approach than that of Kawaoge's however both involve complex and lengthy computations. The model by Law relies on a correlation between maximum temperature and the term,  $\Omega$ , which describes the geometry of the compartment and the ventilation opening however it does not specifically account for the nature of the compartment, the decay period nor defines limits for its use. The model by Lie is essentially that of Kawaoge but in a computationally simplified form. Finally the model by Harmathy is too general in its approach for the purposes of this study.

## **2.8 Selection of Fire Severity Sub-Model**

The aim of the current project is to develop a simple model to estimate the time varying probability of failure of steel beams subject to real fire. In order to achieve the specified aim of the project, the time varying temperature of the compartment, as a function of the significant factors that influence fire severity,

must be calculated. In view of the basic aims of rigour as noted in subsection (1.4), the model by Lie (1974), has been adopted for this purpose. In selecting Lie's model consideration has been given as to the influence of the following factors on the calculated compartment temperature:

- a. the approximate nature of available models.
- b. the uncertainty associated with the size of the fire load.
- c. the type, surface area and distribution of the fuel.
- d. ventilation conditions.
- e. the influence of the bounding surfaces.
- f. the substantial effect that wind velocity and direction can have on the fire development, .

The algorithm is considered suitable for the current project for the following specific reasons:

- a. suitable for initial development of reliability model.
- b. models basic fire phenomena.
- c. predicts with reasonable accuracy the expected compartment temperature.
- d. the algorithm is simple to calculate.
- e. the algorithm can be computed quickly and is therefore suitable for many probability simulations.
- f. the algorithm uses readily available input data.
- g. the data can be expressed in probabilistic terms.

- h time dependent thermal properties of materials can be incorporated into the analysis.
- i the algorithm facilitates literally a minute by minute analysis of the structural element being investigated.
- j. the algorithm acts as an independent module. A more sophisticated temperature time model can be used without altering the structure of the program to estimate structural reliability.

## 2.9 Comparison of Predictions of Selected Fire Severity Submodel with Test Results and Predictions of Other Models.

The model adopted to calculate the compartment temperature-time curve is that proposed by Lie (1974). The model is an analytical expression based on temperature curves for ventilation-controlled fires calculated according to the method described by Kawagoe and Sekine (1963), refer subsection (2.6.1).

The following expression calculates the gas temperature,  $T_g$ , during the fully developed phase of the fire (Curve OA - Figure 2.7) as a function of the opening factor,  $F$ , and the time in hours from the occurrence of flashover:

$$T_g = 250(10F)^{0.1/F^{0.3}} e^{-tF^2} \left[ 3(1 - e^{-0.6t}) - (1 - e^{-3t}) + 4(1 - e^{-12t}) \right] + C \left( \frac{600}{F} \right)^{0.5} \text{ (}^\circ\text{C)} \quad (2.17)$$

where

$$F = \frac{A\sqrt{H}}{A_T} \quad (\text{m}^{-1/2}) \quad (2.23)$$

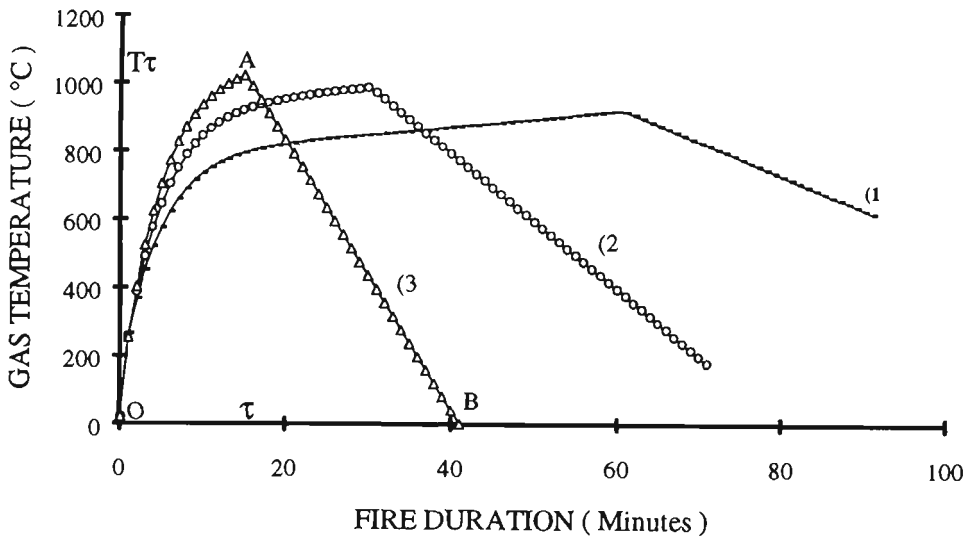


Figure 2.7: Temperature time curve for a range of opening factors 1) =  $0.03 \text{ m}^{1/2}$ ; 2) =  $0.06 \text{ m}^{1/2}$ ; 3) =  $0.12 \text{ m}^{1/2}$ ; (Fire load density =  $40 \text{ kg/m}^2$ ).

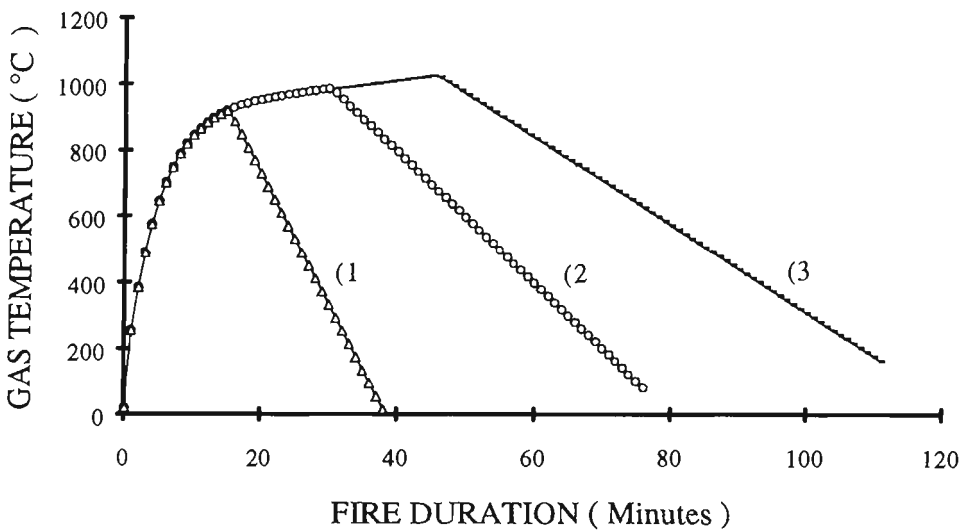


Figure 2.8: Temperature time curve for a range of fire loads. (1 =  $20 \text{ kg/m}^2$ ; (2 =  $40 \text{ kg/m}^2$ ; (3 =  $60 \text{ kg/m}^2$  (Fire load referenced to floor area): Opening parameter,  $F = 0.08 \text{ m}^{1/2}$ .

The constant  $C$  takes into account the thermal properties of the compartment boundary material on the temperature.  $C = 0$  for heavy materials

( $\rho \geq 1600 \text{ kg/m}^3$ ), and  $C = 1$  for light materials ( $\rho < 1600 \text{ kg/m}^3$ ). The

duration of the fire,  $\tau$ , is determined by:

$$\tau = \frac{QA\tau}{330A\sqrt{H}} = \frac{Q}{330F} \quad (\text{hr}) \quad (2.18)$$

where the fire load,  $Q$  (kg/m<sup>2</sup>), is the fire load per unit area of the **surfaces bounding the compartment**. The model presupposes a wood (cellulose based) fuel. In the event of the all or part of the fuel being a material other than cellulose the fire load must be expressed in terms of wood equivalent, in which the calorific value of wood is taken to be 18.8 MJ/kg. The expression (2.17) is valid for:

$$t \leq \frac{0.08}{F} + 1 \quad (\text{hr}) \quad (2.24)$$

and

$$0.01 \leq F < 0.15 \quad (\text{m}^{-1/2}) \quad (2.25)$$

The temperature during the decay period (Curve AB - Figure 2.6) has been assessed from experimental test fires. The temperature course of the fire in the decay period is given by:

$$T_g = -600\left(\frac{t}{\tau}\right) + T_\tau \quad (^\circ\text{C}) \quad (2.19)$$

Characteristic temperature time curves, obtained from expressions (2.17) and (2.19) are illustrated for a range of fire loads and ventilation openings - refer Figures 2.7 and 2.8. It is apparent that for a given fire load, the duration of the fire increases while the maximum temperature decreases as the opening factor

decreases. Conversely for a constant value of opening factor, the maximum temperature and duration of the fire increases as the fire load increases.

### 2.9.1 Comparison with Kawaoge's results

Comparative plots between temperature-time curves obtained by solving heat balance (Kawagoe) and those described by expression (2.17) - refer Figures 2.9 and 2.10 show that in the first two hours after flashover for  $\rho \geq 1600 \text{ kg/m}^3$  ( $C = 0$ ):

- $F = 0.04$  the plots are almost coincident.
- $F < 0.04$  expression (2.17) over-estimates the temperature.
- $F > 0.04$  expression (2.17) under-estimates the gas temperature.

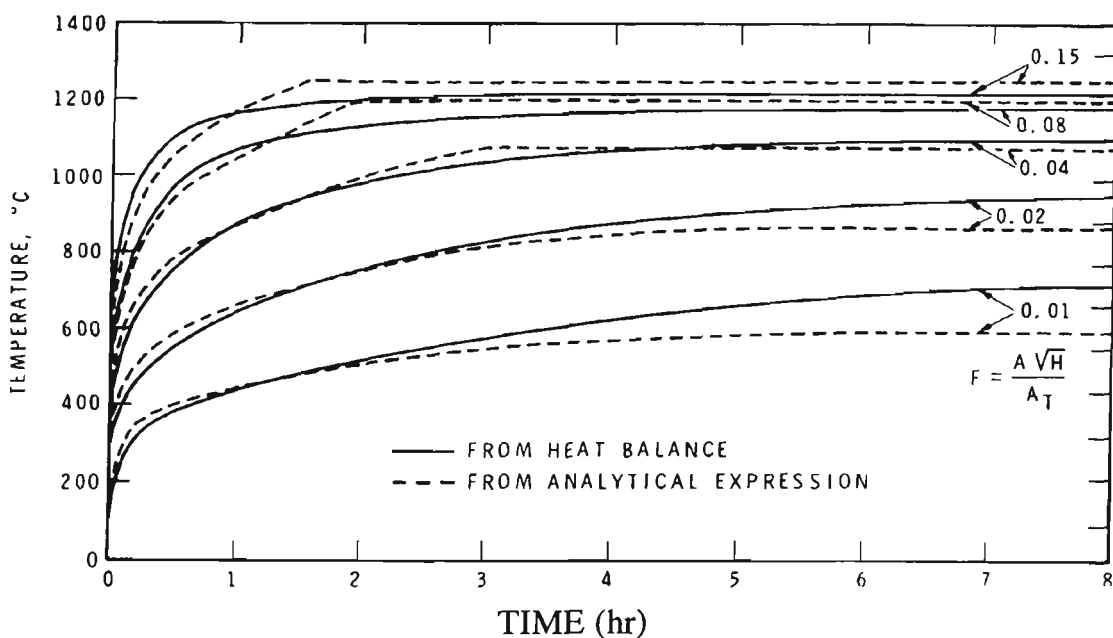


Figure 2.9: Comparison between temperature-time curves obtained by solving a heat balance and those described by expression (2.17) for ventilation controlled fires in compartments bounded by predominantly heavy materials ( $\rho \geq 1600 \text{ kg/m}^3$ ) [after Lie, 1992].

For  $\rho < 1600 \text{ kg/m}^3$  ( $C = 1$ ) the trend is similar although the differences between corresponding curves is greater.

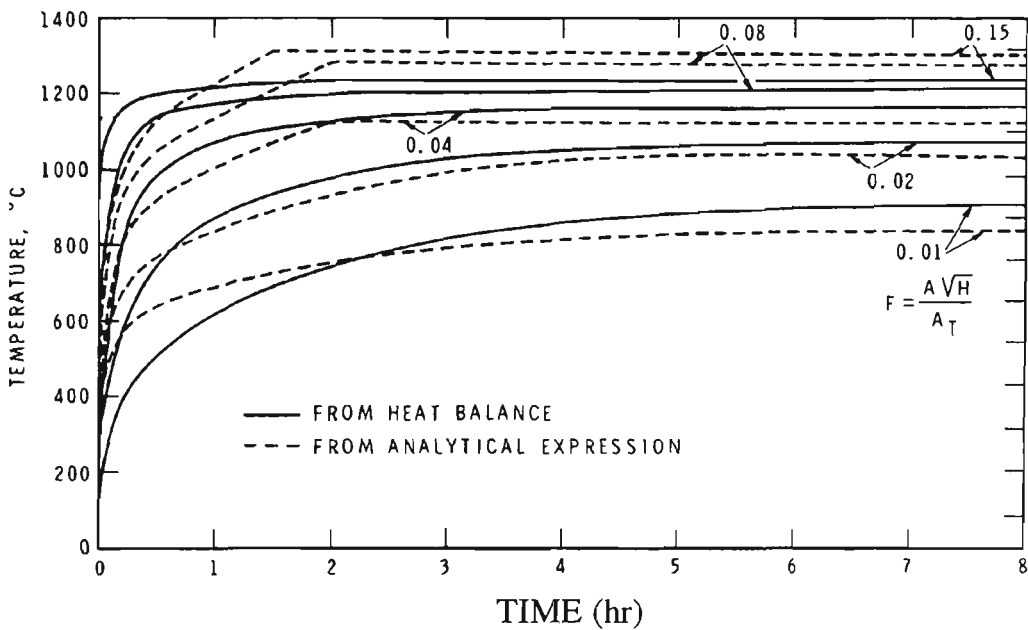


Figure 2.10: Comparison between temperature-time curves obtained by solving a heat balance and those described by expression (2.17) for ventilation controlled fires in compartments bounded by predominantly light materials ( $\rho < 1600 \text{ kg/m}^3$ ) [after Lie, 1992].

Lie was aware of the large degree of uncertainty associated with the calculation of temperature time curves - primarily due to uncertainty in the magnitude of the fire load. In developing his model he set out to predict a curve "whose effect, with reasonable probability, will not be exceeded during the use of the building". It is not clear how this statement is to be interpreted nor how this probability was to be assessed and what constitutes a "reasonable probability".

There appears to be no consistent safety factor incorporated in to the temperature-time curves themselves. The duration of the fully developed fire

and hence the maximum compartment temperature is a function of the fire load, expression (2.19), Lie's statement can be interpreted that fire resistance design should be performed using temperature curves generated by a fire load density equivalent to the 80, 90 or 95<sup>th</sup> percentile of the fire load distribution rather than assuming some inbuilt factor of safety in the temperature-time curves. The foregoing is a salient point given the proposed use of the Lie model in a reliability analysis.

### 2.9.2 Comparison Between Alternative Models.

A comparison of temperature-time curves calculated using the Lie model and the temperature time curves recommended by the Swedish Building Regulations Board for use in the rational fire engineering design of buildings [Pettersson, 1976], Figure 2.11, show good agreement.

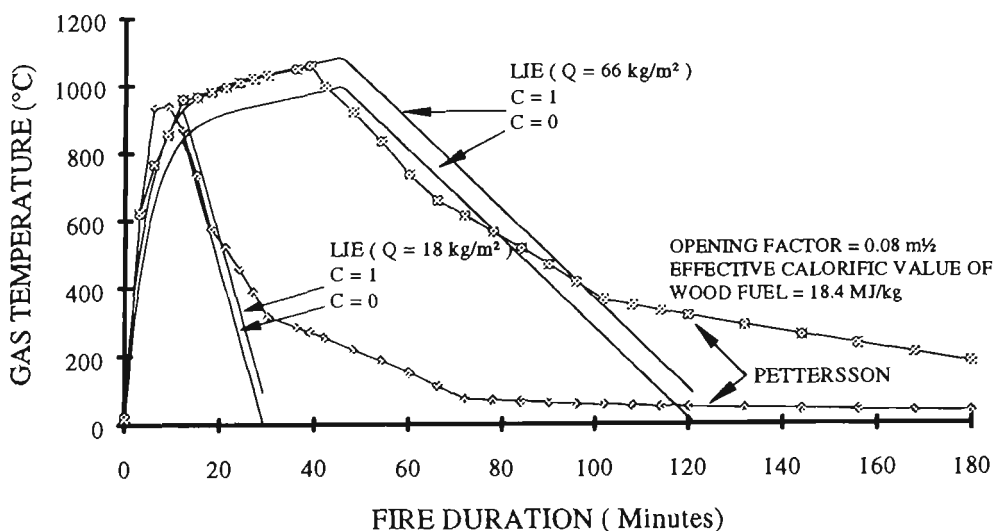


Figure 2.11: Comparison between gas temperature curves calculated using the Lie model and that adopted for use in the Swedish Building Regulations.

The curves illustrated are calculated using an average opening factor (0.08 m<sup>-1/2</sup>) and fire loads of 18 and 66 kg/m<sup>2</sup> (100 and 377 MJ/m<sup>2</sup>) referenced to floor area; representative of a low and high office fire load. The compartment used in the modeling of the Swedish curves has thermal properties corresponding with the average values for concrete, brick and lightweight concrete. Designated Type "A", the thermal inertia  $\sqrt{k\rho c}$  of this compartment is approximately equal to 1166 Jm<sup>-2</sup>s<sup>-1/2</sup>K<sup>-1</sup>. Based on the thermal properties of the "representative" bounding materials adopted by Lie,  $\rho \geq 1600$  kg/m<sup>3</sup> ( $C = 0$ ) corresponds to a thermal inertia of 1558 Jm<sup>-2</sup>s<sup>-1/2</sup>K<sup>-1</sup>, while  $\rho < 1600$  kg/m<sup>3</sup> ( $C = 1$ ) corresponds to a thermal inertia of 780 Jm<sup>-2</sup>s<sup>-1/2</sup>K<sup>-1</sup>. Accordingly the curve representing the average temperature obtained from the two Lie curves would have a thermal inertia equal to a Type A compartment. The Swedish fire load expressed in MJ/m<sup>2</sup> is converted to an equivalent fire load assuming the effective calorific value of wood to be 18.8 MJ/kg. Consideration of the foregoing indicate a difference between the maximum gas temperature predicted by the two models of approximately 40 °C, and a difference in the time to reach maximum temperature of approximately 8 minutes.

### 2.9.3 Comparison between Lie Model and Experimental Results (Butcher)

The theoretical temperature time curves are compared Figures 2.12, 2.13 & 2.14 with temperature curves obtained by experiment [Butcher et. al., 1966].

The compartment in the Butcher fire tests had a floor area of 28 m<sup>2</sup>. The walls were made from brick and the floor and roof were made from refractory concrete slabs. The thermal inertia of the internal bounding surface would correspond with a Type "A" compartment.

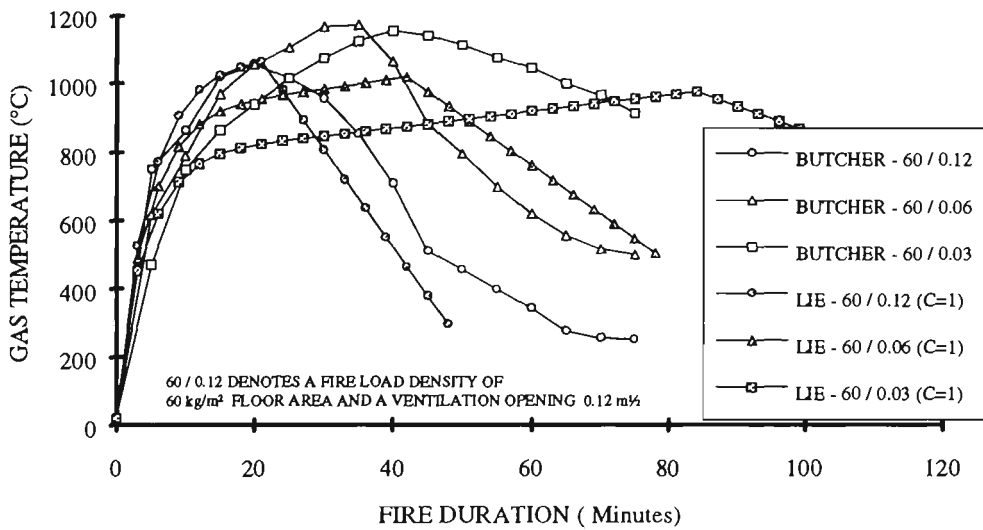


Figure 2.12: Comparison between theoretical and experimental temperature-time curves. Fire load density = 60 kg/m<sup>2</sup>.

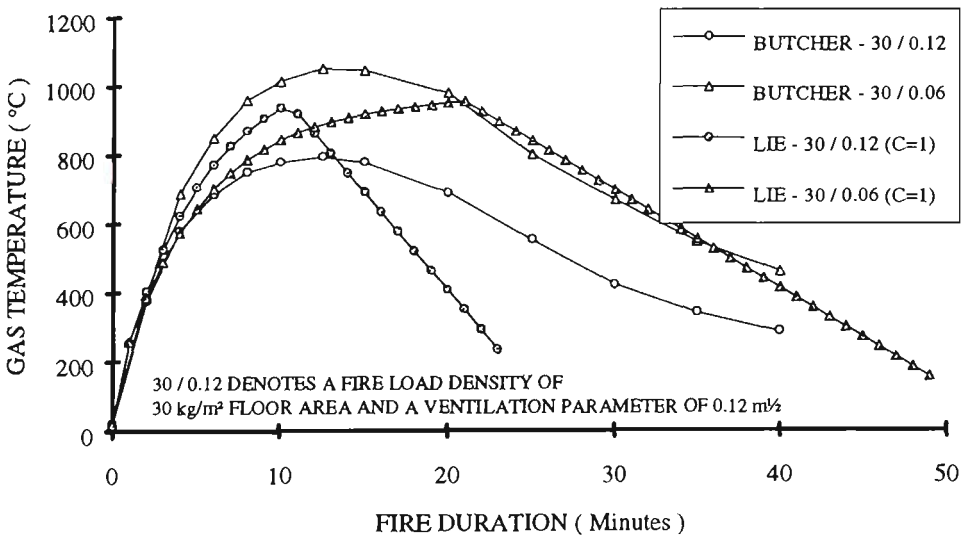


Figure 2.13: Comparison between theoretical and experimental temperature-time curves. Fire load density = 30 kg/m<sup>2</sup>.

The Lie temperature versus time curves have been calculated assuming  $C = 1$ . This means that the calculated temperatures will on average be 45 °C high due to the assumed, lower, thermal inertia. For high fire loads (60 kg/m<sup>2</sup>) and

large ventilation conditions ( $0.12 \text{ m}^{-1/2}$ ), refer Figure 2.12, there is good agreement between the calculated and measured values. For low to medium ventilation conditions ( $0.3 - 0.6 \text{ m}^{-1/2}$ ) the algorithm overestimates the time to achieve the average maximum temperature by 10 to 30 minutes. The algorithm also consistently underestimates the actual gas temperature by as much as  $200 \text{ C}^\circ$ . For low fire loads ( $15 \text{ kg/m}^2$ ), refer Figure 2.14, the algorithm predicts average maximum gas temperatures  $150 - 250 \text{ C}^\circ$  higher than that measured and underestimates the time to achieve the average maximum gas temperature by approximately 5 minutes. Inspection of Figure 2.13 shows that in the case of an average fire load ( $30 \text{ kg/m}^2$ ), there is reasonable agreement between the predicted temperatures and the experimental results.

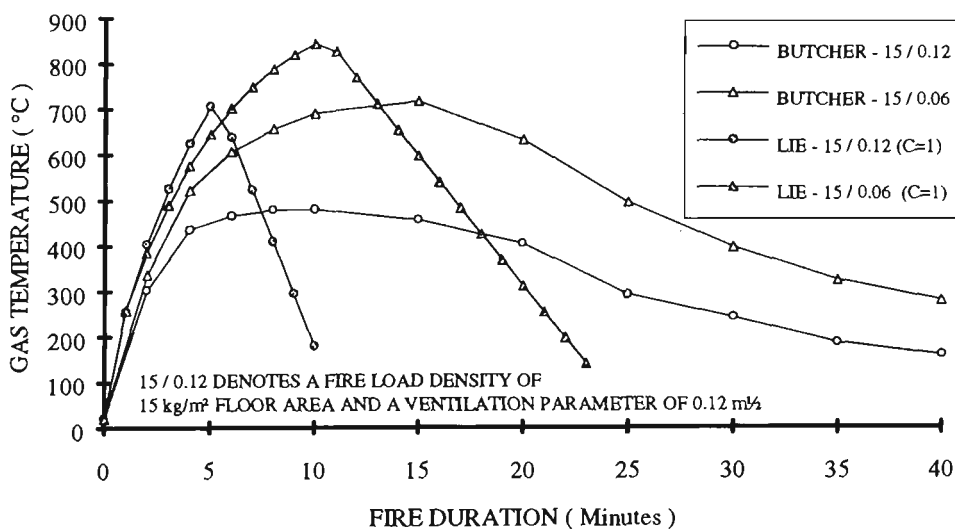


Figure 2.14: Comparison between theoretical and experimental temperature-time curves. Fire load density =  $15 \text{ kg/m}^2$ .

The Butcher fire test data was used in the development of the Swedish model [Magnusson & Therlandersson, 1974]. Given the good agreement between the Lie algorithm and the Swedish temperature versus time curves the degree of

correspondence between the theoretical and experimental results in this case is disappointing.

#### **2.9.4 Comparison between Lie Model and Experimental Results (Lathem)**

A more recent investigation into the rate of heating of steel members in natural fires [Lathem et.al., 1987], has provided compartment temperature versus time plots considered to be typical of multi-storey office blocks; low fire loads and comparatively large ventilation conditions. The compartment had a floor area of 50 m<sup>2</sup> and was constructed of spall resistant insulating refractory brick with a concrete roof slab lined with ceramic fibre tiles. This highly insulating environment (thermal inertia approximately 413  $Jm^{-2}s^{-1/2}K^{-1}$ ) was later modified by lining walls with fire resistant plasterboard and removing the ceramic roof tiles. The thermal inertia of the modified compartment (1060  $Jm^{-2}s^{-1/2}K^{-1}$ ) was now similar to the thermal inertia of the compartment used by Butcher. The modification to the wall and roof lining had a significant effect on the maximum average temperature attained in the fire; specifically, for a fire load of 15 kg/m<sup>2</sup> and 0.06 m<sup>1/2</sup> ventilation opening, the introduction of the plasterboard reduced the maximum average compartment temperature in a cellulosic fire from 851 °C to 700 °C. This result serves to highlight the importance of the thermal properties of the compartment boundary.

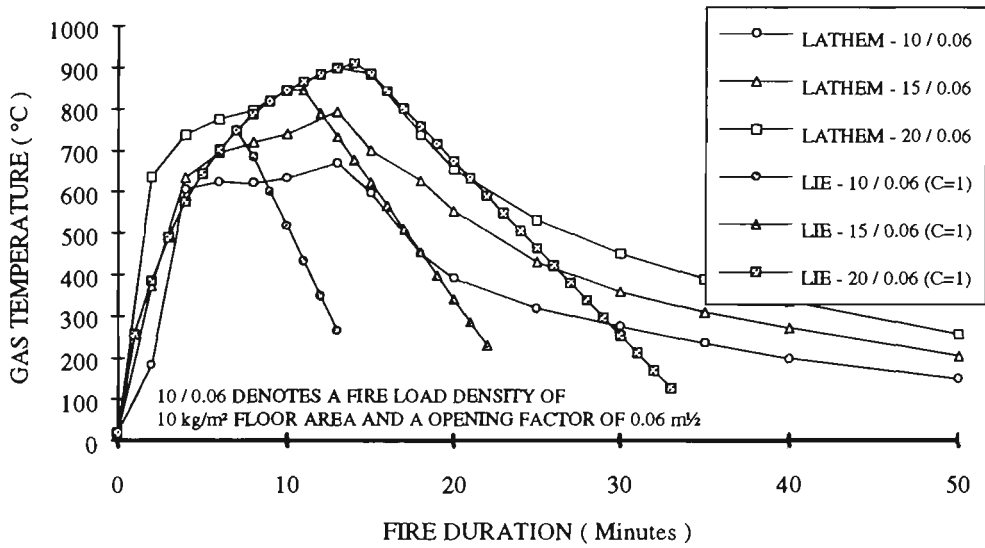


Figure 2.15: Comparison between theoretical and experimental temperature-time curves. Opening factor =  $0.06 \text{ m}^{-1/2}$ . Fire load density = 10, 15 and  $20 \text{ kg/m}^2$  - Author.

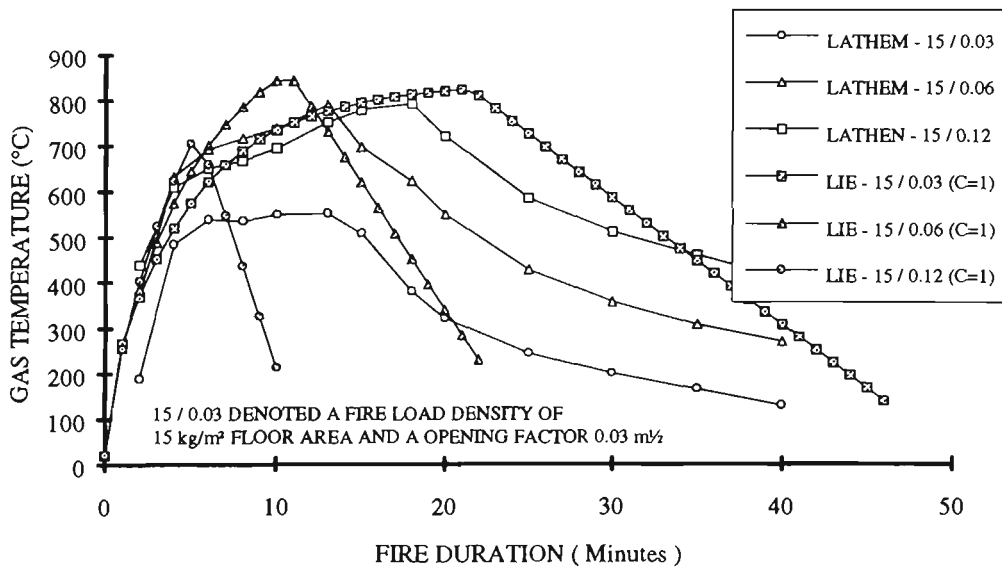


Figure 2.16: Comparison between theoretical and experimental temperature-time curves. Fire load density =  $15 \text{ kg/m}^2$ . Opening factor =  $0.03, 0.06$  and  $0.12 \text{ m}^{-1/2}$  - Author.

The results of a series of test fires in which wooden cribs were simultaneously ignited are shown Figures 2.15 and 2.16. For average values of opening factor (ventilation conditions) agreement between the calculated temperature and the

experimental result is good for fire-loads of 20 kg/m. Similarly agreement between calculated temperatures and experimental results is good when the opening factor is small, becoming less so as the opening factor increases.

The results show that the Lie model predicts, for very low fire-loads, average maximum gas temperatures 150 - 200 C° higher than that recorded in test results. The Lie model also predicts that maximum temperatures will be achieved earlier and that the duration of the fire will be shorter.

## **2.10 Summary**

Based on comparisons with fire test data the accuracy with which the Lie algorithm predicts the maximum gas temperatures varies. At high fire load the maximum temperature may be underestimated by up to 150 °C, while at low fire load the algorithm may overestimate the gas temperature by a similar amount. Of greater concern is the variation between theory and experiment in the time taken to attain the maximum gas temperature. An insulated structural member exposed to a long duration fire will eventually heat to a temperature close to that of the ambient gas temperature. The probability of failure of the member is greatly increased and the time to failure affected.

The insensitivity to the thermal properties of the compartment boundaries is also a weakness in the model. As noted previously the Lie model identifies two broad classes of building materials as represented by their density. One group,

with thermal properties resembling those of a heavy material (high heat capacity and conductivity) and a second group, representing those of light materials (low heat capacity and conductivity). Typical values of thermal inertia range from  $2200 \text{ Jm}^{-2} \text{ s}^{-1/2} \text{ K}^{-1}$  for normal weight concrete down to  $400 \text{ Jm}^{-2} \text{ s}^{-1/2} \text{ K}^{-1}$  for wood. A compartment constructed with materials with low values of thermal inertia will experience significantly higher compartment gas temperatures.

At high fire load and ventilation opening ( $60 \text{ kg/m}^2$  &  $0.12 \text{ m}^{-1/2}$ ) there is good agreement between the theoretical and experimental temperature curves. For larger ventilation opening however considerable disparity occurs between the two sets of curves both in maximum temperature attained and time to maximum temperature. At low fire load ( $15 \text{ kg/m}^2$ ) a similar but opposite trend is evident. There is a reasonable match between the theoretical and experimental curve when the ventilation opening is small ( $0.03 \text{ m}^{-1/2}$ ) becoming less so as the ventilation opening increases.

## 2.11 Conclusion

A number of compartment fire models have been investigated. The model by Lie has been selected for use in the simulation model to determine the reliability of steel beam in fire. Based on comparisons with test data the model gives acceptable representations of compartment gas temperature versus time curves.

The model is suitable for simulation in that it is simple to calculate, requires only two input variables, fire load density and opening factor, both of which have available statistical descriptors.

## **CHAPTER THREE**

### **MODELLING HEAT TRANSFER TO STEEL**

### **3.0 Introduction**

In the following chapter a brief description is given of the mechanisms by which heat is transferred from a fire to a steel section. Alternative methods of calculating the temperature rise in a fire exposed steel beam are investigated and the current recommendations reviewed. The accuracy of the heat transfer submodel selected for use in the proposed simulation model to calculate the time varying probability of failure of steel beams is assessed.

The rate at which the temperature of structural steel increases during exposure to fire depends on a number of factors. Not least amongst these is the gas temperature-time curve to which the steel is exposed. In the previous chapter it was demonstrated that an infinite range of real fire scenarios are possible depending primarily on ventilation, the nature and type of fire load and the compartment in which the fire occurs. To accurately model the increase in temperature of a fire exposed steel beam, the thermal properties of the steel such as thermal conductivity, specific heat and density must be assessed. The geometry and layout of the section are also important considerations. If the steel is insulated then the thermal and material properties of the insulating material must also be assessed.

### 3.1 Heat Transfer

The transfer of heat from one location or material to another is affected by three mechanisms, namely, conduction, convection and radiation. In a fire, heat is transferred from the fire to an exposed object is by convection and radiation. The heat transferred by convection to an object is generally less than 10% of the radiative heat [Trinks and Mawhinney, 1961]. The heat transfer through the steel and insulation material takes place exclusively by the conduction process.

#### 3.1.1 Convection

The transfer of heat by the contact of flowing gas to and over a solid surface is by the process of convection. The heat flux,  $\phi$ , transferred to a solid surface per unit time and area by a gas moving over it is given by [Burmiester, 1983]:

$$\phi = h(T_{\infty} - T_S) \quad (3.1)$$

where  $h$  = convection heat transfer coefficient  
 $T_{\infty}$  = free stream gas temperature  
 $T_S$  = surface temperature of object

The heat transfer process occurs in the region adjacent to the surface within a region known as the boundary layer. The convective heat transfer coefficient,

$h$ , is a function of the boundary layer, its dimensions, nature and velocity of flow as well as the properties of the gas, thermal conductivity, density and viscosity. The calculation of the convective heat transfer from a gas to a surface involves the derivation or measurement of the coefficient  $h$ . This may be accomplished by either: exact mathematical analysis; analogy between heat and momentum transfer; direct measurement of heat transfer coefficients coupled with correlation based on the basis of dimensional analysis.

The convection process can be described as forced, in which case the gas is flowing as a continuous stream over the solid surface, or as natural, where the gas flow occurs as a result of density differences arising from temperature variations in the gas. In both cases the gas flow may be laminar or turbulent. The situation that exists during a compartment fire is complex and at some time during the fire both types of convection will occur and both types of flow. Accordingly the determination of the convective heat transfer coefficient is difficult. For this reason the use of direct measurement and correlation is the preferred method of determining the coefficient  $h$ . Typical values lie in the range 5 -25 W/m<sup>2</sup> °C for free convection and 10 - 500 W/m<sup>2</sup> °C for forced convection in air [Drysdale, 1985]. A theoretical analysis [Wade, 1942] determined that, for free and forced convective heat transfer between a vertical steel plate and air, the coefficient  $h$  to be 6 -8 W/m<sup>2</sup> °C and 8 - 12 W/m<sup>2</sup> °C respectively. Based on approximate calculations of the relative contributions of convective and radiative heat transfer in a boiler [Gray et al., 1974], show that the convective component is comparatively small, less than 10%. As a

consequence in many analysis a simple estimate of the convective heat transfer is adopted or, in some cases, it is neglected.

### 3.1.2 Radiation

All substances are capable of emitting and absorbing energy in the form of thermal electromagnetic radiation. The radiative energy emitted from a substance increases rapidly with temperature. An ideal radiator (a black body) will emit energy at a rate proportional to the fourth power of the absolute temperature of the body. The total energy,  $Q$ , emitted by a body is given by the following semi-empirical relationship [Hottel and Sarofim, 1967]:

$$Q = \varepsilon\sigma T^4 \quad (3.2)$$

where  $T$  = the temperature in degrees Kelvin  
 $\varepsilon$  = emissivity (surface radiation efficiency)  
 $\sigma$  = Stefan-Boltzmann constant

The emissivity,  $\varepsilon$ , of a body or surface is the ratio of the radiative heat flux emitted by the body to that emitted by a black body at the same temperature. Since the rate at which radiation is emitted varies with wavelength, the emissivity varies accordingly. A simplification adopted in the calculation of heat transfer is to assume a grey body. A grey body is defined as one whose

emissivity is constant with wavelength. Some typical values of emissivities are given in Table 3.1.

Surface	Emissivity	Source
Luminous flame	0.6 - 0.9	Drysdale (1985)
Oxidised steel	0.8 - 0.9	"
Concrete floor slab	0.8	"
Firebrick	0.75	"
Beam exposed to direct flame	0.5 - 0.7	Kirby (1986)
Beam protected from direct flame or above high ceiling	0.3 - 0.7	"

Table 3.1: Emissivities of surfaces in fire compartment Drysdale (1985).

In an actual fire the exposed steel receives heat from luminous flames, which has a surface radiation efficiency,  $\epsilon_f$ , greater than 90 %, which approaches that of a black body. It is generally assumed that the radiative heat transfer to an exposed member is approximately that of a black body [Kawagoe, 1963]; [Babrauskas, 1975]; [Lie, 1992].

Because radiation travels in straight lines only part of the radiation emitted from the flame surface will reach the steel member. In order to calculate the radiant intensity at a point distant from the heat source a configuration or geometric view factor,  $\epsilon_g$ , is introduced. Values of  $\epsilon_g$  for various shapes and geometries can be obtained from tables and charts given in the literature [Hottel and Sarofim, 1967]. Since all bodies and surfaces in the fire compartment emit radiation and the steel is completely enclosed, one dimensional radiative exchange between fire and steel is often assumed. The

resultant emissivity,  $\epsilon_r$ , [Simonson, 1967] for one dimensional radiative heat transfer to exposed steel members is:

$$\epsilon_r = \frac{1}{1/\epsilon_f - 1/\epsilon_s - 1} \quad (3.3)$$

where  $\epsilon_f$  = emissivity of the flames  
 $\epsilon_s$  = emissivity of the steel

The resultant emissivity accounts for the emissivity of the flames, combustion gases and exposed surfaces and may take into account the configuration factor [Pettersson, 1976]. The use of the resultant emissivity has been disputed by [Mooney, 1992]. The radiation to which floor beams are subject depends on the width to height ratio of the beam and on the space to height ratio of the beams. Depending on the foregoing the resultant emissivity is reduced approximately 15 - 20% to accommodate the beam geometry and layout [Pettersson, 1976]. The resultant emissivity and the configuration factor have a significant effect on the calculated value of heat transferred between two bodies. Both of these terms can be difficult to determine and are often interdependent. The emissivity and view factors are derived semi-empirically and serve to correlate theory with observed temperatures.

### 3.1.3 Conduction

Conduction is the inter-molecular transfer or flow of heat through solids, liquids and gases. The second law of thermodynamics requires that heat

transfer between and within bodies occurs when a temperature gradient or imbalance in the internal energy of the system exists and that heat will flow from the location of the highest temperature to the location of the lowest temperature. Assuming energy is conserved and given sufficient time a body subject to a temperature gradient will achieve a steady heat flow. The steady state heat flow,  $Q$ , between two points in an isotropic material is given by:

$$Q = \frac{kA(T_1 - T_2)}{d} \quad (3.4)$$

where

$k$	=	constant of proportionality
$T_1 - T_2$	=	temperature difference between points
$d$	=	distance between points
$A$	=	area normal to direction of heat flow

Equation ( 3.4) can be written more generally as

$$\phi = \frac{Q}{A} = -\lambda \frac{\partial t}{\partial x} \quad (3.5)$$

where

$\phi$	=	the heat flux (the heat flow per unit area per unit time across any surface)
$\lambda$	=	coefficient of thermal conductivity

Since steel has a high thermal conductivity transient conductivity need not be considered. Equation (3.5) - Fourier's law - is used to describe one-

dimensional steady state conduction in a slab. Equation (3.5 ) can be expanded to deal with conduction through a system of plane slabs of different material. The constant of proportionality represented by the coefficient of thermal conductivity,  $\lambda$ , is dependent upon the temperature and composition of the material. Values for thermal conductivity are determined from measurements of the time necessary to restore thermal equilibrium to a body exposed to a temperature gradient. Accurate information on the thermal conductivity of materials is essential for predicting the increases in temperature of a body due to heat transfer by conduction.

One-dimensional conduction does not often occur in practice since a body would have to be either perfectly insulated at its edges or so large that conduction would be one-dimensional at the centre. Calculation of the heat transferred into insulated steel beams is essentially two-dimensional at corners of box-protected beams.

### **3.2 Prediction of Temperature of Fire Exposed Members**

A number of methods exist for predicting temperatures of structural members exposed to fire. Of the available theoretical methods available at present, numerical methods are the most popular due to their versatility. Numerical methods are used to predict the temperature distribution in a steel member exposed to fire by solving non linear heat flow equations. These equations can be solved using either finite elements [Zienkiewicz and Cheung, 1967] or finite

difference methods [Dusinberre, 1961]; [Lie, 1977]. Such methods permit the calculation of temperature distributions in one, two or three directions and can accommodate composite sections and box-protected sections in which a volume of air is enclosed by the insulating material.

Computer programs have been developed that analyse the thermal response of structural steel elements and assemblies exposed to fire. The programs Fires-T3 [Iding, 1977], Tasef-2 [Pualsson, 1983] and Tempcalc [Anderberg, 1985] are three such programs which with appropriate sizing of the grid and accurate modelling of boundary conditions, yield accurate results [Wickstrom, 1989]. Fires-T3 employs a finite element method using implicit backward difference , coupled with time-step integration while Tasef-2 uses explicit forward difference time integration.

### **3.2.1 Numerical Method**

The following is a brief description of a two-dimensional finite difference method for the calculation of insulated steel members currently used by the National Research Council of Canada [Lie, 1992].

The cross-section of the protected member is divided into an orthogonal grid of closely spaced nodes. The heat balances of equations (3.1), (3.2) and (3.4) are expressed between adjacent nodes. Nodes located on the outside edge of the insulating material are subject to thermal radiation from the fire and heat

transfer by conduction to adjacent elements. Convective heat transfer to the insulation is usually ignored in this model for the reasons given above (subsection 3.2.1). Allowances can be made for heat generation or absorption due to decomposition or dehydration of the material. Heat transfer between elementary regions within the insulation occurs by conduction only. For box protected steel beams in fire heat transfer to the steel from the inside face of the insulation may occur by either of the three processes described above however convective heat transfer in the air gap is considered insignificant. It has been reported [Lie, 1992] that the rise in temperature due to convective heating is less than 1% of the maximum steel temperature [Lie and Harmathy, 1972]. The steel in contact with the insulation is heated by conduction while the steel in contact with air is heated by radiation. The temperature of the steel core is determined by equating the enthalpy of the steel core to that of the sum of the enthalpy's of the constituent steel pieces. That is the conductivity of the steel is assumed to be infinite and that the steel temperature is uniform over the cross-section of the member.

In order to simplify the calculation the expressions of heat transfer used assume steady-state conditions whereas the temperature of the compartment varies with time. In order to calculate the temperature-time response of the steel the increase in temperature is calculated in a step-wise manner for a suitably small increment of time over which it is assumed steady-state conditions exist in the fire compartment.

### **3.2.2 Comparison with Test Results**

A comparison with calculated and experimental results is reported [Lie, 1992], in which steel columns of various sizes and protected by number of protecting materials show a maximum deviation of approximately 15%. Both the standard temperature-time relation and a temperature-time curve that resembles an actual fire temperature curve was used [Lie and Harmarthy, 1970]; [Konicek and Lie, 1974].

### **3.2.3 Commentary on Numerical Method**

The finite difference method briefly described above can be considered as a reasonably sophisticated model for the calculation of the temperature of insulated steel members. It should be stressed however that even such a model ignores the contribution of convection both from the fire and in the air gap, in the case of box protected members; that the conductivity of the steel is assumed to be infinite; that the reported accuracy of the method is predicated on the density, specific heat, emissivity and thermal conductivity of the protection material being available.

### **3.3 Current Code Methods for the Calculation of the Temperature of Steel Members**

A method for the calculation of the temperature of steel beams and columns exposed to the standard fire is given in the European Recommendations for the Fire Safety of Steel Structures [ECCS, 1983], and by the French Technical Centre for Steel Construction [CTICM, 1976]. The calculation procedure is essentially the same as that proposed in the draft Eurocode EC3, [Design of Steel Structures, 1990] and the draft Actions of Fires [CIB Commission W81, 1992]. The recommendations are based on the Swedish manual Fire Engineering Design of Steel Structures [Pettersson et. al., 1976].

#### **3.3.1 Simplified Heat Transfer Analyses**

##### **3.3.1.1 Simplified Heat Transfer Analyses of Unprotected Steel Members**

The calculation procedures in the European Recommendations for the Fire Safety of Steel Structures [ECCS, 1983] {ECCS} are based on a simplified one-dimensional heatflow analysis in which the basic equations governing heat transfer are used in conjunction with lumped heat capacity analysis. The method is based on the following assumptions:

- a) the beams are exposed to fire on four sides.

- b. the steel offers no resistance to heat flow and therefore at any point in time is at uniform temperature. That is the thermal conductivity of the steel is assumed to be infinite.

Given infinite conductivity of the steel the rate of increase of internal energy of the steel given by:

$$q = C_s \rho_s V \frac{dT}{dt} \quad (3.6)$$

where	$q$	=	the rate of increase of energy	(W)
	$C_s$	=	the specific heat capacity of steel	(J/kg °C)
	$\rho_s$	=	the density of steel	(kg/m <sup>3</sup> )
	$V$	=	the volume of the body	(m <sup>3</sup> )
	$T_s$	=	the temperature of the body	(°C)
	$t$	=	time	(sec)

and the energy transmitted to the body from the fire is given by:

$$q = A \left[ (\alpha_r + \alpha_c) (T_f - T_s) \right] \quad (3.7)$$

where	$A$	=	the surface area exposed to fire	(m <sup>2</sup> )
	$\alpha_r$	=	the coefficient of heat transfer due to radiation from the fire to the exposed surface of the member	(W/m <sup>2</sup> °C)

- $\alpha_c$  = the coefficient of heat transfer due to convection  
from the fire to the exposed surface of the  
member (W/m<sup>2</sup>°C)
- $T_f$  = the temperature of the furnace (°C)

it follows from equations ( 3.6 ) and ( 3.7 ) that:

$$A[(\alpha_r + \alpha_c)(T_f - T_s)] = C_s \rho_s V \frac{dT_s}{dt}$$

$$\frac{dT_s}{dt} = (\alpha_r + \alpha_c) \frac{A}{V} \frac{(T_f - T_s)}{C_s \rho_s} \quad (3.8)$$

in which  $\alpha_c$ ,  $\alpha_r$  and  $C_s$  are given as [ECCS]:

$$\alpha_c = 25 \quad (3.9)$$

$$\alpha_r = \frac{5.67 \epsilon_r}{T_f - T_r} \left[ \left( \frac{T_f + 273}{100} \right)^4 - \left( \frac{T_s + 273}{100} \right)^4 \right] \quad (3.9A)$$

$$C_s = 38 \times 10^{-5} T_s^2 + 20 \times 10^{-2} T_s + 470 \quad (3.10)$$

where  $\epsilon_r$  = the resultant emissivity.

The ECCS recommend a value of 0.5 for the resultant emissivity or the use of equation (3.3) for a more accurate value. Both [Pettersson, 1976] and

- 
- The value of the Stefan-Boltzmann constant given in the ECCS (1983) document and in the Swedish design manual (1976) of 5.77 is incorrect and should be 5.67.

[CTICM, 1976] {CTICM} suggest a value of 0.7 with additional adjustment for view factor for beam construction. It is found that in the case of an insulated beam, the value of the emissivity has little or no effect on the temperature of the steel beam. Variation in the value of the emissivity in the case of an uninsulated beam however can have a significant effect on the temperature-time curve of the member, refer Figure 3.1.

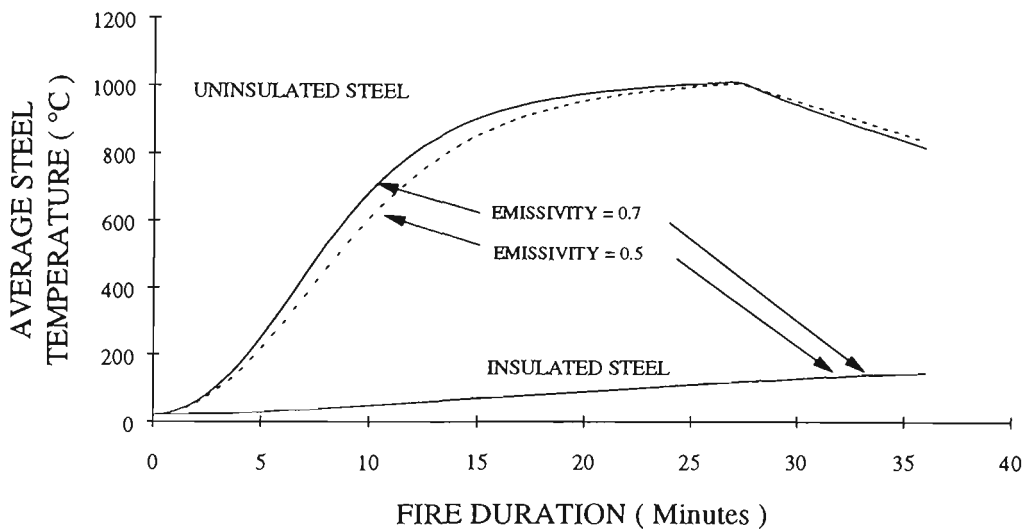


Figure 3.1 — Influence of variation in emissivity on average temperature of insulated and uninsulated steel members.

The recommended value of  $\alpha_c$  is based on experimental investigations of standard and natural fire exposures. A slightly different value of  $23 \text{ W/m}^2 \text{ }^\circ\text{C}$  is suggested by Pettersson and CTICM for  $\alpha_c$ .

The specific heat of steel,  $C_s$ , is a function of the steel temperature. The ECCS recommendations suggest however that a temperature independent value of  $520 \text{ J/kg}^\circ\text{C}$  may be used. The effect of using a single value of specific heat on the calculated temperature versus time curve is compared with that

calculated using a temperature dependent specific heat is demonstrated in Figure 3.2.

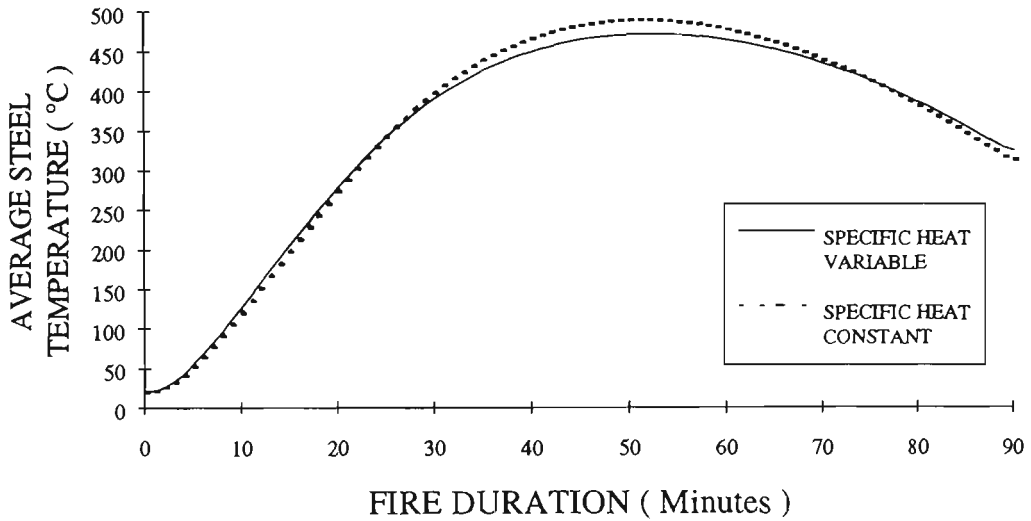


Figure 3.2: Temperature time curve of a lightly insulated steel beam calculated using a temperature dependent specific heat of steel and a constant value specific heat.

By using equation ( 3.8 ) in a step-by step calculation in which the time interval  $\Delta t$  satisfies:

$$\Delta t < \frac{2.5 \times 10^4}{A/V} \quad (3.11)$$

the time-temperature relationship of the steel member is obtained. The ECCS and CTICM both recommend that for any increment of time, the gas temperature,  $T_f$ , used in the calculation of the steel temperature should be the average gas temperature during the time period.

### 3.4.1.2 Simplified Heatflow Analysis of Protected Steel Members

The method follows on from that developed for heat transfer to uninsulated steel members. Two additional assumptions are required as follows:

- a) the insulating material has negligible thermal capacity and therefore has a linear temperature gradient between the fire exposed surface and the inner surface next to the steel.
  
- b) the resistance to heat flow between the inner surface of the insulating material and the steel is negligible.

The temperature rise in fire exposed steel beams can be significantly influenced by the presence of insulation material. Similarly to equation (3.7) the heat transfer from the furnace to the surface of the insulation is given by:

$$q = A_{io}[(\alpha_r + \alpha_c)(T_f - T_{io})] \quad (3.12)$$

where  $A_{io}$  = outer surface area of the insulation per unit length (m<sup>2</sup>)

$T_{io}$  = temperature of outside surface of insulation.(°C)

while the transfer of heat through the insulation by means of conduction based on equation (3.5) is given by:

$$q = \frac{\lambda A_i}{I} (T_{io} - T_s) \quad (3.13)$$

where  $A_i$  = internal surface area of insulation per unit length  
(m<sup>2</sup>)

$I$  = thickness of the insulation material (m)

Using equations ( 3.6 ), ( 3.12 ) and ( 3.13 ) and assuming the conductivity of the steel to be infinite and that  $A_{oi} = A_i$ , the temperature rise in a lightly insulated member is obtained from:

$$dT_s = \frac{(\alpha_c + \alpha_r) + \lambda/d_i}{C_s \cdot \rho_s} \cdot \frac{A_i}{V} \cdot (T_f - T_s) \cdot dt \quad (3.14)$$

The CITCM suggest the following expression for the heat transfer coefficient for lightly insulated beams:

$$(\alpha_c + \alpha_r) = 23.2 + 1.388 \times 10^{-5} (T_f + 273)^3 \quad (3.15)$$

Both Petterson (1976) and the ECCS recommend that the surface heat transfer term  $(\alpha_r + \alpha_c)$  may be ignored when calculating the rise in temperature of an insulated steel beam when the value of this term is small in comparison to the value of the insulation thickness divided by the thermal conductivity of the insulating material,  $d_i/\lambda_i$ . In which case Equation (3.14) may be written as:

$$dT_s = \frac{\lambda/d_i}{C_s \cdot \rho_s} \cdot \frac{A_i}{V} \cdot (T_f - T_s) \cdot dt \quad (3.16)$$

This simplification however will lead to significantly higher average steel temperatures, as much as 100 °C higher, in the case of small values of  $d_i/\lambda_i$ , as shown in Figure 3.3..

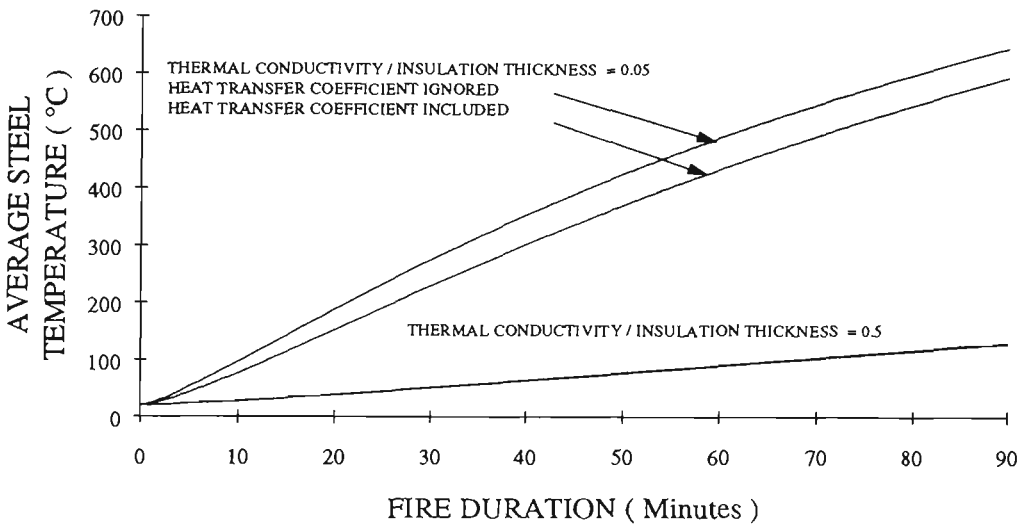


Figure 3.3 — Influence of heat transfer coefficient on calculated steel temperature. When the ratio of insulation thickness to thermal conductivity is small the steel temperature is significantly over-estimated.

Equation (3.14) is based on the assumption that the heat capacity of the insulation is zero, that is, the temperature distribution across the insulation is linear. It has been shown [Rohsenow and Choi, 1961] that this is the case for thin bodies. Insulation may be considered thin if the following inequality is satisfied:

$$C_s \cdot \rho_s \cdot V \geq 2 \cdot C_i \cdot \rho_i \cdot A_i \cdot d_i \quad (3.17)$$

where  $C_i$  = specific heat of the insulation

$\rho_i$  = density of the insulation

In the case of this inequality not being satisfied an alternative equation (3.18) is recommended by the ECCS which is less conservative than (3.14). The alternative equation (3.18) assumes that the heat capacity of the insulation is lumped at a representative depth within the insulation. The equation is given as:

$$dT_s = \frac{\lambda_i}{d_i} \cdot \frac{1}{C_s \rho_s} \cdot \frac{A_i}{V} \cdot \left( \frac{1}{1 + \zeta} \right) \cdot (T_f - T_s) \cdot dt \cdot - \frac{dT_f}{\left( 1 + \frac{1}{\zeta} \right)} \quad (3.18)$$

and  $\zeta = \frac{C_i \cdot \rho_i \cdot A_i \cdot d_i^*}{2 \cdot C_s \cdot \rho_s \cdot V}$  (3.19)

This equation should only be used when  $\zeta > 0.25$ . The lumped heat is assumed by the ECCS to occur at the inside face of the insulation. This results in a significant reduction in the steel temperature due to heat being absorbed by the insulation. This is considered unrealistic [Bennetts et. al., 1986] who suggests that the lumped heat should be at mid-depth in the insulation,  $d_i/2$ , in which case the reduction in the temperature of the steel is halved. The ECCS recommendation could be considered unconservative. An alternative simplified calculation method is also given [ECCS, 1983], in which equation (3.14) is used. In this method the thermal capacity of the steel is increased by

---

\* The definition of this expression in the draft Eurocode EC3 Part 10, is in error - the code uses thermal conductivity in place of thickness of insulation.

one half of the thermal capacity of the insulation material. This method is to be used only with the standard fire exposure.

The draft Eurocode [EC3, 1990] proposes a modified version of equation (3.18) for the calculation of the increase in temperature of all insulated members as follows:

$$dT_s = \frac{\lambda_i}{d_i} \cdot \frac{1}{C_s \rho_s} \cdot \frac{A_i}{V} \cdot \left( \frac{1}{1 + 2/3 \zeta} \right) \cdot (T_f - T_s) \cdot dt \cdot - \left( e^{\zeta/5} - 1 \right) \cdot dT_f \quad (3.20)$$

A comparison of calculated temperature versus time curves calculated using equations (3.18) and (3.20) reveal a considerable difference in Figure 3.4. Using the modification proposed by Proe, there is a much improved match between the curves obtained from the two equations. By assuming the reference depth  $d_i/2.5$  even better agreement is achieved. A comparison of equations (3.15) and (3.20) show reasonable agreement for thicknesses of insulation less than 20 mm.

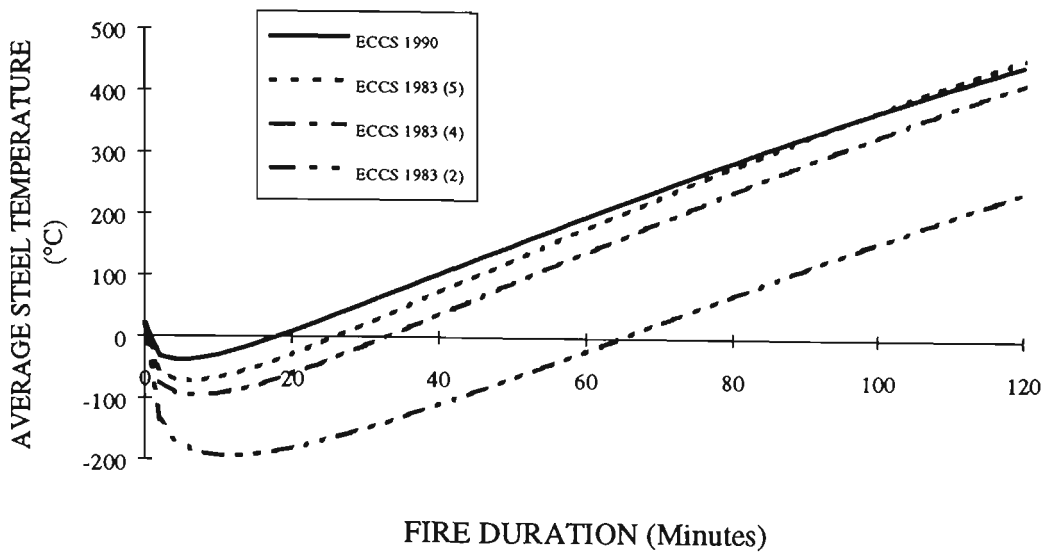


Figure 3.4: Relationship between the 1983 and 1990 recommendations for the calculation of the temperature of heavily insulated steel members. (2) = reference depth = I; (4) - reference depth = I/2; (5) - reference depth = I/2.5. [ Test case 350 UB box insulated with 40 mm fibre silicate ] - Author.

### 3.4.1.3 Considerations for Three Sided Exposure

A beam supporting a concrete slab will typically exhibit a temperature gradient over the depth of the cross-section of the member. The gradient is due to both the large heat capacity of the concrete which results in a transfer of heat from the top of the beam to the concrete, and to the reduced exposed surface area of the steel section due to the top flange being protected from direct exposure to the fire.

The temperature distribution in a fire exposed steel beam can be idealised as either a linear distribution for box protected steel beams, Figure 3.5 A(1&2) or

as two isothermal zones for unprotected or contour protected steel sections, refer Figure 3.5 B(1&2).

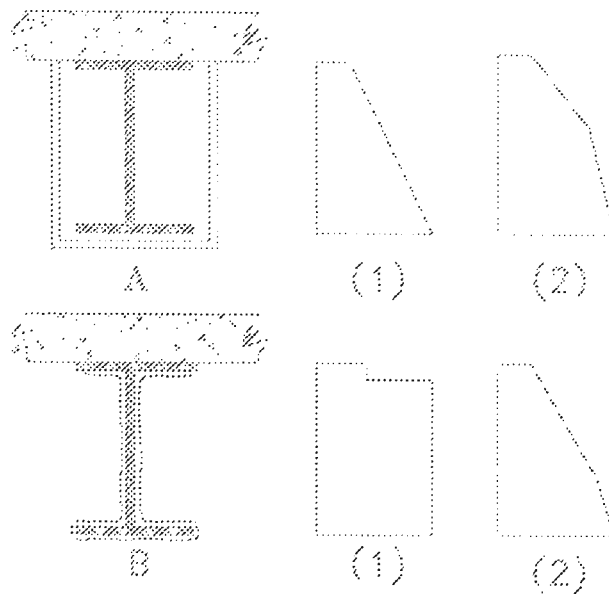


Figure 3.5: Simplified temperature distributions observed in tests.  
 A) - box protected steel section; B) - contour protected steel section

The magnitude and shape of the temperature gradient depends on the length of fire exposure, depth of the beam and the mass of the section. Beams with thin fire protection and /or are heavily loaded are exposed to the fire for a shorter period and are therefore expected to exhibit a small temperature gradient. Deep beams or beams with a small exposed surface area to mass ratio - such as universal bearing piles (UBP) - are expected to display a large temperature gradient. These expectations are supported by test results of bottom flange, web and top flange temperatures from a series of twenty one fire tests of contour protected steel beams supporting a concrete slab [Proe, 1989]. The average difference in temperature between the top and bottom flange was 260 °C. The average ratio of top flange to bottom flange

temperature,  $T_{top}/T_{bottom}$ , was 0.61 in which the largest ratio, smallest temperature gradient, was 0.82 and the smallest ratio was 0.42. Only one lightly insulated section exhibited a shape of temperature gradient as shown in Figure 3.5 B(1) in which the bottom flange and web are essentially the same temperature. In the remaining sections the shape of the temperature gradient corresponds with that shown in Figure 3.5 B(2) in which the web temperature was on average 0.86 that of the bottom flange temperature. From test results it was also apparent that the thermal gradient of heavily insulated contour protected steel beams approaches a linear distribution, refer Figure 3.5 A(1). Table 3.2 shows values of  $T_{top}/T_{bottom}$  derived from test results of maximum and average steel temperatures for box protected beams [BHP, 1983].

Section	Insulation Thickness (mm)	$T_{top}/T_{bottom}$
100 UC	19	0.88
100 UC	50	0.79
200 UBP	25	0.80
200UBP	50	0.56

Table 3.2: Ratio of temperature of top flange to bottom flange for box protected steel beams.

From the foregoing it can be assumed that under normal conditions the  $T_{top}/T_{bottom}$  ratio of a steel beam supporting a concrete slab is likely to vary between 0.9 to 0.5.

The simplified thermal model does not account for the effect of a thermal gradient in the steel. It has been shown however, [Proe, 1900] that it is

appropriate to use the temperature of the steel beam, as a weighted average of the temperature over the cross-section, to calculate the strength of the member at elevated temperature, refer Subsection (4.5.3). Alternatively a factor may be applied in the structural response analysis that allows for the additional reduction in strength of the beam due to the presence of the thermal gradient.

#### **3.4.1.4 Density of Steel**

The density of steel is normally taken to be 7850 kg/m<sup>3</sup> for structural steel. A small decrease in the density, ~ 3%, occurs when Grade 43A structural steel is heated up to a temperature of 700 °C [Wainman, 1990]. The effect of such a small change is considered to be a second order effect in the modelling of the temperature of steel and will be ignored in this analysis.

#### **3.4.1.5 Thermal Conductivity of Steel**

The error associated with the assumption of heat transfer through steel being uniform and instantaneous (infinite conductivity) has been assessed. A comparison of steel temperatures [Barthelemy, 1976] calculated using the simplified method and a two-dimensional analysis using finite elements agree to within 10% for sections with an exposed surface area to mass ratio, ESM, greater than 10. All but the largest universal beam (UB) steel sections and some bearing piles (UBP) available in Australia have an ESM greater than 10.

The effect of ESM on the rate of heating of insulated steel sections insulated with the same thickness of insulation material is shown in Figure 3.6.

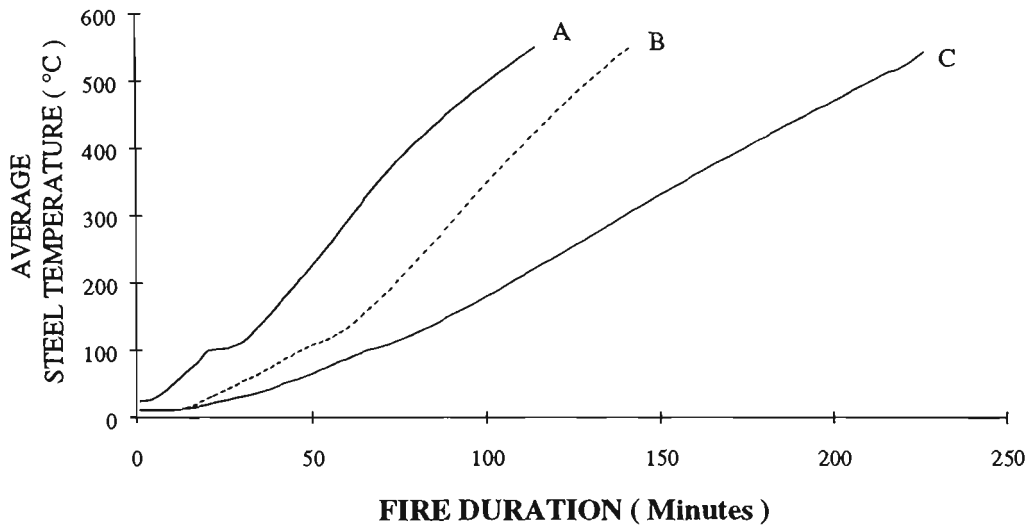


Figure 3.6: Heating rate of insulated steel sections as a function of exposed surface area to mass ratio (ESM). A) - ESM = 40; B) - ESM = 26.7; C) - ESM = 9. Insulation 38 mm Harditherm 700.

### 3.4.1.6 Thermal Conductivity of Insulation

A true measure of the thermal conductivity of insulating material is difficult to obtain. Values of thermal conductivity for a number of insulating materials as a function of the insulation temperature are given in Table 3.2 , [Pettersson, 1976]. No information is given in the reference as to whether the values of thermal conductivity are derived from theoretical considerations, measured values or by correlation with the results of fire tests.

Insulating Material	Temperature °C				
	100	200	300	400	500
Vermiculite Slab	0.099	0.108	0.116	0.13	0.137
Mineral Wool	0.051	0.068	0.094	0.127	0.173
Gypsum Plaster	0.12	0.14	0.157	0.181	0.198

Table 3.3: Thermal conductivity,  $\lambda$ , (W/m°C) of some insulation materials as a function of insulation temperature.

It is evident from Table 3.3 that there are considerable differences in the value of thermal conductivity for different materials and as a function of temperature. It is recognised that the thermal conductivity has a strong influence on the fire resistance of the structural element [Lie, 1992]. The ECCS recommend that the thermal conductivity of the insulation material  $\lambda_i$  be determined experimentally as a function of the mean temperature of the insulating material by using Equation (3.14). Such an approach takes into account the arrangement of the insulation as well as the thermal and mechanical behaviour of the insulating material under fire conditions. It is stressed that such a value of  $\lambda$  is not equivalent to the conventional value of the thermal conductivity as given in handbooks on heat transfer, rather it acts as a correlating factor.

Using Equation (3.14) and experimental values of the thickness of the insulating material, the steel temperature, the slope of the time-temperature response curve and furnace temperature, obtained from the theoretical standard temperature-time relationship, [Bennetts et. al., 1986] and [Barthelemy, 1976] derived equations for thermal conductivity for a number of steel sections and insulating materials as a function of the temperature of the insulating material.

The thermal conductivity versus temperature relationship for the insulating material for temperatures below 100 °C was given by extrapolation. Equations (3.21) and (3.22) were used to determine the value of the moisture content of the material,  $\rho$ . Hence two correlating terms,  $\lambda$  and  $\rho$  are determined in order to match theoretical and measured steel temperatures.

It has been demonstrated by calculation [Pettersson, 1976] that the average temperature of the insulation during exposure to fire is generally approximately the same as the average maximum temperature attained by the steel member. As a result of this the ECCS permit the thermal conductivity of the insulation to be represented by a single value, determined as a function of the expected maximum steel temperature. The result of adopting such a simplification is demonstrated in Figure 3.7 where the temperature versus time curve for an insulated steel beam is calculated using an expression for thermal conductivity

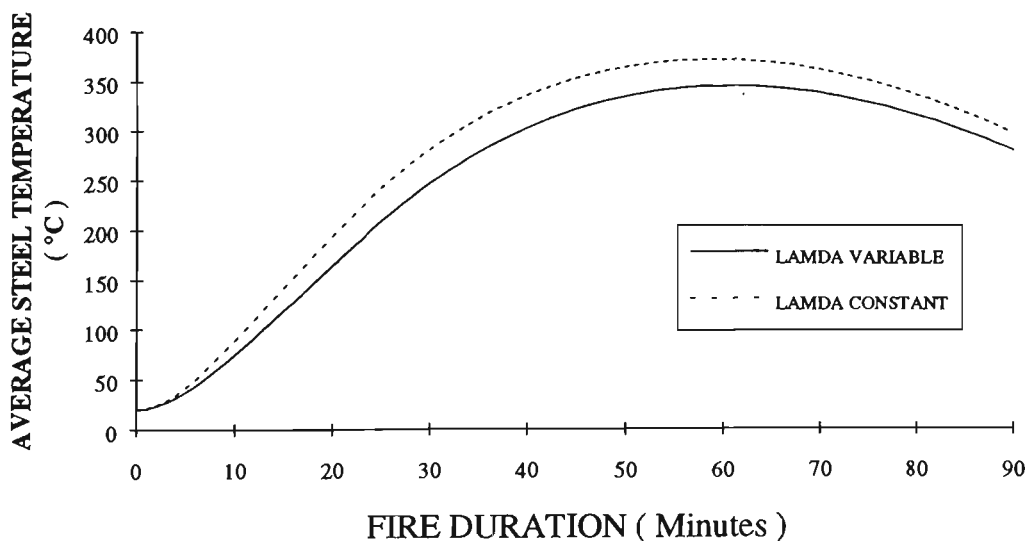


Figure 3.7: Temperature time curve of a lightly insulated steel beam calculated using a temperature dependent thermal conductivity ( $\lambda$ ) of insulation and a constant value of thermal conductivity based on expected maximum steel temperature. (Insulation thickness = 20 mm)

that varies with the steel temperature and a single value of thermal conductivity based on the expected maximum temperature of the steel.

From the work of Bennetts it was apparent that there was considerable variation in the calculated thermal conductivity obtained from the results of tests on similar specimens, and that there was also systematic variation between the various sections. Much of this variation was ascribed to the method of calculating the exposed surface area to mass ratio. Because of this the foregoing method can only be employed in a general way if the mass ratio is taken in to account as a dependent variable.

#### **3.4.1.7 Influence of Moisture**

The presence of water in the insulating material can significantly delay the time to reach a given temperature. Free water in the pores will evaporate when it reaches 100 °C. Because water has a large latent heat of evaporation most of the heat supplied to the material is used to evaporate the water. This process results in a delay time during which the temperature of the steel either increases slowly or remains constant. Figure 3.8 shows some test results, [Hardies, 1981], that exhibit the delay time phenomenon.

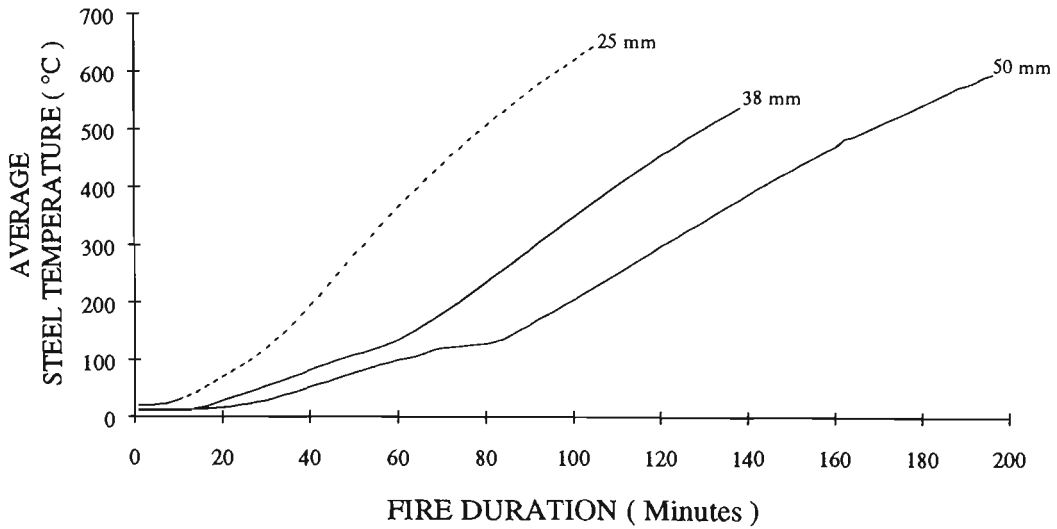


Figure 3.8: Temperature rise of 250 UB steel beams exposed to the standard fire and protected by a range of insulation thicknesses. A plateau in the temperature-time curve at 100 °C becomes evident as the thickness of the insulation increases.

The delay time is a function of the absolute volume of moisture, which for a particular material will increase in proportion to the thickness of the material. Materials in which water of crystallisation is also present will suffer delay time but at temperatures greater than 100°C depending on the rate of heating.

Based on the method by CTICM, the following equation for calculation of the change in temperature,  $\Delta T_s$ , of the steel member over the interval of time,  $\Delta t$ , has been proposed [Bennetts, 1986]:

$$\Delta T_s = \frac{1}{\frac{1}{\alpha} + \frac{1}{2\lambda}} \cdot \frac{1}{C_s \rho_s / A_i V + (4180 \rho l)} (T_f - T_s) \cdot \Delta t \quad (3.21)$$

where  $\rho$  = moisture content of the insulation material by volume

4180 = the heat capacity of water in  $\text{kJ/m}^3 \cdot ^\circ\text{C}$

Equation (3.21) presupposes that the temperature of the insulation to be the average of the furnace (fire) and steel temperature. It further assumes a particular temperature distribution through the insulation, for which there is no theoretical justification, but results in predictions of steel temperatures which are in accordance with experimental results. This expression is considered valid up to a steel temperature of 100 °C. At 100 °C the delay time,  $t_d$ , is calculated by equating the total heat flux to the member ( post 100 °C) to the energy required to vaporise the water as follows:

$$\int_{t_1}^{t_1+t_d} (T_f - 100) dt = 60 \cdot 2.26 \times 10^6 \rho I \left( \frac{1}{\alpha} + \frac{1}{2\lambda} \right) \quad (3.22)$$

where  $2.26 \times 10^6$  = the energy required to convert water to steam at 100°C in kJ/m<sup>3</sup>

The ECCS (1983 and 1990) provide an empirical expression from which to determine  $t_d$  as follows:

$\frac{\rho \cdot \rho_i \cdot d_i^2}{\lambda_i} \times 10^2$	4	8	12	16	20	24	28
$t_d$ (minutes)	5	15	25	30	40	50	55

Table 3.4: Calculation of delay time due to moisture.

### 3.4.2 Regression Method

A method is given in [AS 4100, 1990], for the calculation of the time for steel members to reach a specified limiting temperature. The method, which is applicable to steel members subject to both three and four sided exposure, is based on interpolation of temperature versus time curves from a series of fire tests using the regression equation (3.23) subject to a number of limitations. The relationship between temperature,  $T$ , and time,  $t$ , as a function of the thickness of insulation,  $h_i$ , and the mass to surface area ratio,  $k_{sm}$  is calculated by least-squares regression as follows:

$$t = k_0 + k_1 h_i + k_2 \left( \frac{h_i}{k_{sm}} \right) + k_3 T + k_4 h_i T + k_5 \left( \frac{h_i T}{k_{sm}} \right) + k_6 \left( \frac{T}{k_{sm}} \right) \quad (3.23)$$

where  $k_0$  to  $k_6$  = regression coefficients

A minimum of nine fire tests, in which the thickness of insulation and ESM are varied, are required to determine the regression coefficients. The regression method is limited to the temperature range, 200 °C to 600 °C, - being the interval in which the relationship between time and temperature is observed to be near to linear. The regression method was developed to provide a simple means of determining the fire rating of insulated steel members from test data for use in the design environment. Importantly, it avoids the difficulty of obtaining a measure of the thermal conductivity of the insulating material.

The method is limited in that it can only be used for determining response of structural members to exposure to the standard test fire. The method could possibly be extended to model real fire exposure however the additional number of independent variables would be increased by at least two and as a consequence the number of fire tests required to determine the regression coefficients would become quite uneconomical.

### **3.5 Selection of Heat Transfer Submodel**

It has been demonstrated that for unprotected and protected steel beams exposed to fire on four sides the temperature versus time curve obtained by using the simplified one dimensional heat transfer model is within 10% of the result obtained by using a two-dimensional finite element analysis [Barthelemy, 1976]. Such a level of accuracy corresponds with that required under Aims of Project, refer Subsection (1.1.2). The use of more complex numerical methods to determine the temperature of a section is only appropriate where temperature distribution either through or along the member varies. It was explained in Subsection (3.4.1.3) that a thermal gradient exists in a steel member exposed to fire on three sides. It is still appropriate, however, to use the simplified one-dimensional heat transfer model in this case as the calculated temperature versus time curve corresponds with that of the bottom flange (maximum temperature) of the steel beam. The effect of the thermal gradient can be taken into account by the use of either a strength reduction factor or a modified strength reduction model, refer Subsection (4.5.3).

The fire severity model adopted, refer Subsection (2.8), assumes a uniform gas temperature throughout the compartment volume. While this assumption is not always valid, it precludes temperature variation along the length of the beam. Further, because one of the aims of the project is to determine the strength in bending of a simply supported floor beam it is only necessary to know the temperature of the steel where the bending moment is at a maximum, the mid-point of the beam. Modeling of temperature variation along the beam is, therefore, neither possible with the adopted fire model nor necessary given the aims of the project. The use, therefore, of the simplified one dimensional heat transfer method is justified in that appropriate accuracy is achieved for the calculation of the strength of fire exposed steel beams.

The heat transfer model to calculate the temperature of steel beams in fire that has been adopted for use in the proposed simulation model to calculate the time varying probability of failure of steel beams is based on that published in the European Regional Organisation for Steel Construction document, [ECCS, 1983] - European Recommendations for the Fire Safety of Steel Structures, and by the French Technical Centre for Steel Construction, [CTICM, 1976]. The recommendations are written specifically for "load-bearing steel elements and structural assemblies exposed to the standard fire, providing an alternative to the standard fire resistance test", [ECCS, 1983]. ECCS and CTICM recommend that the concept of "effective fire duration" in which the temperature attained by a sample exposed to a real fire is expressed as the time for the sample to reach the same temperature when subject to the standard fire. The use of this concept is not necessary however as the method outlined in the

recommendations is equally suited to input data based on temperature time curves representing natural fires, [Thor et al., 1977].

### 3.5.1 Selected Submodel Equation for Calculation of Unprotected Steel Temperature

The calculation of the temperature of unprotected steel will follow the method outlined in sub-section 3.4.1. The increase in the average temperature of a steel member is given by Equation (3.8) which was:

$$\frac{dT_s}{dt} = (\alpha_r + \alpha_c) \frac{A}{V} \frac{(T_f - T_s)}{C_s \rho_s} \quad (3.8)$$

#### 3.5.1.1 Heat Transfer Coefficient and Emissivity for Heat Transfer Submodel

In this analysis the coefficient of heat transfer due to convection  $\alpha_c$ , is taken as  $23 \text{ W/m}^2 \text{ }^\circ\text{C}$  [Petterson, 1976], [CTICM, 1976]. The temperature dependent coefficient of heat transfer due to radiation,  $\alpha_r$ , is calculated using Equation (3.9A) obtained from the ECCS recommendations as follows:

$$\sigma_r = \frac{5.67 \epsilon_r}{T_f - T_s} \left[ \left( \frac{T_f + 273}{100} \right)^4 - \left( \frac{T_s + 273}{100} \right)^4 \right] \quad (3.9A)$$

where  $\epsilon_r$ , the resultant emissivity of the flames, combustion gases and exposed surface is taken as 0.5 for a beam exposed to flame on four sides. In the case of an I-beam supporting a concrete slab, in which the flames can penetrate between the girders, both the CTICM and the Swedish Institute of Steel Construction, [Pettersson, 1976], the recommended resultant emissivity factor of 0.7 has been adopted for use in calculating the temperature-time response curve for use in the simulation model

### 3.5.1.2 Specific Heat of Steel adopted in Submodel

The specific heat of steel,  $C_s$ , is a function of the steel temperature. In this analysis the specific heat will be determined from equation (3.10) which was:

$$C_s = 38 \times 10^{-5} T_s^2 + 20 \times 10^{-2} T_s + 470 \quad (3.10)$$

The effect of using equation (3.10) reduces the calculated average maximum steel temperature by approximately 3.5% compared with that obtained from using a temperature independent value of specific heat as shown previously - refer Figure 3.2. When incorporated in to the simulation model the use of the temperature dependent value will reduce the variance of the maximum temperature by 2% . This has a small effect on the estimate of probability of failure.

### 3.51.3 Time Step

Equation (3.8) is applied in small discrete time steps,  $\Delta t$ . A limit for the time increment is specified by equation (3.11) as follows:

$$\Delta t < \frac{2.5 \cdot 10^{-4}}{A_i/V} \quad (3.11)$$

Assuming a maximum value of surface area to volume ratio,  $A_i/V$ , of  $160 \text{ m}^{-1}$ , the effect of the chosen time increment on the calculated maximum steel temperature is shown in Figure 3.9. A recommended time increment of 150 seconds is adequate for the range of sections encountered in practice. A time increment of 60 seconds was adopted however in the simulation model to predict time to failure to the nearest minute. This had the effect of reducing the

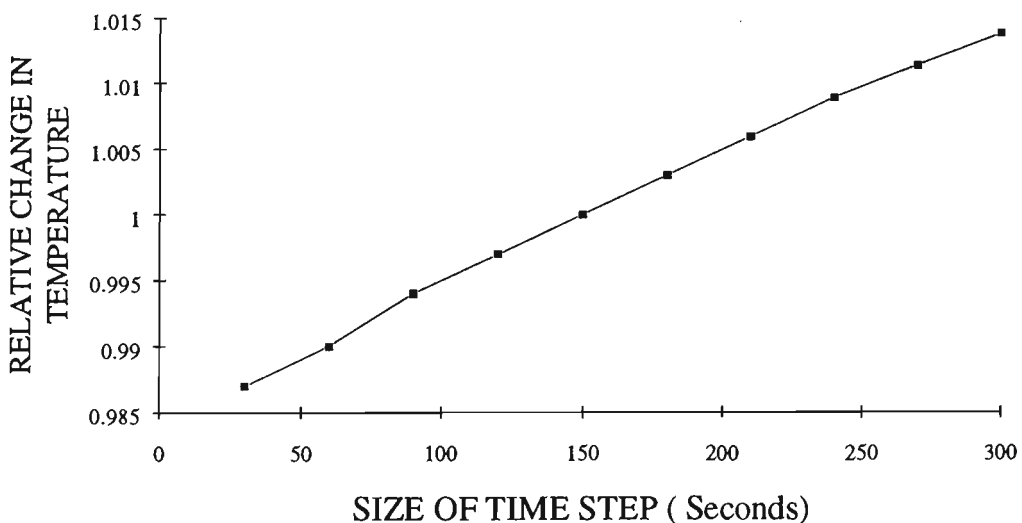


Figure 3.9: Relative change in the calculated average maximum steel temperature as a function of time increment - assuming an  $A_i/V$  ratio of 165 - Author.

calculated maximum steel temperature by 1%. The sensitivity of the calculation of the steel temperature to the size of the time increment decreases as the thickness of the insulation increases.

#### **3.5.1.4 Comparison between Calculated Steel Temperature versus Time Curve and Experimental Test Data - Uninsulated Steel**

It can be demonstrated that the simplified heat transfer model predicts the temperature-time response curve of uninsulated steel sections exposed to either the standard fire or real fires with acceptable accuracy. The calculated steel temperature versus time curve of an uninsulated steel beam supporting a concrete slab was compared with the temperature versus time curve measured in a standard fire test [Pettersson, 1976]. Good agreement (within 30 °C) was obtained between the calculated temperatures and the temperatures measured on the lower flange of the steel beam. The temperature in the top flange was consistently lower than in the rest of the beam. This is due to the top flange being protected from direct radiation and to the continuous conduction of heat away from the top flange into the cooler slab.

The accuracy with which the simplified method is capable of predicting the temperature of a steel beam supporting a concrete slab when exposed to real fire has also been assessed. Gas temperature versus time curves measured in a series of test fires conducted at the joint British Steel Corporation / Fire

Research Station [Lathem et al., 1986], were modelled and used as input  $T_f$  in Equation (3.14) to calculate the temperature of the steel, refer Figure 3.10.

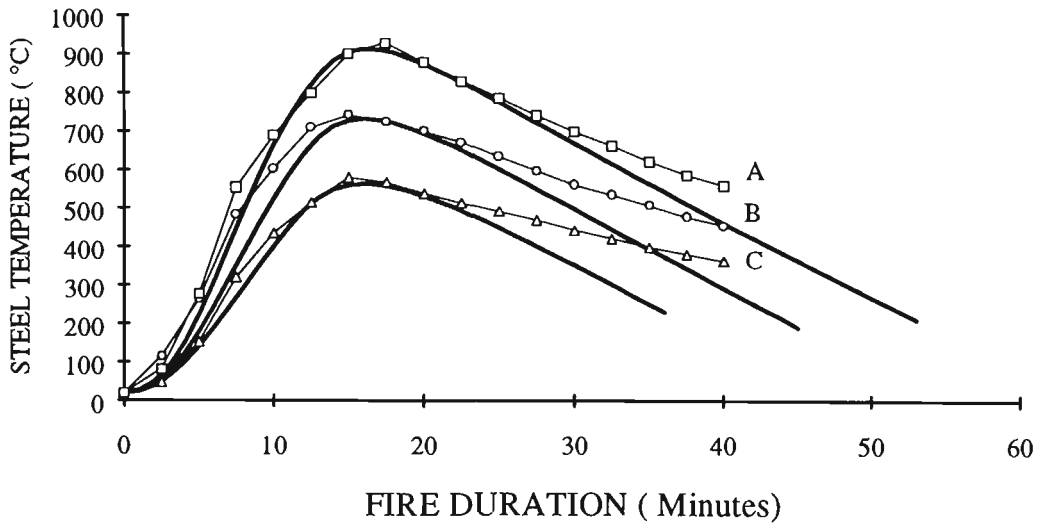


Figure 3.10: Comparison of experimental and calculated steel temperature using Equation (3.14). Measurements taken on lower flange of uninsulated beam supporting concrete slab. Fire test data after Lathem (1987), - open shapes: modelled temperatures - solid line. (Opening Factor =  $0.06 \text{ m}^{1/2}$  Fire load density ( $\text{kg}/\text{m}^2$ ): A = 10; B = 15; C = 20) - Author.

Agreement to within 5% is obtained between the calculated temperature versus time curves and those temperatures measured at the lower flange of uninsulated beams supporting a concrete slab.

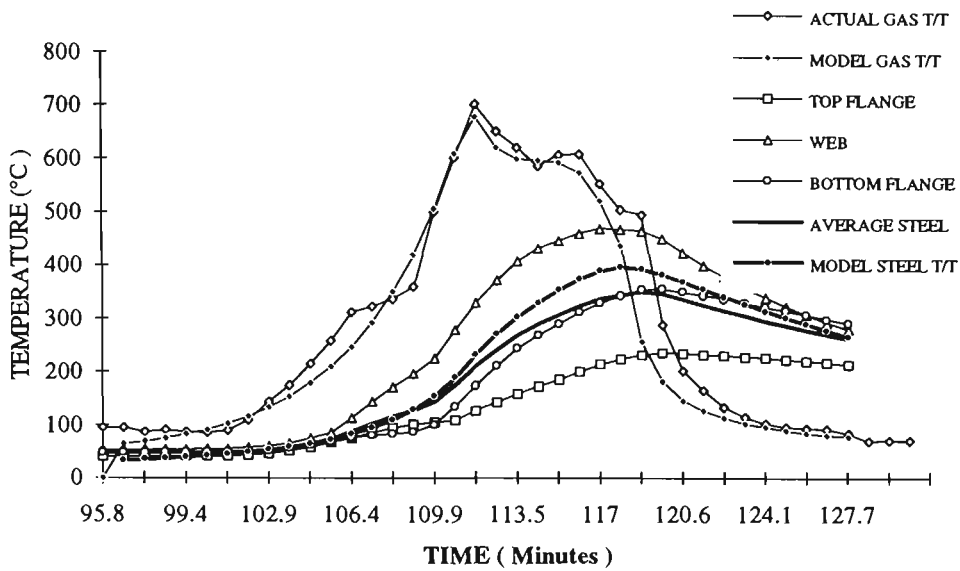


Figure 3.11: Comparison between measured steel temperatures, obtained from simulated office fire, and calculated steel temperature using one-dimensional heat transfer - Author.

Figure 3.11 shows the steel temperature of the web, top and bottom flanges of a castellated 510 UB90 beam recorded during a simulated office fire, [BHP, 1992]. The beam supports a lightweight concrete slab and is shielded from the direct effect of fire by a 30mm thick, cast plaster ceiling tiles. The temperature of the gas in the ceiling space was modelled using a curve fit program and used as input to calculate the steel temperature using Equation (3.14). The resultant emissivity used in the calculation was determined from the charts given in Pettersson [1976]. This is a more difficult situation to model due to the protection afforded the bottom flange by the ceiling tiles: the relatively high surface area to mass ratio of the web: the heat sink effect of the slab. The normal linear temperature distribution over the depth of the steel section is not evident. Unlike the previous example, in which the simplified method predicted the lower flange temperature accurately, there is reasonable agreement - to within 10% - with the average temperature of the steel section. The influence

of the emissivity of the top of the suspended ceiling (which has only been estimated) on the calculated steel temperature will be significant. Despite the complex nature of the situation it is evident that use of the simplified method to predict the temperature of steel exposed to real fire produces acceptable results.

The use of Equation (3.14) for predicting the temperature versus time curve of sections exposed to real fire on four sides [Butcher et al., 1966], is demonstrated in Figures 3.12 and 3.13.

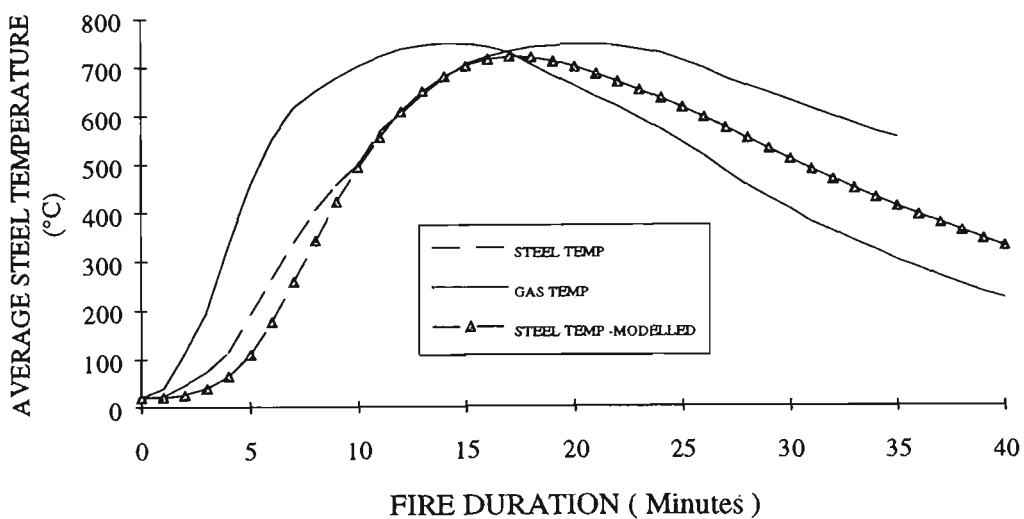


Figure 3.12: Comparison between calculated and test data of free standing column exposed to natural fire. Fire load = 30 kg/m<sup>2</sup>; ventilation = 0.08 m<sup>1/2</sup> - Author.

Figure 3.12 represents a reasonably severe fire (fire load of 30 kg/m<sup>2</sup> floor area) in which the columns are assumed to be surrounded by emissive flames. In this case an emissivity of 0.7 was adopted as recommended for internal columns by Kirby [1986]. Equation (3.14) underestimates the maximum steel temperature by approximately 20 °C but matches well, within 15%, over the temperature range in which loss of strength is likely to be critical.

Figure 3.13 represents a relatively small fire (fire load 7.5 kg/m<sup>2</sup> floor area) in which heat loss to the surroundings was apparent. As a consequence of the foregoing an emissivity of 0.4 was adopted in the calculation of the steel temperature. Again good agreement, within 10%, is achieved between calculated and measured temperature-time curves, the calculated temperature being conservative in this situation.

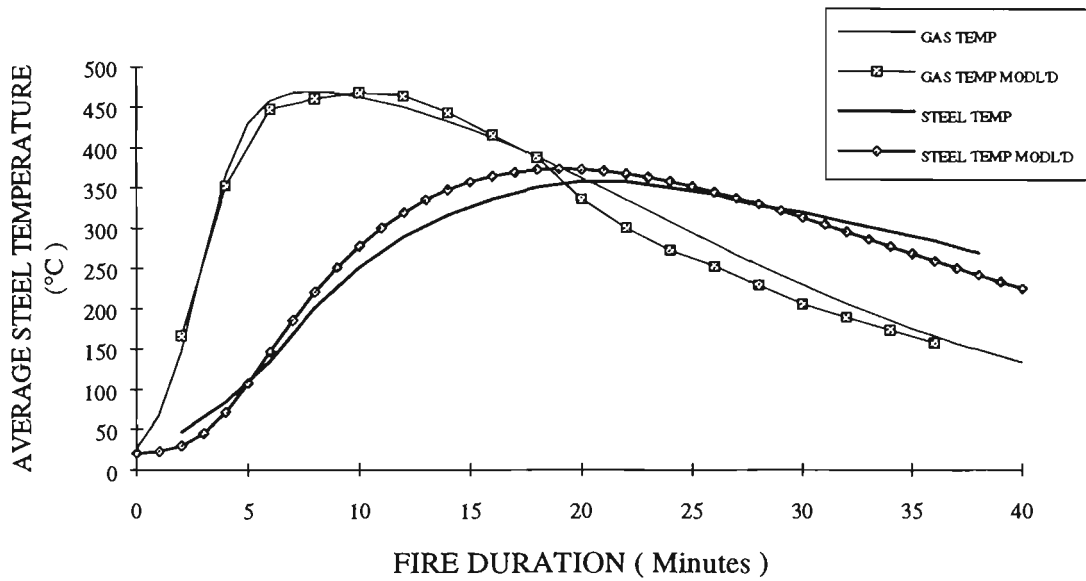


Figure 3.13: Comparison between calculated and test data of free standing column exposed to real fire. Fire load = 15 kg/m<sup>2</sup>; ventilation = 0.12 m<sup>1/2</sup> - Author.

### 3.5.2 Calculation of Temperature for Insulated Steel

The increase in the mean temperature of a steel member protected by dry insulation material was given by equation (3.14) as follows:

$$dT_s = \frac{(\alpha_c + \alpha_r) + \lambda/d_i}{C_s \cdot \rho_s} \cdot \frac{A_i}{V} \cdot (T_f - T_s) \cdot dt \quad (3.14)$$

### 3.5.2.1 Arrangement of Insulation

A number of basic geometries are possible for steel beams protected by insulating material, depending on whether the insulating material is the spray type or board material and whether the beam supports a concrete floor directly on its upper flange or not. Two arrangements have been used in the submodel as shown in Figure 3.14.

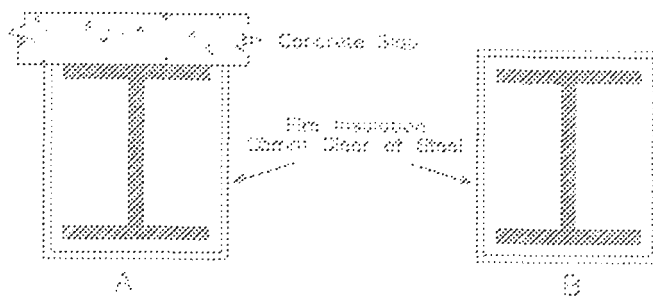


Figure 3.14: Arrangement of insulation: A) - three-sided exposure. B) - four-sided exposure.

The term  $A_i/V\rho_s$  in Equation (3.14) is determined from the length of insulation measured around the interior face of the insulation exposed to fire,  $A_i$ , divided by the cross-sectional area of the steel section and by the density of steel ( $\rho_s = 7850\text{kg/m}^3$ ).

### 3.5.2.2 Thermal Conductivity of Insulation

Harditherm 700, a calcium silicate based board [Thomas and Bennetts, 1982], has been adopted as the only type of insulation material to be considered in this

project. Harditherm is used throughout the construction industry and is representative of the type of insulating board currently available in Australia

The thermal conductivity of Harditherm 700 was assessed by Thomas and Bennetts. The relationship describing the variation in the thermal conductivity as a function of the maximum steel temperature, ( $T_{SM}$ ), was given as follows:

$$\lambda_i = (0.09402 + (9.24 \times 10^{-5} \cdot T_{SM})) \quad (3.24)$$

Equation (3.24) was used in Equation (3.14) to calculate the temperature-time response curve for a number of steel beams insulated with Harditherm 700 and exposed to the standard fire. The results are presented in Figures 3.15 and 3.16.

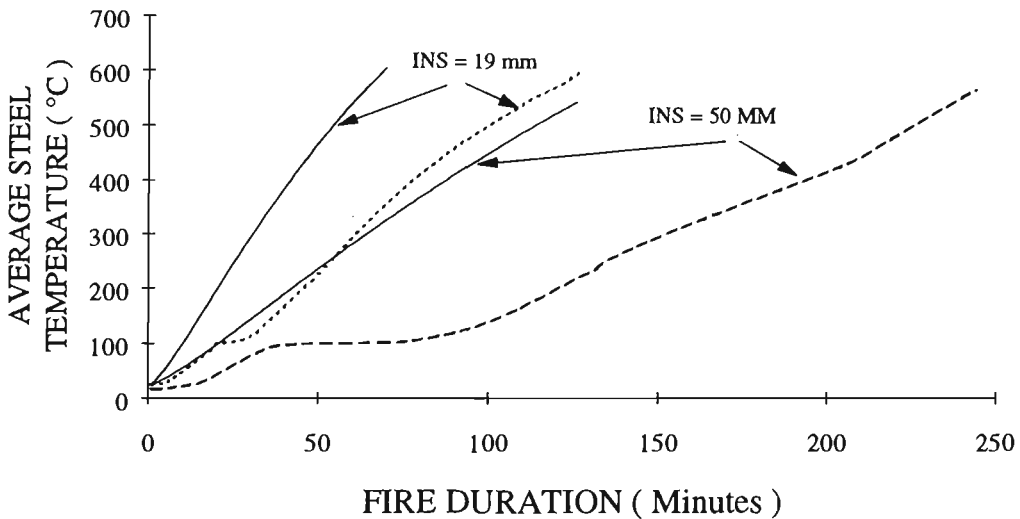


Figure 3.15: Comparison between experimental and calculated temperature-time curves in which Equation (3.24) was used to represent the thermal conductivity of the insulation - 3 - sided exposure. (Dashed line represents test data) -Author.

It is apparent from Figures 3.15 and 3.16 that use of Equation (3.24) does not result in an acceptable match between experimental and calculated temperature versus time curves.

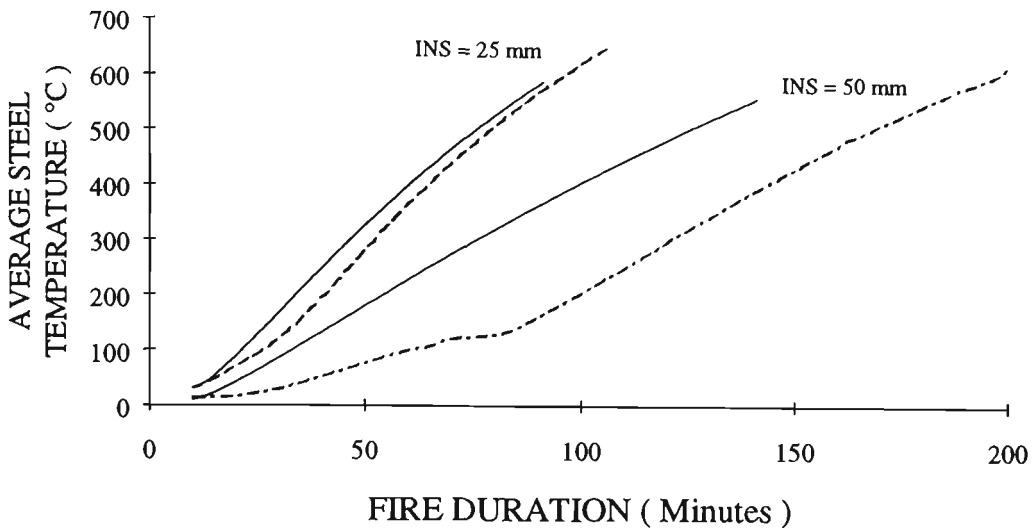


Figure 3.16: Comparison between experimental and calculated temperature-time curves in which Equation (3.24) was used to represent the thermal conductivity of the insulation - 4 - sided exposure. (Dashed line represents test data) - Author.

The poor result can in part be explained by the use of a constant value of thermal conductivity in the calculation. It was demonstrated in Figure 3.2 that use of a constant value for the thermal conductivity results in a significant increase (up to 9%) in the steel temperature. It was further demonstrated, Figure 3.7, that the presence of moisture in the insulating material can significantly alter the shape of the temperature-time curve leading to a significant increase in the time to heat the steel. Finally, variation in the exposed surface area to mass ratio is not specifically accounted for by Equation 3.24 rather it represents an average value of thermal conductivity derived from test results. The sections used in the calculation for Figures 3.14 and 3.15 represent an average value of ESM for beam sections of ~26. Temperature-time curves for sections with higher or lower ESM's would diverge from the experimental curves by an even greater amount. The discrepancies between the calculated and measured steel temperatures will have a significant effect on

both the estimate of probability of failure and time to failure when used in the simulation model.

### 3.6.2.3 Thermal Conductivity of Insulation - Derived From Test Data

As a consequence of the foregoing an alternative expression for thermal conductivity has been derived by correlation with experimental data based on the method described by Bennetts et al (1986).

The experimental data relates to steel beams box insulated with Harditherm 700 insulating material - refer Figure 3.14.

The slope of the steel temperature-time response curve at time  $t_i$  is obtained by calculation of the slope of the straight line joining data points at the beginning and end of the time interval under consideration, Figure 3.17. Two time intervals were tried,  $t_i \pm \Delta t$ ,  $t_i \pm 2\Delta t$ . There was little difference in the final expression for thermal conductivity obtained from using either time interval however the scatter associated with the longer time interval was reduced. The foregoing was a consideration in determining the magnitude of the modelling error to be attributed to thermal conductivity in the simulation model.

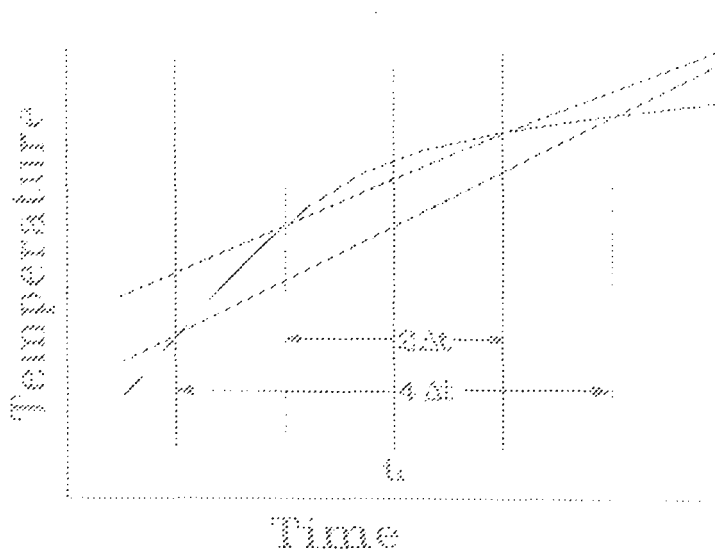


Figure 3.17: Method of calculating slope of temperature-time response curve - Author.

Equation (3.14) was used to derive an expression for thermal conductivity for temperatures greater than 100°C. Rather than use extrapolation to obtain an optimal value of moisture content, measured values of moisture content were used in conjunction with Equation (3.21) to obtain an expression for  $\lambda$  for steel temperatures up to 100°C. This differs significantly from the method of Bennetts et al (1986). The foregoing procedure was adopted because the variation in the measured moisture contents was relatively small (less than 15%) and the sensitivity of the temperature-time curve to variation in the values of thermal conductivity, due to variation in moisture content, was, contrary to the findings of Bennetts, small - refer Figure 3.18.

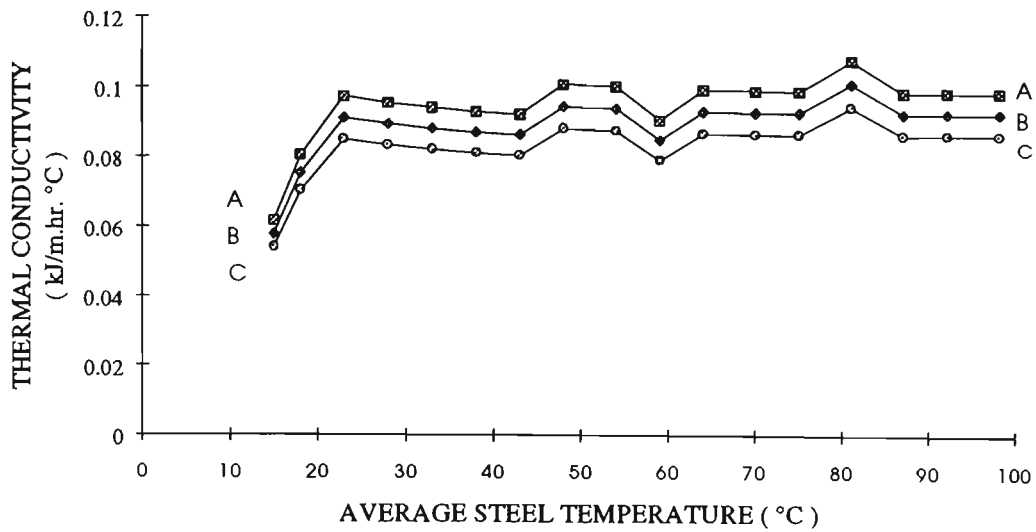


Figure 3.18: Variation in calculated thermal conductivity as a function of moisture content. B) - average moisture content. A) and C) - B)  $\pm$  30% - Author.

The variation in thermal conductivity as a function of temperature and exposed surface area to mass ratio is shown in Figures 3.19 and 3.20 for beams exposed to fire on four sides.

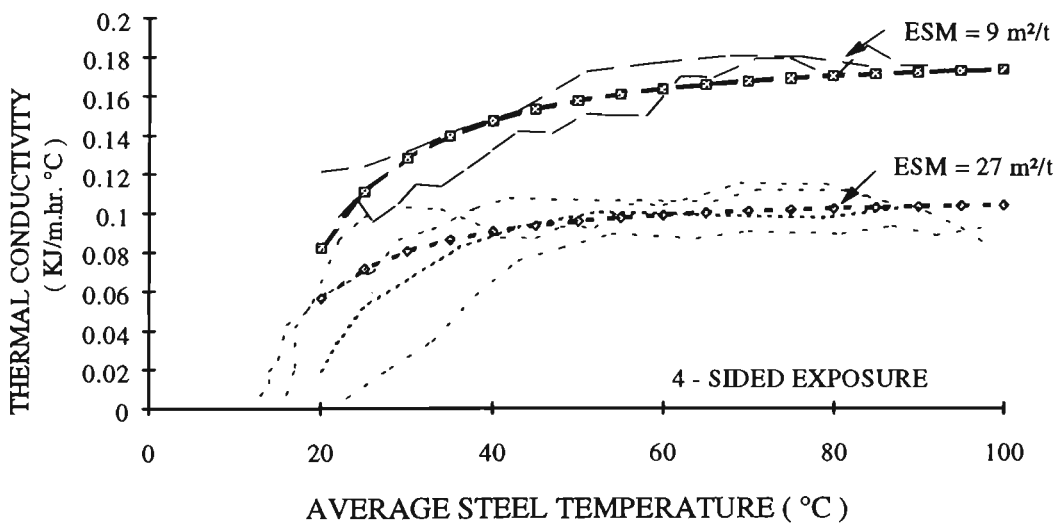


Figure 3.19: Values of thermal conductivity derived using experimental data in Equation (3.21) for temperatures up to 100 °C. Heavy line indicates modelled response - Author.

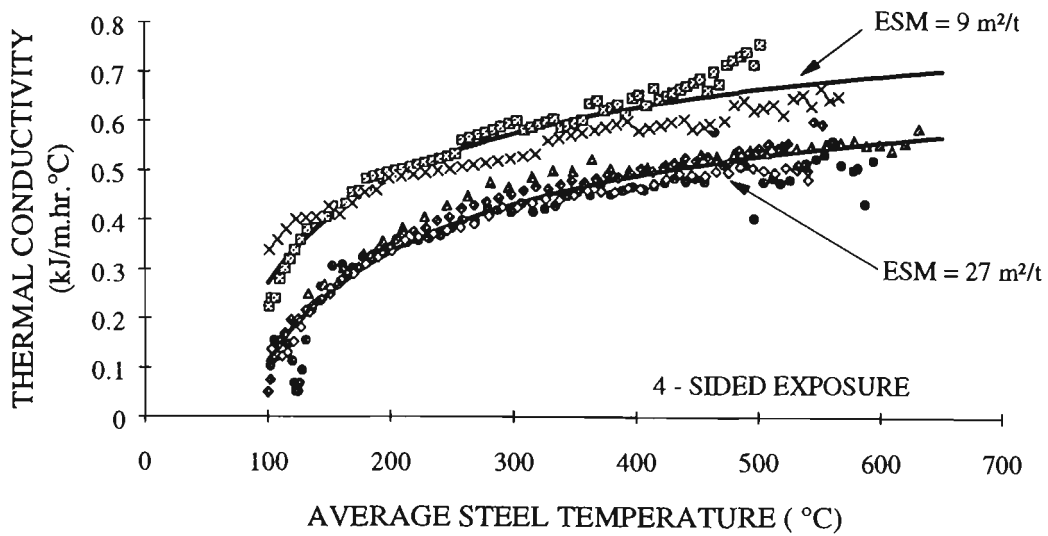


Figure 3.20: Values of thermal conductivity derived using experimental data in Equation (3.14) for temperatures over 100 °C. Heavy line indicates modelled response - Author.

The following expressions have been derived to represent the thermal conductivity ( $\lambda$ ) of Harditherm 700 insulation board in the calculation of the average temperature,  $T_s$ , of box protected steel beams exposed to fire on four sides.

Average steel temperature 0 - 100 °C

$$\lambda = 0.099 + \frac{6.84}{ESM^2} + \frac{(-4.31 - 382.53/ESM)}{T_s^{1.5}} \quad (3.25)$$

Average steel temperature >100 °C

$$\lambda = 0.8504 + \frac{11.03}{ESM^2} + \frac{(-6.94 - 0.023ESM)}{\sqrt{T_s}} \quad (3.26)$$

where  $ESM =$  mass to surface area ratio ( $m^2/tonne$ ).

Delay time due to presence of moisture is given by:

$$0.55 + 0.000135I^3 \quad (3.27)$$

where  $I =$  thickness of insulation (mm).

Equations 3.25, 3.26 and 3.27 are limited to sections in which the mass to surface area ratio lies between the values 9 and 40  $m^2/tonne$  and to thicknesses of insulation no greater than 50 mm.

The following expressions have been derived to represent the thermal conductivity ( $\lambda$ ) of Harditherm insulation board in the calculation of the average temperature of box protected steel beams ( $T_s$ ) exposed to fire on three sides.

Average steel temperature 0 - 100 °C

$$\lambda = 0.2977 - 0.0077ESM + \frac{\left(36.46 - 331.66/\sqrt{ESM}\right)}{T_s^2} \quad (3.28)$$

Average steel temperature >100 °C

$$\lambda = 0.592 - 0.015ESM + \frac{(2093.7 - 0.036ESM^3)}{T_s^{1.5}} + \frac{(-5332.7 + 0.103ESM^3)LnT_s}{T_s^2} \quad (3.29)$$

Delay time due to presence of moisture is given by:

$$0.497 + 0.0087I^2 \quad (3.30)$$

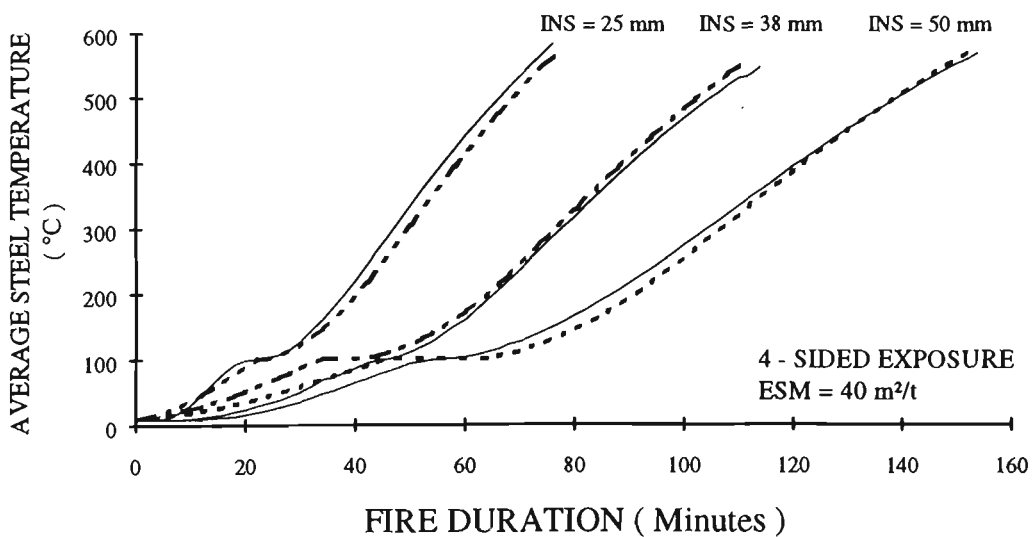
Equations 3.28, 3.29 and 3.30 are limited to sections in which the mass to surface area ratio lies between the values 6 and 27 m<sup>2</sup>/tonne and to thicknesses of insulation no greater than 50 mm.

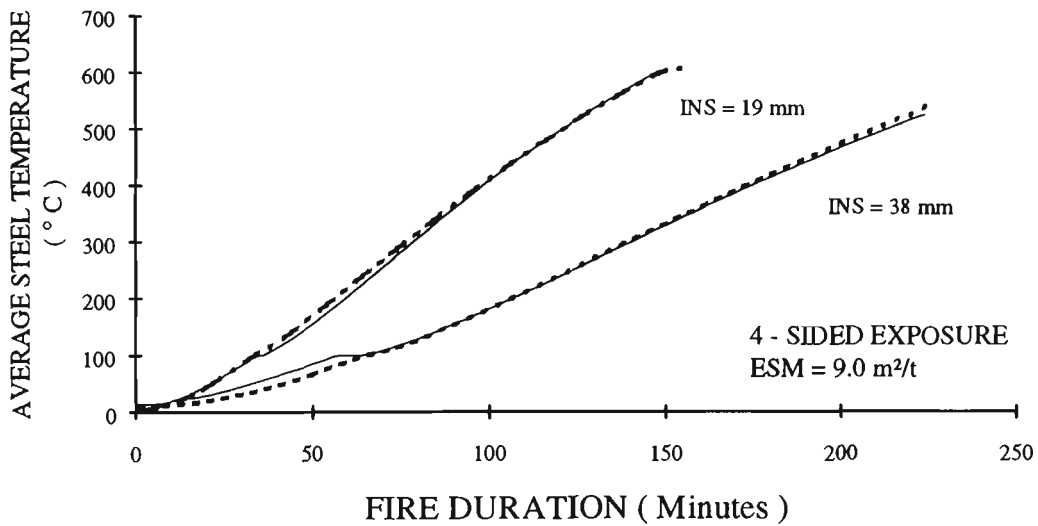
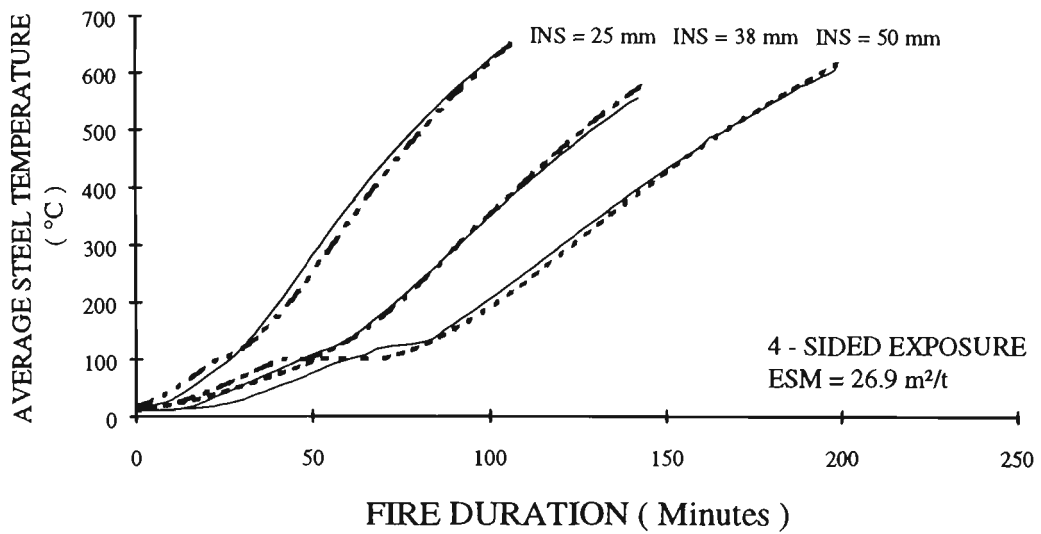
Equations (3.27) and (3.30), which determine the delay time due to moisture, were obtained by curve fitting rather than by the CTICM method described in sub-section (3.4.1.4) the results from which, when used in conjunction with Equations (3.25, 26, 28 and 29), proved to be inconsistent. The use of curve fitting is justified in that the CTICM Equation (3.22) is also based on correlation with experimental data and is very sensitive to the reference depth of the lumped heat. In both the CTICM method and ECCS method (Table 3.3) the delay time is calculated independently of the exposed surface area to mass ratio but requires a value for the thermal conductivity. The value of thermal conductivity obtained from the equations derived above however is a function of the exposed surface area ratio. It is recognised that there is no connection between these two variables and that the derived expressions for thermal

conductivity are correlating terms in order to match experimental data. As such the derived values are inappropriate for use in either Equation (3.22) or Table 3.3.

### 3.6.2.4 Comparison between calculated steel temperature-time curve and experimental test data - insulated steel

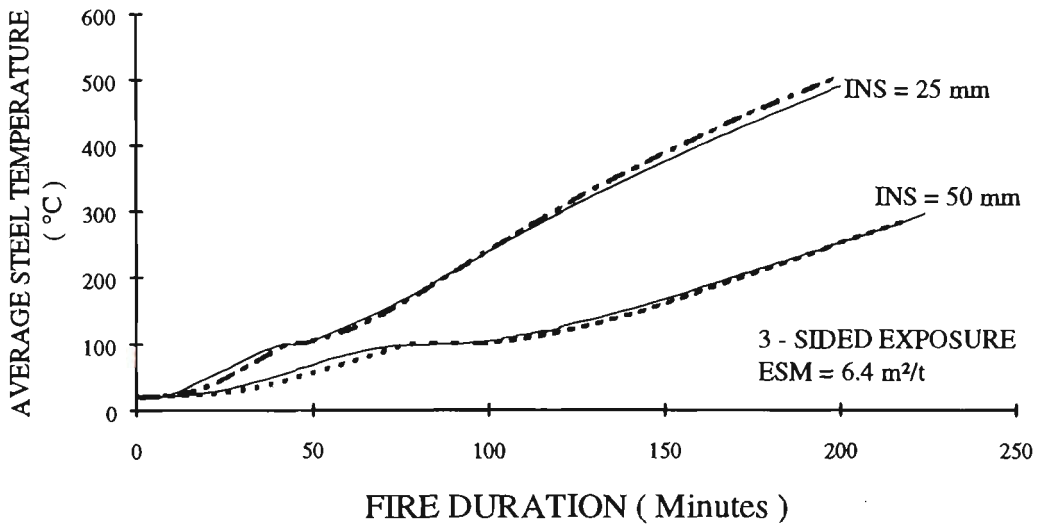
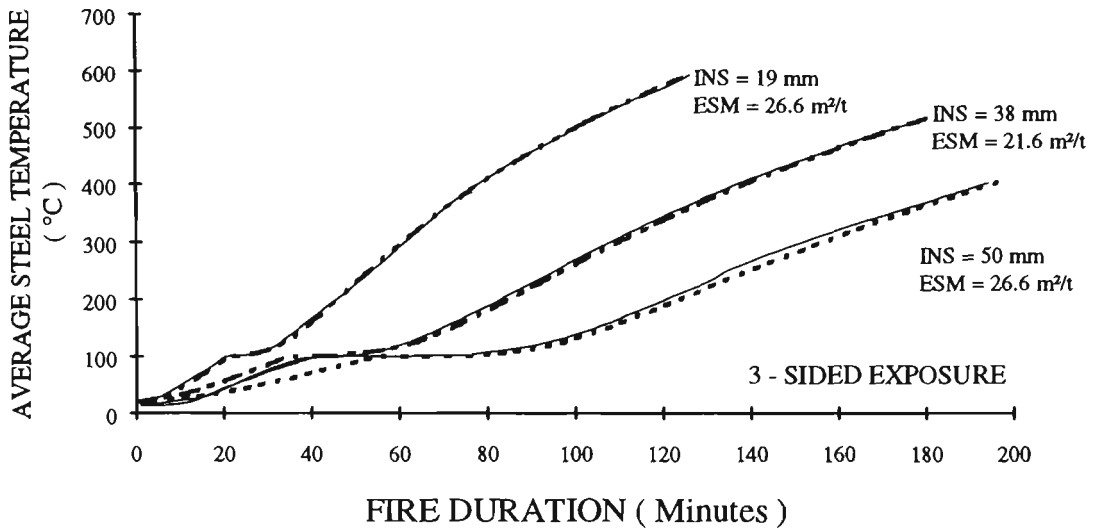
A comparison between measured and calculated steel temperatures using Equations (3.14) and (3.21), in which the thermal conductivity is given by Equations (3.25, 26 and 27), is given in Figures 3.21, 3.22 and 3.23 for a range of insulation thicknesses and mass to surface areas for beams exposed to fire on four sides.





Figures 3.21, 3.22 and 3.23: Comparison of modelled (solid lines) and measured (dashed lines) temperatures of insulated steel beams exposed to fire on four sides for a range of insulation thicknesses (INS) and mass to surface area ratios (ESM). Beams box protected with Harditherm 700 insulation board Author.

A comparison between measured and calculated steel temperatures using Equations (3.14) and (3.21), in which the thermal conductivity is given by Equations (3.28, 29 and 30), is given in Figures 3.24 and 3.25. for a range of insulation thicknesses and mass to surface areas for beams exposed to fire on three sides.



Figures 3.24 and 3.25: Comparison of modelled and measured temperatures of insulated steel beams exposed to fire on three sides for a range of insulation thicknesses (INS) and mass to surface area ratios (ESM). Beams box protected with Harditherm 700 insulation board - Author.

### 3.7 Conclusion

The use of the derived expressions for thermal conductivity result in very good agreement between the calculated temperature versus time curves and the

test data. Although the test data is based on exposure to the standard fire it has been demonstrated in Section (3.5.1.4) that the simplified method can be used to predict the temperature versus time curve of steel sections exposed to real fires.

## **CHAPTER FOUR**

### **MECHANICAL PROPERTIES SUBMODEL**

## 4.0 Introduction

During fire the mechanical properties of steel are affected by its temperature. The effect of change in the mechanical properties of steel on the structural performance of a particular member will depend on the forces in the member due to the action of applied loads, conditions of support and whether the member is axially restrained.

The present study is limited to failure of simply supported, axially unrestrained steel beams in bending. As will be demonstrated in the next chapter the strength of a beam in bending can be predicted by application of simple plastic theory using the two parameters section modulus ( $S$ ) and yield strength ( $F_{sy}$ ). As a consequence of the foregoing only a knowledge of the variation in the yield strength of steel with temperature is required in order to predict the strength of steel beams in bending at elevated temperature.

The chapter commences with a review of the stress-strain relationship of structural steel at elevated temperature and examines the influence of the particular method of measuring the strength of steel at elevated temperature has on proposed strength-temperature relations. Recommended strength reduction curves for structural steel are reviewed and a relationship, based on test data, is presented which predicts the change in strength of Australian structural steel as a function of temperature.

## 4.1 Mechanical Properties of Steel

All of the mechanical properties of steel are strongly influenced by temperature. These include yield strength, modulus of elasticity and coefficient of thermal expansion. As the temperature of steel increases changes occur in the crystalline structure of the steel which effect its behaviour. For the carbon steels typically used in buildings construction in Australia the changes in crystalline structure occur at temperatures greater than 600 - 650 °C [Jeanes, 1980]. Under normal loading a beam is likely to be close to failure or to have failed before such temperatures are attained. Changes in the crystalline structure therefore are ignored in fire engineering design.

### 4.1.1 Stress - Strain at Room Temperature

Two modes of behaviour are evident when a steel specimen is subject to an axial load in a tensile testing machine. On removal of the load, the elongation disappears - the steel displays an elastic response. If, on the other hand, there is residual elongation, the material has exhibited a plastic response. The elastic limit is reached at a strain of approximately 0.15% , the corresponding stress is defined as the yield stress,  $F_{sy}$  . Up to this point the stress is proportional to the strain, the ratio of the stress to strain defines the elastic modulus (E) [Lay, 1982].

## 4.1.2 Stress - Strain at Elevated Temperature

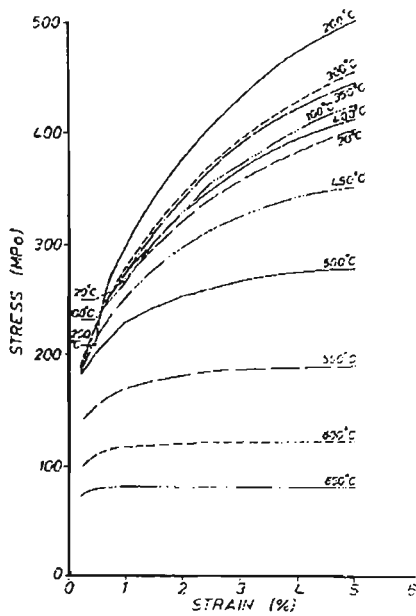


Figure 4.1 - Variation with temperature of the stress-strain curve of Australian Grade 250 steel.

Results from steady state tensile tests on Australian Grade 250 steel show that as the steel is heated above a temperature of approximately 200 °C, its yield stress reduces by about 15% and the tensile strength increases. The strain increases for a given stress and the slope of the initial part of the stress - strain graph reduces.

The elastic modulus therefore reduces with increasing temperature. At elevated temperature (above 300 °C) the clearly defined yield point disappears, refer Figure 4.1. In its place a softly rounded yielding transition develops and the tensile strength progressively decreases [Stevens et al., 1971]. Similar results have been reported for American [Harmathy & Stanzack , 1970], Japanese [Furamura et al., 1985] and British steels [Jerath et al., 1980].

## 4.2 Measurement of Stress-Strain Relationships

Analytical models describing the behaviour of steel at high temperature are based on test data of stress and deformation characteristics at different temperatures. The material properties measured in tests are closely related to

the method used [Anderberg, 1988]. There are a number of testing procedures from which the variation of flow of stress of a steel sample at elevated temperature can be obtained. These can be arranged as transient heating tests and steady state tests.

#### **4.2.1 Steady State Tests**

Steady state tests are often referred to as isothermal. In such tests the unloaded sample is heated at a predetermined rate until thermal equilibrium is attained at the required reference temperature. Depending on the information required, the sample is either stressed or strained at a uniform rate while the resulting elongation or load is recorded. A family of load-elongation relationships can be obtained by repeating the test at different reference temperatures as shown in Figure 4.1.. In stress-rate controlled tests the strain measured before the load is applied corresponds to the thermal strain. Such tests are usually terminated when the 0.2% proof strain is reached. If a specimen is maintained at constant temperature and constant load the creep strain can be measured however in stress rate controlled isothermal tests the stress-strain relationship is often obtained at a high rate of loading whereby the maximum load is applied within one to two minutes thereby avoiding the effect of creep.

### **4.2.2 Transient Heating Tests**

Transient heating tests are often referred to as anisothermal. In these the load on the steel specimen is maintained constant while the temperature of the specimen is increased at a constant rate. A family of strain versus temperature curves are obtained in which each curve corresponds to an applied stress. Heating rates and duration of exposure experienced in real fires can be simulated using this method of testing. As a consequence the effect of high temperature creep is automatically accounted for. Tests carried out under transient conditions are considered to represent the behaviour of structures in fire, and thus provide data of direct relevance to evaluating mechanical properties of steel at elevated temperature.

Information derived from transient heating tests are presented in two forms:

- a) as a series of derived stress/strain curves at elevated temperature;
- b) as a relationship between the ratio of the elevated temperature stress to the yield stress at 20 °C.

### **4.3 Models of Stress-Strain Relationships**

Models by which the stress/strain relationship of steel at elevated temperature are described can be categorised as those that include the effect of creep explicitly, those in which the effect of creep is included implicitly and finally

those that ignore creep. Creep is the change in strain which occurs in a member under constant load conditions. This categorisation by 'creep' reflects the nature of the test data used to derive the model and the intended use for the model.

Sophisticated models that include the effect of creep explicitly [Harmathy, 1967], [Thor, 1973] and [Anderberg, 1983] use the concept of temperature-compensated time proposed by Dorn [1954]. Furamura et al. [1985] presents a creep model for Japanese steel SS41. The model by Thor was used to establish critical steel temperature as a function of load for use in the Swedish manual for the Fire Engineering Design of Steel Structures [1976]. The model by Anderberg is incorporated in to the structural computer package Steelfire [1988 ].

Models of stress-strain relationships that include the creep explicitly are based on the combined results of different steady state tests. Strain at transient high temperatures comprises three components defined by the constitutive equation:

$$\varepsilon = \varepsilon_{th}(T) + \varepsilon_{\sigma}(\sigma, T) + \varepsilon_{cr}(\sigma, T, t) \quad (4.1)$$

where

$\varepsilon_{th}$	=	thermal strain
$\varepsilon_{\sigma}$	=	instantaneous stress related strain
$\varepsilon_{cr}$	=	creep strain

A linear relationship between thermal strain and temperature is generally assumed, the type and strength of the steel having little influence [Anderberg, 1988].

Analytical descriptions of instantaneous stress-strain curves as a function of temperature derived from steady state tests can be approximated by either a number of straight lines, two straight lines connected by an ellipse [Purkiss, 1988] or by a modified expression of Ramberg and Osgood [1943] as used by Magnusson [1974].

Creep strain measured in steady state tests is used in order to predict the contribution of creep during transient heating conditions. Variation in load resistance at transient high temperature can be accounted for in such models by considering strain hardening.

It has been demonstrated by Anderberg, [1988] that models based on steady state heating tests can satisfactorily predict total deformation as a function of temperature and load level in a transient heating test when load levels are low. Significant discrepancies occur however between modelled results and test data at high load level due to an instability phenomenon peculiar to transient heating tests. Since load levels on beams rarely exceeds 60% of capacity in load resistance factored design (LRFD) and will be less during fire, the discrepancies at high load level can be ignored.

Simpler analytical models of stress-strain relationships at elevated temperature that include the effect of creep implicitly are used in computer structural models such as "STABA-F" [1984] and CEFICOSS [1990] in which finite element methods are used to calculate the distortion of frames and sub-assemblies, restraining forces and member capacities. Such material models are based on the results of transient heating tests performed at a particular heating rate in which the effect of thermal strain has been isolated and considered independently. It has been demonstrated that the magnitude of creep strain is influenced by the rate of heating of the steel [Skinner, 1970]. Heating rates can vary widely due to different fire exposures, presence and thickness of insulation material and type of fuel. As a consequence, models in which creep is included implicitly will only account for the effect of creep in an approximate way.

In both the British code of practice for fire resistant design BS 5950: Part 8 [1990] and the Commission of the European Communities EC3: Part 10 [1990] the materials models are based on the results of transient heating tests. The British model is based on the results of a major anisothermal tensile-testing programme in which the performance of structural steels were evaluated for a range of heating rates (2.5 to 20 °C/min) and range of applied stress. In the case of the EC 3 the materials model is based on the results of anisothermal tests on large scale models using scales of 1:4 to 1:6. in which simply supported beams were subject to a range of load ratios (the ratio of actual load to ultimate load-bearing capacity at normal temperature) varying from 0.85 to 0.05 and heating rates varying from 2.67 to 32 °C/min [Rubert et al. 1985].

The complete stress/strain behaviour was derived numerically from the measured deflections

#### **4.4 Models of Variation of Steel Strength with Temperature**

A number of relationships have been proposed that describe the decrease in yield stress with increase in temperature. These are shown in Figure 4.2 and are for the American ASTM A36 steel [Lie and Stanzak, 1974], European regional organisation ECCS [1979], National Research Council of Canada [Lie, 1992], British BS4360 Grade 43 [Jerath et al., 1980], French statutory body CTICM [1976] and Australian Grade 250 steel [Bennetts et al., 1981].

It is apparent from Figure 4.2 that models of loss in strength as a function of temperature vary widely. This is due to in part to variation in the chemical composition of the individual steels used in the tests, the manner in which the steels were processed and whether the steel is strain aged. More importantly much of the variation in the strength models is attributable to differences in choice of strain at first yield, load rate and rate of increase of temperature.

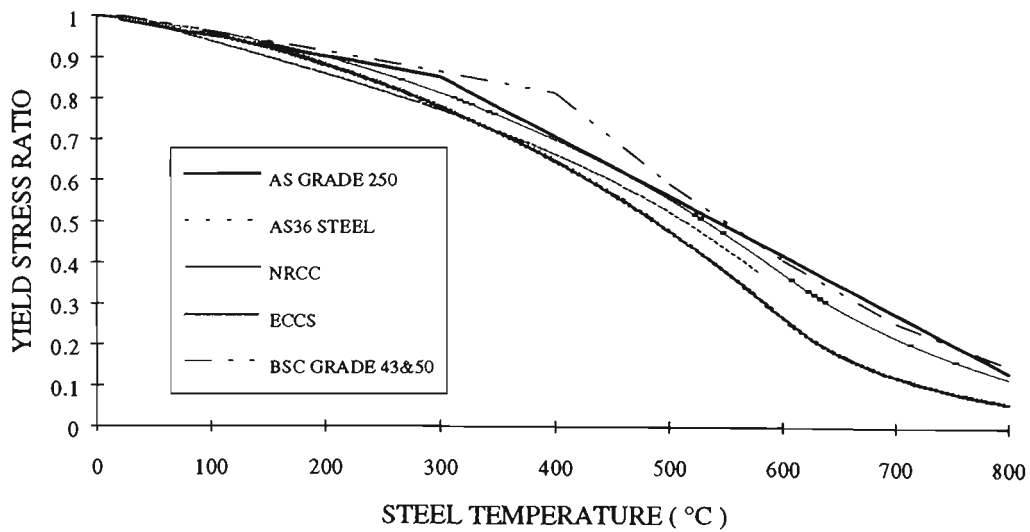


Figure 4.2 Various proposed yield stress reduction models.

Models of variation in yield strength of steel as a function of temperature were derived directly from tensile tests or indirectly from established stress/strain relationships as follows:

- a) steady state tests conducted at very high rate of loading or high rate of strain - creep strain not accounted for.
- b) steady state tests conducted at very low rate of loading or low rate of strain - creep strain accounted for implicitly.
- c) derived from constitutive models based on steady state data - creep strain accounted for explicitly.
- d) transient heating tests - creep strain accounted for implicitly.

Two issues arise from a consideration of the source of the data used in the model:

- a) has the effect of creep been accounted for.
- b) the value of reference strain at which the strength of the steel was assessed.

#### 4.4.1 Influence of Creep and Heating Rate on Time and Temperature of Steel at Collapse

Creep is only present at significant levels in steels under high temperature conditions, that is, at temperatures in excess of 400 °C [Malhotra, 1982]. The occurrence of creep means that the deformation and collapse behaviour of a steel structure depends on the load history and the shape of the fire temperature time curve to which it is subjected. The more highly loaded the member and the longer the high temperature exposure, the greater is the creep effect. This is demonstrated in Table 4.1 which shows the variation in steel temperature from a series of transient tests at a reference strain of 1 % for a range of heating rates [Skinner, 1970].

STEEL TEMPERATURE C				
STRESS LEVEL	HEATING RATE ( °C/min)			
	1.67	4.2	10	30.0
0.33 $F_{sy}$	632	645	671	696
0.66 $F_{sy}$	542	-	574	610

Table 4.1 - Variation in steel temperature at 1% strain for a range of heating rates and two levels of stress, ( AS 1205 Grade 250 steel).

It can be deduced from Table 4.1 that when steel is heated slowly, creep strain has a longer duration over which to develop, therefore the higher the rate

of increase in the strain rate. This results in the strain in the steel being larger at a given temperature than if creep were ignored.

The extent to which the maximum temperature at which the 1% plastic strain is attained is dependent on the heating rate, has been estimated by Kirby [1988]. By combining the results of British tests with that of others [Skinner, 1972], [Copier, 1972] and [Ruge, 1980], he shows that relative to the 10 °C/min heating rate an increase of 10 °C/min increases the temperature at which 1% strain is achieved by 15 °C. The European Code for structural Steelwork, EC3 [1990] strength reduction model represents the lower limit of heating rates (2.67 °C/min) investigated during testing. A model based on the higher heating rate investigated (32 °C/min) would be less conservative, resulting in a shift along the temperature axis of approximately 40 °C.

It has been demonstrated [Magnusson et al., 1976] that the increase in the maximum steel temperature at the time of first yield for the extreme case of a lightly insulated steel beam compared with the case of a heavily insulated steel beam is 20 °C. The heating rate of steel subject to the standard fire varies between 50°C/min (non and lightly insulated members) and 5°C/min (heavily insulated members) [Twilt, 1988]. Therefore considering that heavily insulated steel is most likely to suffer most creep, the calculated critical temperature of steel at collapse is likely to be overestimated by 20 °C if the reduction in  $F_y$  due to creep is ignored. The time of failure would be overestimated by four minutes. This data suggests that creep does not have a substantial effect on time to failure. Thus it can be concluded that the deformation behaviour and hence the collapse temperature of beams is not significantly influenced by the

rate of temperature rise providing that the above mentioned rates of heating are not exceeded and that the maximum steel temperature does not exceed 600°C [Witteveen, et al., 1977] and [Knight, 1975]. Table 5.1 shows however that for the case of a lightly loaded steel beam the temperature exceeds 600 °C for all heating rates.

The influence of creep on the deformation of a fire exposed steel beam has been reported by Anderberg [1988]. When the effect of creep is ignored the time to collapse is increased by 19 %, from 17.2 - 20.4 minutes and the temperature at failure is increased from 700 °C to 760 °C.

The heating rates of steel in real mixed fuel fires can be as high as 80 °C/min [Lathem, 1987]. Thus in real fires creep is even less of an issue. The short duration of real fires does not give creep strains time to develop.

It can be concluded that strength reduction models in which the influence of creep is accounted for will predict a more rapid loss of strength for temperatures greater than 400 °C than those models in which creep is ignored. It can also be concluded that some of the variation in the published strength reduction models is likely to be attributable to the use of data derived from tests performed at different rates of heating and whether, if creep effects have been included, they have been included implicitly or explicitly. The use of transient heating tests performed at low rates of heating as a source of data for strength reduction models are a conservative alternative to steady state tests, which do not include creep effects, and transient heating tests that use high rates of heating, both of which raise the critical temperature.

The effect of creep on the time to failure of a steel beam exposed to real fire has been shown to be a second order consideration. Given the desired

accuracy of the project as declared in subsection ( 1.1.2), the inclusion of a model that takes into account the effect of creep is not warranted.

#### 4.4.2 Effective Yield Stress of Steel at Elevated Temperature

It was noted previously (Subsection 4.1.2) that at elevated temperature the onset of yield occurs over a band of strain value rather than sharply defined at a single value of strain as occurs in ambient conditions. In order to apply elementary plastic theory it is necessary to define an arbitrary point on the stress-strain curve which marks the transition from elastic to plastic behaviour of the steel. This is done by specifying a plastic strain at which the effective yield stress is determined. The choice of strain has a significant effect on the shape of the yield strength reduction curve. A consistent and widely used method of defining the yield point of steel, [Lay, 1982], both at ambient and elevated temperature, is to adopt the concept of proof stress, more specifically an arbitrary plastic strain of 0.2%.

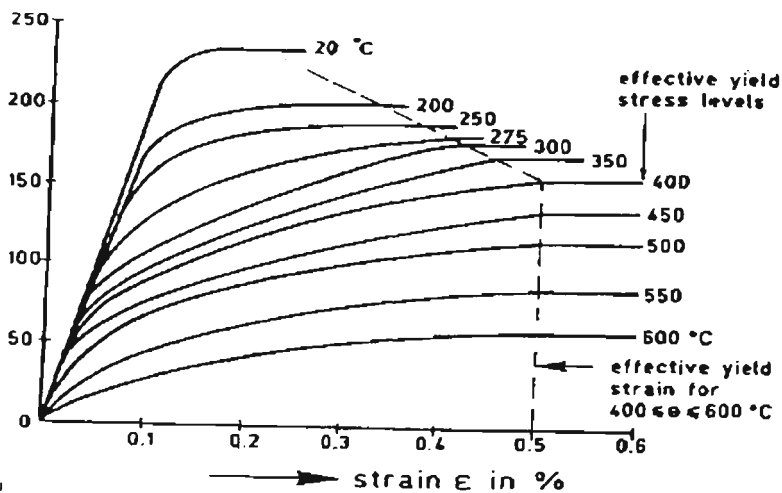


Figure 4.3: Stress-strain curves at elevated temperature for Fe 360 steel [ECCS, 1983].

In the ECCS [1983] recommendations the "effective yield stress" is arbitrarily defined as the total strain beyond which, the stress is constant with strain. This is demonstrated in Figure 4.3 for Fe 360 steel. The effective yield stress is reached at a total strain of 0.16% at ambient temperatures, increasing to 0.5% total strain for steel temperatures  $> 400$  °C. The European Code for structural Steelwork, [EC3, 1990] has adopted a value equivalent to 2% total strain at which to determine the effective yield stress.

The strain at which the effective yield stress of the steel is derived has a significant effect on the shape of the strength reduction curve. This is demonstrated in Figure 4.4 in which the ECCS [1983] recommendation is compared with four strength reduction models derived from the stress-strain relationships of steel given in EC3 [1990]. The four models correspond to the effective yield stress ratio as a function of temperature for strains of 0.2, 0.5, 1.0 and 2.0 %.

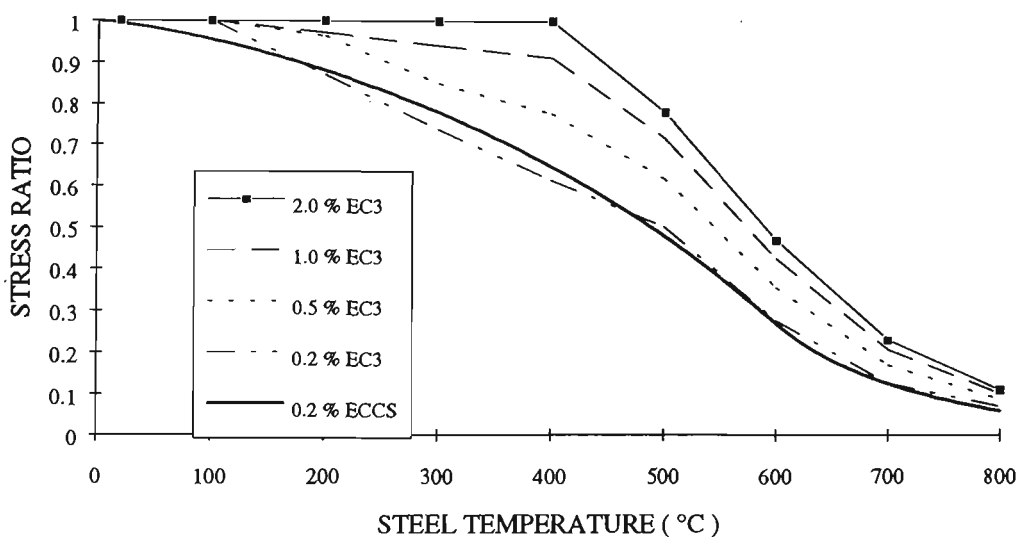


Figure 4.4: Reduction in effective yield stress, expressed as a ratio of yield stress at ambient conditions, for a range of strains at first yield from ECCS [1983] and EC3 [1990].

Between 500 - 600 °C, the temperature at which beams generally fail in fire, the predicted loss of effective stress determined using 0.2% strain, results in a 24 % reduction in the load carrying capacity of the beam than if the 2.0% strain was used. At 400 °C, the temperature at which a heavily loaded beam in fire may be expected to fail, the difference is approximately 38%.

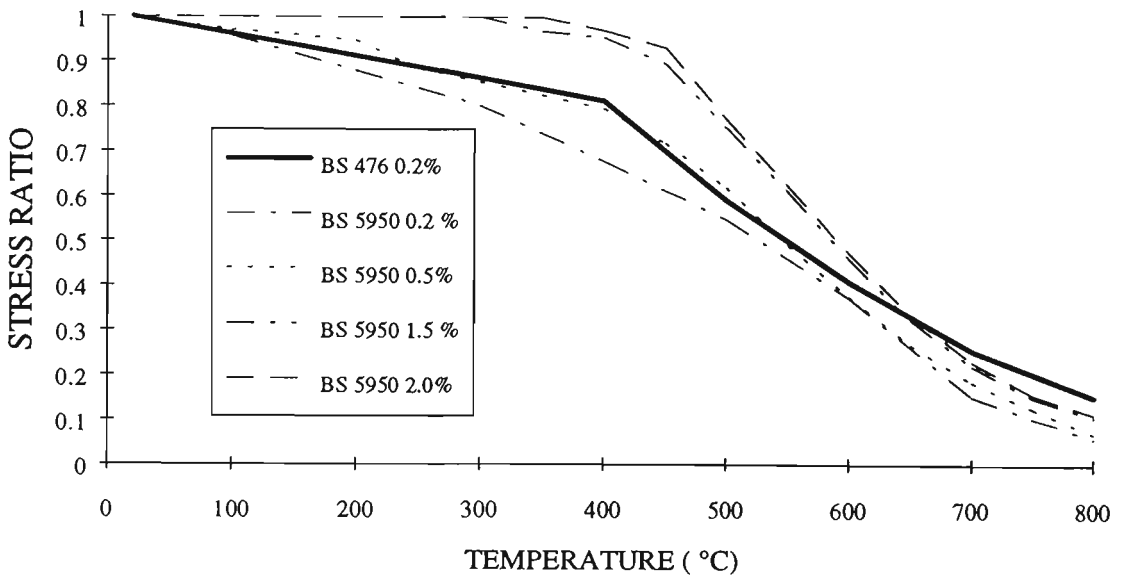


Figure 4.5 - Reduction in effective yield stress, expressed as a ratio of yield stress at ambient conditions, for a range of total strains from British Standards BS 476 [1972] and BS 5950 [1990], (combined Grades 43 and 50 steel sections).

A comparison of strength reduction models from the superseded British Standard BS 476 [1972] and the current code of practice for fire resistant design BS 5950 [1990] show a similar range of values for  $F_y$ , refer Figure 4.5.

It has been accepted practice to use the 0.2% proof strain to define the yield stress. The reason for this is essentially historical in that the relatively simple steady state tensile test requires a reference strain at which to terminate the test [Skinner, 1970]. A value of 0.2% strain had traditionally been used in tension tests at ambient temperature and had resulted in predictions of failure in

bending of steel beams that were in accordance with test results. Tension tests at elevated temperature accordingly adopted this value. Adoption of this value of strain to define the effective yield stress has been justified in that it is a conservative approach which will ensure that at any temperature the corresponding yield stress will be lower than that which would be obtained if the yield stress was associated with a higher proof stress [Bennetts et al. 1981].

A number of studies on the elevated tensile properties of Australian [Skinner, 1970], German [Rubert and Schaumann, 1986] and British [Kirby, 1988] steels demonstrate there is a dramatic change in strain rate during transient tensile tests. Figure 4.6 shows that, irrespective of the applied load, once a total strain of 1% is reached, a small increase in temperature results in large rates of strain due to the rapid emergence of creep strain. During standard fire resistance tests of beams, strains of approximately 2 - 3% have been recorded at the centre of the tensile flange when the deflection attains the limiting value ( $\text{span} / 30$ ) [Kirby, 1988]. It is apparent that when the strain in the tensile flange of a steel beam reaches 1% imminent failure could be expected with a relatively small further rise in temperature. It is because of this close correlation between structural instability and strain that in the two most recent codes of practice for fire resistant design, BS 5950, Part 8 [1990] and Eurocode No 3 [1990], values of strain of 1.5% and 2% respectively have been adopted at which to determine strength reduction factors for non-composite members in bending.

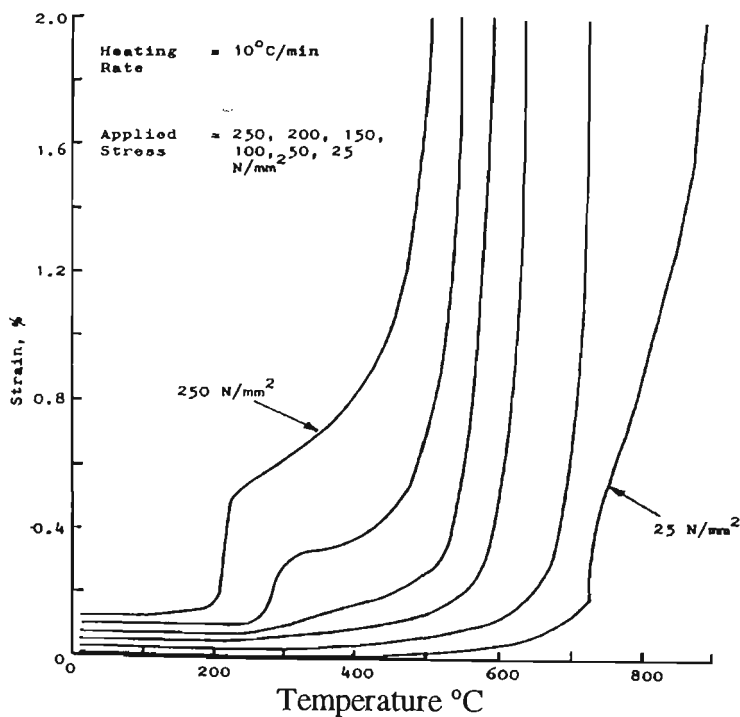


Figure 4.6: Tensile curves for a Grade 43A steel derived from transient tests [Kirby, 1988]

The practical implications of differences in material models has been investigated by Twilt [1988], in which the a comparison is made between models based on ECCS [1983] and data used in the draft British Standard 5950 [1985]. The critical steel temperature (the temperature at which the applied stress equals the temperature affected member capacity ) calculated using a mechanical model for British steel in which the stress at the beginning of yield of steel is determined at 0.5% strain, is 55 °C lower than if the model using the 1% strain was used. Assuming heating rates of steel of 5 - 50 °C/min there is a maximum increase of 11 minutes in the fire resistance period by adopting the model based on the 1% strain. According to Twilt this would result in an approximate increase in thickness of insulation by 20%. A comparison between ECCS and British steel based on 0.5 % strain differed by as much as 100 °C. The seemingly significant difference in critical temperature however translated to an increase in the fire resistance time of five minutes. The author concluded that despite large differences in the value of strain at

which to determine the effective yield stress, for practical situations, these differences do not lead to significant differences in time of failure. Therefore design should be based on time of failure which is insensitive to stress ratio, rather than ensuring steel temperatures are less than some critical value which is very sensitive to the variety of  $F_y$  values recommended in the literature.

It has been demonstrated that models of stress ratio based on higher proof stress differ significantly in shape in comparison with curves based on the 0.2% proof stress. Stress ratio models in which higher proof strains are used result in higher critical steel temperatures and as a consequence, increase the fire resistance period of the steel, depending on the rate of heating, by a few minutes. The use of higher proof stress is justified in that it better predicts structural instability while a lower proof stress would prescribe a lower yield stress and underestimate maximum structural resistance.

Much of the information available on the change in strength of steel when exposed to high temperatures relates to steel subject to steady state heating conditions. It is argued that data based on tests which simulate the thermal exposure to which members are exposed in real fire should be used to derive models of loss of strength with increase in temperature. The two most recent codes of practice for fire resistant design, BS 5959, Part 8 [1990] and Eurocode No 3 [1990] have adopted models based on transient heating conditions in which creep effects are accounted for and realistic strains are used to define effective stress. Such models are better suited for realistic predictions of likelihood of failure and time to failure of fire exposed steel beams. These models further reduce the need to consider creep and facilitate simple and accurate design.

## 4.5 Strength Reduction Model for Australian Steel

### 4.5.1 Current Model

A strength reduction model for Australian steel is based on data obtained from steady state temperature tension tests conducted by Australian Iron and Steel (AIS) and by Melbourne Research Laboratories (MRL) [Bennets et al.,1981] on samples taken from Grade 250 plate and on tests on British Grade 43 steel [BSC, 1980]. The British Grade 43 steel is virtually identical in composition and method of manufacture to that of the Australian Grade 250 steel.

A linear regression was conducted on the combined British Grade 43 and Australian Grade 250 data. Only data points falling within the range 300 - 700 °C were used as this is the range over which the variation of the stress ratio with temperature is nearly linear. The recommended stress ratio - temperature relationship, based on the lower 95% confidence limit to the least squares fit, is given by the following:

$$\begin{aligned} \frac{F_{Y_{T_s}}}{F_{Y_{20}}} &= 1 - \frac{T_s}{2000}, & 0^\circ C < T_s < 300^\circ C \\ \frac{F_{Y_{T_s}}}{F_{Y_{20}}} &= \frac{(895 - T_s)}{700}, & 300^\circ C < T_s < 895^\circ C \end{aligned} \quad (4.2)$$

where

$$\begin{aligned} T_s &= \text{steel temperature } C \\ F_{Y_{T_s}} &= \text{yield strength at temperature } T_s \end{aligned}$$

The Australian model in Equation 4.2 is compared with alternative strength reduction curves in Figure 4.2.

The Australian strength reduction curve given in the Australian Steel Code AS 4100 [1990] is given as:

$$\frac{F_{YT_s}}{F_{Y20}} = 1.0 \quad , \quad 0^\circ C < T_s < 215^\circ C$$

$$\frac{F_{YT_s}}{F_{Y20}} = \frac{(905 - T_s)}{690} \quad , \quad 215^\circ C < T_s \leq 905^\circ C \quad (4.3)$$

This is a slightly simpler version of Equation (4.2) and corresponds to the mean value linear regression of the same data on which Equation (4.2) was based. Equation (4.3) is the adopted expression for use in calculating the period of structural adequacy (PSA) for those structural members required to satisfy the requirements of the Building Code of Australia. Both models are shown in Figure 4.7.

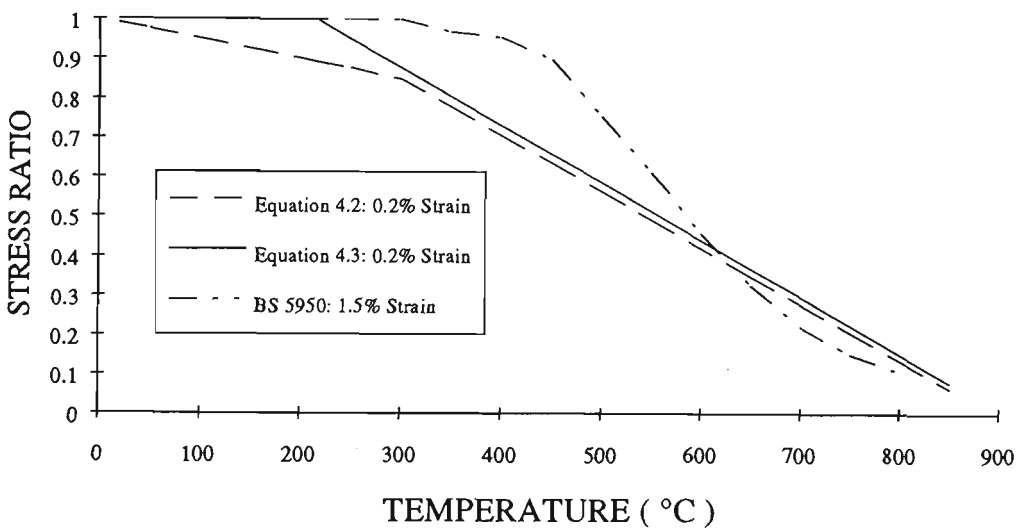


Figure 4.7 - Comparison between strength reduction models based on Equations (4.2) and (4.3) and that given in BS 5950: Part 8.

The strain rates used in the Australian tests were very low, varying from 2 to 17 millistrain per minute. As a consequence some allowance for creep is accounted for implicitly. This allowance is considered adequate, as the period for which the steel is maintained at temperatures in excess of 400 °C, during

exposure to a 4 hour standard fire-resistance test, is not sufficient to justify an explicit allowance for creep [Proe, 1989]. The strength reduction model is based on the 0.2% proof stress. It has been demonstrated in Sub-section (4.4.2) that use of the 0.2% proof strain is very conservative. Since the Australian model is based, in part, on British test data it is suggested that a model for Australian steel based on transient heating and higher proof strain would be similar to the model given in BS 5950, Part 8 for Grade 43A steel. A comparison between the Australian models and the British model is shown in Figure 4.7.

#### **4.5.2 Alternative Strength Reduction Model**

The mechanical properties of steel at elevated temperature may vary due to differences in chemical composition or manufacturing process. Because of this individual steels may require a separate strength reduction model. In Eurocode EC3: Part 10 a [1990] alternative models are given for Fe 360 and Fe 510 steels whereas in BS 5950: Part 8 [1990] for grades A43 and A50 steels a single strength reduction model is given.

The Australian Standard AS 4110 is applicable to steel members for which the value of yield stress used in design does not exceed 450 MPa. It is implicit that the model of variation of yield stress with temperature given in Section 12 of AS 4100, Equation (4.3), which is based on Grade 250 and A43 steel, is considered suitable for grades of steel other than Grade 250.

The results from seventy one steady state tensile tests of samples of Grade 350 plate and samples taken from the web and flanges of Grade 350 universal section have been combined with the Grade 250 and A43 data and is shown in

Figure 4.8 A statistical analysis of the Grade 250 and 350 data demonstrated no significant difference between the two sets of data. The Grade 350 data provides additional data in the temperature range 200 - 500 °C.

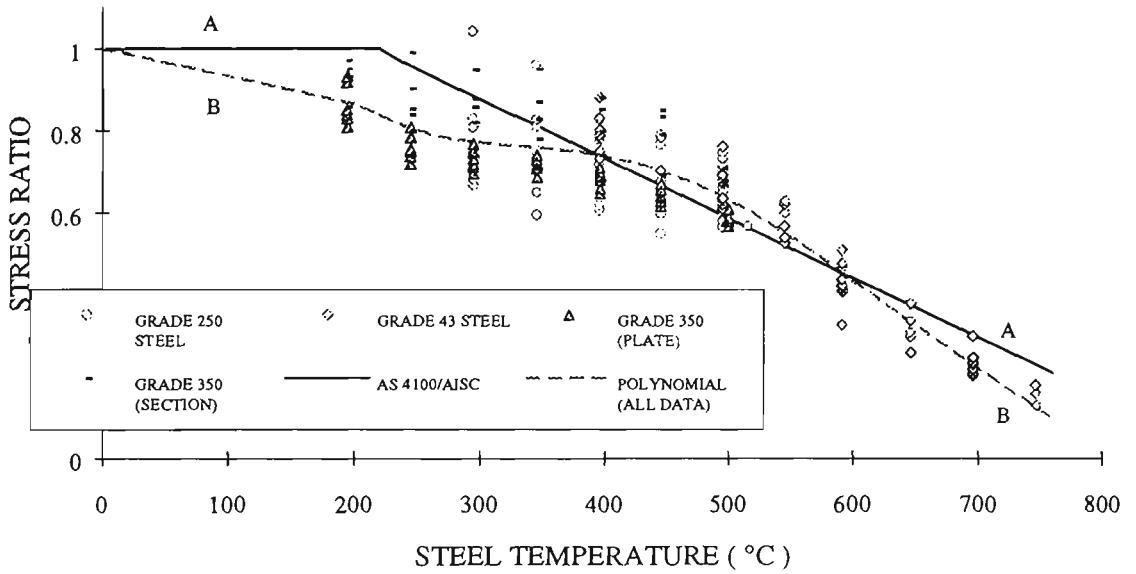


Figure: 4.8 - Strength reduction models. Curve AA - AS 4100. BB - derived polynomial based on test data of Grade 250 and 350 steel.

An alternative strength reduction model has been derived using the combined data and is shown as curve BB in Figure 4.8 and given by the following equation:

$$\frac{F_{Y_{T_s}}}{F_{Y_{20}}} = \begin{cases} \left(1 - \frac{T_s}{1487.6}\right) & T_s \leq 200 \\ A + B \cdot T_s + C \cdot T_s^2 \cdot \text{Log}(T_s) + D \cdot T_s^{2.5} + E \cdot T_s^3 & 200 < T_s \leq 600 \quad (4.4) \\ 0.433 - \left(\frac{(600 - T_s)}{473}\right) & 600 > T_s \leq 800 \end{cases}$$

where  $T_s$  = Steel temperature  
 $A$  = 2.9907  
 $B$  = -0.0238  
 $C$  =  $4.7523E^{-5}$

$$\begin{aligned} D &= -1.5891E^{-5} \\ E &= 1.964E^{-7} \end{aligned}$$

The model is more complex than that given by Equations (4.2) and (4.3) but better represents the available test data. The model is more conservative than the model used in AS 4100 for temperatures up to 400 °C, in that it predicts a more rapid loss of strength with increase in temperature. For temperatures between 400 and 600 °C, the temperature range during which most failures would occur, Equation (4.4) predicts a higher yield strength than Equation (4.3).

An alternative strength reduction model was derived for the following reasons:

- a) an estimate of the modelling error associated with the strength reduction model is required for inclusion as a random variable in the reliability submodel, refer Subsection (8.1.3). An estimate of the modelling error based on Equations (4.2) or (4.3) was not considered to be representative. Both Equation are based on linear regression and represents the test data reasonably well for the temperature range 400 - 600 °C. For temperatures outside this range Equations (4.2) and (4.3) are less effective. In order to reduce the estimate of modelling error Equation (4.4) has been used since the line that best fits the data automatically minimises the standard error of fit.

- b) the model is more general in its application than that given in AS 4100 in that it is based on both Grade 250 and Grade 350 steel.
- c) the temperature range over which the model can be used with confidence, has been extended down to 200 °C. This is particularly important in terms of the simulation of failure of a steel beam in fire. It is evident that there is a finite probability of failure of a steel beam at ambient temperature due to variation in material properties and loading conditions. The model in AS 4100 does not permit failure due to temperature effects until the steel reaches 215 °C. The probability of failure will therefore remain constant until steel is heated beyond this temperature. Results from both steady state and transient heating tensile tests [Kirby, 1988] show that a reduction in the proof stress of steel occurs at temperatures between ambient and 215 °C. It follows that failure can occur at any temperature, and that the probability of failure will increase with increasing temperature.

In order to account for the possibility of failure at low temperatures a materials model must apply to the temperature range likely to be experienced by a steel beam in fire and must be based, as far as possible, on all relevant test data.

### 4.5.3 Alternative Strength Reduction Model - Three Sided Exposure

Equation (4.4) assumes a uniform temperature gradient across the steel section. In Subsection (3.4.1.3) it was noted that steel beams supporting a concrete slab on their compression flange exhibit a temperature gradient over the depth of the beam which alters the strength of each fibre and hence its contribution to the moment capacity of the section.

In this analysis the temperature gradient in the steel beam subjected to exposure on three sides is assumed to be linear from a maximum at the bottom (tensile) flange to a minimum at the top (compressive) flange supporting the concrete slab, refer Figure (3.5). Based on the method described in Subsection (5.2.3) the stress ratio of Australian universal beams were calculated using the strength reduction model given by Equation (4.4) for a range of linear temperature gradients. Figure 4.9 shows the influence of a range of linear temperature distributions, as expressed by the ratio of the top flange temperature to bottom flange temperature,  $T_{top}/T_{bottom}$ , on the stress ratio for a 250UB37.

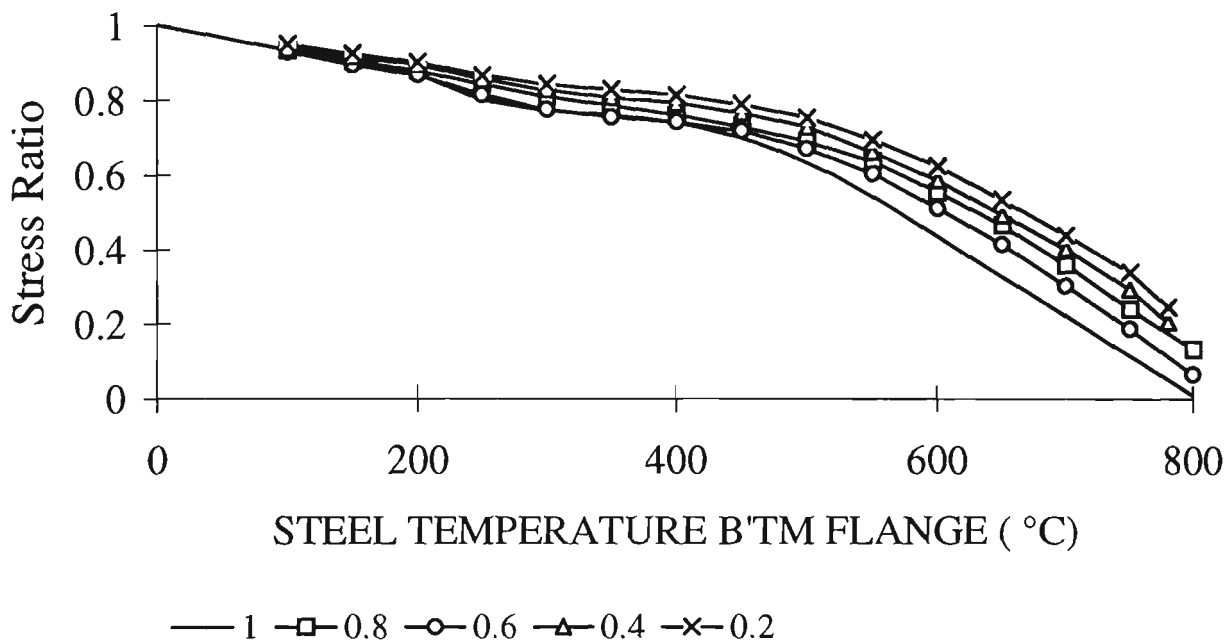


Figure 4.9 - Influence of linear temperature gradient on moment capacity. Numbers in legend indicate ratio of the temperature of the compression flange/ temperature of the tensile flange i.e.  $T_{top}/T_{bottom} = 0.6$  - Author.

It can be seen from Figure 4.9 that, in comparison with a uniformly heated beam, for a given bottom flange temperature, as the temperature gradient increases, the stress ratio increases and therefore the strength of the section

The strength of a steel beam with a temperature gradient can be calculated by either:

- a) using equation (4.3) modified by a strength reduction factor determined for a particular temperature gradient refer Subsection (5.2.3).
- b) use a modified strength reduction model.

In this analysis option a) is suitable for uninsulated steel beams with a temperature gradient for which the proposed heat transfer model, refer

Subsection (3.5.1), predicts the maximum (lower flange) temperature. In the proposed heat transfer model developed in Subsection (3.6.2) for insulated steel beams the average temperature was used as the characteristic temperature for the steel in the exercise of calibration of the heat transfer model. As a consequence an alternative strength reduction model has been developed which for a given average steel temperature and thermal gradient, calculates the strength of the section. A general strength reduction model is proposed for insulated steel beams with a thermal gradient, expressed as a function of the maximum steel temperature, as follows:

$$\frac{F_{YTs}}{F_{Y20}} = \text{Exp}(A1 + B1 \cdot T_s + C1 \cdot T_s^2 + D1 \cdot T_s^3 + E1 \cdot T_s^4) \quad (4.5)$$

Equation (4.5) is assumed to have the same statistical properties as Equation (4.4).

#### 4.6 Comparison between Strength Reduction Model and Test Results

In Figure 4.11 the AISC/AS4100 strength reduction model for the temperature range 450 - 700 °C is shown along with the proposed model, Equation 4.4, and the British model given in BS 5950. Results of stress ratio and temperature at failure from fire tests, [BHP, 1983], of beams exposed to fire on four sides are also plotted. As expected there is not a large difference between the AISC/AS4100 model and the proposed model since over this

temperature range both models are based essentially on the same data. Due to the small number of test results it is not possible to draw definite conclusions however in general the current AISC/AS4100 model and the proposed model correspond with the lower bound of the test data and are therefore conservative. The British model, which is based on transient axial test data, appears to represent the available data well. These observations support the argument that the strength reduction models should be based on transient test data in which the effective stress is determined at strains of 1 or 2% rather than at the nominal 0.2% proof stress.

The numbers adjacent to the data points in Figure 4.11 represent the fire duration time. It is expected that beams exposed to temperatures greater than 400 °C for a long period would show some evidence of creep and as such would represent the lower bound of the data plot. This is not evident from the small sample of test results available.

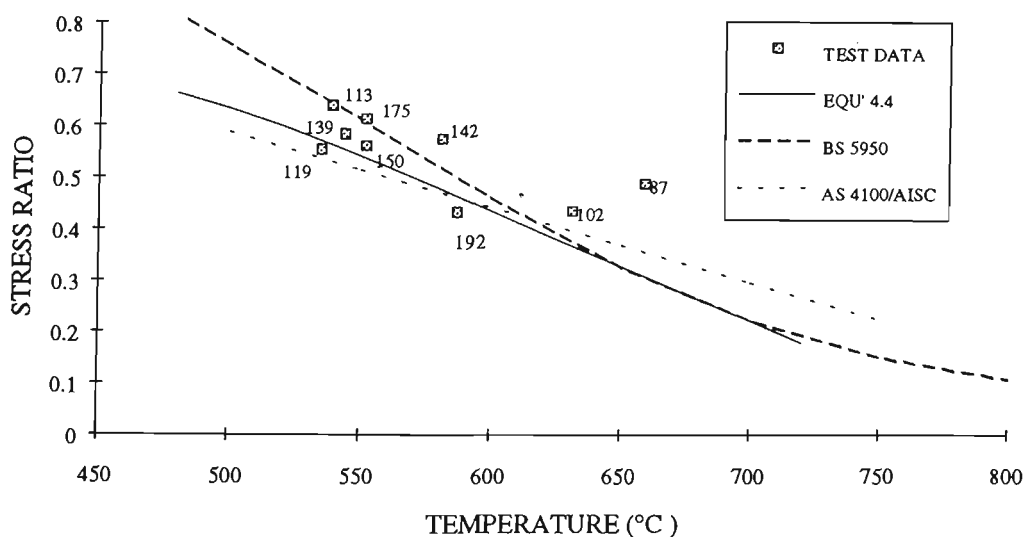


Figure 4.11: Comparison between strength reduction models and test data (four sided exposure) - Author.

The purpose in modelling the loss of strength at elevated temperature is to predict the duration of exposure of fire exposed beams before collapse occurs. The importance of variation in strength reduction models and the degree to which the models represent the available data is best assessed by the influence of the models on the time to failure. In Table 4.3 a comparison between measured time to failure of beams exposed to the standard fire and the calculated time to failure using the current AISC/AS4100 model and the proposed model, Equations 4.4 and 4.5, is given. The measured temperature at failure was used in the calculation. Both models are on average conservative

COMPARISON BETWEEN MEASURED AND CALCULATED TIME TO FAILURE USING MATERIALS MODEL						
MRL TEST NO.	SECTION	EXPERIMENTAL (Minutes)	AS 4100 MODEL	MODEL ERROR %	STRENGTH REDUCTION MODEL (Minutes)	MODEL ERROR %
4 - SIDED EXPOSURE						
BFT 108	250 UB 37	192	198	+ 3.1	196	+ 2.1
BFT 124	250 UB 37	102	97	- 4.9	97	- 4.9
BFT 110	250 UB 37	139	130	- 6.9	137	- 1.4
BFT 93	250 UB 37	175	158	- 9.7	166	- 5.7
BFT 106	100 UC 15	150	143	- 4.7	149	- 0.7
BFT 122	100 UC 15	113	100	-11.5	106	-6.2
BFT 99	100 UC 15	87	74	- 14.9	77	- 11.5
BFT 114	200 UBP 122	143	123	- 13.9	131	- 8.4
BFT 142	127 X 4.9 SHS	151	183	+ 21.2	173	+ 14.5
BFT 143	203 x 9.5 SHS	119	131	+ 10.1	129	+ 8.4
3 - SIDED EXPOSURE						
BFT 168	310 UB 40	201	176	- 12.4	188	- 6.4
BFT 169	100 UC 15	124	131	+ 5.6	125	+ 0.8
BFT 170	100 UC 15	246	238	- 3.3	240	- 2.4
BFT 172	200 UBP 122	241	223	- 7.5	234	- 2.9
BFT 173	200 UBP 122	340	336	- 1.2	346	+ 1.8
AVE' ERROR				8.7		5.2

Table 4.3: Comparison between measured and calculated time to failure using AISC/AS4100 and proposed strength reduction model, Equation 4.4 and 4.5. [Test Data - BHP Melbourne Research Laboratories (MRL), 1983].

in that they both predict earlier time to failure. The average error using the AISC/AS4100 model is -6.3% and -3.5% for the proposed model. These values are a measure of the modelling error associated with each strength reduction model.

Results from two tests in which Square Hollow Section (SHS) were used, test numbers BFT 142 and 143, compare poorly with calculated values. The steel used for these sections is 400 Mpa. Steel of this grade was not used in the formulation of either of the models and as such the strength reduction models may be considered to be inappropriate for steel sections of this grade. Since results indicate that values of calculated time to failure of SHS are unconservative caution should be exercised if steel of this grade is to be used in such an analysis.

The combined modelling error associated with the heat transfer model proposed in Chapter 3 and strength reduction models, Equations 4.4 and 4.5 is shown in Table 4.5 and Figure 4.11. Based on the section size, thickness of insulation and exposure condition (three or four sided) the temperature versus time curve has been calculated for each of the test cases. The time of failure is obtained when the temperature affected moment capacity of each section equal the applied moment. The average combined model error, excluding BFT 142 and 143, is -3.3% with the largest error being -8.8%.

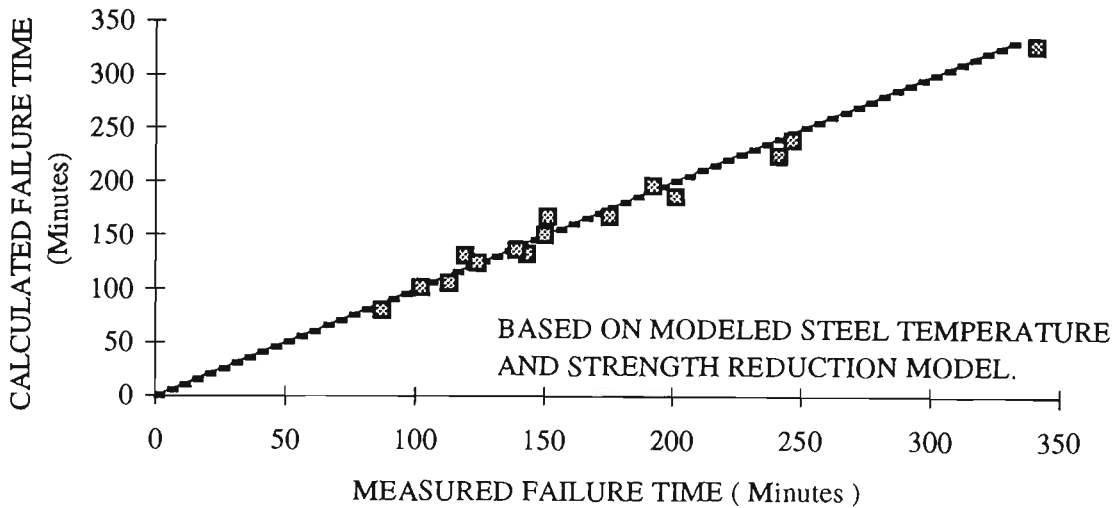


Figure 4.11: Comparison between calculated and experimental time to failure - Author.

**COMPARISON BETWEEN MEASURED AND CALCULATED TIME TO FAILURE USING STRENGTH REDUCTIO & HEAT TRANSFER MODELS**

MRL TEST NO.	SECTION	EXPERIMENTAL (Minutes)	STRENGTH REDUCTION AND HEAT TRANSFER MODEL (Minutes)	MODEL ERROR %
<b>4 - SIDED EXPOSURE</b>				
BFT 108	250 UB 37	192	196	+ 2.1
BFT 124	250 UB 37	102	101	- 1.0
BFT 110	250 UB 37	139	136	- 2.1
BFT 93	250 UB 37	175	167	- 4.6
BFT 106	100 UC 15	150	150	0
BFT 122	100 UC 15	113	105	-6.2
BFT 99	100 UC 15	87	80	-8.8
BFT 114	200 UBP 122	143	132	-7.7
BFT 142	127 X 4.9 SHS	151	167	+10.6
BFT 143	203 x 9.5 SHS	119	131	+10.1
<b>3 - SIDED EXPOSURE</b>				
BFT 168	310 UB 40	201	186	-7.4
BFT 169	100 UC 15	124	124	0
BFT 170	100 UC 15	246	239	-2.8
BFT 172	200 UBP 122	241	224	-7.1
BFT 173	200 UBP 122	340	348	+2.3
<b>Average % Error</b>				<b>-3.3</b>

Table 4.5: Comparison between measured and calculated time to failure using proposed strength reduction model, Equation 4.4 and 4.5 and proposed heat transfer models. [Test Data - BHP Melbourne Research Laboratories (MRL), 1983].

Again there is a large error associated with the SHS, the thermal model predicting a more rapid increase in the steel temperature than occurred in reality. The thermal model developed in Chapter 3 was calibrated using box protected universal beams. It is evident that a separate thermal model would be required for insulated hollow sections.

## 4.7 Conclusion

Much variation exists between available strength reduction models. This variation is attributable to inherent differences in the nature of the data on which the models are based and the assumptions made in the modelling process. It has been demonstrated that rate of heating, creep and the value of strain at which effective stress is measured influence the shape of the strength reduction curve.

An alternative mechanical properties submodel has been derived from available test data: refer to Equations 4.4 and 4.5. The model allows for loss of strength at temperatures below 215 °C and accommodates the increased capacity of sections with temperature gradients. The submodel gives a better prediction of strength than the current model in AS4100. It is well suited to the research in this thesis but is not proposed as an alternative to the model in AS4100 because it is not as simple to use in engineering design.

## **CHAPTER FIVE**

### **STRUCTURAL RESPONSE SUBMODEL**

## 5.0 Introduction

Modeling structural response involves structural analysis that is the application of the principals of equilibrium, compatibility and strength of materials in order to determine the strength and deformation of a structure under load. The structure under consideration in this thesis is a simply supported, axially unrestrained, steel floor beam.

Modelling must be based on a knowledge of the material behaviour and applied loads. For an isolated statically determinate member the forces and moments acting on the member are already known. The strength of a steel beam in bending should be determined for conditions at collapse when steel behaves plastically. Hence plastic analysis only is considered here.

This chapter shows how basic structural theory for ambient conditions is applied to steel at elevated temperature and is adopted for the structural response submodel. Strength is assumed to be limited by bending rather than shear or other modes of failure. From experience, this is true for most practical beams.

## 5.1 Statically Determinate Beams

During a fire temperatures may vary in exposed steel members but during deformation plane sections remain. Variations in stiffness along determinate members do not affect the distribution of bending moment. Therefore analysis for ambient conditions applies to steel beams at elevated temperature. For a simply supported beam subject to a point load  $P$  (kN), the maximum moment,  $M_{MAX}$ , is given by:

$$M_{Max} = M_C = \frac{Pab}{L} \quad (\text{kNm}) \quad (5.1)$$

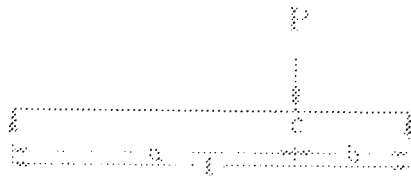


Figure 5.1: Loading arrangement - point load.

For a simply supported beam carrying a uniformly distributed load,  $w$  (kN/m), refer Figure 5.2, the moment at  $x$  is given by:

$$M_x = \frac{wLx}{2} - \frac{wx^2}{2} \quad (\text{kNm}) \quad (5.2)$$

where  $L = \text{span (m)}$

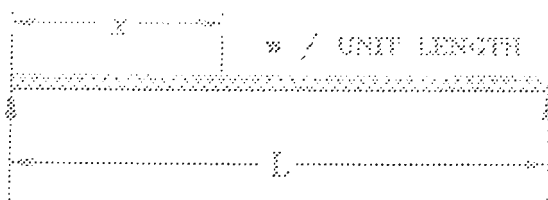


Figure 5.2: Loading arrangement - uniformly distributed load.

Based on linear elastic analysis the moment due to a combination of point and uniformly distributed loads is determined by superposition.

## 5.2 Plastic Analysis

### 5.2.1 Ambient Temperature.

The ultimate load capacity or collapse load of a simply supported steel beam can be determined in accordance with the principles of plastic analysis [Trahair & Bradford; 1988]. Tests show that the distribution of strain stays linear over the depth of the section after yield by means of plastic flow in the yielded region [Moy, 1985], refer Figure 5.3. The assumption of plane sections remaining plane is therefore still valid.

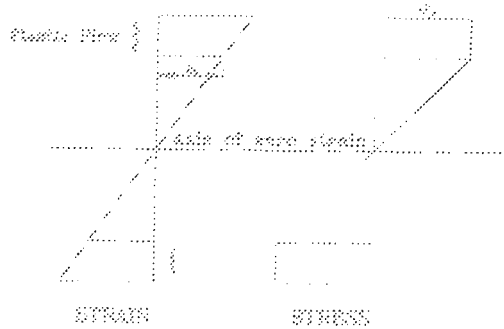


Figure 5.3: Stress-strain distribution for plastic analysis.

The moment capacity  $M_P$  at a plastic hinge is obtained from the product of the plastic section modulus,  $S$ , and the yield or 0.2% proof stress,  $F_Y$ . The calculated maximum moment capacity of a beam is given by:

$$M_P = F_Y \cdot S \quad (5.3)$$

The use of plastic analysis in the design of steel structures at ambient temperatures is governed by Section 4.5 of AS 4100 (1990). The analysis is limited to hot formed, doubly symmetric I-sections which satisfy the requirements specified for a compact section in Clause 5.2.3 AS 4100.

An idealised moment-curvature relationship assumed in plastic analysis is shown in Figure 5.4(a). The actual moment-curvature, shown in Figure 5.4(b), for two sections, is asymptotic to the ideal relationship. The degree to which the ideal curve matches the actual moment curvature is a measure of the accuracy of the model.

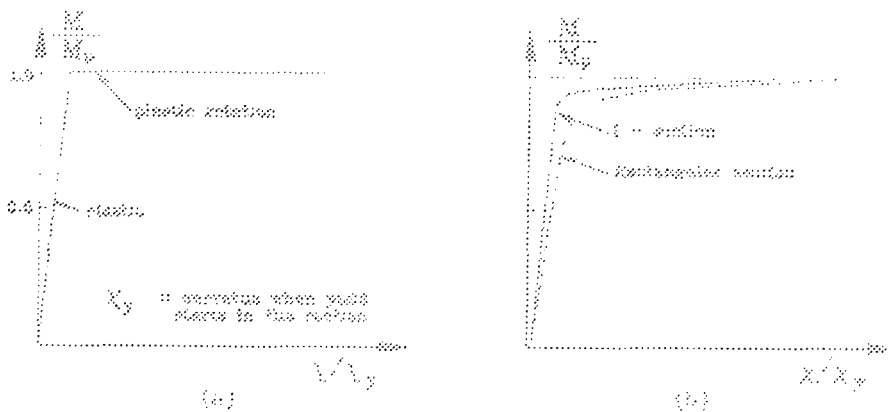


Figure 5.4: (a) - ideal elastic-plastic moment curvature relationship.

(b) - actual moment curvature relationship for different section shapes.

In the plastic analysis of beams elastic strains are ignored as well as the effect of strain hardening which causes the moment-curvature relationship to rise above the fully plastic limit. The analysis further assumes that the effect of high shear forces which cause small reductions in  $M_p$  - due to reductions in the plastic bending capacity of the web - can be ignored. The consequence of these assumptions in the theoretical behaviour of a simply supported beam

supporting a point load is to underestimate the moment capacity of the beam at collapse by up to 24% [Yura et al.; 1978]. In the case of a simply supported beam supporting a uniform load the assumptions lead to an underestimation of the moment capacity of between 2 - 8% [Yura et al.; 1978] and 1.4% [Fukumoto and Kubo; 1977].

## 5.22 Elevated Temperature - Four sided Exposure

The collapse load of a simply supported steel beam at elevated temperatures can be determined using plastic analysis if the relevant value of yield stress is used for each fibre according to the temperature at that point [Proe et al., 1989]. For the case of a steel beam with a uniform temperature throughout, refer Figure 5.5,

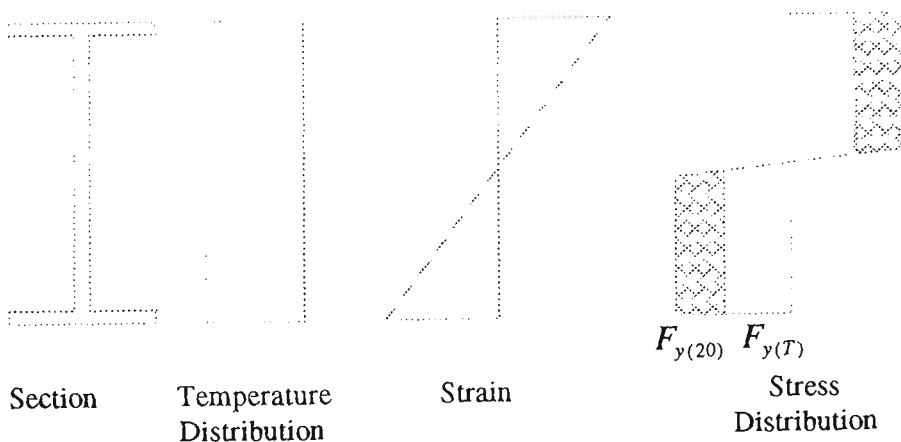


Figure 5.5: Stress distribution four sided exposure.

the temperature affected strength is the same throughout the section therefore the moment capacity at temperature T ,  $M_{pT}$ , is given by:

$$M_{pT} = SF_{yT} \quad (5.4)$$

where  $F_{yT}$  = yield stress of steel at temperature  $T$

### 5.2.3 Elevated Temperature - Three Sided Exposure

In subsection 3.4.1.3 it was demonstrated that the temperature gradient through the depth of the steel section was a function of length of fire exposure, insulation thickness and beam depth. The difference in strength between uniformly heated beams and beams with a temperature gradient is accounted for in the European Recommendations for the Fire Safety of Steel Structures [1983] by means of a calibration factor. The load ratio, the ratio of the applied load in fire to the member load capacity at room temperature, calculated assuming a uniform temperature distribution is modified by a load multiplier which increases the capacity of the beam under fire conditions as the load ratio decreases. The multiplier was determined assuming a 100 °C difference between the bottom and top flange [Pettersson & Witteveen; 1980]. This factor also accommodates the use of a nominal value of yield stress in the ECCS recommendations. The dependence of the multiplier on load ratio is reasonable - a lightly loaded beam will fail at a higher temperature and therefore be expected to develop a greater temperature gradient - however no account is taken of the dependence of load capacity with variation in temperature gradient.

Proe [1989] has demonstrated that for simply supported composite steel beams in fire the strength of the beam, calculated from the room-temperature capacity and a reduction steel yield stress based on the effective uniform temperature, give good results. The effective uniform temperature,  $T_e$ , is the weighted average of the bottom flange, web and top flange temperature  $T_b$ ,  $T_w$  and  $T_t$  defined as:

$$T_e = (2T_b + T_w + T_t) / 4 \quad (5.6)$$

The structural response submodel for three sided exposure is developed from modelling four sided exposure. Since the yield strength of each element of steel, and hence its contribution to the moment capacity of the section, depends both its temperature and its relative position in the section, refer Figure 5.6, Equation (4.4) is no longer directly applicable. The strength of a section has been calculated using a discrete element method as described by Proe et al. [1990], in which the beam depth is divided into 50 elemental fibres. For a given temperature distribution the temperature at the mid-height of each fibre is determined by interpolation. For this analysis the yield stress of each fibre has been obtained from the strength reduction model, Equation (4.4). The neutral axis is determined by balancing compression and tensile forces and hence the moment capacity of the section for the given temperature regime determined. The strength reduction model for three sided exposure, Equation (4.5) given in subsection (4.5.3), was derived in this way.

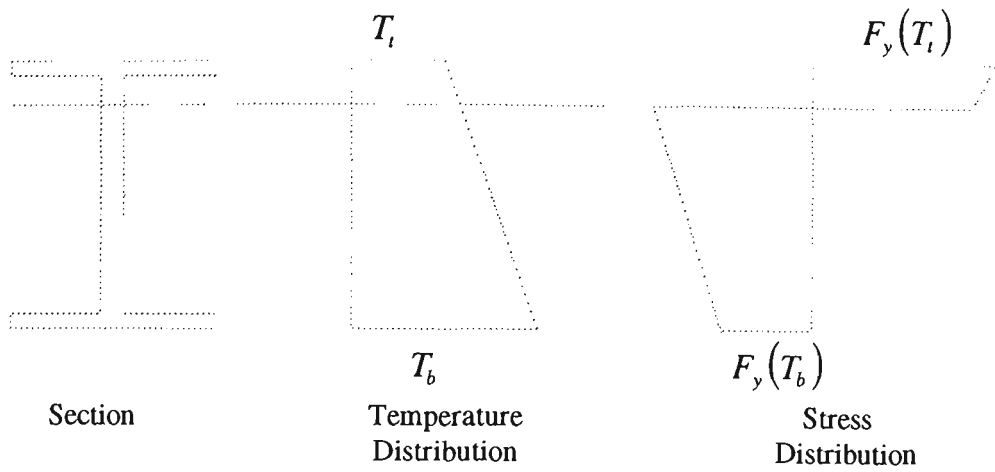


Figure 5.6: Stress distribution, three-sided exposure.

An analysis of all Australian universal beam sections [Proe, ], reveals that a similar fraction of their ambient temperature moment capacity, under any given temperature distribution, is maintained, refer Figure 5.7.

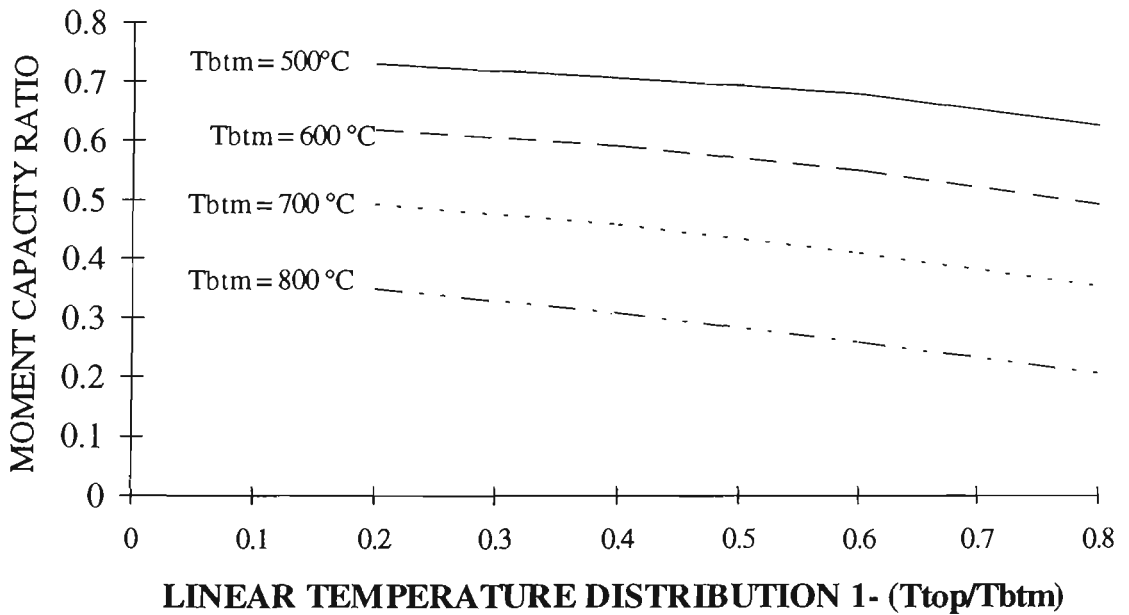


Figure 5.7: Moment capacity ratio as a function of bottom flange temperature ( $T_{btm}$ ) and linear temperature gradient  $1 - T_{top}/T_{btm}$  for Australian sections - Author .

Figure 5.7 shows that, for a bottom flange temperature of  $600^\circ\text{C}$ , there is a 20% relative increase in the moment capacity of the section as the ratio

$T_{top}/T_{btm}$  decreases from 0.8 to 0.4. There are significant gains in strength and as a consequence in the fire duration of beams supporting concrete slabs compared with beams exposed to fire on all sides.

### 5.3 Flexural Capacity

In the determination of flexural capacity the following assumptions are made in the submodel for structural response:

- a) the temperature distribution along the member is uniform.
- b) axial forces due to expansion of the member are not generated.
- c) creep is of little significance.

Temperature variation along a beam can vary by many hundreds of degrees [Pettersson and Witteveen, 1980], depending on the location of the beam relative to the fire, duration of the fire and protection afforded the beam. The formation of a plastic hinge is assumed to occur at the location of maximum moment. This will not necessarily be the case if the temperature of the beam varies. The structural analysis is simplified if the location of maximum temperature matches the location of maximum moment. This assumption corresponds with that relating to the fire severity model in which it is assumed that the fire compartment is uniformly heated.

It is also assumed that if a member is designed for ambient temperatures in accordance with Section 4.5 of AS4100 [1990] and that the strength of the member in bending is adequate under fire conditions, then the member is adequate in regards alternative modes of failure such as shear and connector capacity failure in fire conditions. Little data is available to substantiate this assumption [Kruppa, 1979]. In the case of a beam supporting a concrete slab however, the degree of restraint afforded by the slab will reduce the possibility of the top flange buckling or of flexural torsional buckling. Despite its acceptance as an appropriate method of analysis of structural elements at elevated temperature it should be used with some caution as the stress-strain behaviour of structural steel at elevated temperature is essentially different from that encountered at normal temperatures [Rubert and Schaumann, 1986].

### **5.3.1 Comparison between Measured and Calculated Moment Capacity for Four Sided Exposure**

Error in the prediction of the moment capacity of a beam at elevated temperature is attributable to assumptions associated plastic theory and to inaccuracies in the materials model used to predict the change in yield strength with temperature. It is not possible here to separate these two effects. In Tables 5.1 and 5.2 a comparison between the measured and calculated moment capacity of steel beams with a uniform temperature distribution is given. The material properties models used in the calculations are the recommended model

for Australian steel given in Section 12 of AS 4100 (1990), refer Subsection (4.5.1), and Equation (4.4), refer Subsection (4.5.2).

Moment Capacity Comparison between Experimental and Structural Response Submodel Results				
MRL Test No.	Section	Experimental (kNm)	Structural Res. Submodel (kNm)	Model Error %
4 - Sided Exposure				
BFT 108	250 UB 37	15.7	16.6	+5.7
BFT 124	250 UB 37	15.7	14.3	-8.9
BFT 110	250 UB 37	79.5	71.2	-10.4
BFT 93	250 UB 37	81.8	68.2	-16.6
BFT 106	100 UC 15	13.0	11.8	-8.9
BFT 122	100 UC 15	13.4	11.1	-17.4
BFT 99	100 UC 15	10.94	11.5	+5.4

Table 5.1: Comparison between calculated moment capacity using AS 4100 model and measured capacity at collapse. Test data derived from BHP MRL Reports (1983).

The data in Table 5.1 relates to simply supported beams supporting a centrally located point load. In the experiment beams were deemed to have failed when the maximum deflection exceeded span/30. The critical deflection corresponds with the formation of a plastic hinge and therefore structural collapse.

The model underestimates the moment capacity by as much as 17.4% and on average -7.3%. It appears that in comparison with the results of beams at ambient temperature, in which the moment capacity at collapse was underestimated by as much as 24% [Yura, et al., 1978], the errors associated with the two models may be cancelling one another.

Moment Capacity Comparison between Experimental and Structural Response Submodel Results				
MRL Test No.	Section	Experimental (kNm)	Structural Res. Submodel (kNm)	Model Error %
4 - Sided Exposure				
BFT 108	250 UB 37	15.7	19.4	+23.5
BFT 124	250 UB 37	15.7	16.7	+6.4
BFT 110	250 UB 37	79.5	83.2	+4.8
BFT 93	250 UB 37	81.8	78.56	-3.9
BFT 106	100 UC 15	13.0	13.6	+4.6
BFT 122	100 UC 15	13.4	12.65	-5.6
BFT 99	100 UC 15	10.94	11.4	+4.2

Table 5.1: Comparison between calculated moment capacity using Equation (4.4) model and measured capacity at collapse. Test data derived from BHP MRL Reports (1983).

The model based on Equation (4.4), overestimates the moment capacity at failure in one case (BFT 108) by 23.5%. The average error is 4.86% and 1.75% if the anomalous result (BFT 108) ignored. This is a significant improvement on the recommended model given in AS 4100 and shows that the use of plastic analysis and the strength reduction model, Equation (4.4), is sufficiently accurate for use in the simulation model to predict the probability of failure of steel beams in real fire.

## 5.4 Conclusion

The ultimate moment capacity of simply supported steel beams in fire can be calculated using plastic analysis in which the yield strength of steel is modified for the effects of temperature using the strength reduction model described in subsection (4.5.2). The method is equally suited to steel beams supporting a concrete slab if account is taken of the increased moment capacity due to the

presence of a thermal gradient in the steel. This can be achieved by using either the weighted average temperature or calculating the elevated temperature moment capacity using discrete element analysis.

Plastic analysis is particularly suited for use in the probability simulation because of its simplicity. Comparison with test results have given a measure of the combined error associated with the structural analysis model and the strength reduction model. This information is required as input in the probability model.

## **CHAPTER SIX**

### **LOAD SUBMODEL**

## 6.1 Load Model - Code Requirement

The design of a steel structure for strength limit state in accordance with AS 4100 [1990] shall account for the action effects arising directly from loads.

The total load on a floor is the sum of a dead load and an independent live load that is the resultant of a sustained live load component and a transient live load component. Loads for beams, designed in accordance with strength limit state, are factored and combined to produce the most adverse affects [AS 1170.1, 1989]. The basic combination and load factor appropriate for floor beam design is:

$$1.25G + 1.5Q \quad (6.1)$$

where

G	=	dead load
Q	=	live load

For fire limit state, the design load is obtained from the following combination of factored loads:

$$1.1G + \psi_c Q \quad (6.2)$$

where

$\psi_c Q$	=	live load combination factor for the strength limit state
------------	---	---

The reason for the lower load factor in the fire limit state is that fire is an extreme event. Rational design considers similar probabilities for each limit state. The probability of fire and lower loads is the same as the probability of no fire and extreme load. The dead load and live load specified above are nominal design dead load,  $G_n$ , and live load  $Q_n$  determined according to AS 1170.1 [1989].

## 6.2 Load Model - Probabilistic

Loads are by nature stochastic and time varying. Models of load effect are obtained from load surveys [Choi, 1988 and 1992].

### 6.2.1 Dead Load

Dead load is effectively sustained at a constant value for the life of the structure. Essentially dead load comprises the self-weight of the structure which can be estimated with reasonable accuracy. Dead load effect is considered a random variable with a lognormal distribution [Pham, 1984]. The distribution parameters are as follows:

$$\bar{G} = 1.05G_n \quad \text{and} \quad \text{COV}(G) = 0.1$$

where  $\bar{G}$  = the mean value of  $G$   
(COV) = coefficient of variation

## 6.22 Live Load

Live load comprises two components: a sustained load associated with normal use, termed arbitrary point in time live load (APT),  $L_A$ , and an extraordinary load, which is a transient load due to unusual events, termed peak live load,  $L_p$ . Stochastic properties of arbitrary point in time live load and peak live load are given in Table 6.1 [Pham, 1984].

$A_{Trib.}$ (m <sup>2</sup> )	Arbitrary Point-in-Time Live Load (APT) Weibull Distribution		Peak Live Load Gumbel Distribution	
	$\bar{L}_A/L_n$	COV( $L_A$ )	$\bar{L}_p/L_n$	COV $L_p$
10	0.21	0.90	0.68	0.41
23	0.19	0.79	0.70	0.26
50	0.27	0.72	0.74	0.25
100	0.25	0.78	0.80	0.24
250	0.31	0.67	0.88	0.19

Table 6.1: Statistical properties of office floor live loads ( $A_{Trib.}$  = tributary area)

Table 6.1 shows that live load is dependent on the tributary area,  $A_{Trib.}$ , (the floor area supported by the beam) and that there is a small increase in live load with tributary area. The table also shows that the permanent component

The relationship, between arbitrary point in time live load and peak live load, which is valid for both ambient and elevated temperature conditions is demonstrated in Figure 6.1.

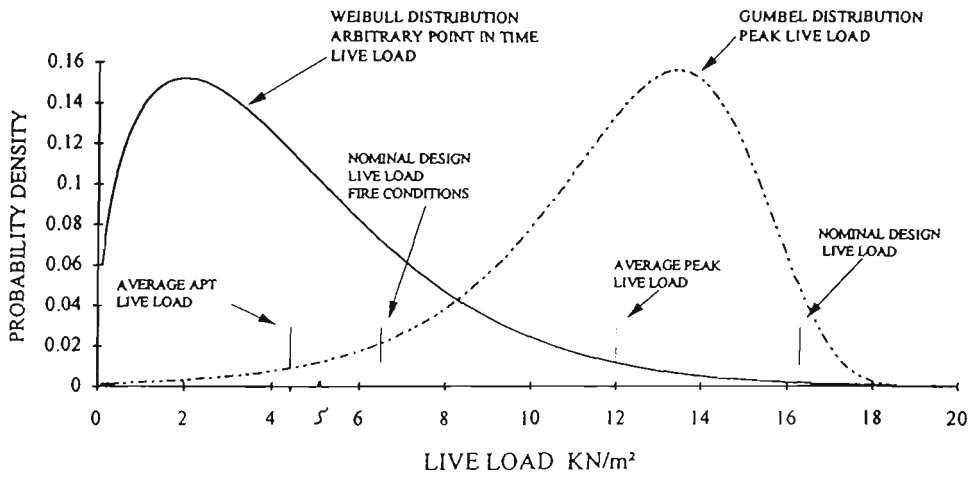


Figure 6.1: Statistical distribution of live load (figure based on 50 m<sup>2</sup>).

The nominal design live load for fire conditions in offices is 50% greater than the average arbitrary point-in-time live load.

## **CHAPTER SEVEN**

### **RELIABILITY MODEL**

## 7.0 Introduction

In this chapter a literature review giving a brief overview of types of reliability models is presented. In accordance with the aims of this project Subsection (1.1.2), a model is selected that predicts probability of failure with time, that is simple and has an accuracy commensurate with other submodels adopted in this project.

## 7.1 Reliability Theory.

### 7.1.1 Calculation of Probability of Failure

The basic structural reliability problem considers a single load and resistance effect. The resistance  $R$  and the load  $S$  are independent random variables, characterised by their probability density functions  $f_r$  and  $f_s$ . In relation to the limit state for strength a structural element will be considered to have failed when its resistance  $R$  is less than the load effect  $S$ . The probability of failure  $p_f$  of the structural element can be expressed in either of the following ways [Melchers, 1987]:

$$p_f = P(R \leq S) \quad (7.1)$$

$$p_f = (R - S \leq 0) \quad (7.2)$$

or in general

$$P[G(R, S) \leq 0] \quad (7.3)$$

where  $G( )$  is termed the limit state function and the probability of failure is identical with the probability of limit state violation.

In classical reliability analysis, assuming  $R$  and  $S$  are independent,  $p_f$  is obtained from:

$$p_f = P(R - S \leq 0) = \int_{-\infty}^{\infty} \int_{-\infty}^{s \geq r} f_r(r) f_s(s) dr ds \quad (7.4)$$

For any random variable  $X$ , the cumulative distribution function  $F_X(x)$  is given by:

$$F_X(x) = P(X) \leq x = \int_{-\infty}^x f_X(y) dy \quad (7.5)$$

hence

$$p_f = P(R - S \leq 0) = \int_{-\infty}^{\infty} F_R(x) f_S(x) dx \quad (7.6)$$

The convolution integral above presupposes that the distribution functions are known. The cumulative distribution function  $F_R(x)$  is the probability that the resistance  $R$  is some value less than  $x$ ,  $R \leq x$  while  $f_S(x)$  is the probability that the load effect will have a value between  $x$  and  $x + \Delta x$  in the limit as

$\Delta x \rightarrow 0$ . Combining the two probabilities and summing over the range of  $x$  provides the total probability of failure. For the special case in which both  $R$  and  $S$  are either normal, lognormal or weibull distributions a closed form of the convolution integral exists. For distribution functions other than those noted or for combinations of distribution functions approximate numerical methods such as the trapezoidal rule are used. For more accurate solutions Simpson's rule or a method based on polynomials can be employed. If  $R$  and  $S$  are not independent or if the reliability problem is formulated using constituent random variables rather than  $R$  and  $S$  then the probability of failure is obtained from the general expression:

$$p_f = P[G(\mathbf{X}) \leq 0] = \int \dots \int_{G(\mathbf{x}) \leq 0} f_{\mathbf{x}}(\mathbf{x}) d\mathbf{x} \quad (7.7)$$

where  $f_{\mathbf{x}}(\mathbf{x})$  is the joint probability density function for the  $n$  vector  $\mathbf{X}$  of basic variables. Computation of this multiple integral is in general not tractable (unless multinormal). Application of numerical integration techniques is time consuming and often result in large-round off errors. There are three approaches to the solution of the multiple integral as follows:

- a) second moment methods that represent the random variable by its first two moments, mean and variance.
- b) advanced second moment methods that transform the original problem such that the probability density function for each variable is approximated by a normal distribution.

- c) Monte Carlo methods which determine the probability of failure by many repeated numerical trials.

### 7.1.2 Second Moment Methods

In this approach estimates of reliability are calculated using random variables represented by their first two moments, mean and variance. This implies a normal distribution for the variables being that it is the only continuous probability distribution completely described by its first two moments. The special case of the two parameter, R and S, reliability problem in which both distributions are normally distributed can be solved analytically. The safety margin  $Z = R - S$  has a mean and variance given by [Melchers, 1987]:

$$\begin{aligned}\mu_z &= \mu_R - \mu_S \\ \sigma_z^2 &= \sigma_R^2 + \sigma_S^2\end{aligned}\tag{7.8}$$

then

$$p_f = P(R - S \leq 0) = P(Z \leq 0) = \Phi\left(\frac{0 - \mu_z}{\sigma_z}\right)$$

$$p_f = \Phi\left[\frac{-(\mu_R - \mu_S)}{(\sigma_S^2 + \sigma_R^2)^{1/2}}\right] = \Phi(-\beta)\tag{7.9}$$

where  $\Phi$  is the standard normal distribution function and  $\beta$  is defined as the "safety index".

If the limit state function is formulated using constituent random variables the foregoing is easily applied since the limit state function, expressed as the safety margin,  $Z(X)$ , is given by:

$$Z(X) = a_0 + a_1 X_1 + a_2 X_2 + \dots + a_n X_n \quad (7.10)$$

and

$$\mu_z = \sum_{i=1}^n a_i \mu_{x_i} \quad \text{and} \quad \text{var}(Z) = \sum_{i=1}^n a_i^2 \text{var}(X_i) \quad (7.11)$$

The safety index  $\beta$  is calculated as before. If the limit state function is not linear it is necessary to linearise  $G(X)$  to obtain the first two moments  $\mu_z$  and  $\sigma_z$ . This is achieved using the first terms of the Taylor series expansion about the point  $\mathbf{x}^*$ . The expansion is often taken about the means of the basic random variables or in more refined second order methods, about the "design point". Such approximating methods are known as mean value second moment (MVSM) and first order second moment methods (FOSM).

The calculated value of  $\beta$  using FOSM methods can vary depending on the way the problem is formulated. A structural reliability problem in which the limit state function is formulated in terms of stress rather than strength can result in a difference of two orders of magnitude in the estimate of probability of failure [Nowak, A.S., 1994]. To obtain a safety index which is invariant, it may be necessary to transform the constituent random variables using the Hasofer-Lind transformation [1974]. The Hasofer-Lind reliability index  $\beta$ , is the shortest distance from the origin to the limit state function in reduced

variable space and is defined as the cumulative area under the marginal distribution curve in the failure region.

The reliability problem is complicated when the limit state equation is non-linear. The point about which the limit state equation is expanded is not known *a priori*. The solution to the reliability problem involves determining the linearisation coordinates in transform space which minimises the distance  $\beta$ . This minimisation problem can be solved using calculus of variations [Shinozuka, 1983] .

For reliability problems involving a large number of constituent random variables and /or complex limit state equations alternative techniques are available. The recommended method of solution [Melchers, 1987] for a non-linear function is the modified gradient projection method. If such a vector cannot be found, algorithms are available [Beveridge and Schechter, 1970; Schittkowski, 1980] which solve a non-linear minimisation problem subject to non-linear inequality constraints. Alternatively a more accessible iterative method has been formulated which allows for an increasingly efficient selection of checking point such that the condition of perpendicularity between the tangent hyperplane and the  $\beta$  direction is achieved [Fiessler et al., 1976; Ellingwood et al., 1980]. The method rapidly converges to a stable value of  $\beta$ . In the case of a highly non-linear limit state function the iterative technique may fail to converge.

The first order methods outlined above are approximate methods to be used when the limit state function is *non-linear*. The second moment technique is *per se* an approximate method in as far as the underlying assumption that the basic random variables are normally distributed is a correct one. A further problem arises in expressing the failure probability by the safety index. The probability of failure is defined as the integral over the transformed region assuming a linear limit state function. At a particular checking point  $P^*$ , the actual failure probability will be greater if the function is concave CC to the origin and smaller if convex AA to the origin Fig. 7.1

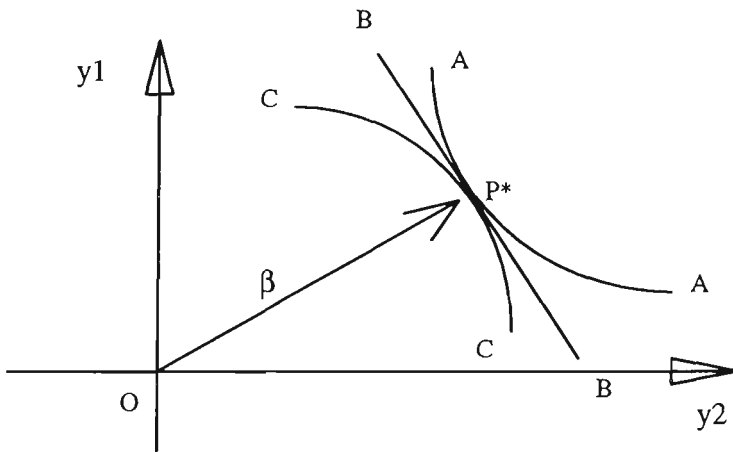


Figure 7.1: Inconsistency in safety index due to variation in volume of failure region.

### 7.1.3 Advanced Second Moment Method

Often information about the distribution functions describing the constituent random variables is available. This additional information can be incorporated in the reliability analysis by transforming non-normal distributions into equivalent normal distributions. An iterative procedure has been proposed

[Leicester, 1985]. In this computational algorithm an initial set of basic random variables corresponding to the coordinates of a hypothetical checking point are assumed.

The method is relatively simple to apply and converges quickly to a final solution. It permits the use of statistical parameters which fully describe the random variable (in as much as the statistical parameters reflects reality). The algorithm is an advance on the iterative method [Rackwitz and Fiessler, 1978] in which information on the distribution function is limited to the simple R - S reliability problem.

#### **7.1.4 Simulation Method**

The Monte Carlo method is a mathematical technique whereby experimentation on real physical system can be simulated numerically. The method proceeds by sampling, at random, a set of values,  $\bar{X}$ , for those system descriptors (variables  $X_i$ ) with known probabilistic properties. The random sampling of the constituent variables occurs subject to the probability density function used to describe each variable. The method is essentially the repeated evaluation of a deterministic model in which the value of one or more of the system descriptors are randomly changed to reflect uncertainty in the magnitude of the variable or in the process itself. If the limit state function

$G(\hat{x}) \leq 0$  is violated the structural element has "failed". If  $N$  trials (experiments) are conducted, the probability of failure is given by:

$$p_f = \frac{n(G \leq 0)}{N} \quad (7.12)$$

where  $n(G \leq 0)$  is the number of trials for which  $G \leq 0$ .

The error  $\varepsilon$  between the actual number of failures and the observed number of failures [Melchers 1987] is approximated by:

$$\varepsilon = k[(1-p)/Np]^{1/2} \quad (7.13)$$

where  $k$  corresponds to the equivalent confidence limit under the standard normal curve.

The method requires the calculation of

When  $R_t \leq S$ ,  $F_t$  increases by 1

$$\text{Total number of failures} = \sum_{t=1}^{t=T_{Dur}} F_t$$

$$p_f = \frac{\sum F_t}{NTr}$$

where

$$\sum F_t = \text{sum of recorded failures at time 't'}$$

$$NTr = \text{number of simulations.}$$

$T_{dur}$  = duration of simulation.

## 7.2 Commentary

The two parameter reliability calculation can be reformulated to handle constituent random variables by employing the limit state function. The resulting joint probability function however can only be solved by numerical integration in which the probability function is evaluated at each integration. Alternatively the second moment method in which the limit state function is linear, as is the case in this study, is easily evaluated. Calculation of the safety index however assumes that constituent random variables are Gaussian and by the central limit theorem the product of normal distribution functions is lognormal [Nowak, 1994]. Mean value second moment (MVSM) method in which the original distribution is approximated at the mean can be used for non-normal distributions however this method is inaccurate if the tails of the cumulative frequency distribution, plotted on normal probability paper, are not a straight lines [Nowak, 1994]. There are two techniques which accommodate non-normal distributions. The first by Rackwitz and Fiessler [1978], transforms non-normal resistance and load effect distributions into approximate normal distributions. The original distributions however must be able to be accurately described by a distribution function. In the second method the basic random variables of the limit state function are transformed into unit normal variates in transform space before the function is evaluated. The safety index is evaluated at the design point. This method is very powerful and can be solved using a

simple computational algorithm. The method is currently limited to consideration of time independent random variables.

To apply classical reliability analysis to estimate the probability of failure of a steel beam it is necessary to know the distribution function of the resistance (R) and load (S) affect, and that R and S are independent random variables. If both R and S have either a Gaussian , Lognormal or Weibull distributions an exact value can be calculated for the probability of failure. Calculation of safety index, using classical reliability, based on any other distribution or combination of distributions is an approximation. In this analysis the R and S effect are the result of the interaction of twelve constituent random variables, refer Chapter 8. The central limit theorem states that the sum of random variables, regardless of type of distribution, will approach a normal distribution and that the product of the same will approach a lognormal distribution. Investigation by the Author in which the resultant distributions for R and S were generated by means of simulation and using the distribution functions of the constituent random variables has shown that the shape of the resultant R and S distributions in this analysis do not correspond with standard distribution functions. The load affect is determined using a lognormal dead load distribution combined with either a gumbel or wiebull (Extreme Value Type 1 and 3) live load distribution. From examination of the load moment distribution, generated using Monte Carlo simulation it is clear the distributions conform to neither a normal or lognormal distribution due to the biased nature of the random sampling. The beam resistance is the product of a random variable (Section modulus) with a normal distribution and a random

variable ( $F_{sy}$ ) which is the result of a complicated non linear function involving six constituent random variables. The mean value and distribution of yield strength, due to its dependence on the temperature of the steel, varies with time refer Figure 7.2.

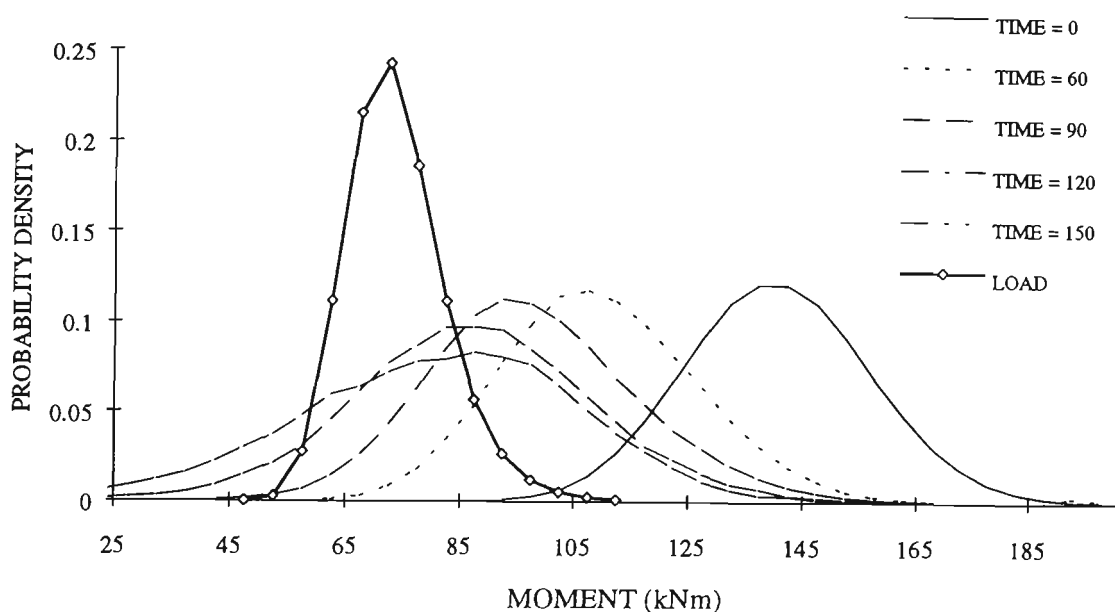


Figure 7.2: Simulated load distribution and variation in mean value and shape of distribution of resisting moment of steel beam exposed to fire for 0 - 150 minutes - Author.

Results from FOSM methods are considered acceptable at high levels of probability ( $10^{-3}$ ) even although the distribution functions are non-normal. At low levels of probability ( $10^{-5}$ ) the error due to tail sensitivity becomes manifest [Ang, 1973]. The potential error due to poor modelling of the tails of the distributions is evident, refer to the insert in Figure 7.3. It can be seen that the area under the tail (a measure of the probability of failure) of the simulated load and the assumed distribution for resistance is significantly larger than the area under the tails of the simulated distributions. That is a larger probability of failure is predicted.

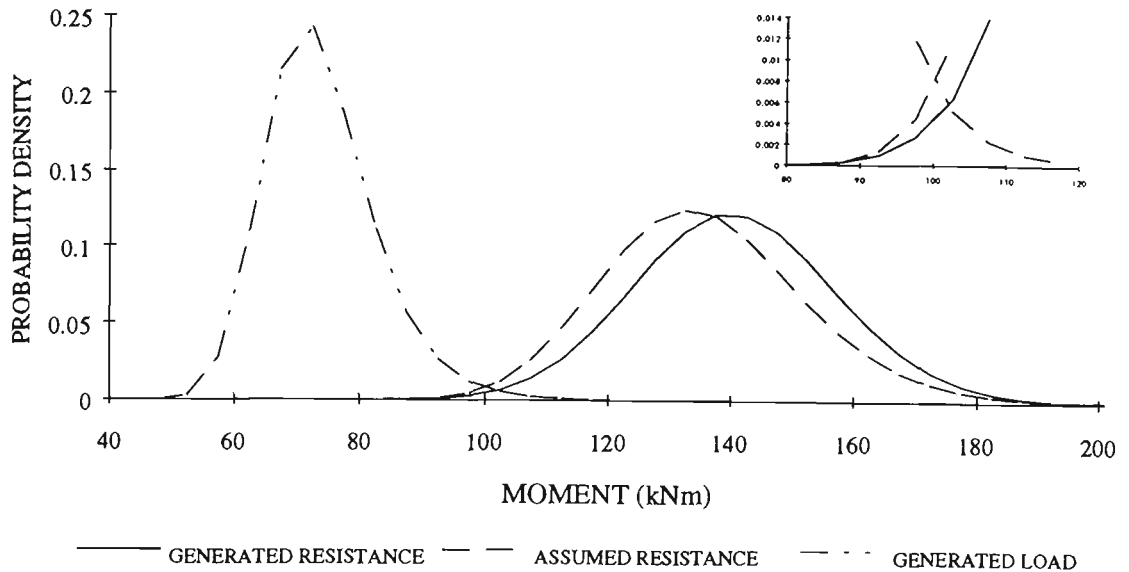


Figure 7.3: Comparison between the shape of the resisting moment distribution obtained by simulation and that obtained using second moment methods in which the resisting moment is assumed to be lognormally distributed - Author.

In order to calculate the time dependent probability of failure it is necessary to calculate the failure rate at each time step. The use of SM or MVSM methods to calculate the overall probability of failure may be appropriate but not so the time incremented failure rate where the probability of failure in any one time interval may be very small. The increasingly skewed distribution of  $F_{sy}$  as a function of fire duration will increase the error.

### 7.3 Reliability Sub-Model

The Monte Carlo simulation method has been adopted to estimate the probability of failure of the steel beam. The Monte Carlo simulation technique

involves "sampling at random to simulate artificially a large number of experiments". If  $N$  trials are conducted, the probability of failure is given by Equation (7.12) as follows:

$$pf = \frac{n(G \leq 0)}{N}$$

where  $n(G \leq 0)$  is the number of trials for which  $G \leq 0$ .

Justification for the use of this technique in preference to using the computationally simpler classical reliability, second moment method or "advanced" second moment methods is based on the following:

The method is more accurate than second moment approach and the computational technique simple to implement. An appropriate level of accuracy of probability of failure is achieved by varying the value of  $N$  hence satisfying the requirements of Subsection (1.1.2). None of the reliability techniques considered above can be used to determine variation in probability of failure with time. The simulation technique can be adapted quite simply to generate a data base of times and modes of failure. The details of how the data base is generated is explained in Chapter 8.

## **CHAPTER EIGHT**

### **MODEL FOR PREDICTING THE PROBABILITY OF FAILURE OF STEEL FLOOR BEAMS IN FIRE**

## **8.0 Reliability Model**

A model to calculate the time varying probability of failure of steel beams (PFSB) in real fire has been developed by combining the following submodels described in previous subsections of this thesis:

- a) Fire severity submodel.
- b) Heat transfer submodel.
- c) Mechanical properties submodel.
- d) Structural response submodel.
- e) Load submodel.
- f) Reliability submodel.

This chapter briefly summarises each submodel, shows how they are linked together and explains input and output data. The program code is given in Appendix A

## **8.1 Model Description**

Each submodel is used sequentially in the reliability model. The operation of each submodel is briefly described:

### 8.1.1 Fire Severity Submodel

The fire severity submodel described in subsection (2.6.5) is adopted from Lie [1974]. The model calculates the variation with time of the gas temperature within an enclosure during a fire. The temperature of the gas within the compartment is assumed to be uniform at any given time during the fire. The fire severity is specified in terms of fire load density and opening factor. Both these parameters are considered random variables and described by a mean, standard deviation and distribution function. The temperature of the gas in the enclosure is calculated at one minute intervals using Equation (2.17) until the fuel is exhausted as determined by Equations (2.1.8). Thereafter the temperature course of the fire in the decay period is calculated using Equation (2.19).

### 8.1.2 Heat Transfer Submodel

The heat transfer submodel described in Subsection (3.4), calculates temperature of steel located within the fire enclosure as a function of the gas temperature versus time curve. The steel temperature is calculated using one-dimensional heat transfer at one minute intervals. For uninsulated steel beams Equations (3.8, 3.9A and 3.10) are used. For steel beams protected by Harditherm 700 insulating board the general Equation (3.16) is used in conjunction with the derived equations for thermal conductivity, Equations (3.25 to 3.27) for beams exposed to fire on four sides and

Equations (3.28 to 3.30) for beams exposed to fire on three sides. The modelling error associated with the derived equations for thermal conductivity is given by the standard error of the fit of the data to the function and is calculated to be 0.0577. The error term is assumed to be normally distributed. Two other parameters are treated as random variables in the heat transfer submodel: insulation thickness; internal dimension insulation configuration. Both are assumed to have normal distributions and have been attributed the following statistical properties:

	Mean	COV
Insulation Thickness	1.0	0.1
Internal Dimension	1.0	0.1

Table 8.1: Statistical properties used in heat transfer submodel.

### 8.1.3 Mechanical Properties Submodel

The mechanical properties submodel calculates the change in the yield strength of steel due to variation in the steel temperature. For a beam exposed to fire on four sides Equation (4.4) is used, refer Subsection (4.5.2). In the case of a beam exposed to fire on three sides and therefore exhibiting a temperature gradient Equation (4.5) is used. Depending on the ratio of top flange temperature to bottom flange temperature the coefficients will vary. The yield strength of steel is calculated at one minute intervals for the duration of the fire. Two parameters are treated as random variables:

yield strength of steel at ambient temperature; strength reduction model of steel. The yield strength of Australian structural steel was given as 295 Mpa with a COV of 0.1 [Birch, 1991]. The modelling error in predicting the change in yield strength with increase in temperature, the standard error of fit was calculated to be 0.073. Both variables were assumed to be normally distributed.

#### **8.1.4 Structural Response Submodel**

This submodel calculates the resisting moment of a simply supported steel beam at elevated temperature using Equation (5.4). The applied moment due to gravity loads is also determined. In the case of a steel beam supporting a concrete slab composite action is not considered. The section modulus ( $S$ ) is considered to have the same properties at ambient and elevated temperature and is taken to be a normally distributed random variable with a mean and COV of 0.97 and 0.03 [Beck, 1983]

#### **8.15 Load Submodel**

Loading configurations considered are uniformly distributed load and a centrally located point load. Both dead and live load are treated as random variables. Models of dead and live load are given in Table(6.1).

### 8.1.6 Reliability Submodel

The reliability submodel uses Monte Carlo simulation. For each simulation or trial a set of values are generated for each of the random variables noted above. The resisting moment of the beam is calculated at one minute intervals and compared with the moment due to load effect which is time independent. The simulation continues as long as the resisting moment is greater than the moment due to load effect or until the fire is exhausted. If, at any time during the simulation, the moment due to load effect is equal to or greater than the resisting moment the beam is considered to have failed. The time of failure is recorded and the next simulation is initiated with a new set of random variables. The process continues until the preset number of trials is completed. A plot of the time varying probability of failure is produced from the record of times at failure and the record of the total number of failures.

Operation of the simulation program requires the generation of random variates to represent the natural variation inherent in the dominant parameters used in the submodels and the uncertainty in the assumptions used in the models. The generation of true random numbers on a computer is not possible without special hardware, instead sequences of independent pseudo-random numbers are generated with statistical properties as close to those of the true random numbers as possible. A library of numerical algorithms (NAG) is available which can be called as sub-routines during program operation. The programs are written using Fortran 77.

Numbers are generated from specified distributions by obtaining one or more real numbers, uniformly distributed between 0 and 1, and applying a suitable transformation.

A consequence of the pseudo-random generation is that it is possible to generate the same sequence of numbers in different jobs. This is an important consideration when conducting sensitivity trials thereby ensuring change in output is due solely to change in the parameter being investigated.

## 8.2 Program Operation

Monte Carlo simulation is not computationally efficient, particularly for estimates of small probabilities of failure. While this can be a problem in estimating the total (time independent) probability of failure, the problem is exacerbated when calculating the time varying probability of failure. The safety index ( $\beta$ ) of steel beams under normal loading and service conditions is given as 3.5 (0.00024) [Pham and Bridge, 1983].

The number of simulations required to ensure a probability of failure with an error less than 20% with 95% confidence is ~ 400,000 and 1.6 million for an error of 10% with 95% confidence, refer Equation (7.13). A simulation in which many millions of trials are computed requires many hours of CPU time on a modern computer. The model PFSB run on a SUN mainframe computer requires 2.8 hours of CPU time to compute one million trials.

There are two reasons why greater numbers of trials are required to estimate the time varying probability of failure:

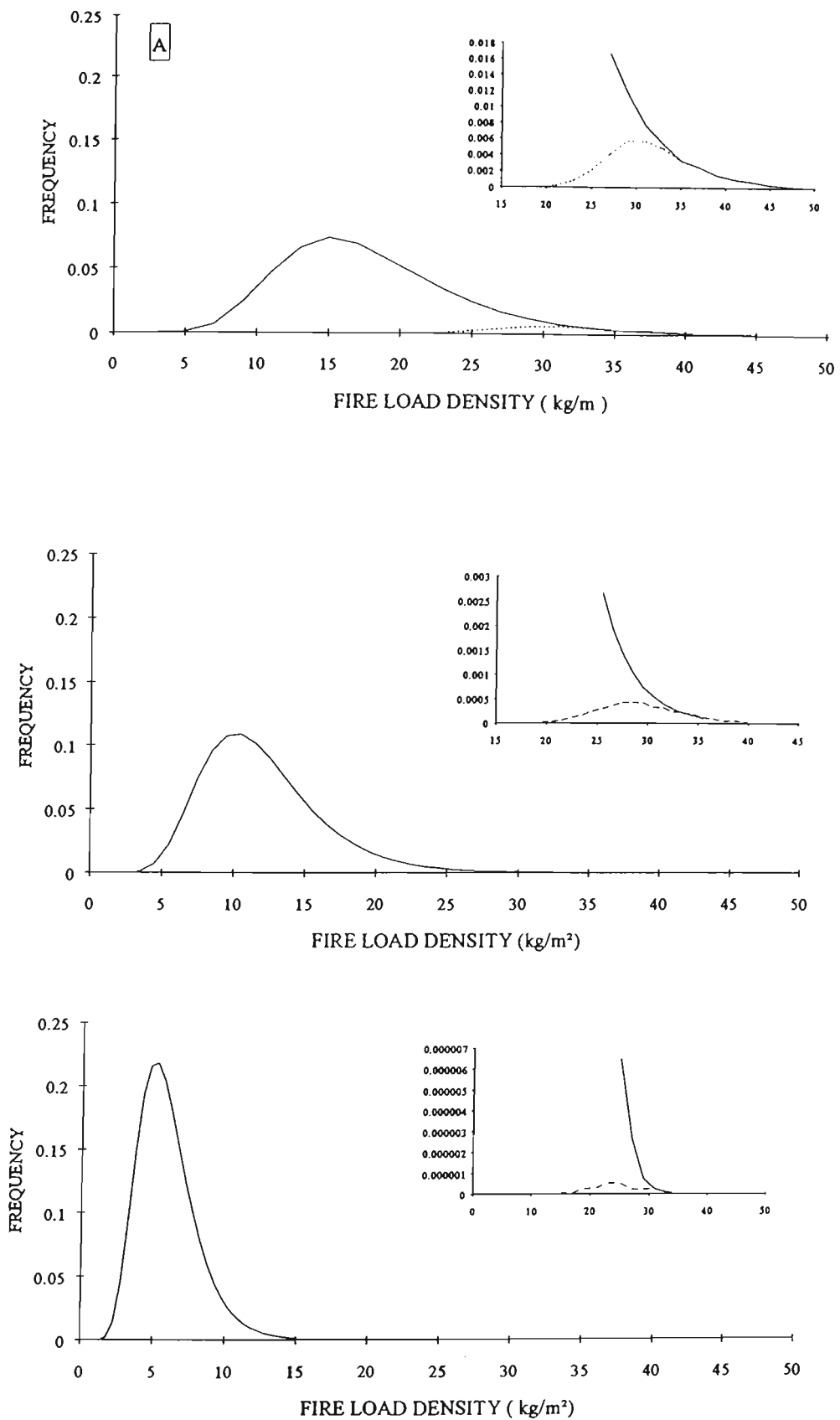
- a) Only those failures that have occurred up to a designated point in time are considered. The conditions that are likely to cause rapid failure such as the simultaneous occurrence of a very high fire load, high gravity load and low yield strength occur with a frequency of approximately one in a hundred thousand (0.00001). For a particular fire condition there may be two or three orders of magnitude difference between the total probability of failure and the probability of failure at a specified time. To achieve statistically significant reliability estimates sufficient failures have to be generated early in the fires history.
  
- b) The load model used for the fire limit state is less than that used for strength limit state. As a consequence the lower bound for failure probabilities for steel beams in fire is smaller. The safety factor for a fire exposed beam due to failure from load effects is approximately 4.3 ( 0.00001) which requires 9.5 million trials to predict the probability of failure at time zero with 20% accuracy and 95% confidence. This is equivalent to approximately 26 hours of CPU time.

## 8.2.1 Variance Reduction

The "crude" Monte Carlo method can be improved by using variance reduction techniques. It is evident that the majority of the simulated fires do not result in failure and are therefore effectively redundant. The simple approach adopted in this thesis is to identify the dominant random variables involved in failure. To estimate the magnitude, range and combinations of those dominant random variables that are likely to result in failure. Use of such 'a priori' information significantly reduces the number of simulations required and hence the CPU time.

The influence of any random variable used in the program PFSB on the probability of failure is assessed by obtaining histograms of selected random variables at failure. It is apparent from conducting this exercise that likelihood of failure is dependent on the steel temperature which in turn is a function of the thickness of insulation and fire load density. Figures 8.1 A), B) and C) show the range of fire load and frequency distributions for three fire loads, 60, 40 and 20 kg/m of floor area (18, 12 and 6 kg/m<sup>2</sup> referenced to total internal surface area, lognormal distribution, COV 0.35). The inserts in each figure show plots of fire load at failure. The number of simulations was the same in all three cases.

It is clear from Figure 8.1. that for the test beam, protected by 20mm insulation board, that as the mean value of the fire load is reduced the probability of failure



Figures 8.1 A-Top), B-Mid) and C-Btm.) - Frequency distribution of fire load density ( main chart) and fire load at failure (insert) [ fire load: A) = 18 kg/m<sup>2</sup> floor area; B) = 12 kg/m<sup>2</sup>; C) = 6 kg/m<sup>2</sup>; opening factor = 0.08 m<sup>1/2</sup>; Ins = 20 mm] - Author. decreases.

This is demonstrated by the size of the area under the frequency distribution of the fire loads that caused failure. It can be seen that as the mean fire load is reduced only those fire load densities one, two and three standard deviations from the mean fire load are likely to cause failure. Further analysis shows that the occurrence of extreme values of parameters other than fire load have a second order effect refer Figure 8.2, in which the affect of variation in thickness of insulation is plotted.. Histograms at failure of gravity load, ventilation parameter and yield strength show that the mean value at failure of each parameter is within one standard deviation of the mean of the original distribution.

A table such as Table 8.2 could be established in the first instance as a guide to assist in future simulations using the program PFSB can be used to efficiently estimate small probabilities of failure. For example a simulation is to be conducted in which an insulated steel beam protected by 20 mm Harditherm 700 insulating board is exposed to a fire severity characterised by a fire load of  $18 \text{ kg/m}^2$  and opening factor of  $0.08 \text{ m}^{1/2}$ . The minimum fire load that is likely to cause failure is  $24 \text{ kg/m}^2$  (approximately one standard deviation past the mean). The number of trials required for statistical significance is 500,000. The program randomly generates this number of fire loads but will only simulate the fire and check for failure if the fire load is greater than or equal to  $24 \text{ kg/m}^2$ . Assuming a lognormally distributed fire load and COV of 0.35, 84.5% of the fires are ignored with a comparable percentage saving in computer time. By setting the limits given in Table 8.2, 90% of all failures are detected.

VENT (m <sup>1/2</sup> )	FIRE LOAD DENSITY (kg/m <sup>2</sup> )					
	24	18	12			6
	INSULATION THICKNESS (mm)					
	20	20	20	30	40	20
0.04						
0.08	28	24.3	20.4			12.3
0.12						

Table 8.2: Table of minimum fire load to be used in simulation for given design fire load ,  
Author.

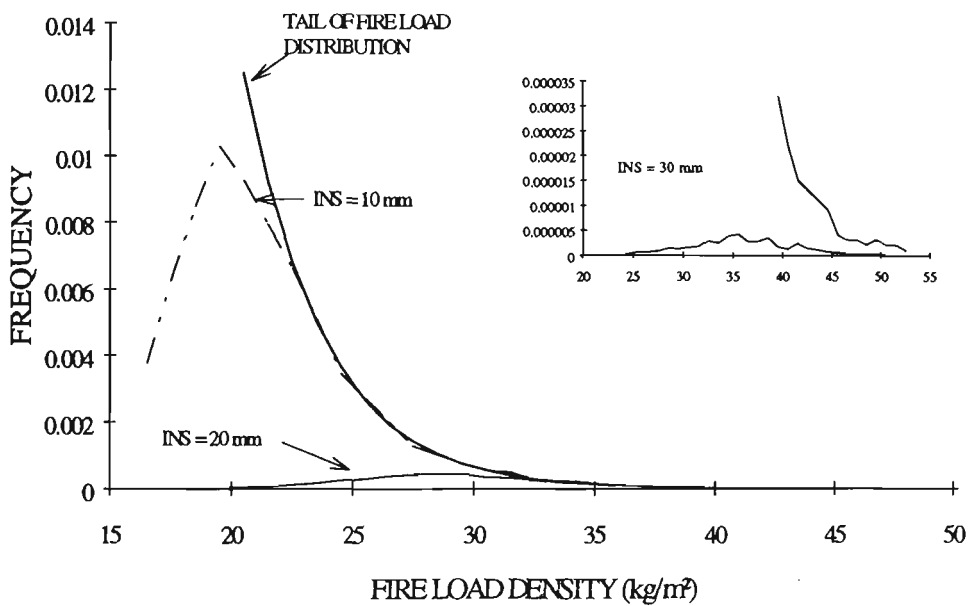


Figure 8.2: Distribution of fire load at failure as a function of insulation thickness [Fire load = 40 kg/m<sup>2</sup>; Ventilation parameter = 0.04 m<sup>1/2</sup>] - Author.

### 8.3 Validation of Model

Inherent difficulties exist in the validation of reliability models. Reliability models are developed as an alternative to experimental testing, the results from which are needed

to validate the model being developed. Due to the expense and difficulty involved in the testing of floor beams subject to real fire there is very little experimental data available which can be used to confirm the results of the model. Validation of PFSB model relies on an indirect comparative approach.

### 8.3.1 General Comparison - Ambient Temperature

A comparison is made in Table 8.3 between estimates of probability of failure calculated using the program PFSB and the expected reliability of structural systems under normal service conditions - as expressed by the safety index. The reliability of a structure is given by the safety index, ( $\beta$ ), refer Equation (7.9). Good agreement - average difference 1.36% - exists between the accepted codified safety index and those values of safety index estimated using PFSB. The maximum difference as expressed as a percentage of the accepted code value is 3.5%.

$\frac{D_N}{D_N + L_N}$	PFSB Simulated	AS 1250 Code Format	PFSB Simulated	AS 4100 Code Format
0	3.4	3.4	3.72	3.75
0.25	3.73	3.8	4.01	4.0
0.50	4.32	4.30	4.35	4.4
0.75	4.53	4.67	4.24	4.4
1.00	4.05	4.13	3.5	3.6

Table 8.3: Comparison between code and simulated safety index for a range of load ratios - Author.

While the program PFSB is primarily developed to estimate failure of steel beams at elevated temperature it is expected that predictions of failure at ambient temperature be consistent with that for structural systems under normal service conditions. In the model, beams exposed to fires of low fire severity suffer little loss of load carrying capacity due to fire. Collapse, if it occurs, is a consequence of the inherent variability in the yield stress of the steel, sectional properties of the beam, the magnitude, type and distribution of the load.

The safety indices used for comparison in Table 8.1 refer to the Australian Standard Steel Code AS1250, based on working stress format and to AS4100, based on limit state format. The statistical models for load and resistance effect used in the development and calibration of the code safety indices are given Table 8.4. Much of this same data has been incorporated into PFSB however the safety index for code calibration was computed using advanced second moment methods [Leicester, 1986] rather than by simulation. It is evident that the use of advanced second moment methods is sufficiently accurate at such probability levels however as noted in Subsection (6.2) second moment methods are not appropriate for determining the incremental change in probability of failure with time.

Parameter	Mean	Coefficient of variation	Type of distribution
Resistance	$2.0R_{Nom}$	0.12	Lognormal
Dead load	$1.05D_{Nom}$	0.10	Lognormal
Live load	$0.74L_{Nom}$	0.25	Weibull

Table 8.4: Statistical models for load and resistance effect used in the code development.

## **CHAPTER NINE**

### **SENSITIVITY ANALYSIS**

## 9.0 Sensitivity Analysis

In the following chapter the influence of the random variables, used in the model PFSB, to model the reliability of an insulated steel roof beam in real fire is assessed. Only those variables expected to have a significant effect (changes greater than 10% ) on the estimate of probability of failure are considered. The influence of selected variables on both the estimated time independent probability of failure and time varying probability of failure are considered. These are:

- a) Fire load density
- b) Ventilation
- c) Insulation thickness
- d) Load ratio
- e) Exposure condition
- f) Strength reduction model

The beam configuration used as the basis of the sensitivity analysis is a 250 UB 37 exposed to fire on three sides. The beam is protected by 20 mm of Harditherm insulating board. The beam is loaded to its design capacity and comprises equal proportions of nominal design dead load and live load. The live load component is modelled as arbitrary point in time live load.

## 9.1 Fire Load Density

Fire load density in this analysis refers to the mass of combustible material per square metre of floor area of the fire enclosure. The fuel, which may comprise a number of natural and synthetic materials, is expressed as an equivalent weight of timber, refer Sub-section (2.5.2).

Fire load density is assumed to be a random variable and described by a mean value, coefficient of variation and a probability density function. The influence of each of these descriptors on the time independent probability of failure and time varying probability of failure is demonstrated.

Based on data from surveys of fire load in office buildings the following mean values of fire load density have been used in the sensitivity analysis; refer (Subsection, 2.5) and characterised for convenience in this analysis as follows:

- a) 20 kg/m<sup>2</sup> low fire load
- b) 30 kg/m<sup>2</sup> medium-low fire load
- c) 40 kg/m<sup>2</sup> medium-high fire load
- d) 60 kg/m<sup>2</sup> high fire load
- e) 80 kg/m<sup>2</sup> very high fire load

## 9.1.2 Probability of Failure - Time Independent

### 9.1.2.1 Mean Value of Fire Load Density

Variation in the estimate of the time independent probability of failure of an insulated steel beam as a function of mean value of fire load density and insulation thickness is given in Figures 9.1 and 9.2. The probability of failure of a steel beam exposed to real fire increases as the fire load density increases. The relationship between the negative logarithm of probability of failure and fire load density is approximately linear as shown in Figure 9.1 and tabulated in Table 9.1. An increase in the mean fire load density of  $10 \text{ kg/m}^2$  at low fire load increases the probability of failure by an order of magnitude while a

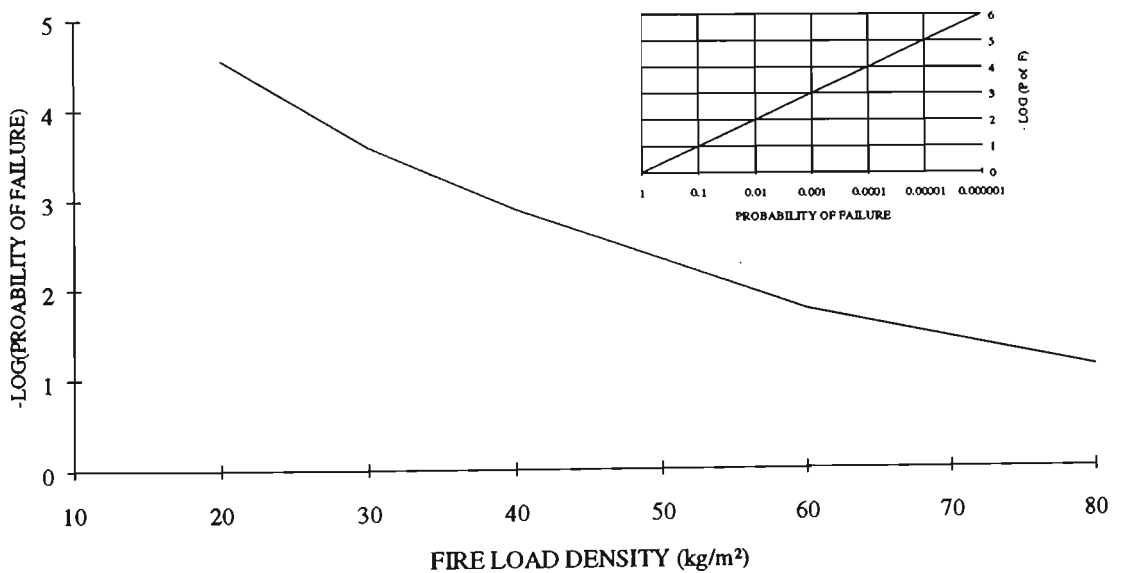


Figure 9.1: Time independent probability of failure as a function of fire load density (FL)  $\text{kg/m}^2$  floor area (opening factor ( OF) =  $0.08 \text{ m}^{1/2}$ , COV = 0.35), [Insert shows relationship between -Log Probability of failure and probability of failure] - Author.

CURVE (Refer Fig. 8.7)	FIRE LOAD kg/m <sup>2</sup> Floor Area	PROB of FAILURE TIME INDEPENDENT
A	20	0.000028
B	30	0.000259
C	40	0.00128
D	60	0.0172
E	80	0.0763

Table 9.1: Time independent probability of failure as a function of fire load density (FL) kg/m<sup>2</sup> floor area (opening factor ( OF) = 0.08 m<sup>1/2</sup>, COV = 0.35).

corresponding increase in the mean fire load at high fire load, and therefore high probability of failure, increases the probability of failure by a factor of approximately 4.5. Thus the rate of change in the probability of failure due to variation in fire load density decreases as the probability of failure increases.

Figure 9.2 shows that irrespective of the rate at which a beam will increase in temperature (as influenced by the insulation thickness), the relative change in probability of failure remains approximately constant.

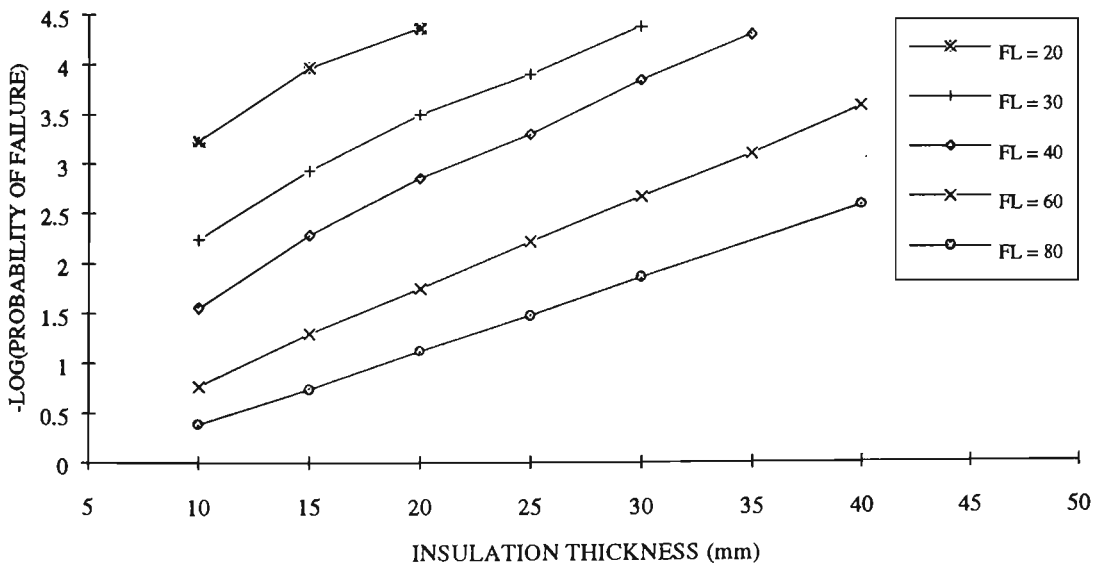


Figure 9.2: Time independent probability of failure as a function of fire load density FL (kg/m<sup>2</sup>) and thickness of insulation (mm) - Author..

### 9.1.2.2 Coefficient of Variation of Fire Load Density

The coefficient of variation (COV) is a measure of the distribution of a variable about the mean value. Alternatively the COV can be considered a measure of the uncertainty associated with a variable. A default value of COV of 0.35 has been adopted for fire load density in the program RSB. This corresponds with the value adopted in the Swedish Fire Engineering Design of Steel Structures [Magnusson, 1976] for offices although higher values have been reported, refer Table 2.2..

Table 9.2 and Figure 9.3 show the variation in probability of failure as a function of COV of fire load density for two mean values of fire load, 40 and 80 kg/m<sup>2</sup>. At a medium-high value of fire load, 40 kg/m<sup>2</sup>, a 100% increase in COV of fire load increases the probability of failure by a factor of fourteen, while at very high fire load, 80 kg/m<sup>2</sup>, the same increase in COV increases the time independent probability of failure by a factor of two.

CURVE Refer Figure 9.9	FIRE LOAD kg/m <sup>2</sup> Floor Area	COEFFICIENT OF VARIATION	PROBABILITY of FAILURE TIME INDEPENDENT
A	80	0.35	0.0728
B		0.52	0.1143
C		0.70	0.1379
D		1.00	0.1515
E	40	0.35	0.00128
F		0.52	0.00677
G		0.70	0.01744
H		1.00	0.03443

Table 9.2: - Probability of failure as a function of fire load density and coefficient of variation of fire load density (OF = 0.08 m<sup>1/2</sup>).

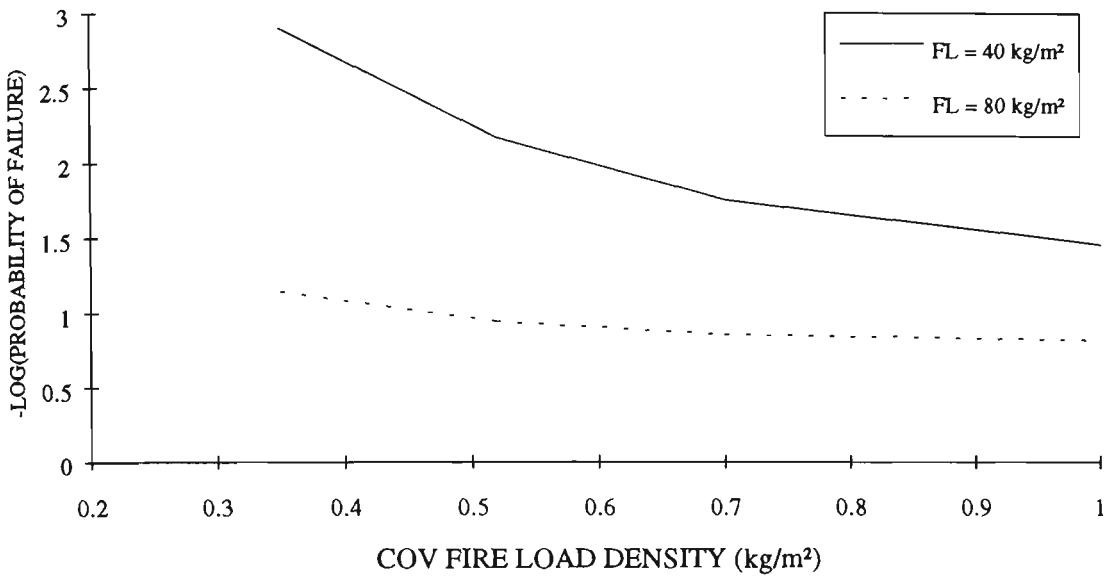


Figure 9.3: Probability of failure as a function of fire load density and coefficient of variation of fire load density ( $OF = 0.08 \text{ m}^{1/2}$ ) - Author.

Figure 9.3 shows that for medium and high fire load density the use of COV greater than 0.7 has little effect on the probability of failure.

Figure 9.4 shows that for highly insulated beams (insulation thickness  $> 40 \text{ mm}$ ) exposed to fires fuelled by very high fire loads there is a nine fold increase in the probability of failure as the coefficient of variation of fire load density is increased by 50%, from 0.35 to 0.52 and an increase by a factor of 22 when the COV is doubled. At small values of insulation thickness (10 mm) any increase in the coefficient of variation has virtually no effect. For highly insulated beams in fires fuelled by medium-high fire loads there is an increase in probability of failure by a factor of ten when the COV is increased by 50% and a forty fold increase when the

COV is doubled. At small values of insulation thickness there is an increase in the probability of failure by a factor of three as the COV is doubled.

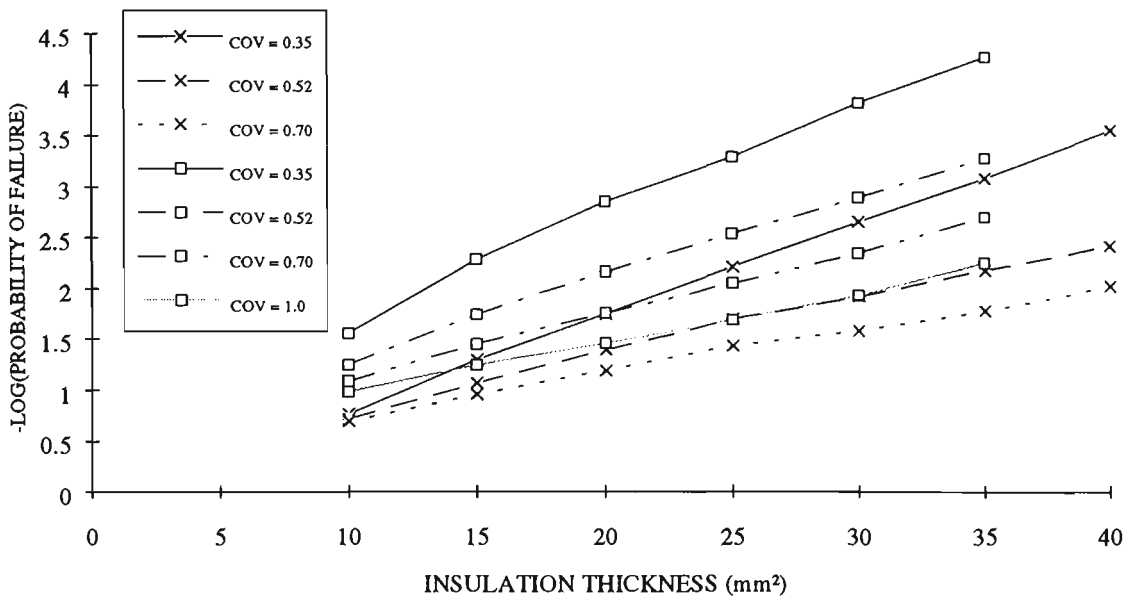


Figure 9.4: Time independent probability of failure as a function of coefficient of variation of fire load density and insulation thickness (based on fire load density of 40 - □ and 60 - × kg/m²; OF = 0.08m<sup>1/2</sup>) - Author.

The reduction in the sensitivity of probability of failure to increases in COV, as demonstrated by the flattening of the slope of the curves in Figure 9.4, is explained in Figure 9.5 in which four theoretical distributions of fire load corresponding to COV's of 0.35, 0.52, 0.7 and 1.0 are given. As the COV increases there is a shift to the left of the mode of the distribution and an increase in the probability of extreme fire loads being generated. Table 9.3 shows that as the COV is increased to one, the rate at which the area under the tail of the

distribution increases, is steadily less. Consequently the likelihood of generating additional high fire loads, that may contribute to failure, decreases. At the same time the skewing of the distribution to the left also reduces the likelihood of generating fire loads that will contribute to failure.

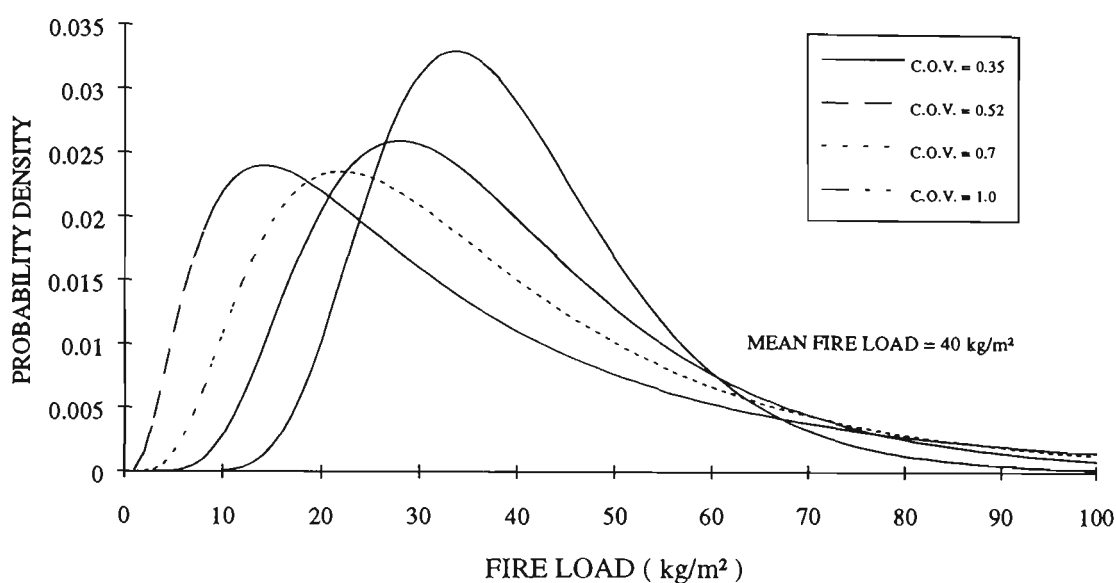


Figure 9.5: Frequency distribution of fire load for a range of values of coefficients of variation - Author.

COV	0.35	0.52	0.70	1.00
% AREA > 60 kg/m <sup>2</sup>	8.6	14.0	17.0	18.3

Table 9.3 - Area under tail of distribution with increase in COV (based on Lognormal distribution).

### 9.1.2.3 Probability Density Function

Different probability density functions may be fitted to fire load survey data with similar levels of confidence. Depending on the function chosen there may be a good match between theoretical and measures values at or about the mean value or about the extreme value statistics or both, refer Figure 9.6. The distribution of fire load density is assumed to be described by a lognormal probability density function, refer Subsection (2.5.1). The effect on the probability of failure of a steel beam in real fire in which the fire load density is assumed to be described by two alternative distribution functions namely, Gamma and Weibull, is given in Table 9.4.

FIRE LOAD	FIRE LOAD = 40 kg/m <sup>2</sup>		FIRE LOAD = 80 kg/m <sup>2</sup>	
	P of F	$\overline{FL}$ @ FAIL	P of F	$\overline{FL}$ @ FAIL
LOGNORMAL	0.00139	24.5	0.07069	39.9
GAMMA	0.00103	21.0	0.07228	38.5
WEIBULL	0.00087	17.6	0.07023	36.2

Table 9.4 Time independent probability of failure as a function of probability density function ( $\overline{FL}$  @ FAIL denotes average fire load density at failure) - Author.

At high fire loads the magnitude of the probability of failure is not influenced by the choice of distribution function. Figure 9.6 shows that despite an obvious difference in the shape of the theoretical distribution of fire load represented by a

lognormal and weibull density function, due to compensating factors, the calculated probability of failure is the same. At medium-high fire load (40 kg/m<sup>2</sup>), in comparison to the lognormal distribution, the probability of failure calculated using a gamma and weibull distribution is 25% and 40% smaller. The smaller probability of failure at low fire load is due to the difference in shape of the tail of the distributions, refer to the insert in Figure 9.6 The number of standard deviations past the mean value of fire load density, at which the average value of fire load density that results in failure occurs, is approximately three in the case of medium-high fire loads and one-and-a-half in the case of very high fire loads. It is apparent therefore consideration needs to be given to the choice of

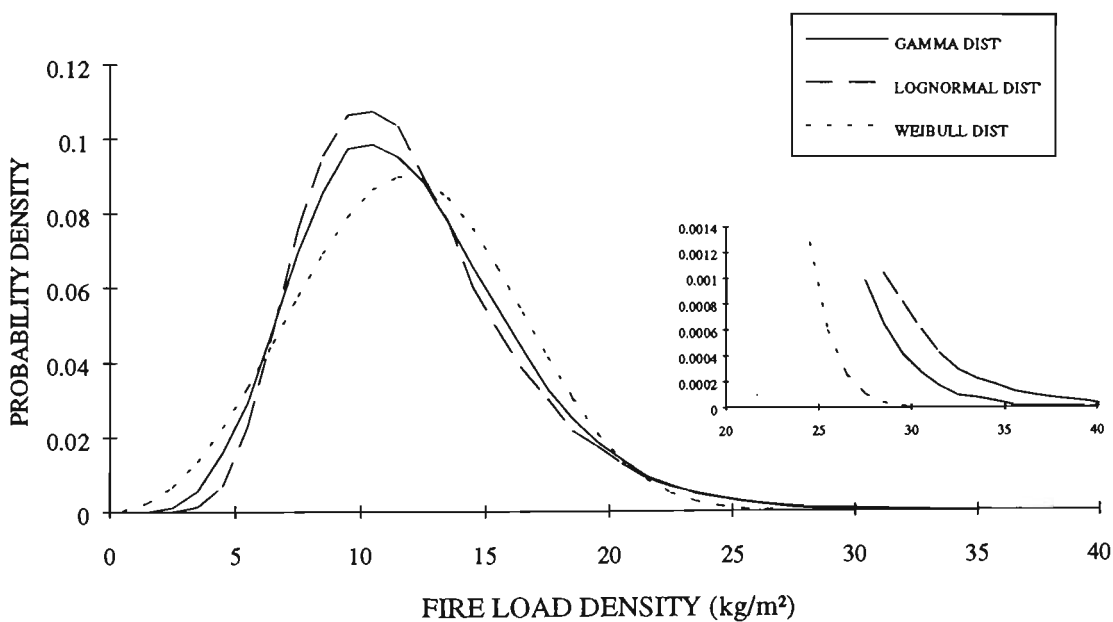


Figure 9.6 - Theoretical distributions of fire load density (based on mean fire load density =40 kg/m<sup>2</sup> and COV = 0.35).

distribution function used to describe fire load when the number of standard deviations between the mean fire load and mean fire load at failure is greater than three. This is likely to occur when low and medium-low fire loads are used and in the case of heavily insulated members where the probability of failure is also likely to be small (less than 0.001).

It can be concluded that at high fire load densities the choice of distribution function is not critical and that at medium and low fire load densities the use of a lognormal distribution function is, compared to the alternative distributions above and, in as far as the distribution represents the data, conservative.

### **9.1.3 Probability of Failure - Time Varying**

Due to inherent variability in fire severity, insulation conditions and loading conditions the length of fire exposure, that a beam likely to fail, can sustain, will vary. Because the design of steel beams for exposure to fire requires that the beam be structurally adequate for a specified fire duration, variation in the probability of failure as a function of time is a more useful estimate of failure than the time independent probability of failure.

### 9.1.3.1 Mean Value of Fire Load Density

Curves representing the time varying probability of failure of the test beam as a consequence of exposure to fires characterised by a range of mean fire load densities is given in Figure 9.7. The time varying probability of failure curve is obtained from the cumulative sum of failures. Typical failure curves comprise five sections and can be idealised as given in Figure 9.8. At time zero, point A on figure 9.8, the probability of failure corresponds with that due to variation in material properties and arbitrary point in time load affects. For the first 10 minutes the failure curve remains almost horizontal, indicating a minimum lag time during which the insulated steel is effectively protected and no temperature effects are possible, region A - B. From 10 to 20 minutes, region B - C, represents failure at temperatures below 100 °C. These failures are due to the simultaneous occurrence of very high values of fire load density, high gravity load and low yield strength, each of which occurs with a low probability, the effect of temperature on the steel contributing little to the occurrence of failure. Region C-D represents the period during which the steel temperature remains constant as moisture in the insulating material is boiled off. As a consequence the probability of failure remains constant during this period.

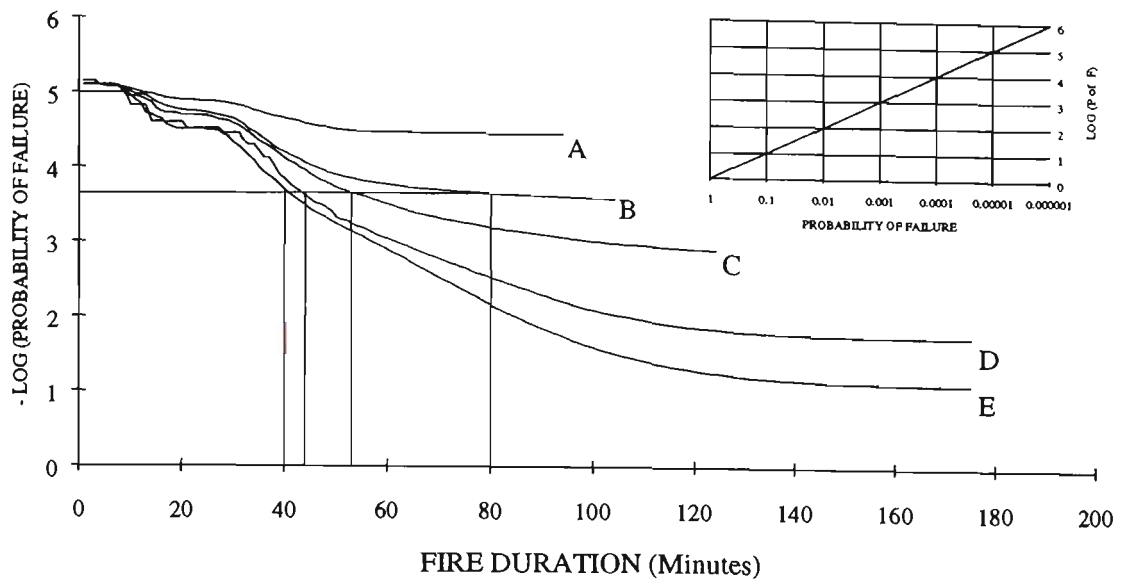


Figure 9.7: Time varying probability of failure as a function of fire load density ( $OF = 0.08 \text{ m}^{1/2}$  A = 20, = 30, C = 40, D = 60, E = 80  $\text{kg/m}^2$ ) - Author.

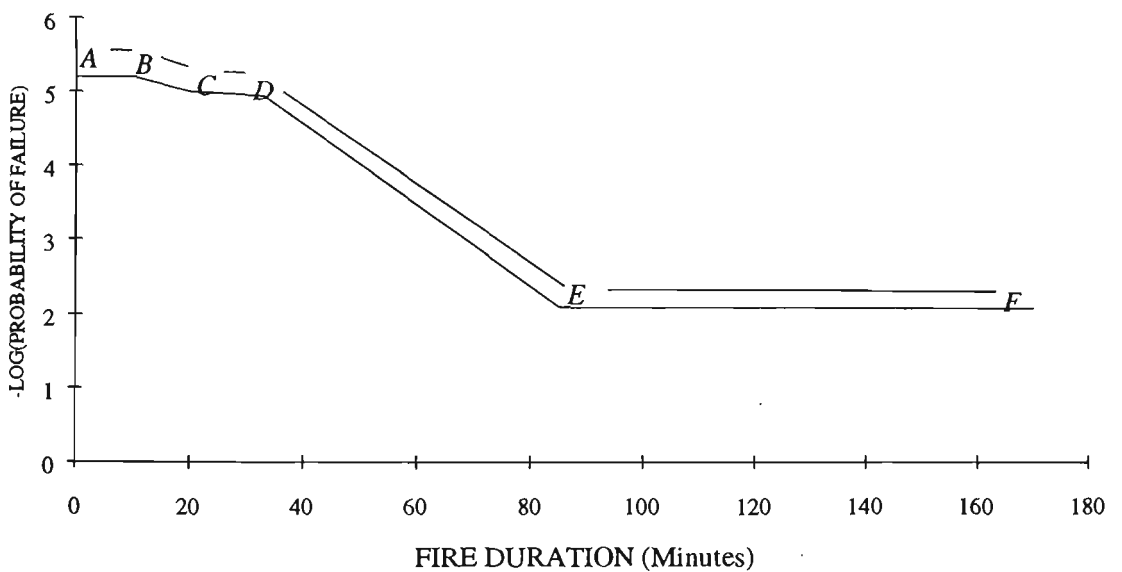


Figure 9.8: Idealised probability of failure curve

As the temperature of the steel continues to rise the frequency of failures increases., region D-E. Eventually all the fires are exhausted and no additional failures can occur, this corresponds with the time independent probability of

failure, region E-F. Depending on the magnitude of the mean fire load density and the degree to which a member is protected by insulating material the time scale in Figure 9.8 will vary.

Figure 9.7 shows that, irrespective of the magnitude of the fire load density, the probability of failure for the first thirty minutes does not vary significantly.

Thereafter there is a rapid divergence between the curves representing various fire load densities. At 60 minutes the test beam is 41 times less likely to fail if it is exposed to a fire fuelled by a low rather than a very-high fire load density. At 120 minutes the beam is 1520 times less likely to fail. At 180 minutes the difference is obtained from the time independent values and corresponds to a factor of 2300. Conversely for a specified target probability of failure the fire resistance period, defined for this analysis as the period of fire exposure sustained before the target probability of failure is exceeded, is reduced as the fire load density is increased. For a target probability of failure of 0.00022 (3.65), corresponding with the probability of structural failure at ambient temperature due to material and load effect, the fire resistance period, for fire load densities of 80, 60, 40 and 30 kg/m<sup>2</sup> reduces from 80 minutes to 53, 44 and 40 minutes respectively. The probability of failure of the test beam, exposed to fires fuelled by small fire load densities, curve A in Figure 9.7, is, at all times, less than that due to structural failure under normal (peak) loading conditions.

### 8.1.3.2 Coefficient of Variation of Fire Load Density

The effect of variation in the COV of fire load density on the time dependent probability of failure of an insulated steel beam is shown in Figure 9.9 for fire load densities of 40 and 80 kg/m<sup>2</sup>. For the particular arrangement investigated variation in the COV of the fire load density has virtually no effect on the time to failure for the first 60 and 90 minutes of fire duration, for the two fire loads investigated. For fires of long duration, variation in the COV has a significant effect on the period of fire resistance achieved for a specified probability of failure. Figure 9.9 shows that for a target probability of failure of 0.0012 (2.9) the period of fire resistance of an insulated steel beam exposed to a fire characterised by a fire load density of 40 kg/m<sup>2</sup> and COV of 0.35 is 150 minutes. For the same probability of failure, a 50 % increase in the COV reduces the time period of fire resistance to 81 minutes. Further increases in the COV to 0.7 and 1.0 however only reduce the period of fire resistance by an additional 4 and 5 minutes respectively.

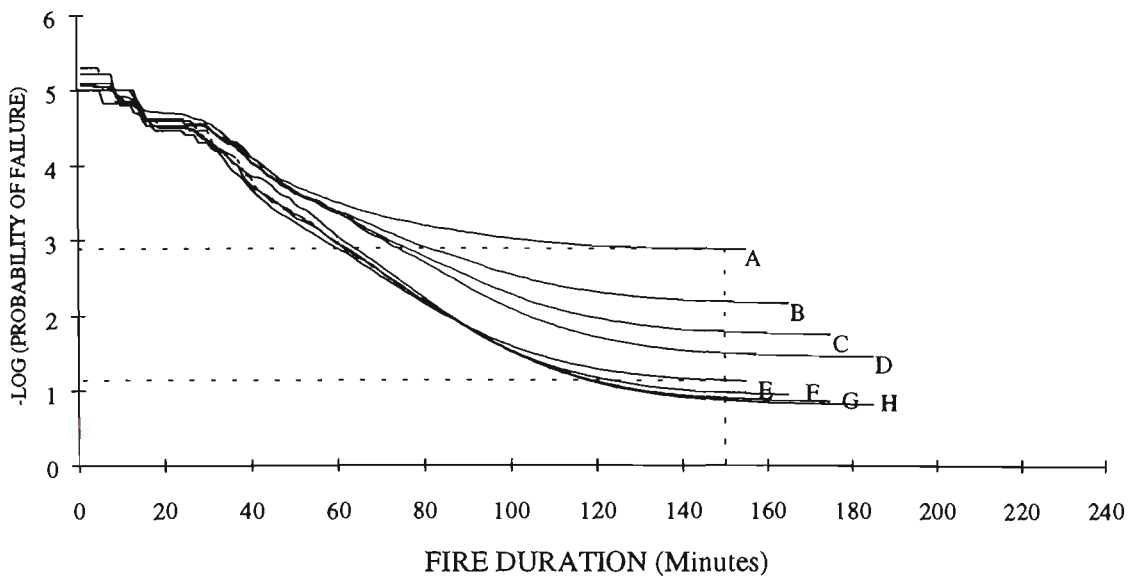


Figure 9.9: Time varying probability of failure as a function of COV of fire load density for two mean values fire load density ( refer Table 9.2 for details) - Author.

At very high ( $80 \text{ kg/m}^2$ ) fire loads, for the same target probability of failure and variation in COV the change in the period of fire resistance is only a few minutes. For a target probability of failure of 0.07 (1.14) and high fire load density a similar trend occurs, as noted previously, in which the period of fire resistance is reduced from 150 minutes to 123, 119 and 118 minutes as the COV is increased from 0.35 to 1.0.

The significance of variation in the COV of fire load density is not readily assessed by inspection of the time independent value of probability of failure. Figure 9.9 shows that consideration of the target probability of failure and period of fire resistance is necessary. It is apparent that, for the arrangement investigated,

for very high fire load densities variation in COV is not important for fire resistance periods less than 90 minutes and in the case of medium fire load densities, 60 minutes.

#### 9.1.4 Conclusion

The magnitude of the fire load density and the uncertainty associated with it, has a significant effect on the probability of failure of an insulated steel roof beam and its period of fire resistance. For the test beam investigated, the probability of failure due to the effect of fires fuelled by low and medium-low fire load densities in combination with arbitrary point in time live load, is no greater than that due to extreme live loads at ambient temperature. It has been shown that the probability of failure of a steel beam, protected by an average thickness of insulation board, increases approximately one order of magnitude per 10 kg/m<sup>2</sup> of fire load at low fire load density and by a factor of five at very high fire load densities. Depending on the target probability of failure, an increase in the mean fire load density of 10 kg/m<sup>2</sup>, reduces the period of fire resistance by 40%. For a given fire load density and target probability of failure doubling the COV increases the probability of failure by more than an order of magnitude and decreases the period of fire resistance by as much as 50%.

It has also been demonstrated that the use of a lognormal distribution to represent fire load density, in as much as it represents the data, is conservative at low fire load densities, in comparison with alternative distribution functions.

## **9.2 Probability of Failure as a Function of Ventilation**

### **9.2.1 Opening Factor**

In Subsection (2.4.2) it was shown that ventilation conditions in the fire enclosure are specified by “opening factor” which is the ratio of the area of ventilation openings in the walls bounding an enclosure to the total internal surface area of the enclosure. Three mean values of opening factor have been used in the sensitivity analysis, 0.04, 0.08 and 0.12 m<sup>1/2</sup>. These sizes were selected for the following reasons;

- a) The model used to generate the temperature time curve is only valid for opening factors between 0.01 and 0.15 m<sup>1/2</sup>.
- b) Opening factors greater than 0.015 m<sup>1/2</sup> are required for flashover (Jansson and Onnermark, 1975).
- c) An opening factor of 0.08 m<sup>1/2</sup> is identified as an overall average (Culver, 1976).

- d) The coefficient of variation of the opening factor is given as 0.1 (Culver,1976).
- e) Based on a COV of 0.1 variability about the selected mean values is achieved without encroaching on the limits of the model.

## 9.2.2 Probability of Failure - Time Independent

### 9.2.2.1 Variation in Mean Value of Opening Factor

Figure 9.10 shows the variation in the estimate of total probability of failure as a function of opening factor.

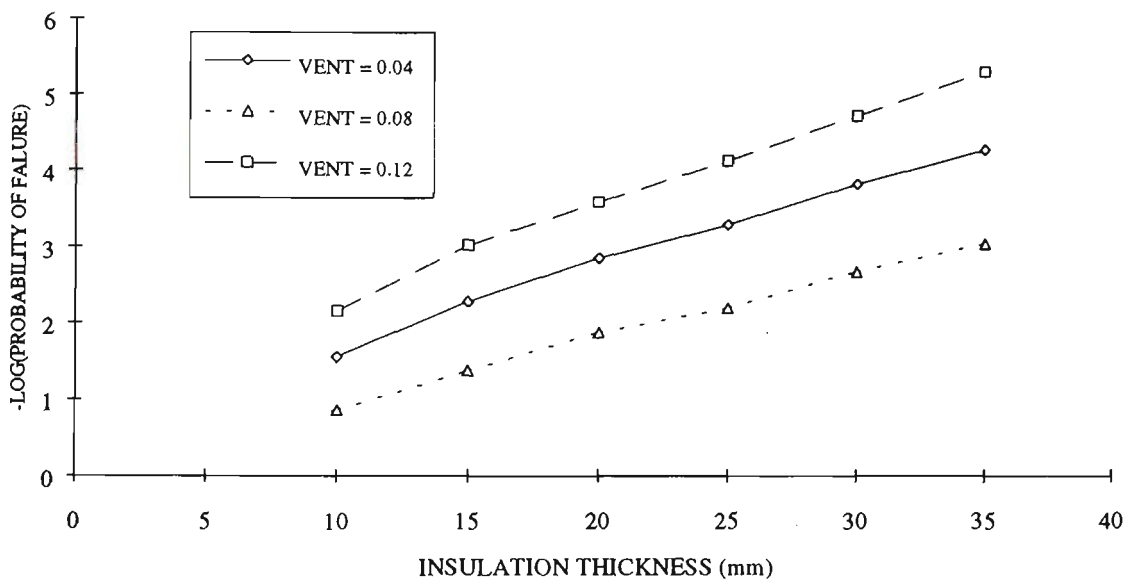


Figure 9.10: Time independent probability of failure as a function of opening factor ( $m^{1/2}$ ) and insulation thickness (mm). COV of opening factor = 0.1 factor ( $m^{1/2}$ ), FL = 40 kg/m<sup>2</sup> -

Author.

Similarly for a beam protected by 10 mm of insulation material, (lightly insulated) and a high probability of failure, the same change in opening factor increases the probability of failure by a factor of 20. It is apparent that, as with fire load density that, at high probability of failure the sensitivity of failure rate to a large change in a basic parameter is greatly reduced.

### 9.2.2.2 Variation in Coefficient of Variation of Opening Factor

An increase in coefficient of variation of the opening factor, from 0.1 to 0.3, increases the probability of failure of a lightly insulated steel beam by a factor of

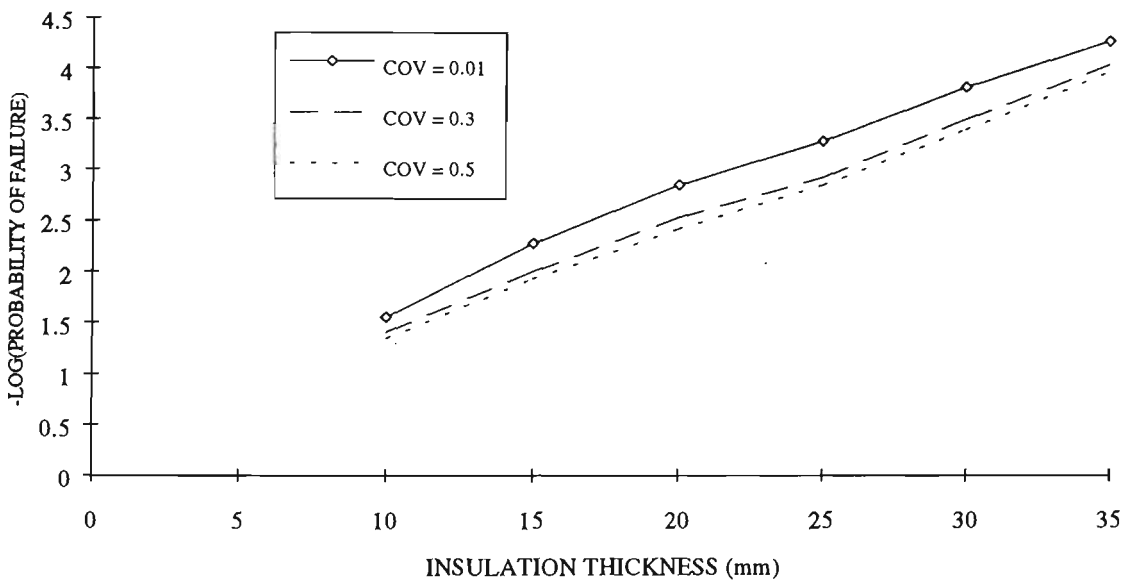


Figure 9.11: Time independent probability of failure as a function of coefficient of variation (COV) of opening factor and insulation parameter (  $OF = 0.08 \text{ m}^{1/2}$  and  $FL = 40 \text{ kg/m}^2$ ) - Author.

1.5, while a five fold increase in the COV increases the probability of failure by a factor of 2.4. For a heavily insulated beam, the corresponding increase in probability of failure is 1.4 and 1.6 respectively, refer Figure 9.11.

It is apparent that the failure rate is relatively insensitive to variation about the mean value of the opening factor and that increasing the COV beyond a value of 0.5 is ineffective. The reason is that there is little skewness in the probability of failure for large opening factor.

### **9.2.3 Probability of Failure - Time Varying**

#### **9.2.3.1 Variation in Mean Value of Opening Factor.**

Curves showing the time varying probability of failure of the test beam for three values of opening factor and two values of fire load density are given in Table 9.5 and Figure 9.12. For the medium-high and very high fire load density variation in the size of the opening factor has little affect on the probability of failure for the first 50 and 100 minutes of fire duration. Thereafter it can be seen that the smaller the opening factor the more rapid the increase in the probability of failure. This phenomenon is due to the influence of the opening factor on the duration of the fire. The size of the opening factor dictates the quantity of oxygen available to the

fire and the rate of heat loss from the fire compartment to the walls and the outside.

CURVE	FIRE LOAD kg/m <sup>2</sup> Floor Area	VENTILATION PARAMETER (m <sup>1/2</sup> )	PROBABILITY of FAILURE TIME INDEPENDENT
A		0.12	0.000275
B	40	0.08	0.00128
C		0.04	0.0146
D		0.12	0.0182
E	80	0.08	0.0763
F		0.04	0.299

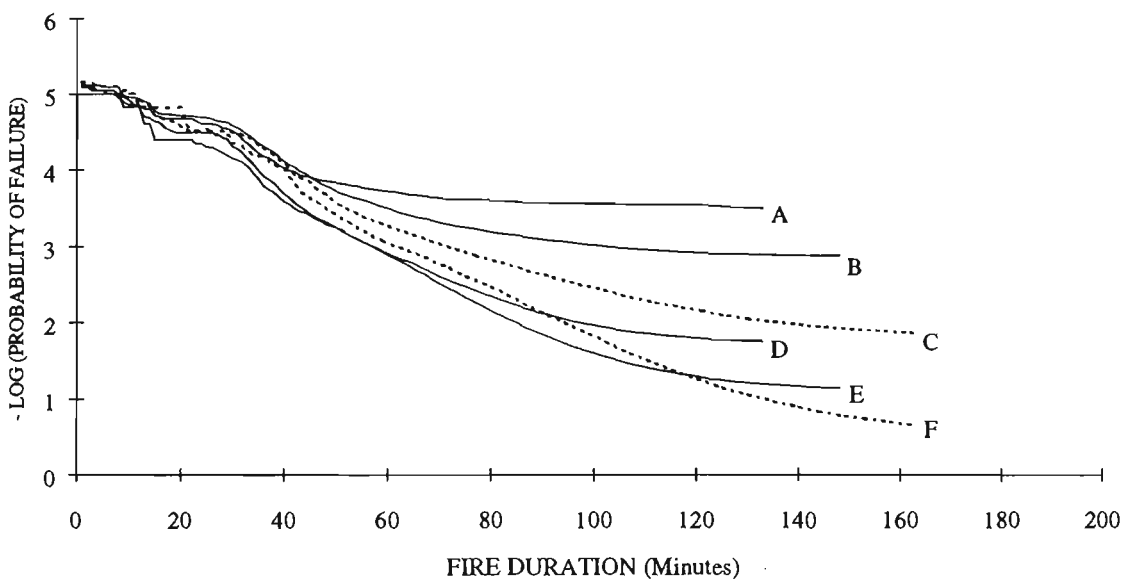


Figure: 9.12 & Table 9.5 - Probability of failure as a function opening factor and two values of mean fire load density - Author.

A fire characterised by a small opening factor will burn longer, but at a slightly lower temperature, than a fire with a large opening factor. As a consequence an insulated steel beam is likely to attain higher temperature since it has longer to heat up and ultimately a greater chance of failure.

### 9.2.3.2 Variation in the Coefficient of Variation of Opening Factor

Based on curves B and E in Table 9.4 the influence of an increase in the coefficient of variation of the opening factor from 0.1 to 0.3, curve B1 and E1, and to 0.5, curves B2 and E2, is demonstrated in Figure 9.13. In the case of a medium-high fire load density, tripling the COV of opening factor has no affect on the probability of failure for the first 100 minutes of fire duration. Thereafter there is a small increase in the probability of failure. For very high fire loads variation in the value of COV is not significant. The explanation given in Subsection (9.2.2.2) seems applicable.

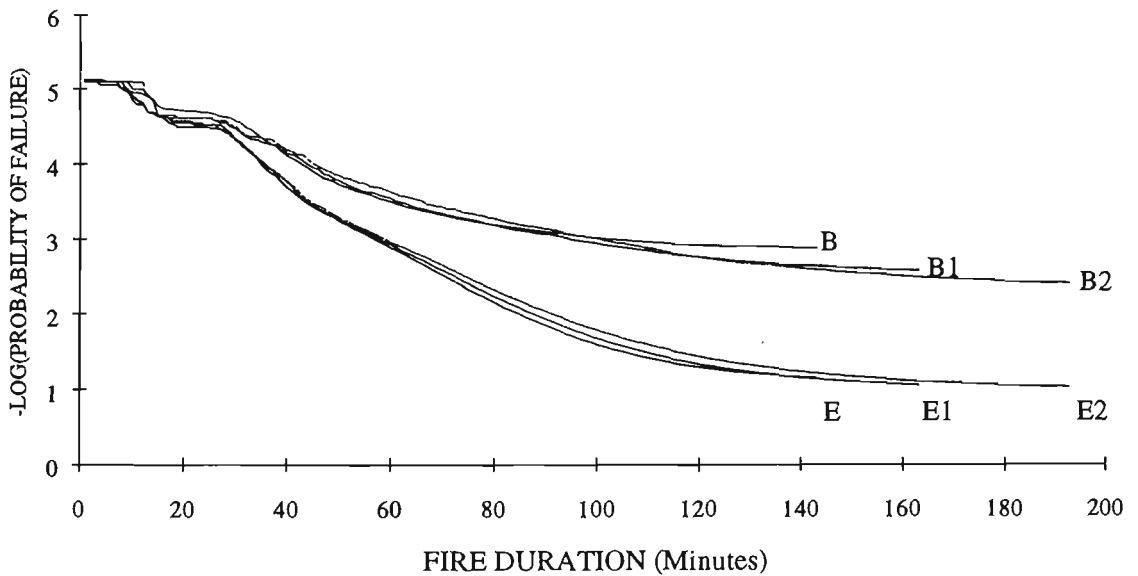


Figure 9.13 - Time varying probability of failure as a function of coefficient of variation of opening factor (refer Table 9.5 for details) - Author.

#### 9.2.4 Discussion

It is convenient in terms of fire modelling that the magnitude of the COV of opening factor is not particularly important. This is because, in reality, variation in the opening factor is likely to be large and to vary during the course of the fire.

The random variability associated with the opening factor can be considered to be composed of two components:

- a) variability due to sampling
- b) induced variability due to the action of fire

a) The opening factor is a measure of the vertical openings in the compartment boundary to the total internal surface area. Statistics based on a survey of all types of offices may well reveal a large spread about the mean value for this parameter. Rather than try to accommodate the effect of the area of window and door space on the severity of a fire in the general case, it makes more sense to assume that a risk assessment, for which this model has been developed, relates to a specific building. The size of the window and door space for specific offices becomes almost deterministic. A small value of coefficient of variation (0.05 - 0.1) is therefore appropriate.

b) It is generally assumed when calculating the opening factor that compartment openings are windows and that all the windows will break after flashover occurs and that doors to the compartment are ajar. The calculated opening factor is therefore taken to be its maximum possible value. Based on observations made during two fire tests conducted by BHP [Almand et al., 1989] in which fire in an office environment was simulated, two scenarios are possible:

- a) the design or maximum opening factor is realised for the full duration of the fire.
- b) the design or maximum opening factor is not realised and that the magnitude of the opening factor varies during the fire.

The two fire tests nominated as O1 and O2, represented a personal office space 4 m square in plan, fitted with contents typical of modern office buildings. A medium-high fire load density ( 42 and 45 kg/m<sup>2</sup>) was used in the tests. In Tests O1 and O2 one wall of the office consisted of a glass window, the opposite wall incorporated a standard timber door. The opening factor was very large and calculated to be approximately  $0.28 m^{1/2}$ . At the start of the tests, in which case the ventilation was effectively zero (other than leakage) difficulty was encountered in initiating the fire in both cases. In test O1 the fire continued to smoulder for 50

minutes without significant development. Similarly in test O2, the fire had almost extinguished itself after 15 minutes. Fire development was achieved only by breaking the glass in two places (Test O1) and by opening the office door to provide ventilation (Test O2). The latter situation corresponding to a ventilation factor of  $\sim 0.03 \text{ m}^{1/2}$ . This supports the contention of Janson and Onnermark that a minimum value of opening factor is necessary for flashover to occur. In both tests there was a rapid increase in the air temperature in response to the increase in ventilation. In Test O1 the increase in air temperature was accompanied by cracking and dislodgment of some of portions of the plate glass windows. The degree to which the "design opening factor " is realised depends on how much of the glass is displaced during the course of the fire. This in turn can depend on the distribution of the flammable materials in the compartment, the height of the room and wind conditions.

The forgoing highlights the fact that the magnitude of the opening factor can vary during the course of a fire and that the calculated maximum value may not be realised in a fire situation. Given that the probability of failure of a protected steel beam in fires fuelled by medium to low fire load densities can increase by over two hundred times as the opening factor is reduced, it is not conservative in such situations to adopt the maximum possible opening factor. Similarly in a small compartment with small windows the area of the door opening may well equal a

quarter to a half of the window area. Doors are very much more resistant to fire and may remain intact for the duration of a fire. The opening factor excluding the door area could be 25 to 50% smaller than the nominal value.

A means of accommodating possible variation in the opening factor during the course of the fire, is to increase the variability about the mean, that is use a large value of COV. It has been demonstrated that, in as far as the fire model used in this analysis represents real fire behaviour, an increase in the COV of the opening factor does not result in a corresponding increase in probability of failure as would be expected for the ventilation conditions prevalent during the fire. It is proposed that a modified mean value or a range of opening factors are used during the fire.

### **9.2.5 Conclusion**

It has been shown that the estimate of the probability of failure is significantly influenced by the ventilation conditions in the fire compartment, as represented by the opening factor. A reduction in the opening factor from 0.12 to 0.04 m<sup>1/2</sup> increases the probability of failure by 200 times. It has also been shown that probability of failure is not sensitive to the magnitude of the coefficient of variation of the opening factor.

It has been noted that , in the case if insulated steel beams, the use of the maximum design opening factor may result in an under estimation of the probability of failure and period of fire resistance, should that value not be realised in reality. In the case of uninsulated steel beams the opposite is true and that the largest possible value of opening factor should be employed to estimate the probability of failure.

### **9.3 Insulation Thickness**

The model RSB is calibrated for one insulation material only at this stage in time, namely Harditherm 700 insulating board. This material is considered representative of the insulating materials presently available and that the performance of this material will in general reflect that of other propriety brands of insulation material.

### 9.3.1 Probability of failure - Time independent

The time independent probability of failure of the test beam as a function of thickness of insulation material for a range of fire load densities is shown in Figure 9.14. At very high to medium-high fire load density for thicknesses of insulation material greater than 10 mm, the relationship between thickness of insulation and probability of failure is approximately logarithmic. The probability of failure is reduced by a factor of approximately 25 for each additional one millimetre of insulation material.

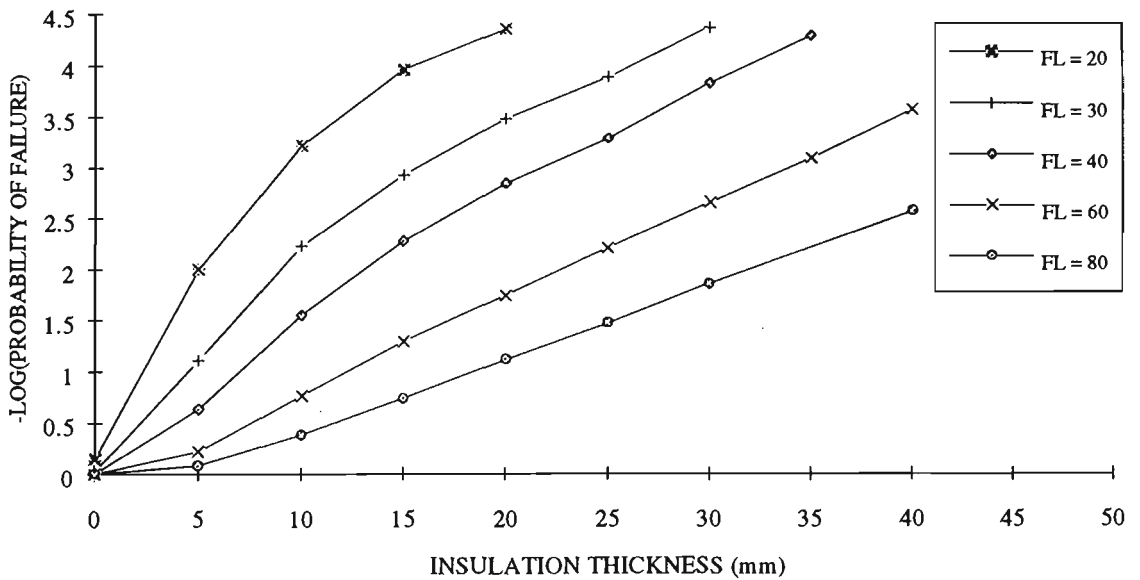


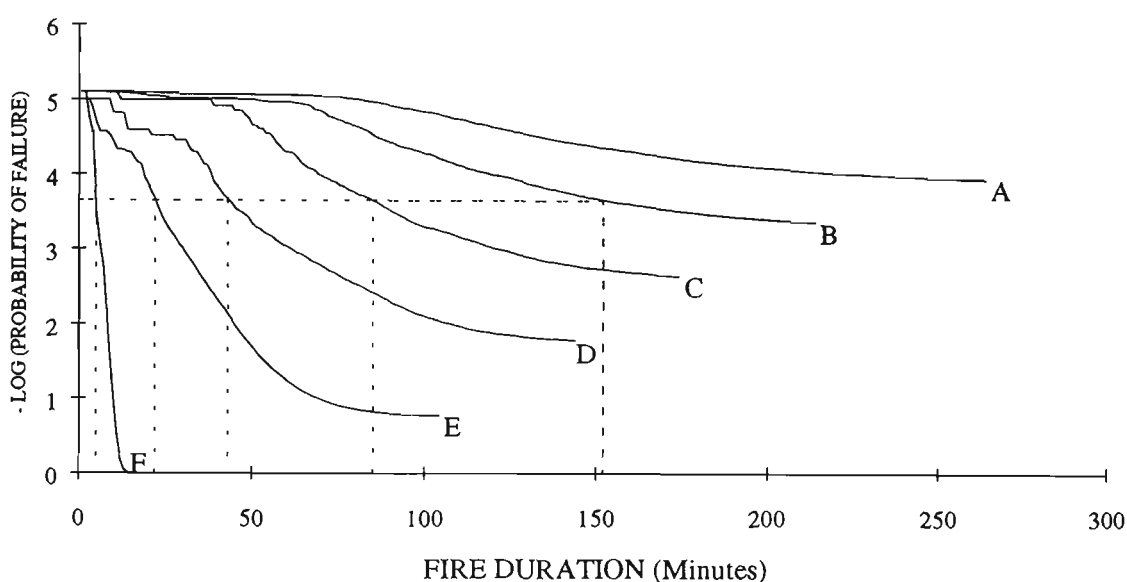
Figure 9.14: Time independent probability of failure as a function of thickness of insulation ( $OF = 0.08 \text{ m}^{1/2}$ ,  $COV \text{ Insulation} = 0.1$ ) - Author.

For thicknesses less than 10 mm the insulation material is not capable of reducing the steel temperature as effectively due to the high gas temperature associated with the large values of fire load density ( in the fire model adopted for a given opening factor, the magnitude of the fire load density defines the maximum gas temperature). For medium-low to low fire load densities, and therefore lower gas temperatures, the insulation material proves to be very effective for this range of fire load, the first 5 mm thickness of insulating material reducing the probability of failure by a factor of 15 to 80 times respectively.

### **9.3.2 Probability of failure - Time dependent**

Curves showing the time varying probability of failure for the test beam for a range of insulation thicknesses is given in Figure 9.15. The corresponding time independent probabilities of failure are given in Table 9.6. It is apparent that with increase in thickness of insulation the fire resistance period, for a specified target probability of failure, increases. For a target probability of failure of 0.00022 (-Log. 3.65) the period of resistance varies from 5 minutes for uninsulated steel to 22, 44, 85 and 152 minutes for insulation thicknesses of 10, 20, 30 and 40 mm respectively.

The probability of failure of steel beams in real fire is modified by the provision of protection. In contrast, an insulated steel beam exposed to the standard fire, the probability of failure is always one. With the use of charts, such as Figures 8.14 and 8.15, the required thickness of insulating material to achieve a target probability of failure and/or period of fire resistance, can be obtained for fires of varying severity



CURVE	THICKNESS OF INSULATION (mm)	PROB of FAILURE TIME INDEPENDENT
A	50	0.000093
B	40	0.00044
C	30	0.00255
D	20	0.0172
E	10	0.1686
F	0	0.9998

Figure 9.15 & Table 9.6: Probability of Failure as a function of Insulation Thickness (Fire Load = 18 kg/m; ventilation parameter = 0.08). Insulating material Harditherm 700 -Author.

## 9.4 Load Ratio and Load Type Ratio

The load ratio being considered is the ratio of the moment due to applied load to the flexural capacity of the beam. The applied load depends on the ratio of dead and live load acting on the beam. The ratio of these two load type varies with time. In this analysis the ratio of load type is considered time invariant. The model of dead and live load used in RSB has been described in Subsections (6.21 and 6.22). The ratios of nominal design dead load to nominal design live load used in the sensitivity analysis are as follows:

DL	:	LL
1	:	3
1	:	1
3	:	1

The dead and live loads for the sensitivity analysis are obtained from the moment capacity of the member using the appropriate capacity reduction factor and load factors. The load type ratio refers to the ratio of dead load and live load before load factors are applied. Figure 9.16 shows the influence of the ratio of load type on the distribution of moment from applied loads, obtained by simulation. Because arbitrary point in time live load is appropriate for strength design in fire situations,

the larger the proportion of the nominal design load effect attributable to live load, the smaller the ratio of applied load to design load.

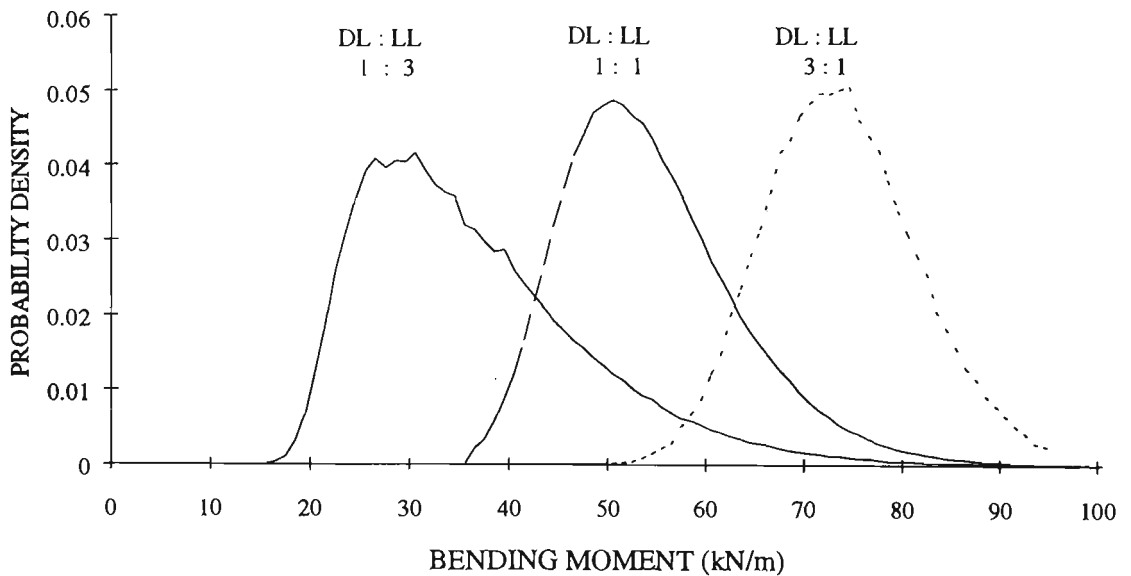


Figure 9.16: Probability density of load moment generated by PFSB for different ratios of dead load to live load (simply supported beam, point load mid-span) - Author.

RATIO	LOAD MOMENT		%
	MEAN	ST' DEV	DESIGN CAPACITY
3 : 1	73.88	7.99	65
1 : 1	54.43	8.91	48
1 : 3	36.82	11.63	32

Table 9.7 - Mean and standard deviation of load moment derived from load models and load ratio expressed as a percentage of design capacity.

The average moment from applied loads and associated standard deviation for the specified load type ratios are given in Table 9.7. Each is expressed as a percentage of the beam design capacity. It can be seen that there is a 50% increase in the design load ratio when the applied load is dominated by dead load compared

with a load effect in which live load is dominant. The COV of the live load dominated load combination is three times larger than that of the dead load dominated load combination. The distribution of the live load dominated load combination is highly skewed towards the right and overlaps the distribution of dead load dominated load combination.

Under normal loading conditions, assuming a DL : LL ratio of 1 : 1, the load ratio is approximately 65% (strength design) and for fire conditions 54%.

#### 9.4.1 Probability of Failure - Time independent

##### 9.4.1.1 Variation in Load Type Ratio

The influence of variation in load ratio, due to variation in load type ratio, on the time independent probability of failure is given in Table 9.8 .

RATIO DL : LL	PROB' OF FAILURE	
	FL = 40 kg/m <sup>2</sup>	FL = 80 kg/m <sup>2</sup>
3 : 1	0.0113	0.1864
1 : 1	0.0016	0.0763
1 : 3	0.00042	0.0364

Table 9.8 - Time independent probability of failure as a function of load ratio.

At medium-high fire load density, in comparison with a DL : LL ratio of 1 : 1, the probability of failure is increased by an order of magnitude when the load effect is dominated by dead load and reduced by a factor of three when live load dominates. At high fire load density the influence of load ratio is much reduced due to the dominating influence of the fire characteristics. It follows that in comparison with the load model used in RSB, the design of steel beams in fire using the current recommendations [AS4100, 1990], in which a load ratio of 54% is used, will result in a higher probability of failure and is therefore conservative.

#### **9.4.1.2 Variation in Load Ratio**

The values given in Table 9.8 are based on full design load adjusted for fire conditions. Under normal service conditions a structural member will rarely be subject to its full design load. In Table 9.9 the probability of failure of the test beam for a range of load ratios is given. Compared with probability of failure for full design load and medium-high fire load the probability of failure is reduced by a factor of 2.7 for 90% load ratio and by a factor of ten if it is only loaded to 70% of its design capacity. At very high fire load densities the reduction is not significant.

DESIGN LOAD RATIO % DL:LL = 1:1	PROB' OF FAILURE	
	FL = 40 kg/m <sup>2</sup>	FL = 80 kg/m <sup>2</sup>
100	0.0016	0.0772
90	0.00062	0.0592
80	0.00029	0.0446
70	0.00015	0.0343

Table 9.9: Time independent probability of failure as a function of a reduced maximum nominal design load ratio (FL = fire load density).

## 9.4.2 Probability of Failure - Time varying

### 9.4.2.1 Variation in Load Type Ratio

The time varying probability of failure of a steel beam in real fire as a function of ratio of load type is given in Figures 9.17 and 9.18 for two fire load densities.

The probability of failure at time zero varies due to variation in the value of the load ratio, refer Table 9.7. In general the smaller the load type ratio the smaller the probability of failure. The probability of failure for load type ratio DL : LL equal to 1 : 1 and 1 : 3 however are almost the same, despite a difference of 16% in moment ratio. This apparent anomaly is explained however by considering the difference in the shape of the distribution of moment due to applied loads. The average value of the moment due to applied load at failure at time zero, determined by simulation for load type ratios 1 : 1 and 1 : 3 is 100.3 and 113.7 kN/m respectively. Due to the highly skewed distribution of the live load dominated load

combination, the area under the tail of the two probability density curves in this region is similar, and as a consequence, the probability of failure is similar.

The shape of the failure curves is as described previously, refer Sub-section 8.1.3.1. The difference in probability of failure at time zero between load type ratios DL : LL of 1:3 and 3:1, is maintained for the duration of the fire. In comparison with a beam in which the nominal dead and live load is equal, a beam in which the applied load is predominantly dead load, has a significantly reduced period of fire resistance.

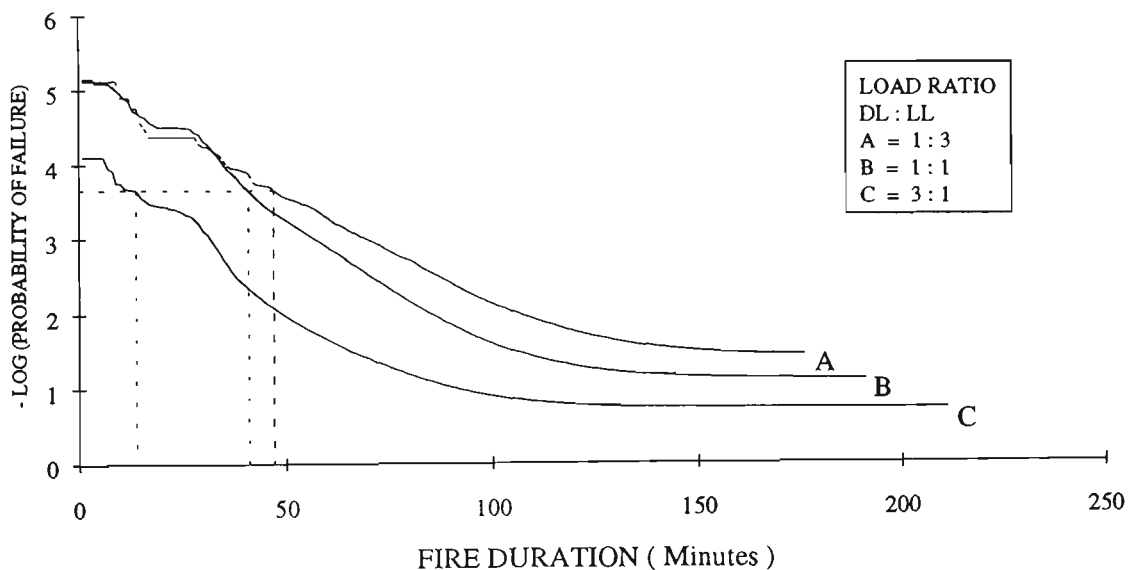


Figure 9.17: Time varying probability of failure as a function of load type ratio of arbitrary point in time live load and dead load (FL =80 kg/m<sup>2</sup>; OF = 0.08 m<sup>1/2</sup> ) -Author.

For a target probability of failure of 0.00022, (-Log. probability of failure 3.7) the period of fire resistance for the test beam investigated is given in Table 9.10 for fire load densities of 80 and 40 kg/m<sup>2</sup>.

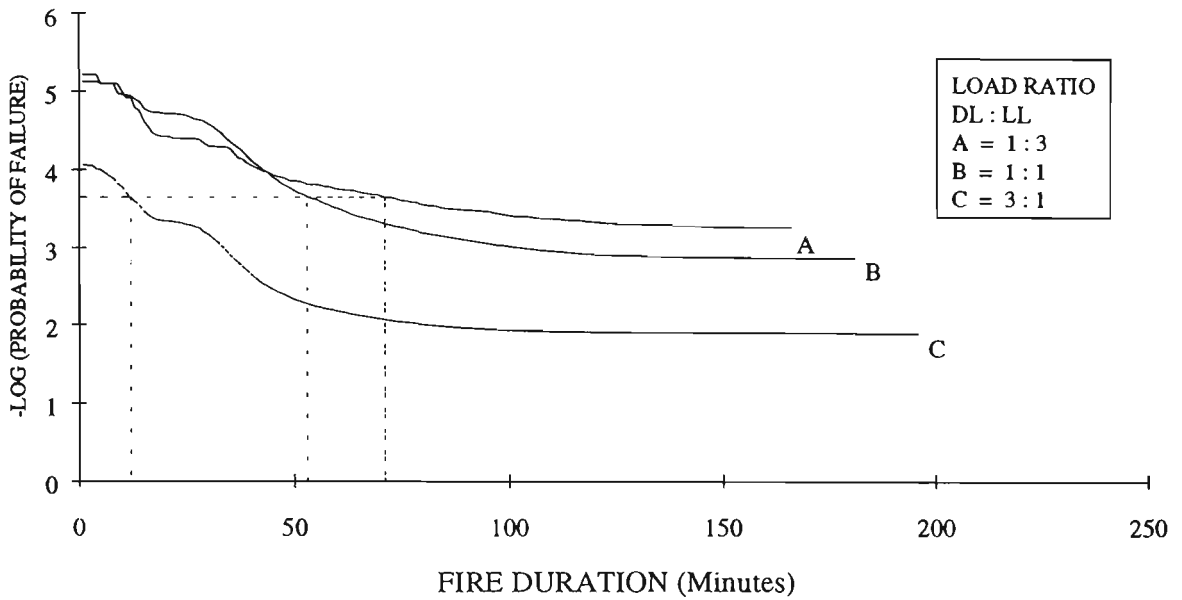


Figure 9.18: Time varying probability of failure as a function of load type ratio of arbitrary point in time live load and dead load (FL =40 kg/m<sup>2</sup>; OF = 0.08 m<sup>1/2</sup>) - Author.

RATIO DL : LL	TIME TO FAILURE (Minutes)	
	FL = 40 kg/m <sup>2</sup>	FL = 80 kg/m <sup>2</sup>
3 : 1	12	13.5
1 : 1	52	40
1 : 3	77	46.5

Table 9.10: Period of fire resistance at probability of failure of 0.00022.

#### 9.4.2.2 Variation in Load Ratio

Curves of variation in the probability of failure as a function of time for a range of load ratios and two fire load densities are given in Figures 9.19 and 9.20. The

probability in failure at time zero decreases as the load ratio decreases. The probability of failure at time zero for a load ratio equal to 33.6% is too small to estimate by simulation (but is estimated by extrapolation to be of the order  $10^{-8}$ ). A 10% reduction in the design load ratio for fire conditions, and each subsequent reduction of 10%, each reduces the probability of failure by an order of magnitude at time zero. For the two fire load densities investigated this effect on the probability of failure is maintained for approximately the first hour of fire duration, thereafter the influence due to load ratio diminishes by 70% in the case of medium-high fire load and 90% for very high fire load, as the magnitude of applied load becomes a less critical.

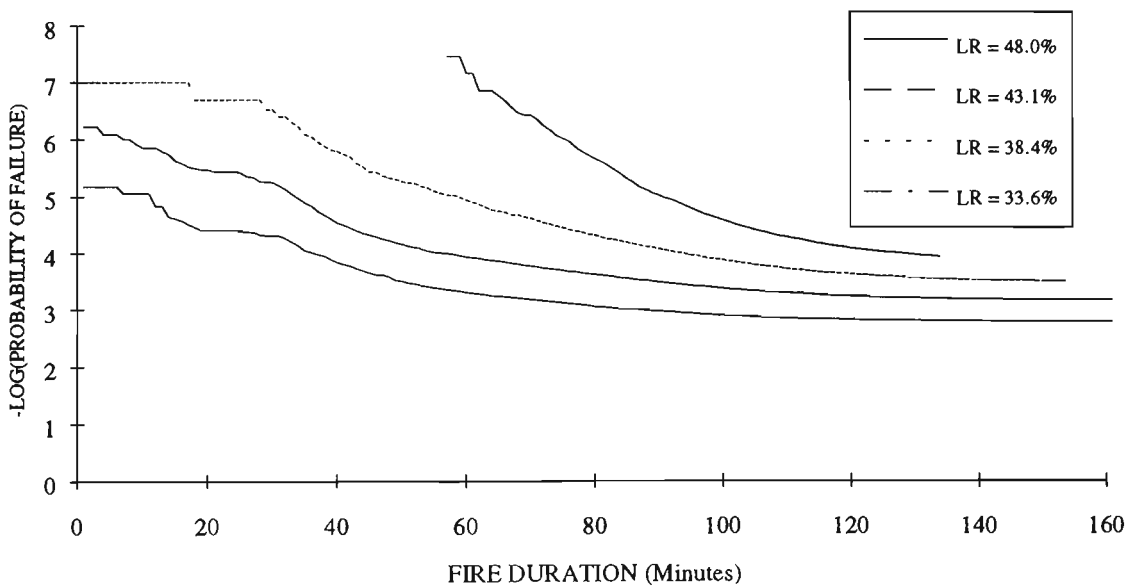


Figure 9.19: Time varying probability of failure as a function of variation in load ratio (FL = 40 kg/m<sup>2</sup>; OF = 0.08 m<sup>1/2</sup>) -Author.

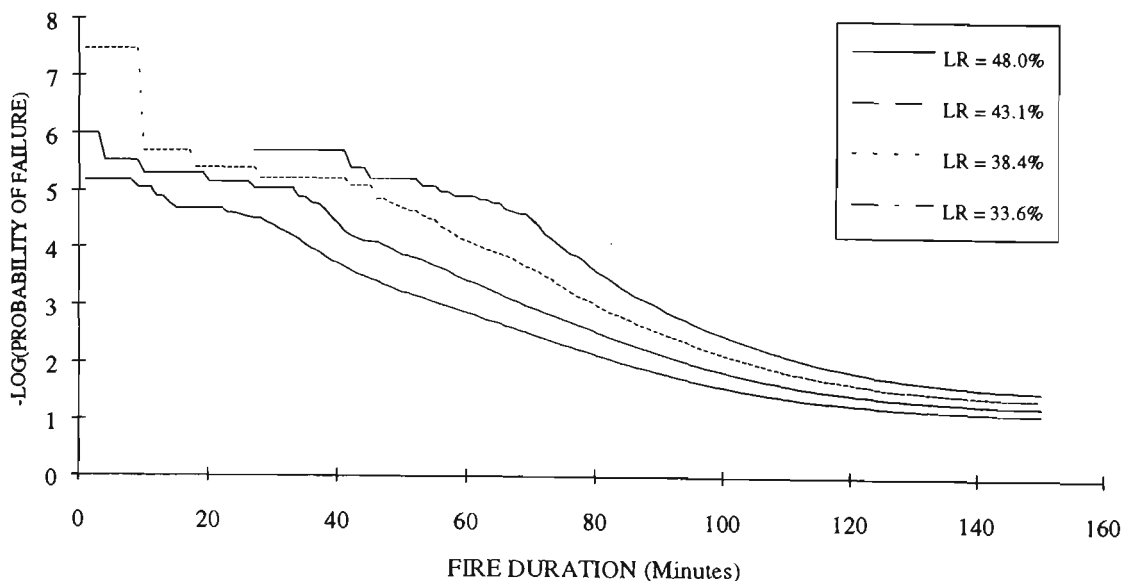


Figure 9.20: Time varying probability of failure as a function of variation in load ratio (FL = 80 kg/m<sup>2</sup>; OF = 0.08 m<sup>1/2</sup>) - Author.

### 9.4.3 Conclusion

Ratio of load type and load ratio both have a significant influence on both the probability of failure and the time variation of probability of failure. It follows that care should be exercised in correctly identifying that proportion of total load effect attributable to dead load. Failure to do so will result in over-estimating the period of fire resistance and underestimating the probability of failure. Conversely significant gains can be obtained in terms of additional safety for a beam designed for full design load under fire conditions but in reality supporting a reduced load.

## 9.5 Exposure Condition

The test case used in the sensitivity analyse so far has been a steel beam supporting a concrete slab, in which case the beam is exposed to fire on three sides. Alternative arrangements are possible however such as a primary steel beam supporting one or more secondary beams, in which case the loading on the structure corresponds to a series of point loads. In this situation flame can envelope the beam, effectively heating it on four sides simultaneously. It has been demonstrated, refer Subsection (3.4.1.3), that due to the smaller exposed surface area and the action of the concrete slab as a heat sink, beams exposed to fire on three sides heat more slowly, and in real fire situations, generally do not attain as high an average steel temperature as those beams exposed to flame on four sides.

### 9.5.1 Probability of Failure - Time Dependent

The variation in probability of failure of a steel beam exposed to fire on three and four sides is given in Figure 9.21, for two fire load densities and a range of insulation thickness. It is apparent that a beam exposed to fire on four sides has a higher probability of failure than a corresponding beam exposed to fire on three sides. For both medium-high and very-high fires loads, a heavily insulated steel

beam heated on four sides is twenty times more likely to fail than if the beam were heated on three sides. A lightly insulated beam, exposed to a fire fuelled by a medium-high fire load density, is ten times more likely to fail in four-sided exposure compared with three-sided exposure.

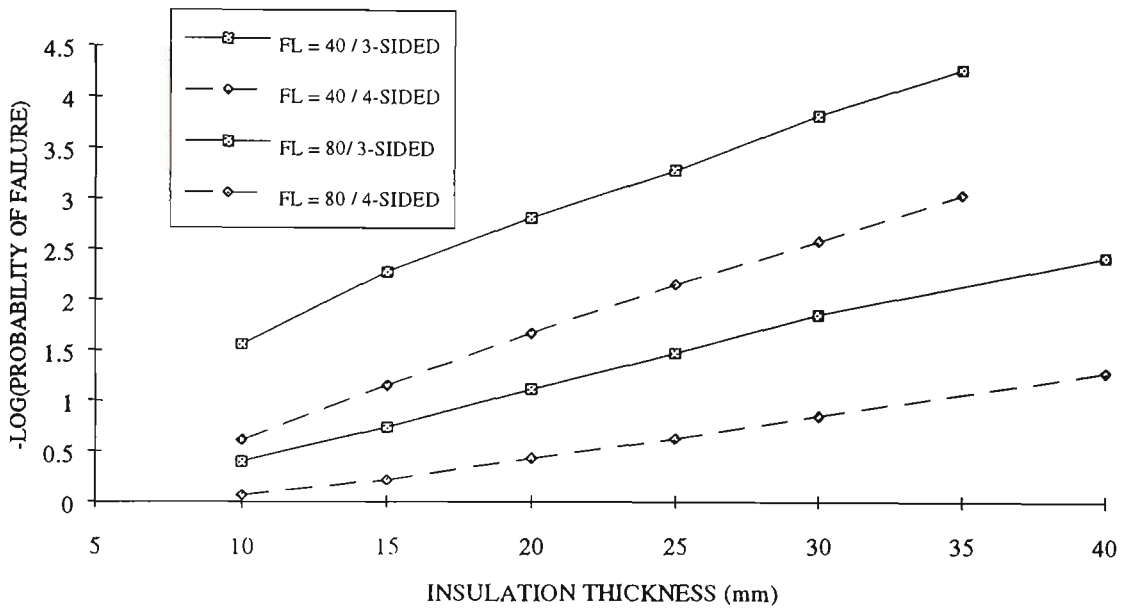


Figure 9.21: Time independent probability of failure as a function of exposure condition for medium-high and very-high fire load density (  $OF = 0.08 \text{ m}^{1/2}$  ) - Author.

### 9.5.2 Probability of Failure - Time Varying

The time varying probability of failure of a beam exposed to fire on three and four sides is given, refer Figure 9.22, for two fire load densities. A beam exposed to fire on four sides has a smaller fire resistance period, for a given target probability of failure, than the corresponding beam exposed to fire on three sides. For both

fire load densities investigated the fire exposure has little influence on the probability of failure during the first forty minutes of fire exposure. Thereafter however, the affect of the more rapid heating rate and higher average temperature of beams exposed to fire on four sides, result in a greater number of failures and an increase in the probability of failure as shown.

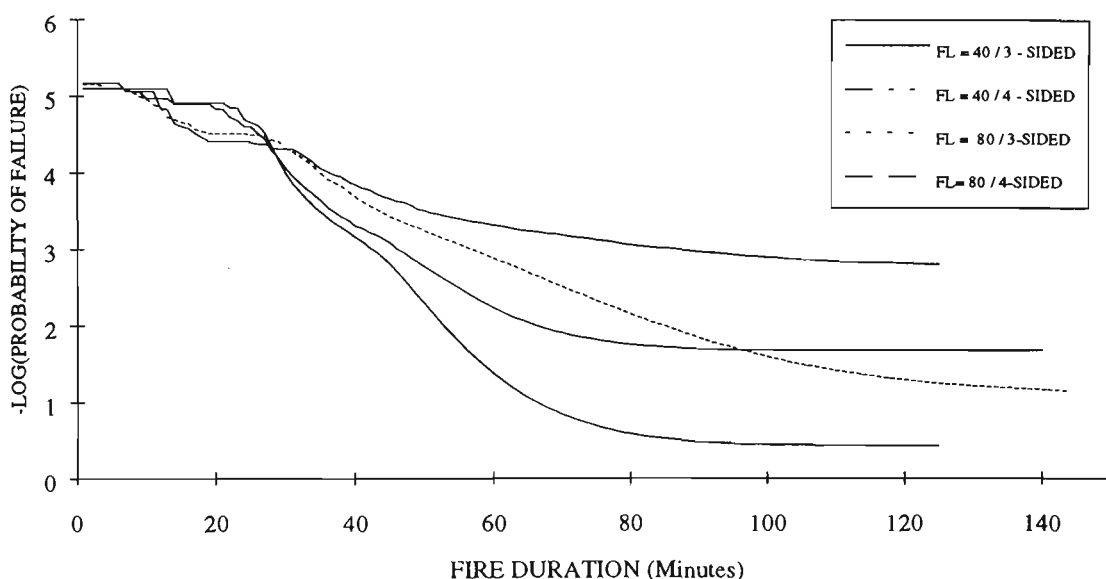


Figure 9.22: Time varying probability of failure as a function of exposure condition for medium-low and high fire load density ( $OF = 0.8 \text{ m}^{1/2}$ ) - Author.

## 9.6 Strength Reduction Model

It was noted previously in Subsection (5.4.2), that a number of strength reduction models are available depending on the value of the proof strain used as a basis for the model. It was suggested that an alternative model for Australian steel, based

on the results of transient test data, would be similar to that used in the British Standard BS 5950. The two British models, one based on a proof strain of 0.02% and the other based on 1.0% proof strain is shown in Figure 9.23.

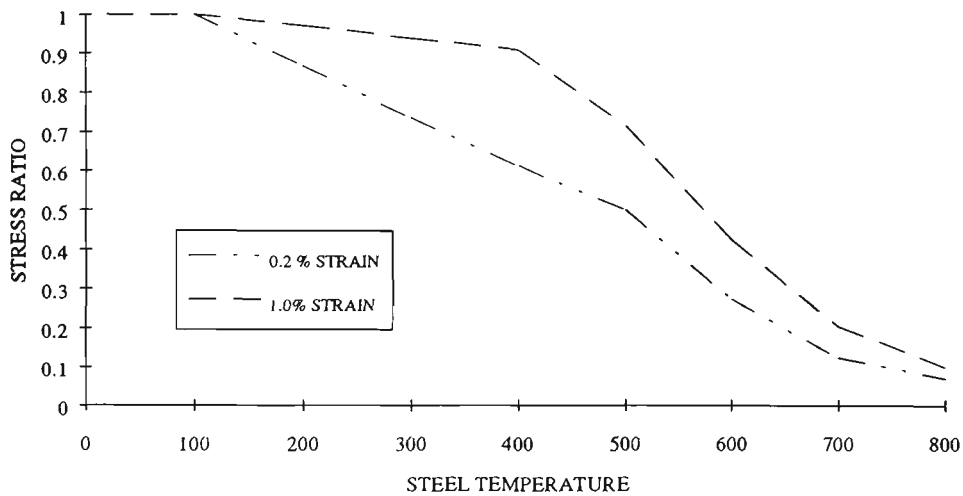


Figure 9.23: Strength reduction model for British steel based on 0.2 and 1.0% proof strain.

### 9.6.1 Probability of Failure

The time varying probability of failure of a steel beam, estimated using the two models, is given in Figure 9.24. Neither model permits loss of strength due to temperature effects until the steel temperature exceeds 100 °C, and in the case of the 1.0% proof strain model there is virtually no loss of strength until the steel temperature exceeds 400 °C. As a consequence the time varying probability of failure remains at the value equivalent to structural failure at ambient temperature

until the beam has been exposed to fire for 47 minutes in the case of the 0.2 % model and 65 minutes for the 1.0% model. After the occurrence of the first failures the probability of failure increases at the same rate for both models. The time independent probability of failure for the 1.0% proof strain model is approximately three times smaller than that predicted using the 0.2% model.

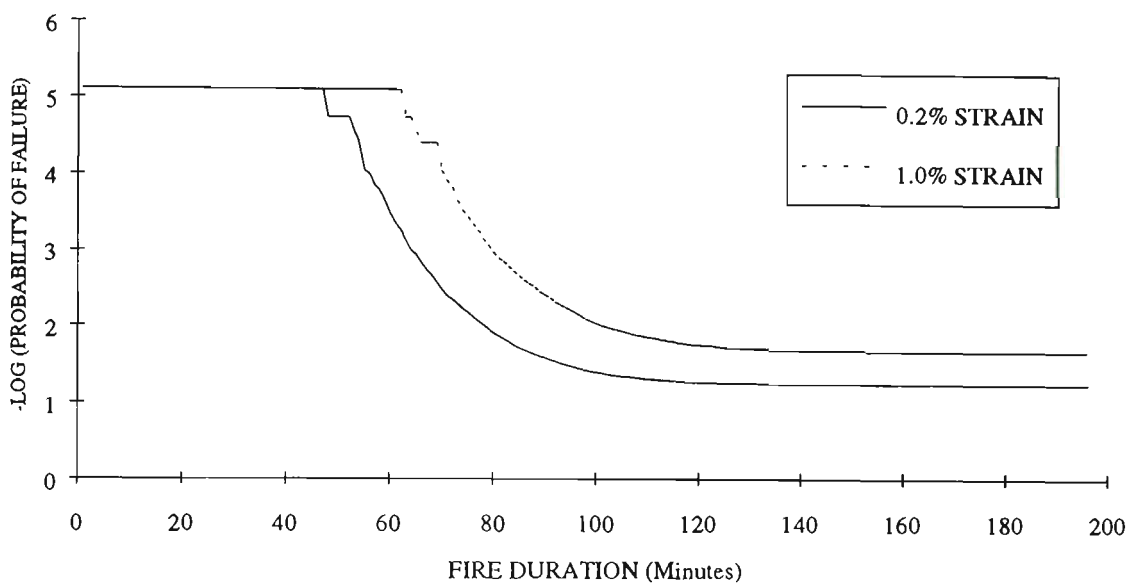


Figure 9.24: Time varying probability of failure for alternative strength reduction models (FL = 60 kg/m<sup>2</sup>; OF = 0.08 m<sup>1/2</sup>; INS = 30 mm; 4-sided exposure) - Author.

## 9.6.2 Conclusion

It is evident that the form of the strength reduction model adopted has a significant influence on the shape of the probability of failure curve and the magnitude of the probability of failure. It also shows that a strength reduction

model based on a small proof strain will result in a conservative estimates of failure and that a model of the same form as the 1.0 % proof strain will increase the period of fire resistance dramatically.

## 9.7 Conclusion

A model has been developed that estimates the time independent and time varying probability of failure of steel beams in real fire. For a specific fire severity, as characterised by fire load density and opening factor, the ratio of beam mass to surface area in the case of a non-insulated beam or the thickness of insulation in the case of a protected beam required to attain a target probability of failure for a specified period of structural adequacy can be determined. The model is a significant advance on the use of the standard temperature versus time curve which does not reflect the true nature of fire nor accommodate the probabilistic approach to the design of steel members for fire.

Based on the results of a sensitivity analysis the following conclusions are made:

The dominant variable influencing the magnitude of the time independent probability of failure is the mean value of the fire load density. An increase in the fire load density of  $10 \text{ kg/m}^2$  at low fire loads, as define in Subsection 9.1, Increases the probability of failure by an order of magnitude while a corresponding

increase in the mean fire load at high fire load increases the probability of failure by a factor of 2. Depending on the target probability of failure, an increase in the mean fire load density of  $10 \text{ kg/m}^2$ , reduces the period of fire resistance by 40%.

The magnitude of the COV of fire load density is significant at low fire load. Doubling of the COV from 0.35 to 0.7 is equivalent to an increase in the mean fire load density of  $10 \text{ kg/m}^2$ . In terms of fire resistance period at low to medium fire load densities for a given target probability of failure doubling the COV decreases the period of fire resistance by as much as 50%. In general the lower the probability of failure whether due low fire severity or thickness of insulation the greater the effect of an increase in the magnitude of COV.

The choice of distribution function used to describe the distribution of fire load density is significant for fire load densities less than  $40 \text{ kg/m}^2$ . At higher fire load densities the probability of failure is of such a magnitude that the shape of the tail of the distribution is less important. For heavily insulated beams where the probability of failure is also likely to be small (less than 0.001) the choice of distribution function becomes significant for fire load densities greater than  $40 \text{ kg/m}^2$ . At medium and low fire load densities the use of a lognormal distribution function is, compared to the alternative distributions above and, in as far as the distribution represents the data, conservative.

For insulated steel beams the probability of failure increases by more than two orders of magnitude as the opening factor decreases. For lightly insulated or unprotected steel variation in the magnitude of the opening factor has little effect on probability of failure. It has also been shown that the probability of failure is relatively insensitive to change in the magnitude of the COV. As a consequence of the foregoing and because the magnitude of the opening factor can vary during the course of a fire it is not conservative to automatically adopt the maximum possible opening factor for use in the design for fire. It is proposed that a weighted mean value or a range of opening factors with a small COV is used in the fire engineering design of steel members rather than a theoretical maximum value of opening factor or mean value and large value of COV.

The insulating material Harditherm 700 had a significant effect on the magnitude of the time independent probability of failure of a fire exposed steel beam. It was found that 10mm thickness of Harditherm 700 decreased the probability of failure by an order of magnitude. Additional 10mm layers of Harditherm 700 decreases the time independent probability of failure logarithmically. It was also found that for a specified target probability of failure the first 10mm of Harditherm 700 increased the time to failure approximately five times compared to that of uninsulated steel. Each additional 10mm layers of Harditherm 700 doubled the time to failure.

Compared to insulated steel beams exposed to fire on four sides, steel floor beams supporting a concrete slab on its top flange have a smaller time independent probability of failure by an order of magnitude.

At medium-low fire load density, in comparison with a dead load : live load ratio of 1 : 1, the probability of failure is increased by an order of magnitude when the load effect is dominated by dead load and reduced by a factor of three when live load dominates. At high fire load density the influence of load type ratio is much reduced.

An insulated steel beam can survive exposed to real fire without increasing the probability of failure past that for normal structural failure at ambient conditions due to the smaller load ratio for fire conditions. Using the probability of structural failure at ambient temperatures as a benchmark a 250 UB beam protected by 20mm of insulation material and designed for gravity loads appropriate for fire conditions will survive a fire fuelled by a medium-low fire load for 70 minutes and a fire fuelled by a very high fuel load for 38 minutes.

## References

- Almand, K. H. et. al., Fire in Offices, BHP, Melbourne Research Laboratories, Report MRL/PS/89 1989.
- ASCE Manuals and Reports on Engineering Practice - No 78, 1992.
- Anderberg, Y., PC-TEMPCALC, Institutet for Brandtekniska, Fragor, Sweden, 1985.
- Anderberg, Y., Modelling Steel Behaviour, Fire Safety Journal, 13 1988.
- Ang, H. S., Structural Risk Analysis and Reliability Based Design, A.S.C.E. Journal of Structural Division, Sept. 1973.
- ASTM E-119 83, Standard Methods of Fire Tests of Building Construction and Materials, Philadelphia, 1983.
- Australian Steel Code AS 4100 (1990).
- Australian Institute of Steel Construction Handbook of Fire Protection Materials for Structural Steel, 1990.
- Babrauskas, V & Williamson, B.W 1979. Post-flashover Compartment Fires; Basis of a Theoretical Model. Fire And Materials, Vol 2, No 2.
- Babrauskas, V., COMPF2, A Program for Calculating Post-flashover Fire Temperatures, National Bureau of Standards, NBS TN 991, 1979.
- Barthelemy, B., Heating Calculation of Structural Steel Members, Journal of the Structural Division, A.S.C.E. August, 1976.
- Beck, V. R. The Prediction of Probability of Failure of Structural Steel Element Under Fire Conditions, The Institution of Engineers, Australia, 1985.
- Bennetts, I.D.et al., Some Factors Relevant to the Testing of Materials in the Standard Fire Test. BHP Report MRL/PS23/81/002, 1981.
- Bennetts, I. D. et. al., Simulation of the Fire Testing of Structural Elements by Calculation, Steel Construction, Vol 19, 1986.
- Beveridge, G.S.G. and Schechter, R.S., "Optimization; Theory and Practice", McGraw Hill, New-York, 1970.
- Birch, Personal Communication, BHP Whyalla 1991
- Bontti, P. Kree, and Kruppa, J., Estimation des Charges Mobililieres d'Incendie dans les Immeubles a Usage de Bureaux, Construction Metallique, No 3, CTICM, September, 1975.

- British Standard 5950, Draft: The Structural Use of Steelwork in Building: Part 8: Code of Practice for the Fire Protection of Structural Steelwork, BSI 1985.
- British Code of Practice for Fire Protection of Structural Steelwork BS. 5950: Part 8, United Kingdom, 1990.
- British Standards Institution, Fire Tests on Building Materials and Structures, BS 476, 1972.
- British Steel Corporation, Elevated Temperature Tensile Properties of Structural Steels, Report No. T/RS/1189/11/80/C, 1980.
- Building Code of Australia
- Cajot, L. G., et al., CEFICOSS, Fire Engineering Design for Steel Structures, CIB W14, Workshop on Structural Fire Safety, Fire Safety Journal, Vol 6, No1,1985.
- Copier, W. Y., Report No. BI-72-73/05.3.11.640, Institute for Building Materials and Building Structures, Delft, 1972.
- Croce, P. A., A study of room fire development: the second full scale fire test of the home fire project, Factory Mutual Research Corporation Serial210114.4, RC 75-T31, 1975.
- CTICM Methode de Prevision le Calcul du Comportement au Feu des Structures en Acier, Construction Metallique, Vol 13, No 4, 1976.
- Culver, C. G., Survey Results for Fire Loads and Live Loads in Office Buildings, NBS Building Science Series 85, 1976.
- Dorn, J. E., Some Fundamental Experiments on High Temperature Creep, J. Mech. Phys. Solids, 3 (1954).
- Dusinberre, G.M. "Heat transfer calculations by finite differences." International Textbook Co. Scranton, PA, 1961.
- Drysdale, D. An Introduction to Fire Dynamics., John Wiley And Sons Chichester, 1985.
- ECCS Technical Committee 3, Fire Safety of Steel Structures 1983.
- Elingwood, B. & Shaver. J.R., Effects of Fire on Reinforced Concrete, ASSC, 1980.
- Ellingwood, B., Galamdos, T.V, MacGregor, J. G. and Cornell, C.A., Development of a Probability Based Load Criterion, Nat. Bureau of Standards, 1980.
- European Convention for Constructional Steelwork, Committee 3 Fire Safety of Steel Structures, 1979.
- Eurocode No 3, Commission of the European Communities, Design of Steel Structures, Part 10: Structural Fire Design 1990.
- Eurocode No 3, Draft - Design of Steel Structures. Commission of the European Communities, 1991.

- Fuimoto, Y. and Kubo, M., An experimental Review of Lateral Buckling of Beams and Girders, Int. Coll. On Stability of Steel Structures Under Static and Dynamic Loads, ASCE, pp 541 - 562, 1977.
- Furamura, F, et al., Nonlinear elasto-plastic creep behaviour of structural steel. J. Constr. Eng., 1985.
- Grubitts, S.J., Fire Safety Engineering in Australia, International Fire Safety Conference, Sydney, 1992.
- Hardie, James. Co Pty Ltd, Fire Test Reports for Harditherm 700 Insulation Board.
- Harmathy, T.Z. Fire and Materials, Vol5, 1981
- Harmathy, T. Z., Postflashover Fires - An overview of the research at the N. R. C. of Canada, Fire Technology, August , 1986.
- Harmathy, T. Z., Combust. Flames, 31, 265-273, 1978.
- Harmathy, T. Z. Fire Safety Design and Concrete, 1992.
- Harmathy, T. Z. & Stanzack, W. W., Elevated Temperature and Creep Properties of some Structural and Prestressing Steels. ASTM STP 464, 1970.
- Hasofer, A. M. and Lind, N. C., An Exact and Invariant First Order Reliability Format, J. of Eng. Mech. Div. A.S.C.E. Vol. 100, 1974.
- Hass, R. et al., STABA-F, Fire Engineering Design for Steel Structures, International Iron and Steel Institute, Fire Engineering Design of Steel Structures, State of the Art, Brussels, 1993.
- Hottel, H. C. and Sarofim, A.F., Radiative Heat Transfer, McGraw-Hill, N.Y. 1967.
- Iding, R. H., Nizamuddin, Z. and Bresler, B., UCB FRB 77-15, University of California, Berkeley, 1977.
- Jeanes, D. C., Methods of Calculating Fire Resistance of Steel Structures, SFPE, Boston 1980.
- Jerath et al., Elevated Temperature Tensile Properties of Structural Steels. BSC Report T/RS/1189/11/80/C 1980.
- Kawagoe, K, Fire Behaviour I rooms, Rep. Buil. Res. Institute No 27. 1958.
- Kawagoe, K. & Sekine, T. B.R.I. Occasional Report No 11, Tokyo, 1963.
- Kirby, B. R. and Preston, R. R., High Temperature Properties of Hot-rolled Steels for use in fire Engineering Design Studies, Fire Safety Journal, 13, 1988.
- Knight, D. C., Predicting the Performance of Steel Members During Fire Conditions, Symposium on Steel Composite Structures, Dresden, 1975.

- Lathem, D. J., Kirby, B. R. and Thomson, G., The Temperatures Attained by Unprotected Structural Steelwork in Experimental Natural Fires, *Fire Safety Journal*, 12, 1987.
- Law, M, A Basis for the Design of Fire Protection of Building Structures, *The Structural Engineer*, Vol. 61A, Jan., 1983.
- Lie & Stanzak, American ASTM A36 steel 1974.
- Lie, T.T., National Research Council of Canada, 1992.
- Lie, T.T., Characteristic Temperature Curves for Various Fire Severities, *Fire Technology*, 1974.
- Lie, T.T., *Structural Fire Protection: Design Manual of Practice*. 1992.
- Leicester, R. H., *Computation of A Safety Index*, Institute of Engineers, Australia, 1985.
- Lay, M. G., *Structural Steel Fundamentals*, ARRB 1982.
- Magnussen, S. E. and Thelandersson, S., A Discussion of Compartment Fires, *Fire Technology*, August 1974.
- Magnusson, S. E. et al., *Fire Engineering Design of Steel Structures*, Publication 50, Swedish Institute of steel Construction, Stockholm 1976.
- Magnusson, S.E & Thelandersson, S., Temperature Time Curves for the Complete Process of Fire Development. *Acta Polytechnica*, No 65, Stockholm, 1974.
- Magnusson, S. E., Safety Problem of Fire Exposed Steel Structures, Division of Structural Mechanics, Lund Institute of Technology, Lund 1974.
- Malhotra, H.L., *Design of Fire-Resisting Structures*, Chapman and Hall, 1982.
- McAdams, W. A., *Heat Transmission*, McGraw-Hills, 1954.
- Mehaffey, J.R and Harmathy, T. Z. Failure Probabilities of Constructions Designed for Fire Resistance, *Fire and Materials*, Vol 8, (2), 1984.
- Melchers, R.E., *Structural Reliability, Analysis and Prediction*, Pub - John Wiley and Sons, 1987.
- Moy. S.S.J., *Plastic Methods for Steel and Concrete Structures*, Macmillan Publishers Ltd., 1985.
- Nowak, A. S., *Reliability of Structures*, Short Course Notes, Ann Arbor, Michigan , 1994.
- Paulsson, M., TASEF-2, Lund Institute of Technology, Lund, Sweden, 1983.
- Pettersson, O., Swedish Institute of Steel Construction, Publication 50, Sweden, 1976.

- Pettersson, O. and Witteveen, J. On the Fire Resistance of Structural Steel Elements Derived from the Standard Fire Tests or by Calculation, *Fire Safety Journal*, 1980.
- Pham, L. 1985. Load Combinations and Probabilistic Load Models for Limit State Codes, Institution of Engineers, Australia.
- Pham, L. and Bridge, R. Q., Safety Indices for Steel Beams and Columns Designed to AS 1250 - 1981, *Civil Engineering Transactions*, 1985.
- Proe, D. J., Ultimate Strength of Simply Supported Composite Beams in Fire, MRL /PS69/89/007, 1989.
- Proe, D. J. *Steel Construction*, 1986.
- Purkiss, J. A. Developments in the Fire Safety Design of Structural Steelwork *J. Construction Steel Research* 11 (1988)
- Proe, D. J. Ultimate Strength of Simply Supported Composite Beams in Fire, BHP MRL Report PS69/89/007, 1989.
- Rackwitz, A. M. and Fiessler, F. B., Structural Reliability Under Combined Random Load Sequences, *Computers and Structures*, Vol. 9, 1978.
- Ramberg, W. and Osgood, W., Description of Stress-Strain Curves by Three Parameters, NACA Technical Note No. 902, 1943.
- Rocket, J. A. , Fire Induced Gas Flow in an Enclosure, *Combustion Science and Technology*, 12, 165-175, 1976.
- Rubert, A. and Schaumann, P., Structural Steel and Plane Frame Assemblies under Fire Action, *Fire Safety Journal*, 10, 1986.
- Ruge, J. and Winkelmann, O., Brandverschatten von Bauteilen, Sonderforschungsbereich 148, Arbeitsbericht 80, 1978, Part 2, Braunschweig, June 1980.
- Shinozuka, M., "Basic Analysis of Structural Safety", *Journal of the Structural Division, ASCE*, 109, No.3, pp.721-740, 1983.
- Schittowskii, K., "Nonlinear Programming Codes: Information, Tests, Performance", *Lecture Notes in Economics and Mathematical Systems* No 183. Springer, Berlin, 1980.
- Skinner, D. H., Masters Thesis, Melb. Uni. 1970.
- Skinner, D. H., BHP Tech. Bull., (2) 1972.
- Standards Association of Australia, Steel Structures Code AS 4100 - 1900.
- Standards Association of Australia, Loading Code AS 1170 Part 1. 1989.
- Standards Association of Australia, Fire Resistance Test of Structures, AS 1530, Part 4

- Stevens, A. G. et al., Tensile Data on Four Structural Steels, BHP Melb. Res. Lab. MRL6/5, 1971.
- Thomas, I.R et al, Fire Test of the 140 William Street Office Building, BHP report BHPR/92/043, 1992.
- Thomas, P. H., Heselden, A. and Law, M., Fully Developed Compartment Fires - Two kinds of Behaviour, Fire Research Technical Paper, HMSO, 1967.
- Thomas, P. H., Heselden, A., Fully Developed Fires in Single Compartments, Fire Research Note No. 923, Fire Research Station, Borehamwood, 1972.
- Thomas, P. H., Modelling of Compartment Fires, Fire Safety Journal, 5, 1983.
- Thor, L. Deformations and Critical Loads of Steel Beams Under Fire Exposure Conditions, Lund Institute of Technology, Lund, Sweden, 1973.
- Trahair, N. S. and Bradford, M. A., The Behaviour and Design of Steel Structures, Chapman and Hall, 1988.
- Trinks, W. and Mawhinney, M.W. (1961). "Industrial furnaces." Carnegie Inst. Technology, Wiley, New York, N.Y.
- Twilt, L., Strength and Deformation Properties of Steel at Elevated Temperatures: Some Practical Implications, Fire Safety Journal, 13 1988.
- Wade, S.H., Evaporation of Liquids in Currents of Air, Transactions of the Institution of Chemical Engineers, 20, 1-14, 1942.
- Warren Centre Project Report and Technical Papers, University of Sydney, 1989.
- Witteveen, J. et al., The stability of Braced and Unbraced Steel Frames at Elevated Temperatures, Proc. Second International Colloquium on the Stability of Steel Structures, Liege, 1977.
- Yura, J. A. and Galambos, T. V., The Bending Resistance of Steel Beams. Journal of the Structural Div, ASCE, Vol 104 NoST9, 1978.
- Zienkiewicz, O.C., and Cheung, Y.K. (1967) "The finite element method in structural and continuum mechanics." McGraw-Hill Publishing Co. Ltd., London, England.

**APPENDIX A**  
**PROGRAM CODE**

```

REAL SFSY, SSQRES, RAVE, RSTDEV, GAMA, sumfl, avfl, fy(420)
REAL G, H, A, B, ETV, MOIST, ESM, DELAY, flc(420), vnt(420), lm(420)
REAL SPAN, FV, MAXTEMP, TAU, DELTAt, GTEMP(420), L, LSTDEV
REAL Er, MGAST, STEMP(420), ALPHAR, ALPHAC, LAMDA, COHT, SPHT, ETV2
REAL RHOS, HCONST, RES(420), PFAIL, FSY1, SMOM, LAVE, SSQMOM
REAL HIGHT, SMAX, SSQMAX, AVMAX, STDMAX, ETV1, RAN, Z0
REAL MAXKT, KT(420), AVMAXKT, HIGHKT, HGAS, AVGAS, SSQGAS, STDGAS, SHGAS
REAL SHRES, SHOT, SSQHOT, AVHRES, AVSTH, STDTH, HRES(420), TOT
REAL MAXTEMPS(1), sstemp(420), ASSGTEMP(420), ssgtemp(420)
REAL SRES(1), LMOM, FSY2, A1, B1, C1, D1, E1, J, ASSTEMP(420)
REAL A4, B4, C4, D4, TERM1, TERM2, DELAY, HEATFLUX, HEATFLUXS
REAL LAMDAS, L1S, FY6(420), LAMDA3, SFAIL(420), STEMPA
REAL DUR, DUR1
REAL LF, LFAVE, SSQLF, LFSTDEV, IN(40), SIZE, START, STEP
INTEGER Z(40), I, PLOT

```

```

INTEGER TIMEP, SIDES, x

```

```

INTEGER T, N, C, IFAIL, NUMB, CC(420), FLAG, D, TIME, FLAG2
DATA A4, B4, C4, D4 / -3.98691, 723.163, 130.98859, 36.7262 /
DATA A5, B5, C5, D5 / -19.9906, 757.516, 134.2853, 41.0875 /
DATA A6, B6, C6, D6 / -25.8946, 729.46, 98.7086, 31.8308 /
DATA A7, B7, C7, D7 / 20.2186, 937.1582, 77.1994, -2.2195 /
DATA A8, B8, C8, D8 / -38.4666, 812.9669, 53.5437, 18.667 /
DATA A9, B9, C9, D9 / -15.3263, 788.4967, 118.2398, 33.3218 /
DATA A10, B10, C10, D10 / -7.0097, 679.6237, 82.2179, 21.22236 /
DATA SFSY, SSQFSY, AVE, STDEV, Er / 0, 0, 0, 0, .5 /
DATA A, B, SPAN, DELTAt / 3.8620, 0.099750, 3.0000, 0.01667 /
DATA G, H, CC(300) / 2.0, 1.929, 0 /
DATA FLAG, D, RHOS, NUMB / 0, 0, 7850, 0 /
DATA A1, B1, C1 / -0.15266728, -0.26755251, 0.027977605 /
DATA D1, E1 / -0.00103877, 0.73690988 /
DATA A11, B11, C11, D11 / -31.2946, 810.879, 111.154, 36.3925 /
DATA A12, B12, C12, D12 / 12.599, 1121.81, 117.26, -1.8433 /
DATA A13, B13, C13, D13 / -141.3276, 884.436, 77.177, 44.319 /
DATA A14, B14, C14, D14 / 23.04152, 925.5311, 167.2161, -1.973986 /
DATA A15, B15, C15, D15 / 39.6368, 828.0219, 139.599, -2.19859 /
DATA A16, B16, C16, D16 / 34.6659, 839.762, 89.8403, -2.0085 /
DATA A17, B17, C17, D17 / 30.6379, 842.4778, 78.4072, -1.87303 /
DATA A18, B18, C18, D18 / 33.978, 8793.033, 1304.439, -1.6396 /
DATA A19, B19, C19, D19 / 19.859, 1341.42, 303.214, -1.46224 /
DATA A20, B20, C20, D20 / -60.4856, 1136.8317, 321.1538, 126.0356 /
DATA A21, B21, C21 / 1.0371021, -.0016071906, 6.2331477E-6 /
DATA D21 / -2.0394809E-7 /
DATA A31, B31, C31 / -4.4231E-10, -7.273E-8, -9.091E-6 /
DATA D31, E31 / 3.0684E-8, -3.222E-11 /
DATA A22, B22, C22, D22 / -21.079, 22.11085, 1832.594, -338.54787 /
DATA A23, B23, C23, D23 / 34.699, 2908.449, 598.32175, -1.58798 /
DATA A24, B24, C24, D24 / 39.1465, 865.0871, 164.35177, -1.8095 /
DATA A25, B25, C25, D25 / -66.28, 1550.252, 361.44, 134.44 /
DATA HEATFLUXS, DELAY, DTIME / 0, 0, 0 /
DATA A32, B32, C32 / -5.72937E-10, -9.2940447E-8, -1.146027E-5 /
DATA D32, E32 / 3.937839E-8, -4.081085E-11 /
DATA A40, B40, C40 / -6.9855747E-10, -9.696143E-8, -1.022577E-5 /
DATA D40, E40 / 4.0689259E-8, -5.19966178E-11 /
DATA A41, B41, C41 / -9.7155698E-10, -1.2089863E-7, -1.15293079E-5 /
DATA D41, E41 / 5.13115668E-8, -7.3050438E-11 /

```

```

DATA A42,B42,C42/1.0412109,-.0016343359,6.8647299E-6/
DATA D42/-2.2453881E-7/
DATA A43,B43,C43/1.0299269,-.001348,5.636498E-6/
DATA D43/-1.884478E-7/
DOUBLE PRECISION FSY
DOUBLE PRECISION G05DDF,G05DGF,G05DEF,G05CAF,G05DPF
DOUBLE PRECISION S,GVAR,L1M,FY0
DOUBLE PRECISION LLOAD,RLOG,FL,VENT,INS,K,AREA,VOL

EXTERNAL G05DDF,G05DGF,G05DEF,G05CAF,G05DPF,G05CBF
CALL G05CBF(0)
IFAIL = 0

```

```

C DESIGNATE NAME OF OUTPUT FILE
OPEN (06,FILE= 'H4')

```

```

C DESIGNATE THE NUMBER OF SIMULATIONS "N" REQUIRED
N = 100000

```

```

C TO OBTAIN A PLOT OF THE VALUES OF PARTICULAR VARIABLES
C AT FAILURE FPLOT = 1; NORMAL FPLOT = 2
C ( AND FOR EXAMPLE SET "SIZE" = FSY
C SET VALUES FOR START AND STEP TO DIMENSION HISTOGRAM)
FPLOT = 1

```

```

IF ( FPLOT .EQ. 1 .OR. FPLOT .EQ. 2) THEN
START = 0
STEP = 2.0
IN(0) = START
DO 480 I = 1,36
IN(I) = STEP + IN(I-1)
480 CONTINUE
END IF

```

```

DO 21 T = 1,N

```

```

LLOAD = G05DPF(1.4079D0,16.21180D0,IFAIL)
RLOG = (G05DEF(4.05150D0,0.0997D0))
LMOM = ((LLOAD + RLOG)*(SPAN ))/4
C LMOM = G05DEF(3.29490D0,0.10040D0)
SMOM = LMOM+ SMOM
SSQMOM = (LMOM**2) + SSQMOM
C IF ( LMOM .LT. 45) THEN
C GO TO 21
C END IF

```

```

FL = G05DEF(2.8320D0,.34D0)
C IF ( FL .LT. 25) THEN
C GO TO 21
C END IF

```

```

FSY = G05DDF(295.0D0,29.5001D0)
C IF ( FSY .GT. 280 ) THEN
C GO TO 21
C END IF

```

```

IF (FPLOT .EQ. 2 ) THEN
SIZE = FL
LF = LF + SIZE
SSQLF = (SIZE**2) + SSQLF

IF ( SIZE .GE.IN(0) .AND. SIZE .LT. IN(1)) THEN
Z(1) = Z(1) + 1
END IF
IF ( SIZE .GE.IN(1) .AND. SIZE .LT. IN(2)) THEN
Z(2) = Z(2) + 1
END IF
IF ( SIZE .GE.IN(2) .AND. SIZE .LT. IN(3)) THEN
Z(3) = Z(3) + 1
END IF
IF ( SIZE .GE.IN(3) .AND. SIZE .LT. IN(4)) THEN
Z(4) = Z(4) + 1
END IF
IF ( SIZE .GE.IN(4) .AND. SIZE .LT. IN(5)) THEN
Z(5) = Z(5) + 1
END IF
IF ( SIZE .GE.IN(5) .AND. SIZE .LT. IN(6)) THEN
Z(6) = Z(6) + 1
END IF
IF ( SIZE .GE.IN(6) .AND. SIZE .LT. IN(7)) THEN
Z(7) = Z(7) + 1
END IF
IF ( SIZE .GE.IN(7) .AND. SIZE .LT. IN(8)) THEN
Z(8) = Z(8) + 1
END IF
IF ( SIZE .GE.IN(8) .AND. SIZE .LT. IN(9)) THEN
Z(9) = Z(9) + 1
END IF
IF ( SIZE .GE.IN(9) .AND. SIZE .LT. IN(10)) THEN
Z(10) =Z(10) + 1
END IF
IF ( SIZE .GE.IN(10) .AND. SIZE .LT. IN(11)) THEN
Z(11) =Z(11) + 1
END IF
IF ( SIZE .GE.IN(11) .AND. SIZE .LT. IN(12)) THEN
Z(12) =Z(12) + 1
END IF
IF ( SIZE .GE.IN(12) .AND. SIZE .LT. IN(13)) THEN
Z(13) = Z(13) + 1
END IF
IF ( SIZE .GE.IN(13) .AND. SIZE .LT. IN(14)) THEN
Z(14) = Z(14) + 1
END IF
IF ( SIZE .GE.IN(14) .AND. SIZE .LT. IN(15)) THEN
Z(15) = Z(15) + 1
END IF
IF ( SIZE .GE.IN(15) .AND. SIZE .LT. IN(16)) THEN
Z(16) = Z(16) + 1
END IF
IF ( SIZE .GE.IN(16) .AND. SIZE .LT. IN(17)) THEN
Z(17) = Z(17) + 1
END IF

```

```

IF ( SIZE .GE.IN(17) .AND. SIZE .LT. IN(18)) THEN
Z(18) = Z(18) + 1
END IF
IF ( SIZE .GE.IN(18) .AND. SIZE .LT. IN(19)) THEN
Z(19) = Z(19) + 1
END IF
IF ( SIZE .GE.IN(19) .AND. SIZE .LT. IN(20)) THEN
Z(20) = Z(20) + 1
END IF
IF ( SIZE .GE.IN(20) .AND. SIZE .LT. IN(21)) THEN
Z(21) = Z(21) + 1
END IF
IF ( SIZE .GE.IN(21) .AND. SIZE .LT. IN(22)) THEN
Z(22) = Z(22) + 1
END IF
IF ( SIZE .GE.IN(22) .AND. SIZE .LT. IN(23)) THEN
Z(23) = Z(23) + 1
END IF
IF ( SIZE .GE.IN(23) .AND. SIZE .LT. IN(24)) THEN
Z(24) = Z(24) + 1
END IF
IF ( SIZE .GE.IN(24) .AND. SIZE .LT. IN(25)) THEN
Z(25) = Z(25) + 1
END IF
IF ( SIZE .GE.IN(25) .AND. SIZE .LT. IN(26)) THEN
Z(26) = Z(26) + 1
END IF
IF ( SIZE .GE.IN(26) .AND. SIZE .LT. IN(27)) THEN
Z(27) = Z(27) + 1
END IF
IF ( SIZE .GE.IN(27) .AND. SIZE .LT. IN(28)) THEN
Z(28) = Z(28) + 1
END IF
IF ( SIZE .GE.IN(28) .AND. SIZE .LT. IN(29)) THEN
Z(29) = Z(29) + 1
END IF
IF ( SIZE .GE.IN(29) .AND. SIZE .LT. IN(30)) THEN
Z(30) = Z(30) + 1
END IF
IF ( SIZE .GE.IN(30) .AND. SIZE .LT. IN(31)) THEN
Z(31) = Z(31) + 1
END IF
IF ( SIZE .GE.IN(31) .AND. SIZE .LT. IN(32)) THEN
Z(32) = Z(32) + 1
END IF
IF ( SIZE .GE.IN(32) .AND. SIZE .LT. IN(33)) THEN
Z(33) = Z(33) + 1
END IF
IF ( SIZE .GE.IN(33) .AND. SIZE .LT. IN(34)) THEN
Z(34) = Z(34) + 1
END IF
IF ( SIZE .GE.IN(34) .AND. SIZE .LT. IN(35)) THEN
Z(35) = Z(35) + 1
END IF
IF ( SIZE .GE.IN(35) .AND. SIZE .LT. IN(36)) THEN
Z(36) = Z(36) + 1
END IF

```

```

      END IF
C      X = X + 1

C      FIRE = 0 FOR REAL FIRE: FIRE = 1 FOR STANDARD FIRE
      FIRE = 0
C      TO USE EXPERIMENTAL STEEL TEMP CURVE TC = 1
      TC = 0
cc     BHP MODEL = 1:  JRL MODEL = 2
      MODEL = 2
      SIDES = 3
      RATIO = .8
c     CONCRETE SLAB SUPPORTED BY A 100UC: UC100 = 1
      UC100 = 0
c     CONCRETE SLAB SUPPORTED BY A 200UB: UB200 = 1
      UB200 = 0

      K = G05DDF(1.0148D0, .047800D0)
C      K = 1
      VENT = G05DDF(0.040D0, 0.004D0)
C      VENT = G05DEF(-2.5310 , 0.09971)
      IF( VENT .LT. .01) THEN
          VENT = .01
      END IF
      IF (VENT .GT. 0.15) THEN
          VENT = 0.15
      END IF

      INS = G05DDF(0.02000D0 , 0.0020000D0)
C      INS = 0.019
      S = G05DDF(470.450D0, 14.550D0)
C      S = 470.45

      GVAR = G05DDF(1.0D0, 0.00001D0)
      VOL = G05DDF(0.004750D0, .0000001D0)
C      VOL = 0.00475
      MOIST = 0.0376
      AREA = G05DDF(0.757D0, 0.07570D0)
C      AREA = 0.757
      FV = AREA/VOL

      ESM = FV/7.85
      IF ( ESM .GT. 40) THEN
          ESM = 40
      ELSE IF( ESM .LT. 5) THEN
          ESM = 5
      END IF

C      GAMA = G05DGF(G, H, IFAIL)
C      ETV1 = G05DBF(1.0)
C      ETV = -(LOG(ETV1)*2.648)+12.061000
C      DLOAD = G05DDF(13.33, 0.533)
c      E0 = G05DDF(1.0, 0.1)
c      LMOM = ((GAMA + RLOG)*(SPAN**2))/8

```

```

c      LMOM =      40
c      LMOM = ((E0 * (DLOAD + LLOAD)) * (SPAN**2)) / 8
12  IF (FSY      .GT. 500.0) THEN
    NUMB = NUMB + 1
    END IF
    C = 1
c      !!! NOTE - MINIMUM STEEL TEMPERATURE = 20 DEGREES !!!
    GTEMP(1) = 20
    STEMP(1) = 22
    LAMDA = 0
    FLAG = 0
    FLAG2 = 0
    HEATFLUXS = 0

    TEMPH = 0
c      SRES(T) = 0
    HIGHT = 0
c      THERMAL CONDUCTIVITY MEAN AND STD'DEV BASED ON CURVE FIT
cc      LIM = G05DDF(0.0D0, 1.00D0)

c      STRENGTH MODEL COEFFICIENTS
cc      FY0 = G05DDF(0.0D0, 1.00D0)

c      REMEMBER TIME SET TO 1.0 MIN.....
c      SET DURATION OF THE FIRE
    DUR = 5
    DO 19 L = DELTAt, DUR, DELTAt
c      DO 19 L = 1.0, 150.0, 0.5
        C = C + 1
        TIME = C
        IF ( FIRE .EQ. 0) THEN
            GO TO 889
        END IF
c      STANDARD TEMP/TIME CURVE
        GTEMP(C) = (345*LOG10((8*L*60)+1))*GVAR) + GTEMP(1)
        GO TO 888
c      GAS TEMP BASED ON BHP O2 TEST -CEILING
c      IF ( L .LE. 26 ) THEN
c      GTEMP(C) = 1 / (0.029455438 + (-1.2472793E-6*L**3) + (-0.0012928895
c      + *1**.5))
c      ELSE
c      GTEMP(C) = (-34602440 + (90847.785*L) + (3.5680628E8/L**.5)
c      + + (-2.1465183e10/L**1.5) + ((2.576449E10*LOG(L))/L**2))
c      END IF
c      GAS TEMP BASED ON BHP O2 TEST AVERAGE
CB      GTEMP(C) = 1 / (0.023540254 + (-.009666658*L) + (.001421961*L**2)
CB      + + (-8.3048099E-5*L**3) + (1.684907E-6*L**4))
889      TAU = FL / (330*VENT)
        MAXTEMP = 250 * ((10*VENT)**(.1 / (VENT**.3))) * EXP(-TAU*VENT**2) *
        + ((3*(1-EXP(-.6*TAU)) - (1-EXP(-3*TAU)) + (4*(1-EXP(-12*TAU)))))
c      + + (600/VENT)**0.5
c      PRINT*, TAU, MAXTEMP
c      IF ( L .LE. TAU ) THEN
        GTEMP(C) = 250 * ((10*VENT)**(.1 / (VENT**.3))) * EXP(- L *VENT**2) *
        + ((3*(1-EXP(-.6* L )) - (1-EXP(-3* L )) + (4*(1-EXP(-12* L )))))

```

```

C      + +(600/VENT)**0.5
        ELSE
GTEMP(C) = (-600*(L/TAU-1))+MAXTEMP
        END IF
888      IF (GTEMP(C) .LE. 19) THEN
        GOTO 20
        END IF
MGAST = (GTEMP(C)+GTEMP(C-1))/2.0

C      HEAT TRANSFER TERMS IN KJOULES/M DEGREES HOURS
ALPHAC = 83.6
C      THERMAL CONDUCTIVITY after BENNETTS
C      LAMDA = G05DDF(0.33910,0.000001)

        IF ( SIDES .EQ. 3) THEN
GO TO 997
        END IF
C      DERIVED EXPRESSIONS FOR THERMAL CONDUCTIVITY - 4 SIDED
        IF ( STEMP(C-1) .GT.100) THEN
LAMDA =(0.8504+(11.03/ESM**2)+((-6.904-0.023*ESM)/
+ STEMP(C-1)**0.5))+(L1M*0.0577)
        ELSE
LAMDA = (0.099+(6.84/ESM**2)+((-4.31-(382.52/ESM**2))/
+ STEMP(C-1)**1.5))
        END IF
DELAY = 0.55 + (0.000135 * ((1000*INS)**3))
GO TO 996
C      DERIVED EXPRESSIONS FOR THERMAL CONDUCTIVITY - 3 SIDED
997      IF (STEMP(C-1) .LT. 100) THEN
LAMDA = 0.2977-(0.00768*ESM)+((36.426-(331.66/ESM**0.5))/
+ STEMP(C-1)**2)
        ELSE
LAMDA = ((0.592-(0.015*ESM)+((2093.7-(0.036*ESM**3))/
+ STEMP(C-1)**1.5)+((( -5332.7+(0.103*ESM**3)) *
+ LOG(STEMP(C-1)))/STEMP(C-1)**2)))+(L1M*0.0577)
        END IF
DELAY = 0.497 +(0.0087*((1000*INS)**2))

C      ECCS COEFFICIENT OF HEAT TRANSFER - UNINSULATED STEEL
C      ALPHAR = 2.04E-7*Er*((MGAST+273)**2 + (STEMP(C-1)+273)**2)
C      + *(STEMP(C-1) + MGAST +546)

C      CTICM COEFFICIENT OF HEAT TRANSFER - UNINSULATED STEEL
C      ALPHAR = 1.25E-7((MGAST+273)**2 + (STEMP(C-1)+273)**2)
C      + *(STEMP(C-1) + MGAST + 546)

C      CTICM COEFFICIENT OF HEAT TRANSFER - INSULATED STEEL
996      ALPHAR = 5E-7 *(GTEMP(C)+273)**3
COHT = 1/((1/(ALPHAR+ALPHAC))+(INS/LAMDA))
TERM1 = ((1/(ALPHAR+ALPHAC))+(INS/(2.0*LAMDA)))

SPHT = ((3.8E-7*STEMP(C-1)**2)+(2E-4*STEMP(C-1)) + 0.472)
c      IF (INS .EQ. 0) THEN
c      GO TO 39
c      END IF
TERM2 = (((SPHT*RHOs)/FV)+4180*MOIST*INS)

```

```

IF (STEMP(C-1) .LT. 100) THEN
STEMP(C) = ((1/TERM1)*(1/TERM2)*(MGAST-STEMP(C-1))*DELTA
+
) + STEMP(C-1)
GOTO 998
END IF
IF (FLAG2 .GT. 1) THEN
GOTO 13
END IF
STEMP(C) = 100
FLAG = FLAG + 1
IF (FLAG .GT. DELAY) THEN
FLAG2 = 1
GO TO 13
ELSE
GOTO 998
END IF
13 HCONST = (COHT*DELTA *FV) / (SPHT*RHOs)
STEMP(C) = ((GTEMP(C)-STEMP(C-1))*HCONST )+STEMP(C-1)

C WRITE(06,40) GTEMP(C),MGAST,STEMP(C)

C UNINSULATED STEEL
C 39 HCONST = ((ALPHAR+ALPHAC)*0.01667*FV) / (SPHT*RHOs)

C STEMP(C) = ((GTEMP(C)-STEMP(C-1))*HCONST )+STEMP(C-1)

998 HIGHT = STEMP(C)
C print*, c,stemp(c),fsy,lamdas,lamda
RES (C) = 0
C ssgtemp(c) = ssgtemp(c) + gtemp(c)
C SSTEMP(C) = SSTEMP(C) + STEMP(C)
C CC(C) = CC(C) +1
C KT(C) = (AREA/VOL)*(LAMDA/INS)
C IF ( KT(C) .GT. KT(C-1) ) THEN
C HIGHKT = KT(C)
C END IF
C IF ( TC .EQ. 1 ) THEN
C STEMP(C) = A20+(B20/(1+((L*60)/C20)**D20))
C STEMP(C) = A20+(B20/(1+EXP(-((L*60)-C20)/D20)))
C STEMP(C) = A15+(B15/(1+((L*60)/C15)**D15))

IF (STEMP(C) .LE. 22 ) THEN
STEMP(C) = 22
END IF
END IF

IF ( MODEL .EQ. 1) THEN
GO TO 991
ELSE IF (MODEL .EQ. 2) THEN
GO TO 884
END IF
884 IF (SIDES .EQ. 3) THEN
GO TO 995
END IF
C STRENGTH REDUCTION MODEL *** 4 SIDED EXPOSURE***

```

```

IF (STEMP(C) .LT. 200) THEN
FSY2 = FSY*(1-(STEMP(C)/1482.6))
GOTO 100
END IF
IF (STEMP(C) .LT. 700) THEN
FYM = ((2.9907+(-.0238*STEMP(C)))+(4.7523E-5*STEMP(C)**2
+ *LOG(STEMP(C)))+(-1.5891E-5*STEMP(C)**2*STEMP(C)**.5)
+ +(1.964E-7*STEMP(C)**3))+(FY0 * 0.07316) )
IF (FYM .GT. 1 ) THEN
FYM = 1
END IF
FSY2 = FSY * FYM
GOTO 100
END IF
IF (STEMP(C) .GT. 800 ) THEN
STEMP(C) = 800
END IF
IF (STEMP(C) .LE. 800) THEN
FSY2 = FSY*(0.2219-((STEMP(C) - 600)/472.95))
END IF
GO TO 100

```

C STRENGTH REDUCTION MODEL \*\*\*\* BHP MODEL \*\*\*

```

991 IF (STEMP(C).LE. 215 ) THEN
c PRINT *, 'BHP'
FSY2 = FSY
GOTO 100
END IF
IF (STEMP(C) .GT. 905) THEN
STEMP(C) = 905
END IF
FSY2 = FSY*((905 - STEMP(C))/690)
GO TO 100
995 IF ( UC100 .EQ. 1) THEN
GO TO 883
END IF
IF ( UB200 .EQ. 1) THEN
GO TO 882
END IF
IF (RATIO .EQ. .6) THEN
GO TO 880
ELSE IF ( RATIO .EQ. .8) THEN
GO TO 881
END IF

```

C STRENGTH REDUCTION MODEL \*\*\*\* 3 - SIDED EXPOSURE \*\*

```

C RATIO = 0.6 WEB EQ 2039
880 STEMPA = STEMP(C)*1.1977
IF (STEMPA .LT. 200) THEN
+ FSY2 = FSY*(A42+ B42*STEMPA+ C42*STEMPA**2
+ +D42*STEMPA**2.5)
GOTO 100
END IF

IF ( STEMPA .GT. 800) THEN
STEMP(C) = 800
END IF

```

```

FYM = ((A42+ B42*STEMPA+ C42*STEMPA**2
+D42*STEMPA**2.5))+(FY0*0.07316)
IF ( FYM .GT. 1 ) THEN
    FYM = 1
END IF
FSY2 = FYM * FSY
c    print*, ' 360UB 0.6'
GO TO 100

C    THE 1.15 AND 0.908 TERMS BELOW ARE TO CHECK 0.2% & 1% STRAIN
C    FSY2 = FSY
C    ELSE
c    FSY2 = FSY*(1.1517143+(stemp(c)*-0.001394643))
C    FSY2 = FSY*(0.9180147+(-1.86728e-6*STEMP(C)**2)+
C    +    (0.0106656*(STEMP(C)**0.5)))

c    FSY2 = FSY*(-0.851286+(0.0136607*STEMP(C))+
c    +    (-2.957142E-5*stemp(c)**2)+(1.75E-8*stemp(c)**3))

C    STRENGTH REDUCTION MODEL *** 3 SIDED EXPOSURE ***
C    RATIO = 0.82  BASED ON 360 UB  WEB  EQ 2039
881  STEMPA = STEMP(C)*1.0
    IF (STEMP(C) .LT. 200) THEN
        FSY2 = FSY*(A21+ B21*STEMPA+ C21*STEMPA**2
+          +D21*STEMPA**2.5)
    GOTO 100
    END IF

    IF ( STEMPA .GT. 800) THEN
        STEMP(C) = 800
    END IF

FYM = (A21+ B21*STEMPA+ C21*STEMPA**2
+D21*STEMPA**2.5 )+(FY0*0.07316)
IF ( FYM .GT. 1 ) THEN
    FYM = 1
END IF
FSY2 = FYM * FSY
c    print*, ' 360UB.8'
GO TO 100

C    STRENGTH REDUCTION MODEL ***** 3 - SIDED EXPOSURE **
C    RATIO = 0.82  BASED ON 200 UBP WEB EQU 6102
882  IF (STEMP(C) .LT. 200) THEN
        FSY2 = FSY*(EXP(A31+ B31*STEMP(C)+ C31*STEMP(C)**2
+          +D31*STEMP(C)**3 +E31*STEMP(C)**4))
    GOTO 100
    END IF
    IF ( STEMP(C) .GT. 830) THEN
        STEMP(C) = 830
    END IF
        FSY2 = FSY*(EXP(A31+ B31*STEMP(C)+ C31*STEMP(C)**2
+          +D31*STEMP(C)**3 +E31*STEMP(C)**4))
c    print*, '200UB'

```

GO TO 100

STRENGTH REDUCTION MODEL \*\*\*\*\* 3 - SIDED EXPOSURE \*\*

RATIO = 0.82 BASED ON 110 UC WEB EQ6102

IF (STEMP(C) .LT. 200) THEN

FSY2 = FSY\*(EXP(A32+ B32\*STEMP(C)+ C32\*STEMP(C)\*\*2  
+D32\*STEMP(C)\*\*3 +E32\*STEMP(C)\*\*4))

GOTO 100

END IF

IF (STEMP(C) .GT. 830) THEN

STEMP(C) = 830

END IF

FSY2 = FSY\*(EXP(A32+ B32\*STEMP(C)+ C32\*STEMP(C)\*\*2  
+D32\*STEMP(C)\*\*3 +E32\*STEMP(C)\*\*4))

print\*, '100UC'

GO TO 100

100 RES(C) = (FSY2 \*S \*K )/1000

IF (RES(C) .GE. LMOM) THEN

GOTO 19

END IF

SFAIL(C) =SFAIL(C) + 1.0

IF( FPLOT .EQ. 1) THEN

SIZE = FL

LF = LF + SIZE

SSQLF = (SIZE\*\*2) + SSQLF

IF ( SIZE .GE.IN(0) .AND. SIZE .LT. IN(1)) THEN

Z(1) = Z(1) + 1

END IF

IF ( SIZE .GE.IN(1) .AND. SIZE .LT. IN(2)) THEN

Z(2) = Z(2) + 1

END IF

IF ( SIZE .GE.IN(2) .AND. SIZE .LT. IN(3)) THEN

Z(3) = Z(3) + 1

END IF

IF ( SIZE .GE.IN(3) .AND. SIZE .LT. IN(4)) THEN

Z(4) = Z(4) + 1

END IF

IF ( SIZE .GE.IN(4) .AND. SIZE .LT. IN(5)) THEN

Z(5) = Z(5) + 1

END IF

IF ( SIZE .GE.IN(5) .AND. SIZE .LT. IN(6)) THEN

Z(6) = Z(6) + 1

END IF

IF ( SIZE .GE.IN(6) .AND. SIZE .LT. IN(7)) THEN

Z(7) = Z(7) + 1

END IF

IF ( SIZE .GE.IN(7) .AND. SIZE .LT. IN(8)) THEN

Z(8) = Z(8) + 1

END IF

IF ( SIZE .GE.IN(8) .AND. SIZE .LT. IN(9)) THEN

Z(9) = Z(9) + 1

END IF

```

IF ( SIZE .GE.IN(9) .AND. SIZE .LT. IN(10)) THEN
Z(10) =Z(10) + 1
END IF
IF ( SIZE .GE.IN(10) .AND. SIZE .LT. IN(11)) THEN
Z(11) =Z(11) + 1
END IF
IF ( SIZE .GE.IN(11) .AND. SIZE .LT. IN(12)) THEN
Z(12) =Z(12) + 1
END IF
IF ( SIZE .GE.IN(12) .AND. SIZE .LT. IN(13)) THEN
Z(13) = Z(13) + 1
END IF
IF ( SIZE .GE.IN(13) .AND. SIZE .LT. IN(14)) THEN
Z(14) = Z(14) + 1
END IF
IF ( SIZE .GE.IN(14) .AND. SIZE .LT. IN(15)) THEN
Z(15) = Z(15) + 1
END IF
IF ( SIZE .GE.IN(15) .AND. SIZE .LT. IN(16)) THEN
Z(16) = Z(16) + 1
END IF
IF ( SIZE .GE.IN(16) .AND. SIZE .LT. IN(17)) THEN
Z(17) = Z(17) + 1
END IF
IF ( SIZE .GE.IN(17) .AND. SIZE .LT. IN(18)) THEN
Z(18) = Z(18) + 1
END IF
IF ( SIZE .GE.IN(18) .AND. SIZE .LT. IN(19)) THEN
Z(19) = Z(19) + 1
END IF
IF ( SIZE .GE.IN(19) .AND. SIZE .LT. IN(20)) THEN
Z(20) = Z(20) + 1
END IF
IF ( SIZE .GE.IN(20) .AND. SIZE .LT. IN(21)) THEN
Z(21) = Z(21) + 1
END IF
IF ( SIZE .GE.IN(21) .AND. SIZE .LT. IN(22)) THEN
Z(22) = Z(22) + 1
END IF
IF ( SIZE .GE.IN(22) .AND. SIZE .LT. IN(23)) THEN
Z(23) = Z(23) + 1
END IF
IF ( SIZE .GE.IN(23) .AND. SIZE .LT. IN(24)) THEN
Z(24) = Z(24) + 1
END IF
IF ( SIZE .GE.IN(24) .AND. SIZE .LT. IN(25)) THEN
Z(25) = Z(25) + 1
END IF
IF ( SIZE .GE.IN(25) .AND. SIZE .LT. IN(26)) THEN
Z(26) = Z(26) + 1
END IF
IF ( SIZE .GE.IN(26) .AND. SIZE .LT. IN(27)) THEN
Z(27) = Z(27) + 1
END IF
IF ( SIZE .GE.IN(27) .AND. SIZE .LT. IN(28)) THEN
Z(28) = Z(28) + 1
END IF

```

```

IF ( SIZE .GE.IN(28) .AND. SIZE .LT. IN(29)) THEN
Z(29) = Z(29) + 1
END IF
IF ( SIZE .GE.IN(29) .AND. SIZE .LT. IN(30)) THEN
Z(30) = Z(30) + 1
END IF
IF ( SIZE .GE.IN(30) .AND. SIZE .LT. IN(31)) THEN
Z(31) = Z(31) + 1
END IF
IF ( SIZE .GE.IN(31) .AND. SIZE .LT. IN(32)) THEN
Z(32) = Z(32) + 1
END IF
IF ( SIZE .GE.IN(32) .AND. SIZE .LT. IN(33)) THEN
Z(33) = Z(33) + 1
END IF
IF ( SIZE .GE.IN(33) .AND. SIZE .LT. IN(34)) THEN
Z(34) = Z(34) + 1
END IF
IF ( SIZE .GE.IN(34) .AND. SIZE .LT. IN(35)) THEN
Z(35) = Z(35) + 1
END IF
IF ( SIZE .GE.IN(35) .AND. SIZE .LT. IN(36)) THEN
Z(36) = Z(36) + 1
END IF
END IF

```

```
GOTO 20
```

```

19 CONTINUE
20 SMAX = HIGHT + SMAX
c MAXTEMPS(T) = HIGHT
c IF ( HIGHT .GT. 500 ) THEN
c END IF
c TRES = TRES + SRES(T)
c TSQRES = (SRES(T)**2) + TSQRES
c SSQMAX = (HIGHT**2) + SSQMAX
C SHRES = HRES + SHRES

c MAXKT = HIGHKT + MAXKT
c SSKT = (HIGHKT**2) + SSKT
C STEMPH = TEMPH + STEMPH
C SSQTH = (TEMPH**2) + SSQTH
C SHGAS = SHGAS + HGAS
C SSQGAS = (HGAS**2) + SSQGAS
21 CONTINUE
c AVHRES = SHRES/REAL(N)
c AVSMAX = SMAX/REAL(N)
c STDMAX = SQRT(((REAL(N)*SSQMAX) - (SMAX**2)) / (REAL(N) *
c + (REAL(N)-1)))
C AVGAS = SHGAS/REAL(N)
C STDGAS = SQRT(((REAL(N)*SSQGAS) - (SHGAS**2)) / (REAL(N) *
C + (REAL(N)-1)))
c AVMAXKT = MAXKT/REAL(N)
c STDKT = SQRT(((REAL(N)*SSKT) - (MAXKT**2)) / (REAL(N) *
c + (REAL(N)-1)))
c WRITE(06,400) AVMAXKT,STDKT
400 FORMAT(1X, 'AVMAXKT = ',F8.2,3X, 'STDEV = ',F8.2)

```

```

c      WRITE(06,22)   AVSMAX,STDMAX
22     FORMAT(1X,'AV MAX STEEL TEMP = ',F6.2,3X,'STDEV = ',F6.2)
c      WRITE(06,27)   AVGAS,STDGAS
c27    FORMAT(1X,'AV MAX GAS TEMP = ',F6.2,3X,'STDEV = ',F6.2)
      DO 140 C = 2,300
          TFAIL = TFAIL + SFAIL(C)
          sumfl = sumfl + flc(C)
140    CONTINUE
      PFAIL = TFAIL/REAL(N)

      WRITE(06,45) PFAIL,NUMB,SFAIL(2),N
c      PRINT*, TFAIL
c      AZRES = ZRES/TFAIL
c      AVSTH = SHOT/REAL(TFAIL)
c      STDTH = SQRT(((TFAIL *SSQHOT) - (SHOT**2)) / (TFAIL *
c + (TFAIL -1)))
c      WRITE(06,23)   AVSTH,STDTH
23     FORMAT(1X,'AV FAIL TEMP = ',F6.2,3X,'STDEV = ',F6.2)
c      RAVE = SRES/REAL(TFAIL)
c      RSTDEV = SQRT(((SSQRES*TFAIL ) - (SRES**2)) / (TFAIL *
c + (TFAIL -1)))

      LAVE = SMOM/REAL(N)
      LSTDEV = SQRT(((SSQMOM*REAL(N)) - (SMOM**2)) / (REAL(N) *
+ (REAL(N) -1)))

      IF ( FPLOT .EQ. 1) THEN
      LFAVE = LF/REAL(TFAIL)
      Lfstdev = SQRT(((SSQLF*REAL(TFAIL)) - (LF**2)) / (REAL(TFAIL) *
+ (REAL(TFAIL) -1)))
      END IF

      IF ( FPLOT .EQ. 2 ) THEN
      LFAVE = LF/REAL(N)
      Lfstdev = SQRT(((SSQLF*REAL(N)) - (LF**2)) / (REAL(N) *
+ (REAL(N) -1)))
      END IF

c      AVETV = SETV/REAL(N)
c      WRITE(06,30) AZRES
      WRITE(06,35) LAVE,LSTDEV
30     FORMAT(1X,'AVE FAIL RES = ',F6.2)
35     FORMAT(1X,'AVE LMOM = ',F8.2,1X,'STDEV = ',F6.2)

c40    FORMAT(1X,3X,F8.2,3X,F8.2,3X,F8.2)
c      AARES = TRES/REAL(N)
c      STDRES = SQRT(((REAL(N) *TSQRES) - (TRES **2)) / (REAL(N) *
c + (REAL(N) -1)))
c      WRITE(06,49) AARES,STDRES
151    FORMAT(1X,F8.2)
49     FORMAT(1X,F8.2,1X,F8.2)
994    FORMAT(1X,'NUMBER OF SIDES EXPOSED = 'I2,10X,F8.2,10X,I5)
45     FORMAT(1X,'THE PROBABILITY OF FAILURE = ',F9.7,4X,I3,4X,F8.2,4X,I8)
c      DO 141 C = 2,300
c      IF (HRES(C) .GT. 00 ) THEN
c      TOT = TOT + 1

```

```

C      END IF
C141  CONTINUE
C      DO 145 C = 2,300
C      SHRES = HRES(C) + SHRES
C145  CONTINUE
C      DO 1551 T = 1,N
C      IF (SRES(T) .GT. .1 ) THEN
C      WRITE(06,151) SRES(T)
C      END IF
C1551 CONTINUE
C      TIMEP =0
      dur1 = dur*60
      DO 150 C = 2,dur1
      IF ( CC(C) .GT. 1 ) THEN
      ASSTEMP(C) = SSTEMP(C)/(CC(C))
      assgtemp(c) = ssgtemp(c)/(CC(c))
      END IF
      TIMEP = 1 + TIMEP
      WRITE(06,50) TIMEP,SFAIL(C)
      WRITE(06,50) C,TIMEP,SFAIL(C),flc(c),vnt(c),fy(c),lm(c)
      WRITE(06,50) C,TIMEP,ASSGTEMP(C),ASSTEMP(C),CC(C),RES(C),LMOM
50    FORMAT(1X,I5,3X,F8.2)
      c 50  FORMAT(1X,I5,3X,I5,3X,F8.2,3X,F8.2,3X,F8.4,3X,F8.2,3X,F8.2)
      c 50  FORMAT(1X,I5,3X,I5,3X,F8.2,3X,F8.2,3X,I6,3X,F8.2,3X,F8.2)
      C      WRITE(06,51) TIMEP, ASSTEMP(C)
      C 51  FORMAT(1X,I5,3X,F8.2)
      150  CONTINUE
      DO 160 T = 1,N
      IF ( FTEMP(T) .GT. 1 ) THEN
      WRITE(06,165) MAXTEMPS(T)
      c165  FORMAT ( F8.2)
      c      END IF
      c160  CONTINUE

      IF (FPLOT .EQ. 1 .OR. FPLOT .EQ. 2 ) THEN
      WRITE(06,635) LFAVE,LFSTDEV
      635  FORMAT(1X,'AVE VALUE = ',F8.2,1X,'STDEV =',F6.2)
      DO 481 I = 1,36
      WRITE(06,634) IN(I-1),IN(I),Z(I)
      481 CONTINUE
      END IF
      634  FORMAT (1X,F5.2,3X,F5.2,3X,I6)

      END

```